Long-term assessment of aerosol chemical composition in the interior of South Africa

P Maritz

orcid.org 0000-0001-6658-0843

Thesis submitted in fulfilment of the requirements for the degree *Doctor of Philosophy in Science with Atmospheric Chemistry* at the North-West University

Promoter:	Prof JP Beukes
Co-Promoter:	Prof PG van Zyl
Assistant Promoter:	Dr C Liousse

Graduation May 2019

20229143

PREFACE

Introduction

This PhD thesis was submitted in chapter format. However, the chapter contents were approached a bit differently than the conventional style, which usually entails separate chapters for literature and experimental/methods. The candidate chose to rather group literature, experimental/methods, as well as results and discussions associated with specific themes together in chapters. A thorough description and mind map that outlines the entire dissertation are presented in Chapter 1.

Formatting and current status of articles

According to the rules of the North-West University, a PhD candidate should submit at least one article to a reputable journal before the PhD dissertation is submitted for examination. It is therefore relevant to report on the current status of articles originating from this dissertation.

The contents of Chapter 2 were prepared and submitted to an ISI-accredited journal, i.e. Journal of Atmospheric Chemistry, which is a Springer Journal.

The contents of Chapters 3 and 4 are being prepared for submission to an ISI-accredited journal, i.e. Atmospheric Chemistry and Physics (European Geosciences Union), or Atmospheric Environment (Elsevier).

Declaration regarding co-authors

All the co-authors of the above-mentioned submitted article, compiled from Chapter 2, had the opportunity to comment thereon. All co-authors will also be given the opportunity to comment on the article that will be compiled from Chapters 3 and 4.

ACKNOWLEDGEMENTS

Firstly, I would like to thank my Father in Heaven for giving me the ability, patience and strength to complete my study.

A special thanks to the following people:

- To my supervisors, Paul and Pieter - Thank you so much for your support, patience, encouragement and guidance during the years it took to complete my studies and for always being available to assist me. I appreciate everything you have done.
- To my parents, Marie and Pieter - Thanks for making it possible to receive a tertiary education and for inspiring me.
- To my best friend and husband, Didrich - Thanks for all the love and encouragement through this challenging time.
- Thanks to my brother, Pieter, and his wife, Anita, my friends (Kerneels, Tracey, Ralph, Faan, Andrew, Katrina, Suzelle, Bertus, Fébé, Jaco, Natascha, Pierre, Alta and Jan-Stefan) for their support.
- Thanks to Cecile van Zyl for assisting with the language editing.
- Financial assistance of the National Research Foundation (NRF) towards this research is hereby acknowledged. Opinions expressed and conclusions arrived at, are those of the author and are not necessarily to be attributed to the NRF.

Thank you
Petra

ABSTRACT

The impacts of atmospheric particulate matter (PM) are co-determined by chemical composition. PM with aerodynamic diameter ≤ 2.5 µm ($PM_{2.5}$) typically contains a significant fraction of organic- (OC), elemental carbon (EC), water-soluble inorganic ions and organic acids (OA), which can affect climate, air quality, human health, acid deposition and visibility. Exceedances of PM with aerodynamic diameter ≤ 10 µm (PM_{10}) associated standard limits are frequent in many regions in the South African interior (SAAQIS, 2018). However, very little data have been published regarding PM's chemical composition. This research presents a multi-year aerosol dataset for South Africa, as determined at two regional background sites (Skukuza and Louis Trichardt, i.e. SK and LT), and two sites that are more directly impacted by nearby industrial emissions (Vaal Triangle and Amersfoort, i.e. VT and AF) operated within the Deposition of Biogeochemical Important Trace Species (DEBITS) project.

24-hour $PM_{2.5}$ and PM_{10} aerosol samples were collected on quartz and Teflon filters, once a month from March 2009 to December 2015, at each of the four sites. The quartz filters were analysed on a Desert Research Institute (DRI) analyser 2001 Model and a Sunset OCEC Dual Optical Lab Instrument (Version 6.4) for OC and EC contents, while the Teflon filters were analysed with an ion chromatograph (IC) to obtain the water-soluble inorganic and OA contents.

Results indicated that the mass fractions of organic carbon (OC) and elemental carbon (EC) at all four sites were lower than what is typical within a developed world context; not due to lower concentrations, but due to the larger fractional contributions from especially sulphate (SO_4^{2-}). Open biomass burning was found to contribute to elevated OC and EC levels on a regional scale. However, household combustion for space heating in semi- and informal settlements made a substantial local (e.g. at VT) and noticeable regional (e.g. at AF and SK) OC and EC contribution. Additionally, industrial and/or vehicle emissions contribute to the baseline OC and EC levels year-round, while oxidation of volatile organic compounds (VOCs) during the wet season will also contribute to OC levels.

The highest concentration of water-soluble ions was reported for the $PM_{2.5}$ size fraction, and in this size fraction SO_4^{2-} had the highest concentrations, followed by OA. Spatial assessment showed that the VT had the highest SO_4^{2-} and NH_4^+ concentrations, followed by AF, SK and LT, while the NO_3^- concentrations were the highest at VT, followed by SK, AF and LT. NH_4^+ was found to be the most probable cation to neutralise the acidic ions in the $PM_{2.5}$ size fraction at all the sites. Back trajectories, diagonal correlation graphs, principal component analysis (PCA), calculations of sea-salt fractions (SSFs) and non-sea-salt fractions (nSSFs), as well as other empirical calculations were used to determine possible source contributions from marine, terrigenous, fossil fuel use, biomass burning, NH_4^+-associated and OA-associated sources. At

all sites in the $PM_{2.5}$ size fraction, fossil fuel use, NH_4^+-associated and terrigenous sources contributed most to the water-soluble ion and OA content. However, the fractional marine influence at SK and LT were higher than at the other sites. Aerosol mass closure indicated that organic matter (OM), derived from the OC mass, was the most significant contribution to the $PM_{2.5}$ aerosol mass percentage at all sites, with SO_4^{2-} making the second largest contribution at all sites.

Keywords: Aerosol, Deposition of Biogeochemical Important Trace Species (DEBITS), International Network to study Deposition and Atmospheric chemistry in Africa (INDAAF), organic carbon (OC), elemental carbon (EC), water-soluble inorganic ions, organic acids, chemical composition, mass closure

LIST OF ABBREVIATIONS

amsl:	above mean sea level
PBL:	planetary boundary layer
VT:	Vaal Triangle
AF:	Amersfoort
SK:	Skukuza
LT:	Louis Trichardt
BVOCs:	biogenic volatile organic compounds
BC:	black carbon
eBC:	equivalent black carbon
EC:	elemental carbon
OC:	organic carbon
TC:	total carbon
PM:	particulate matter
VOC:	volatile organic compound
AERS:	Anion Electrolytically Regenerated Suppressor
ARL:	Air Resources Laboratory
ACSM:	Aerosol Chemical Speciation Monitor
CERS:	Cation Electrolytically Regenerated Suppressor
CCN:	cloud condensation nuclei
DEBITS:	Deposition of Biogeochemical Important Trace Species
DLs:	detection limits
DMPS:	differential mobility particle sizer
DRI:	Dessert Research Institute
ENSO:	El Niño Southern Oscillation
FTIR:	Fourier transform infrared
GC-MS:	gas chromatograph mass spectrometry
HULIS:	humic-like substances
HNMR:	proton nuclear magnetic resonance
HYSPLIT:	Hybrid Single-Particle Lagrangian Integrated Trajectory
IMPROVE:	Interagency Monitoring of Protected Visual Environments
NIOSH:	National Institute of Occupational Safety and Health
IC:	ion chromatograph
IN:	ice nuclei
INDAAF:	International Network to study Deposition and Atmospheric chemistry in Africa
IGAC:	International Global Atmospheric Chemistry

NCEP:	National Centre for Environmental Prediction
OA:	organic acids
POC:	primary organic carbon
RSD:	relative standard deviation
SOC:	secondary organic carbon
SOA:	secondary organic aerosol
WSOC:	water-soluble organic carbon
WISOC:	water-insoluble organic carbon
WMO:	World Meteorological Organisation
US-EPA:	United States Environmental Protection Agency
USA:	United States of America
µg/L:	microgram per litre
ppb:	parts per billion
µEq/L:	micro-equivalents per litre
M:	molar mass
Eq.wt:	equivalent weight
AE:	anionic contribution
CE:	cationic contribution
ID%:	ion difference percentage
NF:	neutralisation factor
SSF:	sea-salt fraction
nSSF:	non-sea-salt fraction
EF:	enrichment factor
PCA:	principal component analysis
KOH:	potassium hydroxide
MSA:	methanesulphonic acid
NH_4NO_3:	ammonium nitrate
$Ca(NO_3)_2$:	calcium nitrate
$CaSO_4$:	calcium sulphate
$Mg(NO_3)_2$:	magnesium nitrate
$MgSO_4$:	magnesium sulphate
$NaNO_3$:	sodium nitrate
HCl:	hydrogen chloride
H_2SO_4:	sulfuric acid
S:	sulphur
N:	nitrogen
F^-:	fluoride
Na^+:	sodium

K^+:	potassium
Mg^{2+}:	magnesium
Ca^{2+}:	calcium
$(COOH)_2$:	oxalic acid
CH_3COOH:	acetic acid
CHOOH:	formic acid
C_2H_5COOH:	propionic acid
NH_3:	ammonia
N_2:	dinitrogen
N_2O:	nitrous oxide
NH_4HSO_4:	ammonium sulphate
$(NH_4)_2SO_4$:	ammonium bisulphate
NH_4NO_3:	ammonium nitrate
NaClO:	sodium hypochlorite
$CaCl_2O_2$:	calcium hypochlorite
$C_3Cl_3N_3O_3$:	trichloro-S-triazinetrione
NaCl:	sodium chloride
NO_2:	nitrogen dioxide
H_2S:	hydrogen sulphide
Cl^-:	chloride
KCl:	potassium chloride
Na_3AlF_6:	tri-sodium hexafluoro-aluminate or cryolite
$CaCO_3$:	calcite
$CaMg(CO_3)_2$:	dolomite
$CH_2(COOH)_2$:	malonic acid
$(CH_2)_2(CO_2H)_2$:	succinic acid
SO_2:	sulphur dioxide
CO_2:	carbon dioxide
SO_4^{2-}:	sulphate
NO_3^-:	nitrate
NH_4^+:	ammonium

TABLE OF CONTENTS

LIST OF TABLES

LIST OF FIGURES

CHAPTER 1

BACKGROUND, MOTIVATION, OBJECTIVES AND APPROACH

In this chapter… *the background and motivation are presented in section 1.1, the objectives in section 1.2, and approach in section 1.3.*

1.1 Background and motivation

The impacts of atmospheric aerosols on climate and general air quality are determined by their physical (e.g. size, mass, structure, and optical properties) and chemical properties (chemical composition) (Seinfeld and Pandis, 2016). Typical chemical species present in atmospheric aerosols include alumina-silicates (e.g. from wind-blown dust), black carbon (BC) or elemental carbon (EC) (depending on analytical technique applied, with definitions according to Petzold et al., 2013), organic carbon (OC), sulphates (SO_4^{2-}), nitrates (NO_3^-), ammonium (NH_4^+) and trace metal species. Aerosols are generally classified according to their size, e.g. PM_{10} (aerodynamic diameter ≤ 10 µm), $PM_{2.5}$ (aerodynamic diameter ≤ 2.5 µm), PM_1 (aerodynamic diameter ≤ 1 µm), and $PM_{0.1}$ (aerodynamic diameter ≤ 0.1 µm) (Slanina and Zhang, 2004). General detrimental effects of atmospheric aerosol pollution on human health include increased cardiopulmonary and respiratory diseases (Gauderman et al., 2004), while $PM_{0.1}$ can diffuse through the membranes of the respiratory track into the blood stream (Oberdorster et al., 2004). Major environmental impacts of atmospheric aerosol pollution include acid deposition and eutrophication (Lazaridis et al., 2002). The baseline of uncertainty associated with aerosol radiative forcing is large, and depends on the afore-mentioned aerosol characteristics, which can vary significantly on a regional and global scale (Slanina and Zhang, 2004; IPCC, 2013).

Atmospheric BC (or EC, depending on analytical technique applied) is emitted as a primary species, while OC can consist of primary and secondary aerosols (Putaud et al., 2004). Major sources of OC and BC include incomplete combustion of fossil fuels, biomass burning and traffic emissions. OC can be formed through the oxidation of volatile organic compounds (VOCs) from both anthropogenic and biogenic sources. BC absorbs terrestrial long-wave radiation that has a warming effect on the atmosphere, while OC, depending on its chemical properties, could absorb or reflect incoming solar radiation (Bond et al., 2013; Laskin et al., 2015). It is generally accepted that OC has a net cooling effect (Ramanathan and Feng, 2009;

Bond et al., 2013; Caserini et al., 2013; IPCC, 2013). BC is considered to be the second most important contributor to global warming, after carbon dioxide (CO_2) (Bond and Sun, 2005; IPCC, 2013). Aerosol SO_4^{2-} and NO_3^- are formed through the oxidation of sulphur and nitrogen oxides (which include cloud processing), respectively, which are gas species that can cause health problems. SO_4^{2-} and NO_3^- are two of the most important species in aerosol and wet deposition (Vet et al., 2014). The deposition of inorganic compounds can be beneficial (e.g. nutrients) or detrimental (e.g. eutrophication) to the environment (Charlson et al., 1992). Particulate SO_4^{2-} and NO_3^- enhance the reflectivity of atmospheric aerosols, which has a cooling effect (IPCC, 2013). Sulphur and nitrogen oxides are generally emitted from fossil fuel combustion processes (Graedel and Crutzen, 1995; Van Loon and Duffy, 2005; Lourens et al., 2011). NH_4^+, derived from ammonia (NH_3) emissions, is usually associated with agricultural activities and some industrial processes (Brasseur et al., 1999; Van Loon and Duffy, 2005; Seinfeld and Pandis, 2016).

Although Africa is regarded as one of the largest source regions of anthropogenic atmospheric OC and BC (Liousse et al., 1996; Kanakidou et al., 2005), it is one of the least studied continents. Within Africa, southern Africa is an important source region. Biomass burning (anthropogenic and natural) is endemic across this region (Swap et al., 2003), especially during the dry season when almost no precipitation occurs in the interior (Laakso et al., 2012). South Africa is the economic and industrial hub of southern Africa, with large anthropogenic point sources (Lourens et al., 2011; Pretorius et al., 2015), which lead to elevated levels of atmospheric SO_4^{2-} and NO_3^- (Dhammapala, 1996; Martins, 2009; Engelbrecht, 2009). Agricultural cultivation activities, during which fertilisers are added that can contribute to elevated levels of aerosol NH_4^+, are widely practised in South Africa (DAFF, 2016). Conradie et al. (2016) also indicated significant influences from terrigenous and marine sources on ionic species in rain water in South Africa.

Notwithstanding the elevated levels of aerosol OC and BC, as well as various inorganic ionic species in the ambient atmosphere of the South African interior, and the importance of these species within human health, environmental and climate perspectives, relatively limited papers related to such topics have been published in the peer-reviewed public domain. Reviews of such literature related to OC and BC, as well as water-soluble inorganic ions and organic acids, are presented in sections 2.1 and 3.1, respectively. From these reviews, it is evident that no long-term OC and BC data have been published for South African regional background sites, with very limited publications considering water-soluble inorganic ions and organic acids. Chiloane et al. (2017) presented some PM_{10} OC and EC concentration data for a limited number of regional background sites. However, these authors only used the data to give regional context to an industrially impacted site that was considered in greater detail. Aurela et al. (2016)

presented PM_{10}, $PM_{2.5}$ and PM_1 OC and EC, as well as water-soluble inorganic ions and organic acid concentrations, determined from a very limited number of aerosol samples for a single regional background site. Tiitta et al. (2014) presented relatively detailed descriptions of eBC, organic aerosol, SO_4^{2-}, NO_3^- and NH_4^+ contents only for PM_1 measured at a regional background site sampled over a one-year period. Venter et al. (2018a) recently published water-soluble ionic contents for a regional background site, as well as an industrial and household combustion influenced site, but did not quantify OC and EC/BC.

1.2 Objectives

The general aims of this study were to conduct a long-term assessment of the OC and EC, as well as water-soluble chemical compositions of aerosols in the South African interior. The specific objectives of this study were as indicated below.

1. Perform long-term assessment of OC and EC aerosol concentrations in the South African interior. This assessment should include evaluating spatial and temporal patterns, mass fractions of the total aerosol mass and possible source contributions.
2. Conduct similar (to Objective 1) assessment of aerosol water-soluble inorganic ions and organic acids at the same sampling sites.

1.3 Approach

In order to meet the objectives, it was decided to deal with each objective in a separate chapter, i.e. Chapter 2 for Objective 1 and Chapter 3 for Objective 2. This is a somewhat unorthodox approach, since there are not separate literature and experimental/method chapters in this thesis. However, this approach allowed the candidate to present literature and experimental aspects that were focused on each of the objectives, instead of, for instance, presenting a separate literature survey that is very broad. In Chapter 4, mass closure of the overall aerosol mass, including species considered in Chapters 2 and 3, will be considered. Therefore, Chapter 4 is linked to both Objective 1 and 2. In the final chapter, i.e. Chapter 5, the main conclusions of the three separate chapters were summarised, the project was evaluated in terms of the objectives and future perspectives presented. A simple mind map of the entire thesis is presented in Figure 1-1.

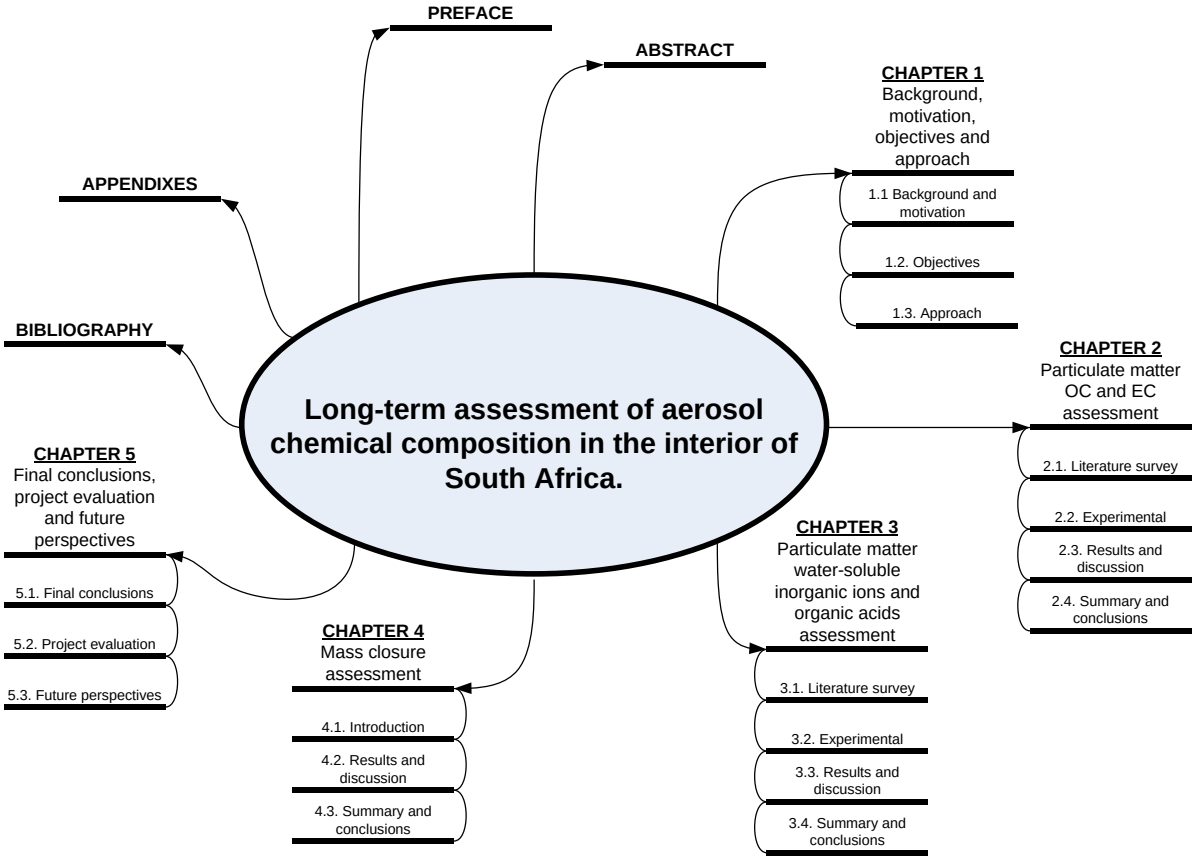

Figure 1-1: Mind map of entire thesis

CHAPTER 2

PARTICULATE MATTER OC AND EC ASSESSMENT

In this chapter… *Literature relevant to organic- (OC) and elemental carbon (EC) is presented in section 2.1. In section 2.2, experimental aspects, including sampling sites (section 2.2.1), sampling methods (section 2.2.2), analyses (sections 2.2.3), air mass histories (section 2.2.4), and fire locations (section 2.2.5) are discussed. Results and discussions are presented in section 2.3, which includes the spatial- (section 2.3.1), temporal assessment (section 2.3.2) and source insights (section 2.3.3). Section 2.4 summarises the conclusions from this chapter. This chapter is linked to Objective 1, as stated in section 1.3.*

2.1 Literature survey

2.1.1 Impact of aerosols

As indicated in Chapter 1, atmospheric aerosols are of great interest to the scientific community, because they directly and indirectly affect global and regional climate (Jen and Wu, 2008; Ramanathan and Feng, 2009; Laakso et al., 2010 and references therein; IPCC, 2013; Seinfeld and Pandis, 2016), general air quality (Venter et al., 2012; Butt et al., 2015), human health (Gauderman et al., 2004; Huttunen et al., 2012; Butt et al., 2015; Siponen et al., 2015), acid deposition and/or eutrophication (Lazaridis et al., 2002; Pöschl, 2005; Seinfeld and Pandis, 2016), and visibility (Fourie, 2006; Zhao et al., 2013; Seinfeld and Pandis, 2016; Yu et al., 2016; Mukherjee and Agrawal, 2017). Atmospheric aerosols directly influence climate by scattering and absorbing solar radiation, and indirectly influence climate by causing an indirect radiative effect when aerosol particles act as cloud condensation nuclei (CCN) and ice nuclei (IN), which modulates cloud properties (IPCC, 2013; Seinfeld and Pandis, 2016; Gunsch et al., 2018). The fine particulate matter (e.g. typically $PM_{2.5}$) is mostly responsible for the adverse health effects caused in humans (e.g. cardiovascular- and pulmonary diseases) (Pope III and Dockery, 2006). Visibility is reduced by particulate matter that scatters and absorbs sunlight (Seinfeld and Pandis, 2016). The influences of aerosols (including the radiative forcing characteristics) and their atmospheric lifetime (which can be in the range of hours to weeks) are determined by their physical and chemical properties (e.g. size, mass, structure, chemical composition, concentration of compounds and optical properties), which can differ on global and regional scales (Charlson et al., 1992; Slanina and Zhang, 2004; IPCC, 2013; Seinfeld and Pandis,

2016). Obviously, aerosol lifetime is also much longer in free troposphere or stratosphere than in the planetary boundary layer (PBL).

2.1.2 Size classification and chemical composition of aerosols

Aerosols/particulate matter (PM) can be classified according to their size, e.g. PM_{10} (i.e. aerodynamic diameter ≤ 10 µm), $PM_{2.5}$ (i.e. aerodynamic diameter ≤ 2.5 µm), PM_1 (i.e. aerodynamic diameter ≤ 1 µm) and $PM_{0.1}$ (i.e. aerodynamic diameter ≤ 0.1 µm) (Slanina and Zhang, 2004; Pöschl, 2005). $PM_{2.5}$ particles typically consist of sulphates (SO_4^{2-}), nitrates (NO_3^-), strong acids, ammonium (NH_4^+), trace metal species, water (Pfeiffer, 2005; Hsu et al., 2017), carbonaceous species (i.e. OC, black carbon (BC) or EC, depending on the analytical technique applied, according to Petzold et al., 2013). PM_{10} would also include a significant aeolian dust fraction (Tyson and Preston-Whyte, 2000; Pfeiffer, 2005). Aerosol BC is considered to be the second most important species contributing to global warming, after carbon dioxide (CO_2) (Bond and Sun, 2005; IPCC, 2013). Although it is compound specific, incoming solar radiation is largely reflected by OC compounds, which cause a cooling effect on the atmosphere (Ramanathan and Feng, 2009; Bond et al., 2013; Caserini et al., 2013; IPCC, 2013).

2.1.3 OC and EC sources

Primary aerosols are defined as being directly emitted from sources into the atmosphere and secondary aerosols are formed through gas-to-particle conversion processes in the atmosphere. BC and/or EC aerosols are emitted as primary atmospheric species, while OC can be emitted as primary (POC) species from both natural and anthropogenic sources or secondary OC (SOC) can form in the atmosphere (Putaud et al., 2004; Szidat et al., 2009). Atmospheric aging processes (i.e. heterogeneous reactions and gas-to-particle partitioning) could result in the chemical composition changing over time (Moffet and Prather, 2009; Riemer and West, 2013). For instance, the oxidation of volatile organic compounds (VOCs) from biogenic and/or anthropogenic sources can lead to SOC. The primary sources of OC and BC or EC include incomplete combustion of fossil fuels (e.g. coal and oil), open biomass burning, traffic emissions and household combustion (e.g. for space heating and cooking) (Pöschl, 2005; Fourie, 2006; Bond et al., 2013; Seinfeld and Pandis, 2016).

2.1.4 Classification and terminology

OC was defined by Shah and Rau (1990) (according to Petzold et al., 2013) as many compounds that consist of carbon, which are chemically combined with hydrogen and/or elements such as oxygen, sulphur, nitrogen, phosphorous and chloride. The chemical composition of OC is very complex and therefore single component identification is relatively difficult, although not impossible. Broadly, OC can be divided into two subcategories, i.e. water-soluble OC (WSOC) and water-insoluble OC (WISOC) (Zappoli et al., 1999; Sullivan and

Weber, 2006). WSOC consists of oxygenated compounds such as di- and polycarboxylic acids, fatty acids, as well as carbohydrates and their derivatives, while WISOC consists of alkanes, alkanals, alkanons, waxes, proteins, plant fragments and bio-aerosols (i.e. small living organisms) (Pöschl, 2005; Szidat et al., 2009). Both of the afore-mentioned OC sub-categories impact the atmosphere (Facchini et al., 1999). WSOC has hygroscopic properties that act effectively as CCN and thereby affect climate by increasing the amount and lifetime of clouds (Wozniak et al., 2012). According to Decesari et al. (2000), WSOC can be divided into three main groups (i.e. neutral compounds, mono-/dicarboxylic acids and polyacids) by using acid/base characteristics. Kiss et al. (2002) and Mayol-Bracero et al. (2002) refer to polyacidic compounds as HULIS (i.e. humic-like substances). HULIS can be of either primary or secondary origin (Sullivan and Weber, 2006). Furthermore, hydrophilic WSOC consists of highly oxygenated compounds that have low molecular weights (e.g. aliphatic carboxylic acids, carbonyls, saccharides and amines), whereas hydrophobic WISOC consists of compounds with higher molecular weights (e.g. aliphatic carboxylic acids and carbonyls, aromatic acids, phenols, organic nitrates, cyclic acids and fulvic acids) (Bae and Park, 2013). Generally, WSOC is taken up easier by biological systems (e.g. human blood and lungs) than WISOC, which contributes to the adverse human health effects of WSOC mentioned earlier (Swanson et al., 2007; Mills et al., 2008a). Categorisations of OC can also be done based on functional groups, as is common in organic chemistry, through the use of analytical techniques such as Fourier transform infrared (FTIR) spectroscopy, proton nuclear magnetic resonance (HNMR) spectroscopy or gas chromatography followed by mass spectrometry (GC-MS) (Liu et al., 2012; Matsumoto et al., 2014). All the afore-mentioned OC classifications, along with their volatility characteristics, can assist scientists in understanding the chemical properties, formation mechanisms, sources and impacts of atmospheric OC better (Yu et al., 2004a; Matsumoto et al., 2014). The volatility of OC reflects the molecular weights of the compounds that make up the OC (Miyazaki et al., 2007). Huffman et al. (2009) reported that SOC particles had similar volatilities, which were lower than that of other organic particles, however, Ehn et al. (2014) stated that the volatility of secondary organic aerosol (SOA) ranges from extremely low to semi-volatile.

Goldberg (1985) generally defined BC as a substance that was produced through incomplete combustion of fossil fuels and biomass burning (Petzold et al., 2013). Bond et al. (2013) describe BC as a strong absorbent of visible light, it is refractory, it has a volatising temperature close to 4000K, it is insoluble in water and organic solvents (e.g. methanol and acetone), and it consists of small carbon spherules with a diameter that could range from <10nm up to 50nm. According to Petzold et al. (2013), the recommended definition of BC is that it is a light-absorbing atmospheric aerosol carbonaceous substance, but different measurement techniques are required for a more quantitative description. Therefore, equivalent BC (eBC) refers to BC

data acquired with an optical absorption method, with mathematical conversion required to transform the light absorption coefficient to mass concentration (Petzold et al., 2013). Shah and Rau (1990) defined EC as an only carbon consisting substance, meaning that it is not bound to any other elements and can exist in a crystalline or amorphous structure (Petzold et al., 2013). Petzold et al. (2013) recommended that the term EC, instead of eBC, be used for data that are specific to carbon content of carbonaceous matter and analysed by a thermal-optical method.

In the current study, EC was measured, not BC or eBC. However, as is evident from the above-mentioned discussions, the terms are not the same. Therefore, in subsequent discussions, the terms EC, BC and eBC are used according to the definitions recommended by Petzold et al. (2013).

2.1.5 OC and EC in southern and South Africa

Africa is considered as one of the largest source regions of anthropogenic OC and BC (Liousse et al., 1996; Kanakidou et al., 2005). Within Africa, southern Africa is a major sub-source region. Open biomass burning (anthropogenic and natural), which emits significant amounts of carbonaceous aerosols, is widespread across southern Africa during the dry season (Formenti et al., 2003; Swap et al., 2004; Tummon et al., 2010; Laakso et al., 2012; Vakkari et al., 2014). Open biomass burning plumes from southern Africa occasionally impact Australia and South America (Swap et al., 2004). Emissions from such fires in southern Africa, as well as transportation across the continent, have been studied through campaigns of the Southern African Fire Atmospheric Research Initiative (i.e. SAFARI-92 and SAFARI-2000). In addition to open biomass burning, South Africa is the industrial and economic centre of southern Africa, with numerous large anthropogenic point sources that could potentially emit carbonaceous aerosols. These include an array of very large coal-fired power stations (Mphepya et al., 2004; Collett et al., 2010; Lourens et al., 2011; Beukes et al., 2013a; Pretorius et al., 2015; Chiloane et al., 2017; Venter et al., 2017), large petrochemical operations that apply coal pyrolysis processes (Lourens et al., 2011; Chiloane et al., 2017) and many pyro-metallurgical smelters (e.g. base metals, ferroalloys, steel) that use carbonaceous reducing agents such as anthracite, char and coke (Barcza, 1995; Roos, 2011; Kleynhans et al., 2016). Almost none of these industries do de-SO_x (i.e. removal of sulphur) or de-NO_x (i.e. removal of nitrogen) their process off-gas. A significant portion of South Africa's population also lives in semi- or informal settlements, where people are still to a large degree reliant on ineffective household combustion using relatively low grade coal and/or wood for cooking and space heating (Venter et al., 2012; Van Zyl et al., 2014; Giannakaki et al., 2016). Due to the mixed first- and third-world nature of the South African economy, the vehicular fleet is also relatively aged when compared with first-

world countries (Lourens et al., 2012; Lourens et al., 2016). Therefore, significant carbonaceous aerosol emissions can also be expected from this sector (Cao et al., 2004; Venter et al., 2012).

Notwithstanding the occurrence of numerous potential areas and point sources of OC and BC (or EC) in South Africa, very little ambient OC and BC (or EC) data have been published for this region in the peer-reviewed public domain. Formenti et al. (2003) reported OC and EC for a limited number of filters sampled during SAFARI 2000 on board an aircraft during September 2000 in a smoke haze layer over the Atlantic Ocean, offshore from Namibia and Angola. Collett et al. (2010) presented an hourly average diurnal plot for eBC measured at the Elandsfontein monitoring station in the industrialised Highveld from April 2005 to March 2006. Hirsikko et al. (2012) and Venter et al. (2012) used eBC data collected at Marikana (station in close proximity to semi- and informal settlements, and pyro-metallurgical smelters) in 2008 to 2009 in order to explain other observations without considering eBC in detail, while Laakso et al. (2012) did the same for eBC data collected at Elandsfontein (station in industrialised Highveld) from 2009 to 2011. eBC mass concentration data gathered at Welgegund (a background site) were used by Hyvärinen et al. (2013) to explain a new method, which entailed correcting eBC concentrations measured with a multi-angle absorption photometer (MAAP). Tiitta et al. (2014) used the same data to explore the chemical composition of PM_1 aerosols, which included eBC and organic aerosols. In Kuik et al. (2015), the weather research and forecasting model, which included chemistry and aerosols (WRF-Chem), was used to model anthropogenic emission contributions to total eBC mass concentrations for four months in 2010. These authors found considerable meteorology modelling underestimations and uncertainties, i.e. changes in wind direction and the early beginning of the rainy season, which could have increased the wet deposition. Size resolved (i.e. PM_1, $PM_{1-2.5}$ and $PM_{2.5-10}$) categorisation of organic compounds in aerosols, according to organic functional groups, collected over a year sampling period at Welgegund, revealed that the organic composition of aerosols in South Africa is complex (Booyens et al., 2015). Feig et al. (2015) presented an initial analysis of eBC concentration data measured at eight monitoring stations in the Vaal Triangle and Highveld Priority areas, which included the seasonality, influence of meteorological conditions and the relationship with PM_{10} and $PM_{2.5}$ concentrations. Aurela et al. (2016) presented very limited OC and EC mass concentration data derived from samples collected over 14 days during 2007 and 2008 at a regional background site (Botsalano). Recently, Chiloane et al. (2017) presented eBC spatial and temporal (diurnal and seasonal) assessments for various sites, as well as source contributions for a single sampling site in the industrial Highveld. No spatial (e.g. covering several sites) and seasonal data have been presented for OC.

2.1.6 Literature conclusions

Specifically considering the OC and BC (or EC)-related literature published in the peer-reviewed public domain (section 2.1.5) indicates the lack of long-term ambient OC and EC data for South African regional background sites. Although some eBC work has been done for southern Africa, year-round data for OC and OC/EC ratio is absent. The data set in this study is the only one providing OC/EC ratio values and enables studying inter-annual variability in OC and OC/EC values. Objective 1 was therefore correctly formulated and if the goals set out in this objective are achieved, a significant contribution to science can be made by this study.

2.2 Experimental

2.2.1 Sampling sites

Aerosol $PM_{2.5}$ and PM_{10} samples were collected at four different sampling sites in the northern interior of South Africa, operated within the Deposition of Biogeochemical Important Trace Species (DEBITS), International Network to study Deposition and Atmospheric chemistry in Africa (INDAAF) project (Galy-Lacaux et al., 2003; Martins et al., 2007), which is endorsed by the International Global Atmospheric Chemistry (IGAC) programme and the World Meteorological Organisation (WMO). These four INDAAF sites were Vaal Triangle (VT), Amersfoort (AF), Skukuza (SK) and Louis Trichardt (LT). The locations of these sites within a regional southern African context are presented in Figure 2-1. Mphepya et al. (2004) previously introduced the sites AF and LT, while Mphepya et al. (2006) introduced SK and Conradie et al. (2016) previously introduced all these sites (i.e. VT, AF, SK and LT); therefore, only brief site descriptions are presented in Table 2-1. Figures 2-1a to 2-1d present Google Earth images of the areas surrounding these four measurement sites, which corresponds with the spatial extent of the small rectangles indicated on the zoomed-in map in Figure 2-1. The information presented in Figure 2-1 and Figure 2-2, as well as Table 2-1, will be contextualised with the results presented later.

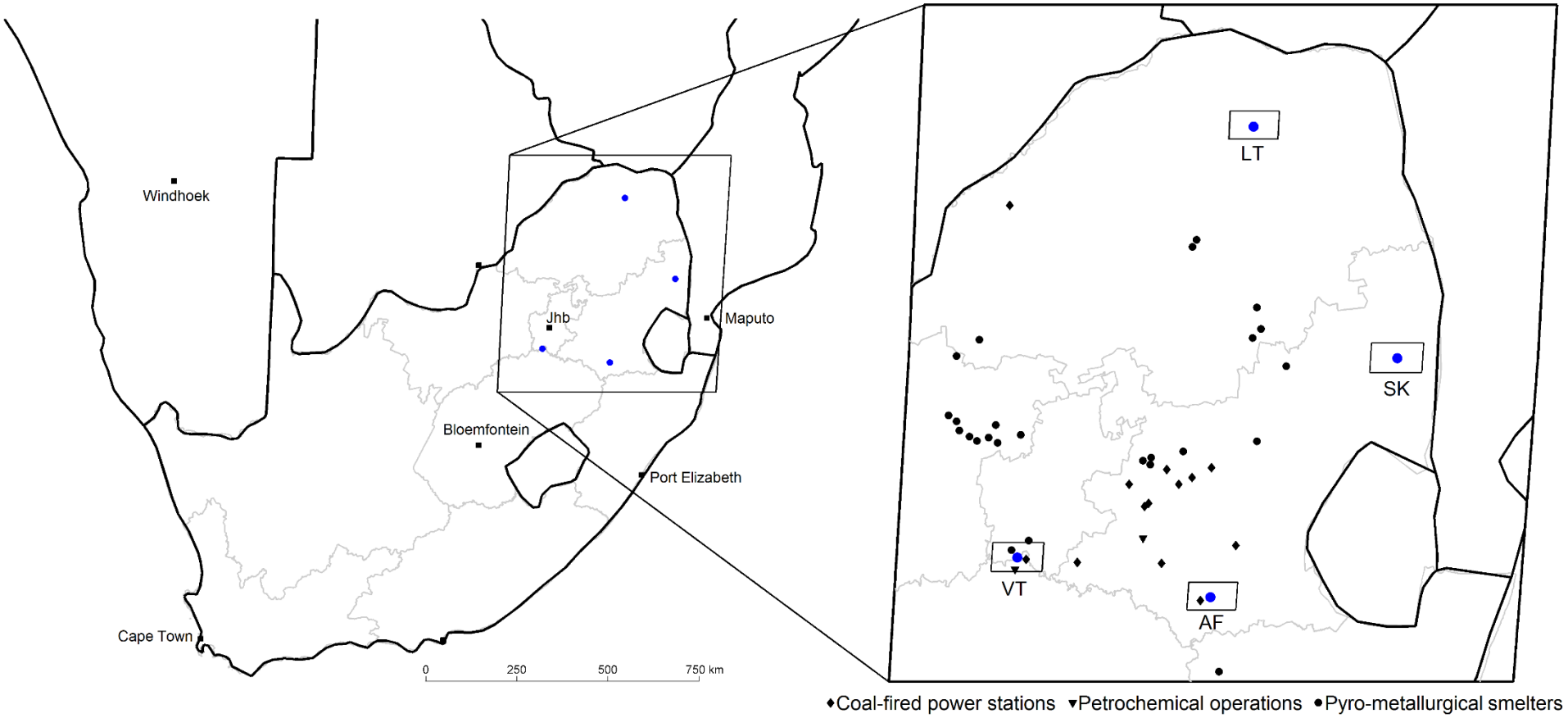

Figure 2-1: **Map of South Africa and zoomed-in area, indicating the location of the INDAAF sites, as well as provinces of South Africa and large point sources**

Table 2-1: Short description of the INDAAF sites in southern Africa

Name, location and elevation	Description
Vaal Triangle (VT) 26°43'29"S 27°53'05"E, 1320 m amsl	Located in a grassland biome. The Vaal Triangle area is highly industrialised. Air quality, which is affected by emissions from industries, traffic and household combustion, is a major concern. Therefore, the area has been proclaimed a national air pollution hotspot in terms of the South African National Environmental Management Act: Air Quality (Gazette, 2005).
Amersfoort (AF) 27˚04'13"S 29˚52'02"E, 1628 m amsl	Located in a grassland biome. The sites are situated on the perimeter of the internationally well-known NO_2 hotspot discernible from satellite observations over the Mpumalanga Highveld of South Africa (Lourens et al., 2012). Therefore, it can be expected that large point sources will affect air quality here. The area wherein the site is located has also been proclaimed a national air pollution hotspot in terms of the South African National Environmental Management Act: Air Quality (Gazette, 2005).
Skukuza (SK) 24˚59'35"S 31˚35'02"E, 267 m amsl	Located in the savannah biome. It should be regarded as a regional background site, situated in one of the largest protected areas, i.e. Kruger National Park, in the world.
Louis Trichardt (LT) 22˚59'10"S 30˚01'21"E, 1300 m amsl	Located in the savannah biome. It should be regarded as a regional background site, where the surroundings are predominantly used for agricultural purposes.

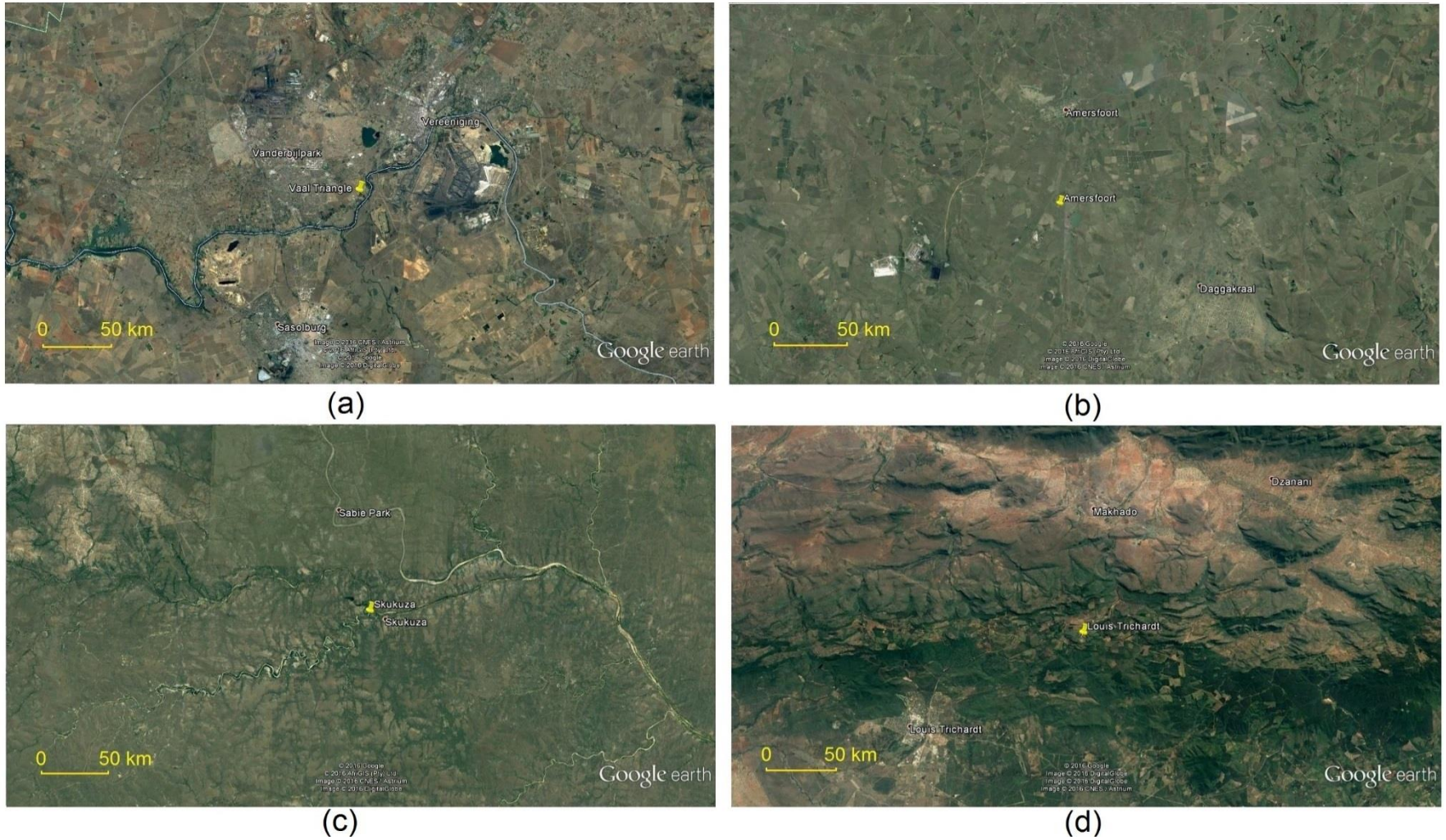

Figure 2-2: Google Earth images of the immediate areas surrounding the four INDAAF sites, i.e. VT (a), AF (b), SK (c) and LT (d), which correspond with the small rectangles indicated on the zoomed-in map in Figure 2-1

Picture 2-1: Instruments deployed at SK (photo courtesy of Carin van der Merwe).

Laakso et al. (2012) briefly discussed the meteorology of the South African Highveld and the interaction between meteorological patterns and pollutant levels. According to Lourens et al. (2012), and Laakso et al. (2012), the Highveld is internationally considered as an NO_2 emission hotspot and significant amounts of CO_2, SO_2 are also emitted there. Additionally, high SO_4^{2-} and NO_3^- loads occur in the area (Josipovic et al., 2010; Conradie et al., 2016). Industrial emissions, other emissions (e.g. household combustion, biogenic) and solar radiation result in a very reactive pollution mix, which can build up due to a dominant anti-cyclonic recirculation pattern (Tyson and Preston-Whyte, 2000). This occurs as a result of a dominant continental high pressure cell over South Africa's interior, especially from June to middle October. Additionally, pollutants are trapped by low-level inversion layers, which increase the ambient concentrations thereof (Tyson and Preston-Whyte, 2000). These inversion layers are strong during the evening and early mornings, but break up in the presence of sunlight heating. Korhonen et al. (2014) reported that the PBL over the Highveld starts to grow three to four hours after sunrise, coinciding with the breakup of the afore-mentioned inversion layers. However, the high-powered lidar used by Korhonen et al. (2014) could only detect aerosols above 400m and therefore could not observe some of the early morning PBL transition. Gierens et al. (2018) presented a method that is more suitable for studying the early morning development of the PBL, by using ceilometer data. Most of the precipitation occurs from middle October to April, which promotes pollutant washout, while

almost no precipitation occurs from May to middle October, which further enhances pollutant build-up.

2.2.2 Sampling methods

24-hour $PM_{2.5}$ and PM_{10} aerosol samples were collected on quartz filters with a deposit area of 12.56 cm^2, once a month from March 2009 to December 2015 at each of the four sites. This collection strategy was used, since it was the only logistically feasible approach – it was impossible to conduct continuous measurements. A total of 656 samples were collected for both size fractions ($PM_{2.5}$ and PM_{10}) at all four sites, i.e. 164 samples for each site. A total of 328 blank samples were also collected, i.e. 82 for each site.

To prevent contamination, surgical gloves and tweezers were worn to handle the quartz filters. Before sampling, the quartz filters were baked at 900°C in a fit-for-purpose furnace (used solely for this application) for four hours. Thereafter, the filters were cooled in a desiccator. The prebaked filters were visually inspected for flaws. The accepted filters were weighed with a Mettler Toledo scale (XS1005 DualRange) that was calibrated and accredited by SANAS. Afterwards the filters were stored in airtight Petri dish holders (in a laboratory with relatively humidity less than 20.0%) until they were used for sampling. MiniVol samplers were used during sampling (Baldauf et al., 2001). These samplers were developed by the United States Environmental Protection Agency (US-EPA) and the Lane Regional Air Pollution Authority. Programmable timers with battery backups for power cuts, allowed samples to be collected at a constant flow of 5 L/min over the 24-hour sampling periods. Prior to sampling, sampler flow rate was verified with a handheld flow meter.

After sampling, the filters were again stored in Petri dish holders and additionally placed in plastic zip lock bags. These were then transported in a mobile refrigerator to the laboratory, where they were stored in a standard commercial refrigerator. 24 hours before analysis, the samples were removed from refrigeration and weighed with the Mettler Toledo scale just before analysis.

2.2.3 OC and EC analysis

Although EC cannot always be directly related to eBC (Watson et al., 2005), for South Africa it has been stipulated that EC can be used as a proxy for eBC (correlation coefficient r = 0.83 between eBC and EC) (Sehloho et al., 2017). This implies that EC mass concentrations determined by off-line sampling and laboratory analysis, as presented in this study, can be used to extend the limited spatial coverage of online eBC measurements.

Numerous methods can be used to analyse OC and EC samples collected on filters (Chow et al., 2001). The Interagency Monitoring of Protected Visual Environments (i.e. IMPROVE) thermal/optical (TOR) protocol instead of the National Institute of Occupational Safety and Health (i.e. NIOSH) protocol was used in this study. Although both protocols deliver the same amount of total carbon (TC), both also result in lower EC with the transmittance values, due to the optical pyrolysis adjustment being higher for transmittance than reflectance. This lower EC was more significant for very black filters, which could not detect blackening (due to pyrolysis) by reflectance or transmittance (Chow et al., 2001). In this study the appearance of the filters after sampling was light to dark brown, which would not influence EC values as much as black filters. Furthermore, the NIOSH protocol adds some of the EC measured, to the OC value during analyses, which is indicated by increased light transmission and reflectance at 850°C. This could be due to mineral oxides in the sample that supplies oxygen to carbon particles that is in close proximity, at this extremely high temperature. In contrast, the IMPROVE protocol separates the OC and EC more accurately during analyses (Chow et al., 2001), therefore, this protocol was the better choice for analysing samples on both instruments described below and also in order to attempt consistency for the analyses of samples (Chow et al., 1993; Chow et al., 2004; Environmental, 2008; Guillaume et al., 2008). Due to logistical reasons, samples collected in the period March 2009 to February 2015 were analysed on a Desert Research Institute (DRI) analyser 2001 Model at the Laboratoire d'Aérologie (France), while samples collected from March 2015 to December 2015 were analysed on a Sunset OCEC Dual Optical Lab Instrument (Version 6.4) at the North-West University (South Africa) (Birch and Cary, 1996; Birch, 1998). Both instruments have a detection limit of 0.2µg carbon/cm^2 (Chow et al., 1993; Turpin et al., 1990), with a relative standard deviation (RSD) of 5.0% (Chow et al., 1993; Birch and Cary, 1996). The exact procedures applied to these instruments were relatively recently presented by Maritz et al. (2015) and Chiloane et al. (2017), and are therefore not repeated here. The analysis in France was done by the candidate under the supervision of an experienced analyst of the DRI analyser, although the analysis in South Africa was also done by the candidate on a Sunset OCEC Dual Optical Lab Instrument, the analysts at Sunset Laboratory Inc. did assist where necessary.

To ensure that the results obtained from the two different analytical instruments were similar, 12 randomly selected samples from each measurement site were analysed by both instruments. The OC and EC mass concentrations obtained differed by less than 3.0%, which is better than the precision (how close repetitive analyses are to one another) of ≤5.0%, specified for these types of analytical instruments (Birch and Cary, 1996). Although a reference sample was not analysed to indicate the accuracy (how close to the true value) of

the methods applied, the notion that the results were also accurate was supported by the two independent methods applied at two independent laboratories having very similar results.

2.2.4 Air mass histories

Back trajectories of air masses were obtained using the Hybrid Single-Particle Lagrangian Integrated Trajectory (HYSPLIT 2014) model (version 4.8) (Draxler and Hess, 1997). Meteorological data from the GDAS archive (of the National Centre for Environmental Prediction (NCEP) of the United States National Weather Service), which is achieved by the Air Resources Laboratory (ARL) (ARL, 2014), were used. Trajectories were modelled for 96 hours backwards and arriving on the hour, at a height of 100 m above ground level. Therefore, for each 24-hour sample, 25 such back trajectories were calculated (one more than the sampling hour period, since both the trajectories at start and end hour were included). The maximum error margins reported for back trajectories calculated in this manner are 15.0 to 30.0% (Stohl, 1998; Riddle et al., 2006; Vakkari et al., 2011). Individually calculated hourly-arriving back trajectories were overlaid on a southern African map, divided into 0.2x0.2° grid cells. A colour code indicating the percentage of trajectories passing over each 0.2x0.2° grid cell was used, with red indicating the highest number of trajectory overpasses.

2.2.5 Fire locations

The MODIS collection 5 burned area product (Roy et al., 2008; MODIS, 2014) was used to determine fire locations.

2.3 Results and discussion

2.3.1 Spatial assessment and contextualisation of concentrations

In Figure 2-3, box and whisker plots of the $PM_{2.5}$ (a) and PM_{10} (b) OC and EC concentrations for the entire sampling period, for each measurement site, are presented together with median OC/EC ratios, as well as box and whisker plots of the $PM_{2.5}$ OC/EC ratios (c) for each site.

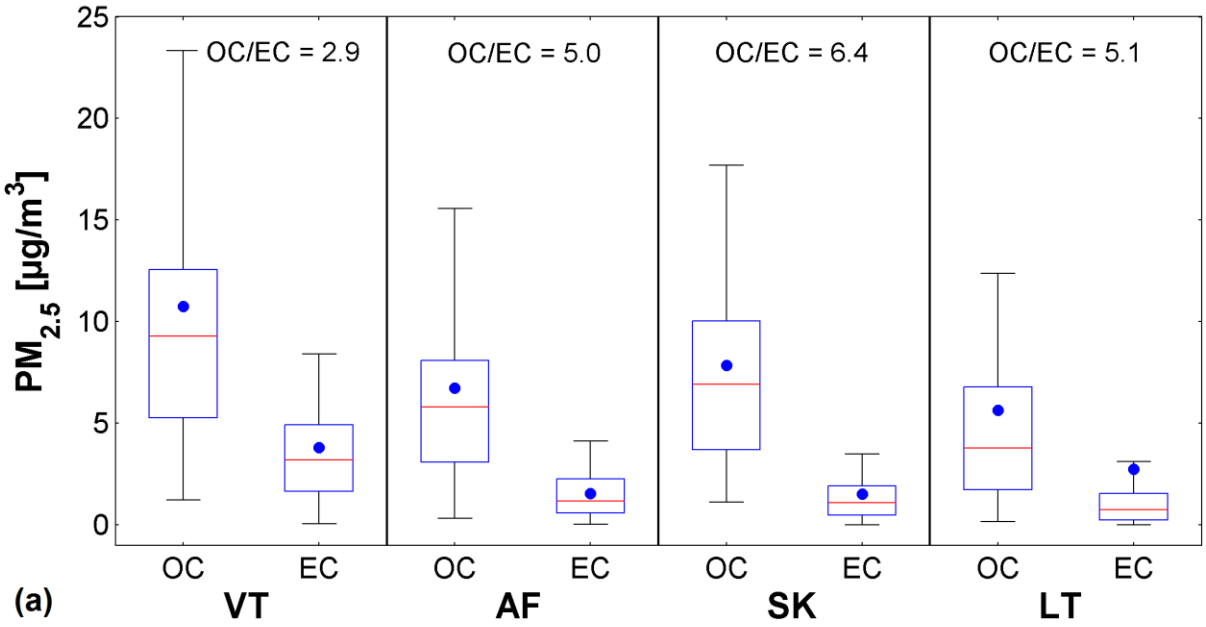

Figure 2-3: **$PM_{2.5}$ (a) and PM_{10} (b) OC and EC concentrations and OC/EC ratios (c) at the four INDAAF sites. The red line indicates the median, the blue dot the mean, the top and bottom edges of the box indicate the 25th and 75th percentiles and the whiskers the ±2.7 σ (99.3% coverage if the data have a normal distribution). Median OC/EC ratios are also indicated**

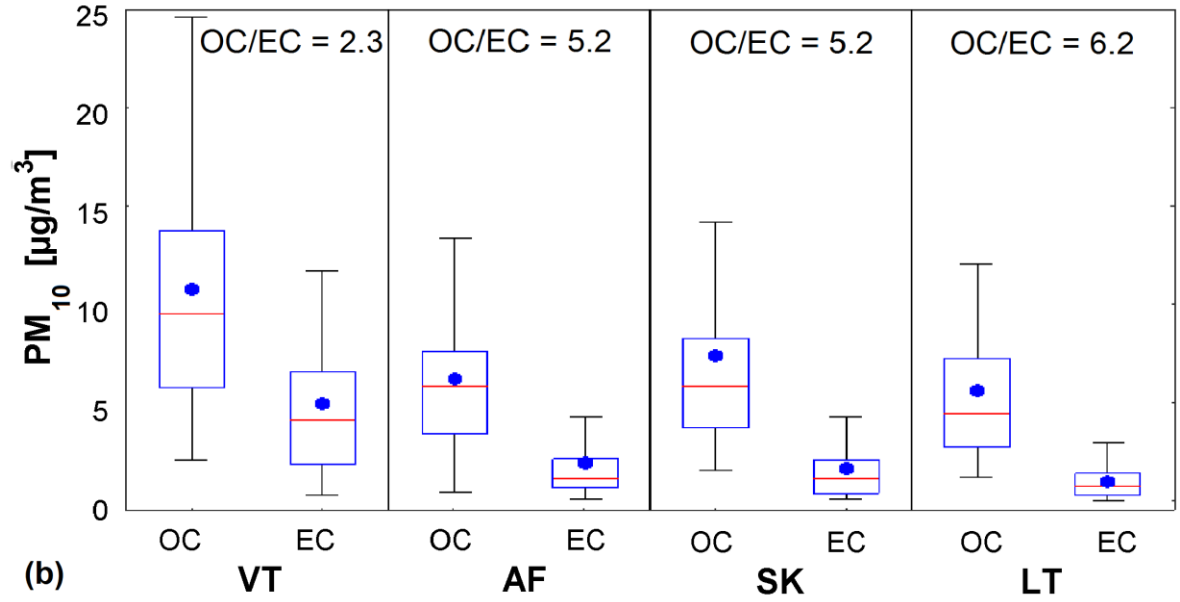

Figure 2-3 (continued): **$PM_{2.5}$ (a) and PM_{10} (b) OC and EC concentrations and OC/EC ratios (c) at the four INDAAF sites. The red line indicates the median, the blue dot the mean, the top and bottom edges of the box indicate the 25th and 75th percentiles and the whiskers the ±2.7 σ (99.3% coverage if the data have a normal distribution). Median OC/EC ratios are also indicated**

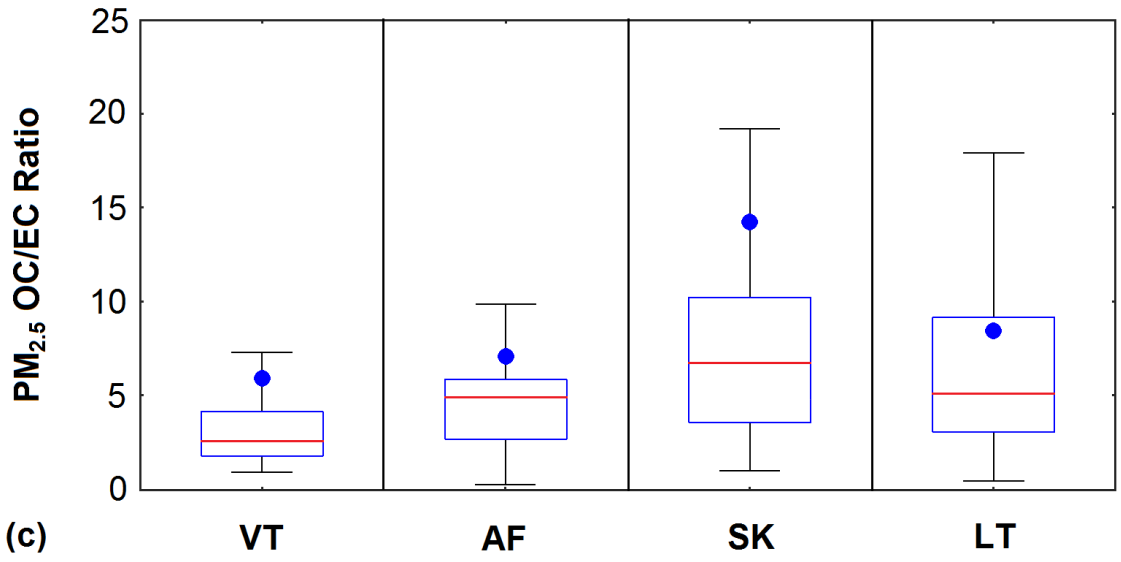

Figure 2-3 (continued): $PM_{2.5}$ (a) and PM_{10} (b) OC and EC concentrations and OC/EC ratios (c) at the four INDAAF sites. The red line indicates the median, the blue dot the mean, the top and bottom edges of the box indicate the 25th and 75th percentiles and the whiskers the ±2.7 σ (99.3% coverage if the data have a normal distribution)

Considering all OC and EC results for all sites combined, it was determined that the contributions of $PM_{2.5}$ OC and EC median mass concentrations to the PM_{10} median mass concentrations were 95.5 and 97.5%, respectively, which clearly indicates that both OC and EC occurred predominantly in the $PM_{2.5}$ size fraction. Therefore, all the subsequent results only indicate the $PM_{2.5}$ size fraction.

It is evident from Figure 2-3a that OC was higher than EC at all four of the South African INDAAF sites. The OC and EC concentrations were the highest at VT, with particularly EC levels being substantially elevated when compared to the other three sampling sites. Therefore, the OC/EC ratio of VT, i.e. 2.9, was also meaningfully lower than for the other sites. AF had the second lowest OC/EC ratio of 5.0, followed by LT with 5.1 and then SK with the highest ratio of 6.4. Figure 2-3c indicates the box and whisker plots of the $PM_{2.5}$ OC/EC ratios for each site, which supports the afore-mentioned observation from Figure 2-3a. These OC/EC ratios provide insight into the proximity of emitting sources in relation to the measurement site locations. The VT site is located within a highly populated (also with high traffic volumes), industrialised region (e.g. metallurgical smelters, coal-fired power stations and petrochemical operations), with numerous semi- and informal settlements (where a significant fraction of homes uses household combustion for space heating and cooking) within close proximity. The close proximity of these sources to the VT site results in the EC, which is a primary emitted species of which the concentration will reduce due to dry and wet deposition (Thatcher and Layton, 1995; Massey et al., 2012) during atmospheric

transport, to be higher than at sites that are further away from sources. However, the OC levels at VT likely do not yet reflect the full consequence of SOC, due to the nearby proximity of sources. In contrast, the higher OC/EC ratios at the other sites (i.e. AF, SK, LT) indicate that the emitting sources are likely to be further from the measurement locations. More complete oxidation of volatile species to form SOC and reduction in EC concentrations due to dry and wet deposition of the particles, will result in higher ratios.

Although the VT OC and EC concentrations are elevated above that reported for the regional background sites reported here, i.e. SK and LT, the concentrations at VT are well below that measured in heavily polluted areas such as New Delhi, India (average OC and EC of 25.6 and 12.1 μg/m^3, respectively) (Sharma et al., 2016), Mumbai, India (average OC and EC of 40.0 and 15.0 μg/m^3, respectively) (Herlekar et al., 2012) and Beijing, China (average OC and EC of 14.0 and 4.1 μg/m^3, respectively) (Ji et al., 2016). However, the concentrations at the background sites (SK and LT) are significantly higher than what has been described for true remote background sites such as 10 sites across Europe (average EC that varies between 0.15 to 0.22 μg/m^3) (Cavalli et al. 2016), National Atmospheric Observatory Košetice, Czech Republic (average OC and EC of 2.85 and 0.65 μg/m^3, respectively) (Mbengua et al. 2018), Terceira Azores, Portugal (Site: AZO 02) (average OC and EC of 0.33 and 0.04 μg/m^3, respectively) (Pio et al., 2011), Sonnblick, Austria (Site SBO 02) (average OC and EC of 0.90 and 0.14 μg/m^3, respectively) (Pio et al., 2011) and Barrow, Alaska, USA (annual average eBC of 0.041 μg/m^3) (Bodhaine, 1995). This indicates that these South African regional background sites are impacted by OC and EC sources. Contributing sources will be discussed later.

As far as the candidate could ascertain, the only study that has been printed in the peer-reviewed public domain that indicates OC and EC aerosol mass fractions/percentages for South Africa is Aurela et al. (2016), who presented average PM_1 mass percentages (OC and EC mass percentages of 39.0 and 3.0%, respectively) for samples taken over very short time periods (14 days in 2007 and 2008) at one site only. Therefore, considering the paucity of such data, mass percentages of $PM_{2.5}$ OC and EC, corresponding to the mass concentrations presented in Figure 2-3, are presented in Figure 2-4.

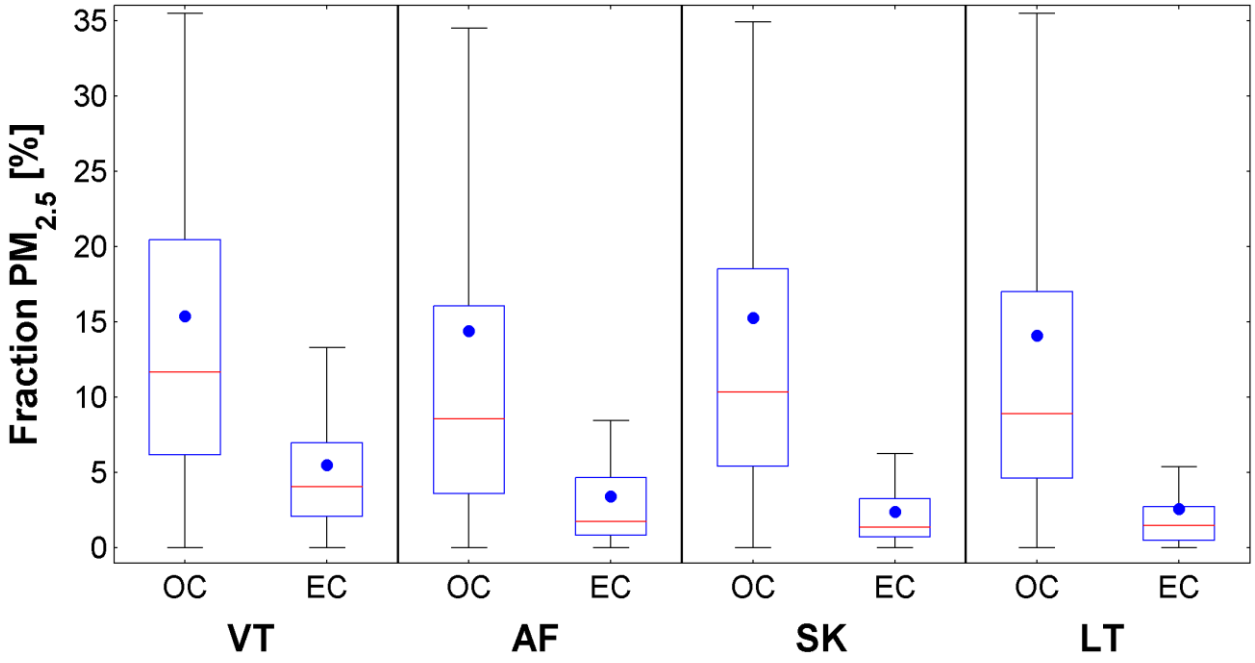

Figure 2-4: $PM_{2.5}$ mass percentage of OC and EC for the four INDAAF sites in South Africa. The red line indicates the median, the blue dot the mean, the top and bottom edges of the box indicate the 25th and 75th percentiles and the whiskers the ±2.7 σ (99.3% coverage if the data have a normal distribution)

The average OC $PM_{2.5}$ mass percentages varied between 14.1 (LT) and 15.4% (VT), while the average EC $PM_{2.5}$ mass percentages varied between 2.3 (SK) and 5.5% (VT). Although one should not compare PM_1 with $PM_{2.5}$ results, it is obvious from the afore-mentioned results that the 39.0% OC PM_1 aerosol mass reported by Aurela should not be considered as representative of the entire South Africa. In addition, Titta et al. (2014) reported PM_1 eBC mass fraction as 5.0% for Welgegund, which corresponds well with the EC mass fraction percentages (Figure 2-4). Datasets covering larger spatial areas and longer time periods, as presented here, give a better estimate of the true situation. Mbengua et al. (2018) found $PM_{2.5}$ OC mass percentages to be 11.0% and $PM_{2.5}$ EC to be 14.0% at one rural background site (National Atmospheric Observatory Košetice, Czech Republic). Putaud et al. (2004) described $PM_{2.5}$ OC mass percentages to be 20.0 to 30.0% (at rural sites) and 22.0 to 38.0% (sites in close proximity to cities and at kerbside sites), while $PM_{2.5}$ EC mass percentages were 5.0 to 11.0% (at rural sites) and 5.0 to 23.0% (sites in close proximity to cities and at kerbside sites), for more than 20 European sites in winter. It therefore seems that the mass percentages of both OC and EC, at all four South African sites reported here, are somewhat lower than within a typical European context. Chemical mass closure was not undertaken, and therefore the contributions from other species cannot be explicitly stated. However, it is certain that SO_4^{2-} will contribute significantly to the $PM_{2.5}$ content. This is in contrast to most of the developed world where a decline in aerosol SO_4^{2-} concentrations has been reported (Zhang et al., 2007b). Recently, Conradie et al. (2016) showed that SO_4^{2-} was the dominant ion in rain water at the same South African INDAAF sites discussed in this paper, and that

the situation in the period 2009 to 2014 was worse (lower pH and higher strong acid content) than similar studies conducted a decade earlier (Mphepya et al., 2004; Mphepya et al., 2006). Aurela et al. (2016) indicated that PM_1 contained 44.0% SO_4^{2-} at a regional background site, while Tiitta et al. (2014) reported 33.0% SO_4^{2-} in non-refractive PM_1 (and 27.0% if eBC was included) for more than one year of Aerosol Chemical Speciation Monitor (ACSM) measurements conducted at Welgegund. Compared to the developed world, the lower contribution of OC and EC to the $PM_{2.5}$ mass percentages reported here (Figure 2-4) is therefore not due to lower mass concentrations of OC and EC (Figure 2-3), but rather due to comparatively higher SO_4^{2-} content of aerosols measured in South Africa.

2.3.2 Temporal (seasonal) assessment

Figure 2-5a and Figure 2-5b indicate average (blue dot) and median (red line) values of the monthly OC (a) and EC (b) concentrations measured over the entire sampling period of 82 months (March 2009 until December 2015) for all the sites, respectively.

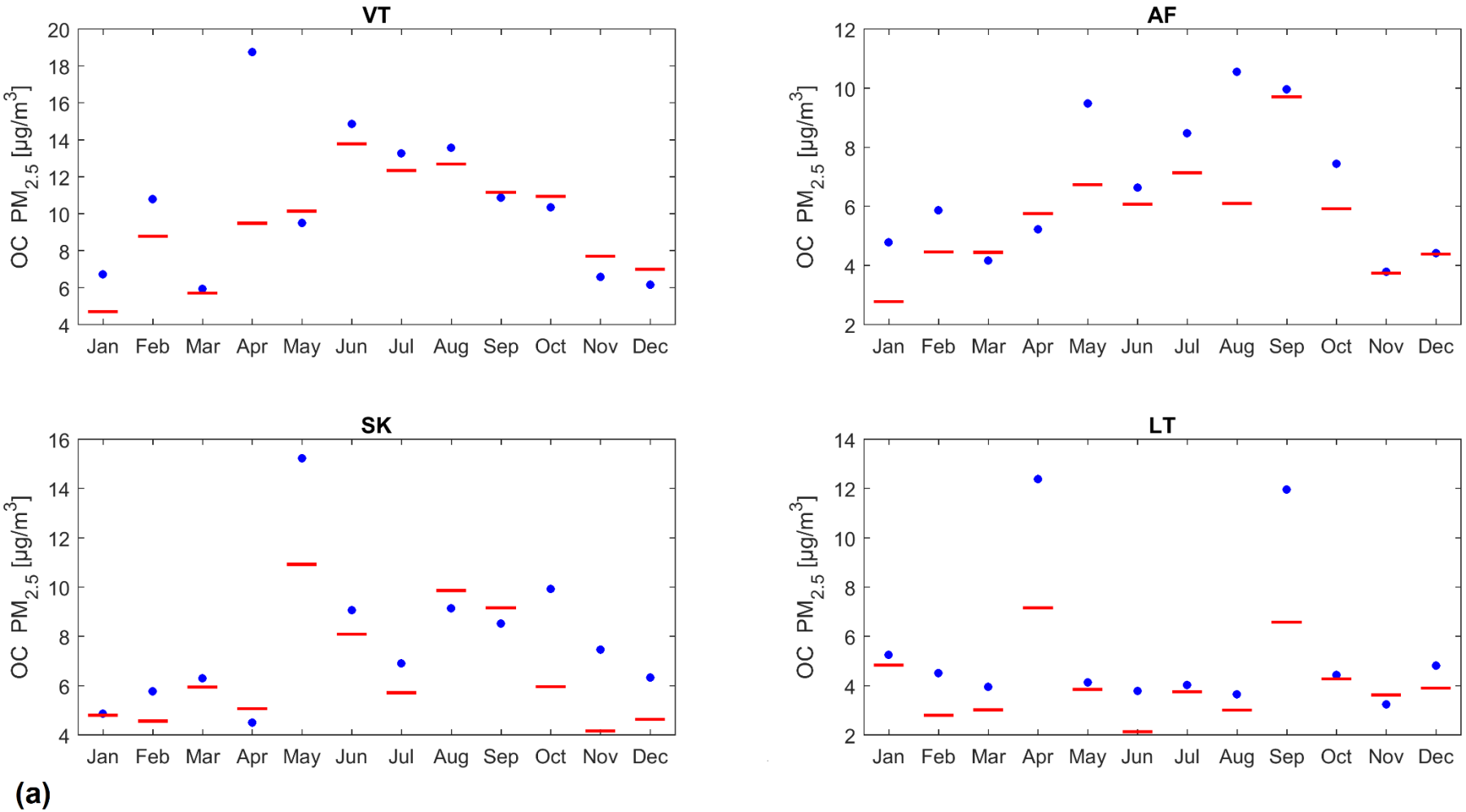

Figure 2-5: **$PM_{2.5}$ monthly temporal distribution of OC (a) and EC (b) for each site over the entire monitoring period. Similar to Figure 2-3 and Figure 2-4, the blue dots indicate mean values and the red lines median values**

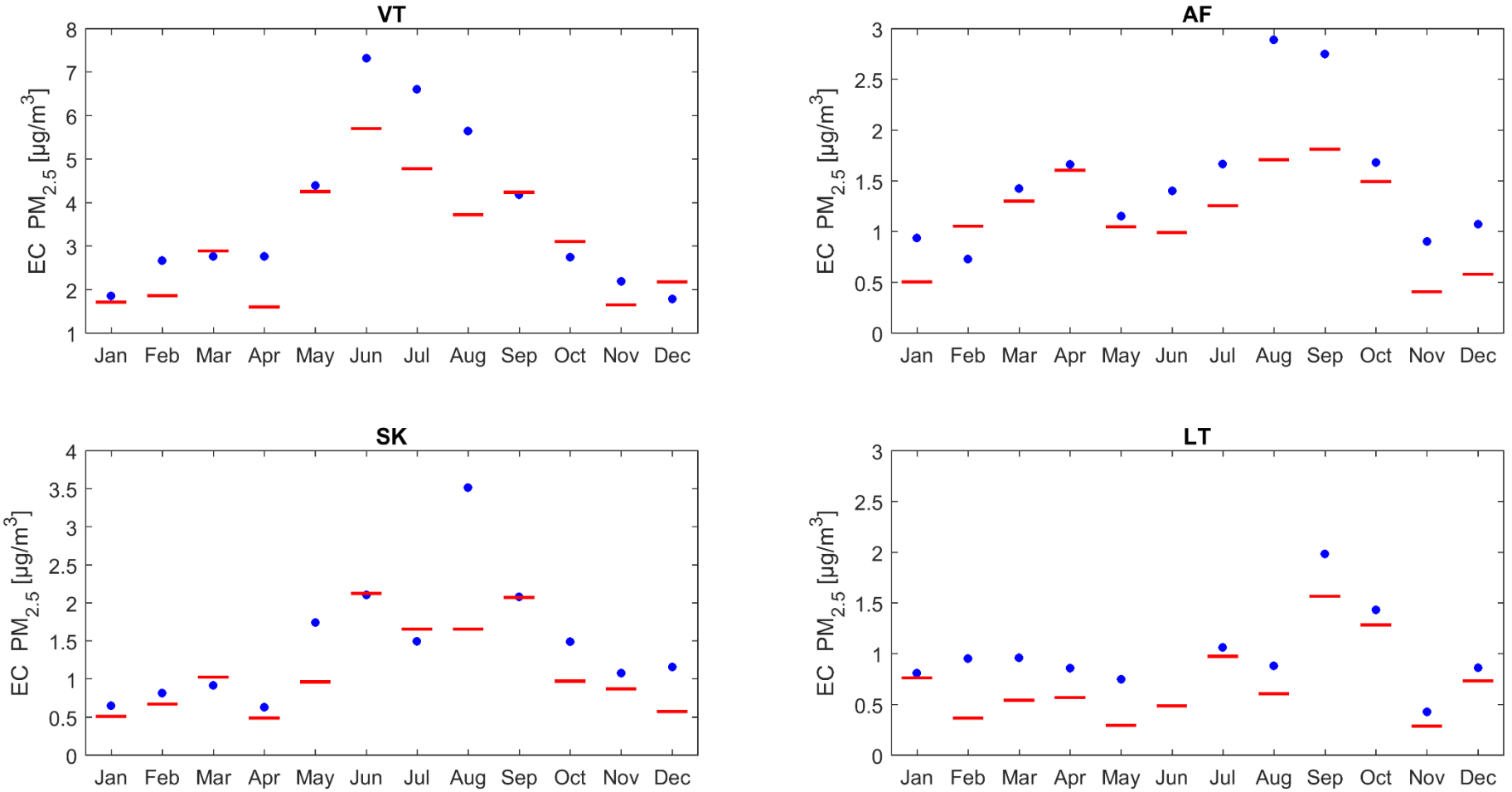

Figure 2-5 (continued): $PM_{2.5}$ monthly temporal distribution of OC (a) and EC (b) for each site over the entire monitoring period. Similar to Figure 2-3 and Figure 2-4, the blue dots indicate mean values and the red lines median value

From Figure 2-5, relatively distinct seasonal patterns can be observed for all the measurement sites. OC and EC concentrations peaked in the cold winter months (June to August) at VT, which clearly indicates that household combustion for space heating in semi- and informal settlements is most likely the main source of both OC and EC at this site. The presence of low-level inversion layers during the evening and early morning (Korhonen et al., 2014; Gierens et al., 2018) during this time of the year, which trap low-level emissions such as household combustion, also exacerbate the situation. Additionally, it is expected that the afore-mentioned low-level during inversion layers will to a large degree prevent high-stack industry emissions from making a significant contribution in June to August, during the evenings and early mornings (Gierens et al., 2018). Previously, Venter et al. (2012) and Chiloane et al. (2017) indicated that household combustion in semi- and informal settlements is a significant source of eBC (with EC measured as a proxy for eBC in this study) in South Africa during winter; however, as far as the candidate could ascertain, these are the first results published in the peer-reviewed public domain that indicate the influence of this type of combustion on elevated levels of OC in South Africa. Regional open biomass burning will also make a contribution to OC and EC levels measured at the VT. In contrast to the VT, maximum OC and EC levels for LT were observed in September, which coincides with the peak frequency of open biomass burning in southern Africa. Open biomass burning frequencies will be discussed in greater detail in the next section. For the AF and SK sites, no single seasonal source seems to dominate, with elevated OC and EC levels occurring in the period from approximately May to October. This period coincides with the cooler later autumn (May), cold winter (June to August) and early spring, prior to the start of the rainy season (September to middle October). It therefore seems feasible that both household combustion for space heating and open biomass burning are contributing substantially to elevated OC and EC levels at these sites. Low-level inversion layers in the colder months will not trap these low-level emissions for long, since the growth of the PBL is a bit slower during these months and do not limit the impact of high-stack emissions from industry too much (which is especially relevant to the AF site). It is obvious that both these sites will also be impacted by open biomass burning that occurs on a regional basis, but it was not necessarily expected that household combustion for space heating would make such a significant contribution at both sites. However, recently, Chiloane et al. (2017) reported that household combustion was the dominant eBC source during winter at Elandsfontein, which is situated approximately 100km west north-west from AF. Similar to AF and SK, Elandsfontein is not in close proximity to semi and- informal settlements, yet the afore-mentioned authors suggested that household combustion had a regional impact on eBC. Therefore, the current results imply that household combustion for space heating also has a regional impact in terms of OC and EC levels, which affect AF and SK.

All sites had the lowest OC and EC levels during late spring (November), summer (December to February) and early autumn (March), which corresponds with the rainy season in the South African interior (Conradie et al., 2016) that will enhance pollutant washout. Low-level thermal inversion layers are also not common during this period and the PBL tends to be deeper (Korhonen et al., 2014). Additionally, household combustion for space heating and open biomass burning are uncommon during this period. Contributing sources would typically be industry, traffic and household combustion for cooking, which occur throughout the year, and additionally biogenic VOC emissions (Jaars et al., 2016) that are oxidised to form OC.

In addition to the temporal OC and EC patterns considered in this section, similar OC/EC ratio temporal patterns are presented in Figure A-1 (Appendix A), which can be referenced in future work.

2.3.3 Additional source insights

In the previous section, it was demonstrated that household combustion for space heating and/or open biomass burning were significant sources of OC and EC in the northern interior of South Africa. In Figures 2-6a to 2-6d, the monthly observed Modis fire pixels from the MODIS collection 5 burned area product (Roy et al., 2008), over the entire sampling period (i.e. March 2009 until December 2015), within 100 and 250 km radii around each measurement site, are presented. From these results, it is evident that most of the open biomass burning fires occur from June to October, with August and September having the highest fire frequencies, irrelevant of which site or year is considered. This supports the earlier deduction that open biomass burning is likely the dominant source of elevated OC and EC levels during this time of the year. Considering Figure 2-6, it is clear that all the measurement sites considered in the study will be influenced by open biomass burning. It was evident that AF, SK and LT had elevated OC and EC levels during the peak biomass burning period (Figure 2-5), when compared to VT. The strong (due to population density) household combustion source at VT, however, prevented the biomass burning contribution to be clearly observable in the seasonal cycles (Figure 2-5). The VT seasonality is therefore likely to be the sum of both sources, i.e. household combustion and biomass burning.

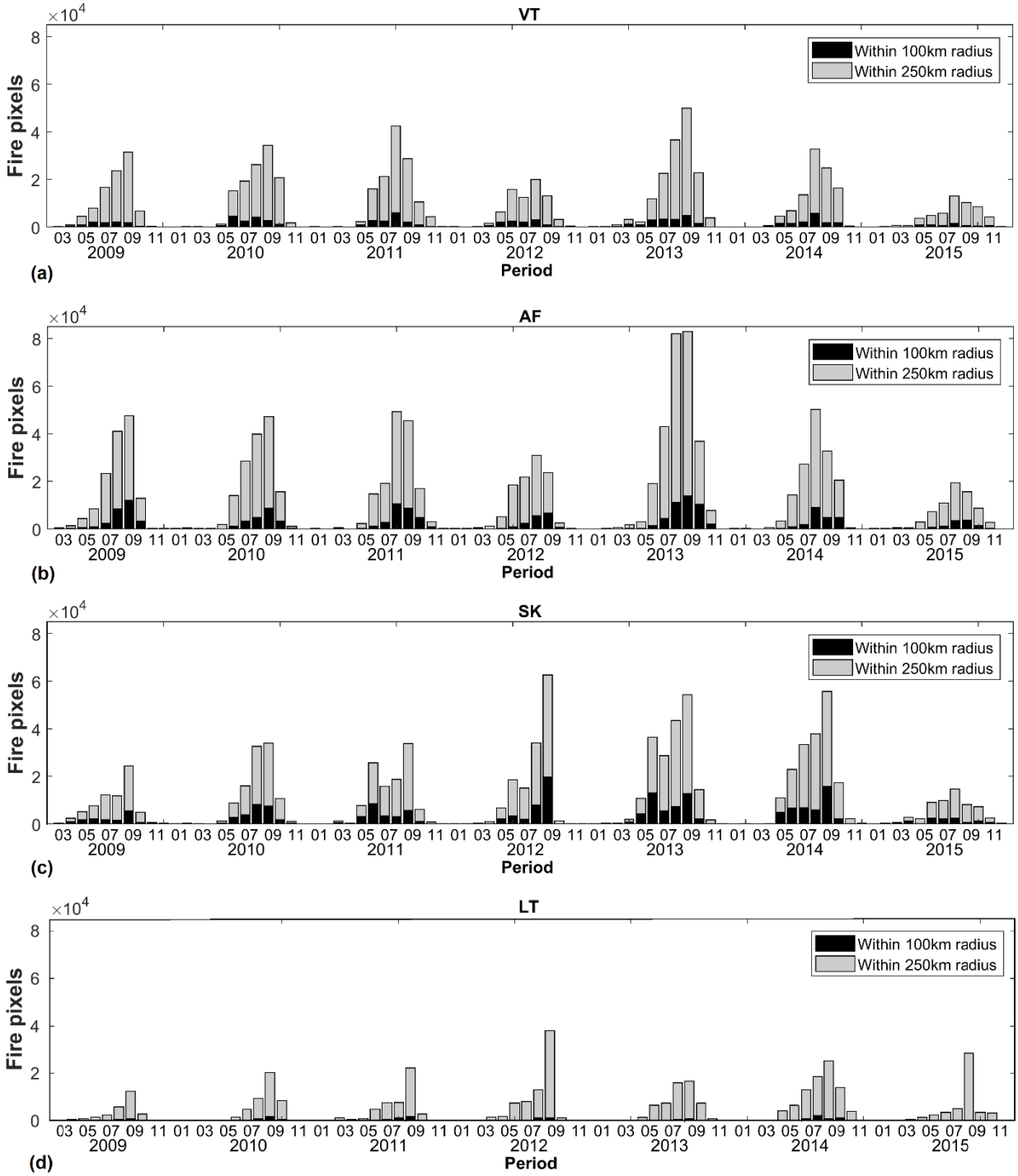

Figure 2-6: Modis fire pixels (Roy et al., 2008) within 100 and 250km radii of VT (a), AF (b), SK (c) and LT (d), over the entire sampling period

From Figure 2-6, it is interesting to note that LT had the least amount of fires within the 100 and 250 km radii. At first, this seems to contradict the deduction made earlier from the seasonal cycles (Figure 2-5) that open biomass burning is the most important source of OC and EC at this site. However, in order to contextualise the influence of open biomass burning, the location of fires in relation to air mass movements needs to be considered. Similarly, the regional

influence of household combustion on OC and EC levels needs to be considered within the context of possible areas from where such emissions are likely, in relation to air mass movements.

Figure 2-7 indicates the locations of Modis fires pixels in 2013 (a) and 2015 (b) in southern Africa. Two years are shown, since it is well known that there is significant inter-annual variation in the occurrence of open biomass burning in southern Africa. This is mainly a result of the variation in El Niño Southern Oscillation (ENSO) conditions. La Niña results in above average rainfall in southern Africa, while El Niño causes less than average rainfall, which results in more or less biomass being available, respectively, for fires in different years (Mafusire et al., 2016). In order to contextualise the possible emission areas for household combustion, the population density for southern Africa is presented in Figure 2-8. Both these aspects, i.e. location of open biomass burning fires and population density, will subsequently be discussed within the context of air mass movements, which are indicated by the overlay back trajectory maps (Figure 2-9) that were drawn for all the sampling days at the sampling sites, over the entire monitoring period (i.e. March 2009 to December 2015).

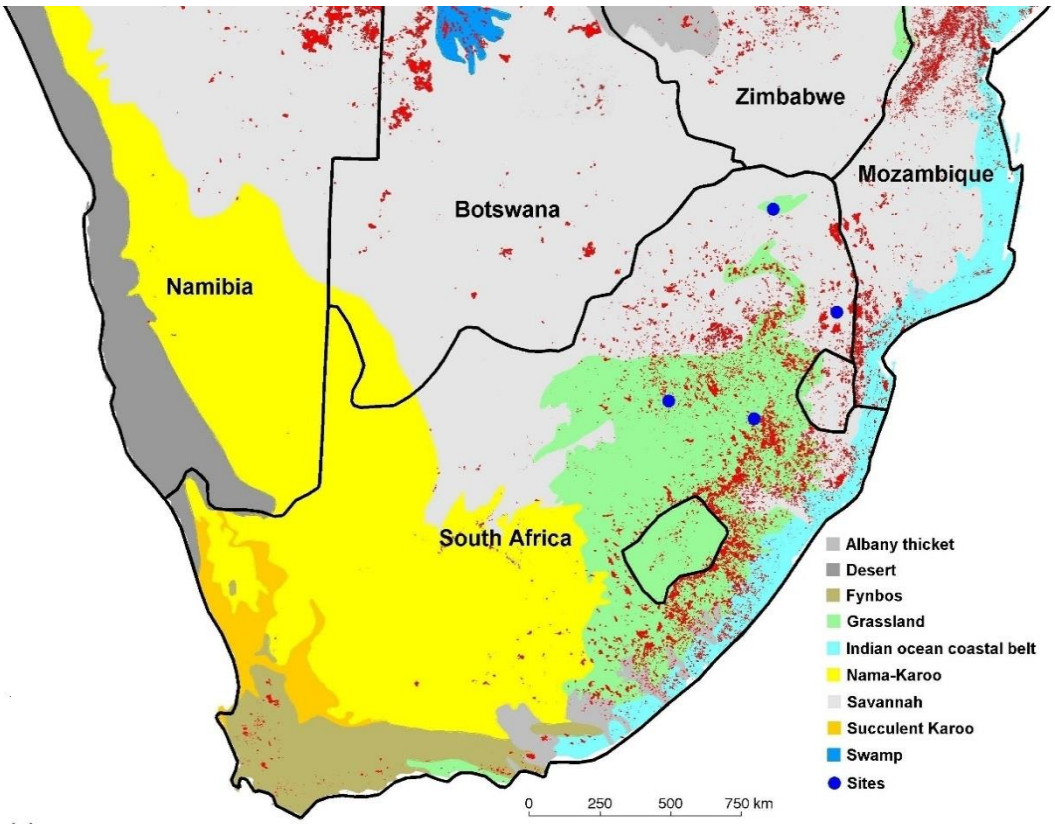

(a)

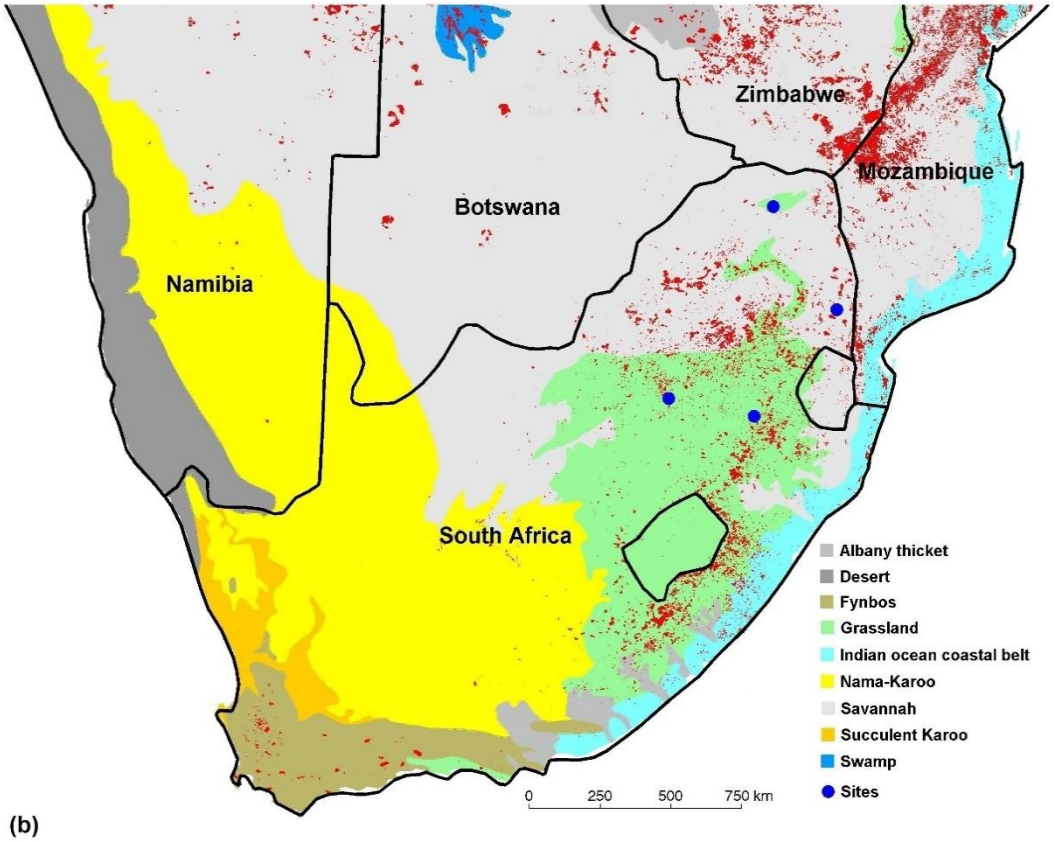

(b)

Figure 2-7: Modis fire pixels for 2013 (a) and 2015 (b) (Roy et al., 2008), superimposed on biomes (Mucina and Rutherford, 2006)

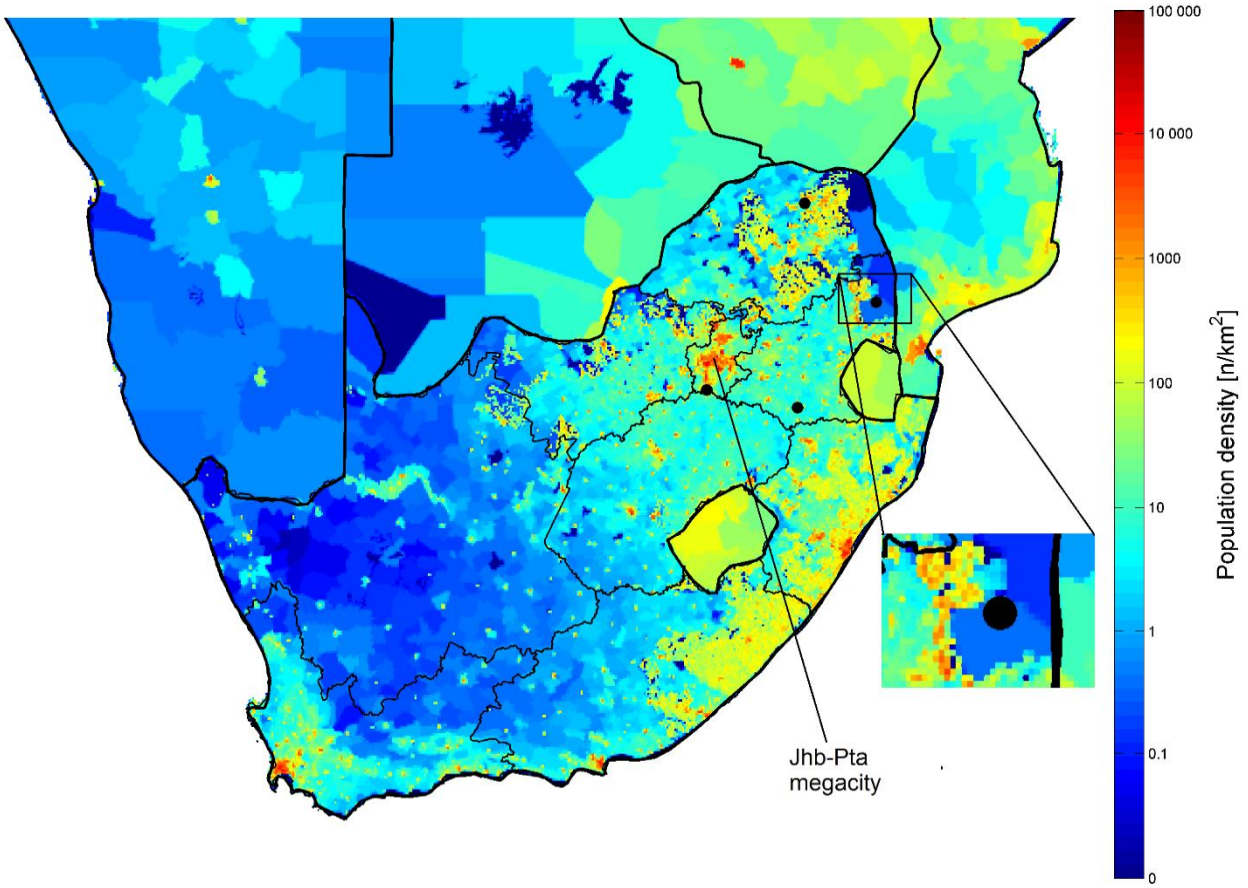

Figure 2-8: Population density for southern Africa (CIESIN, 2010). Also indicated are the locations of the Johannesburg-Pretoria (Jhb-Pta) megacity (with more than 10 million inhabitants) and a zoomed-in area around the SK measurement site

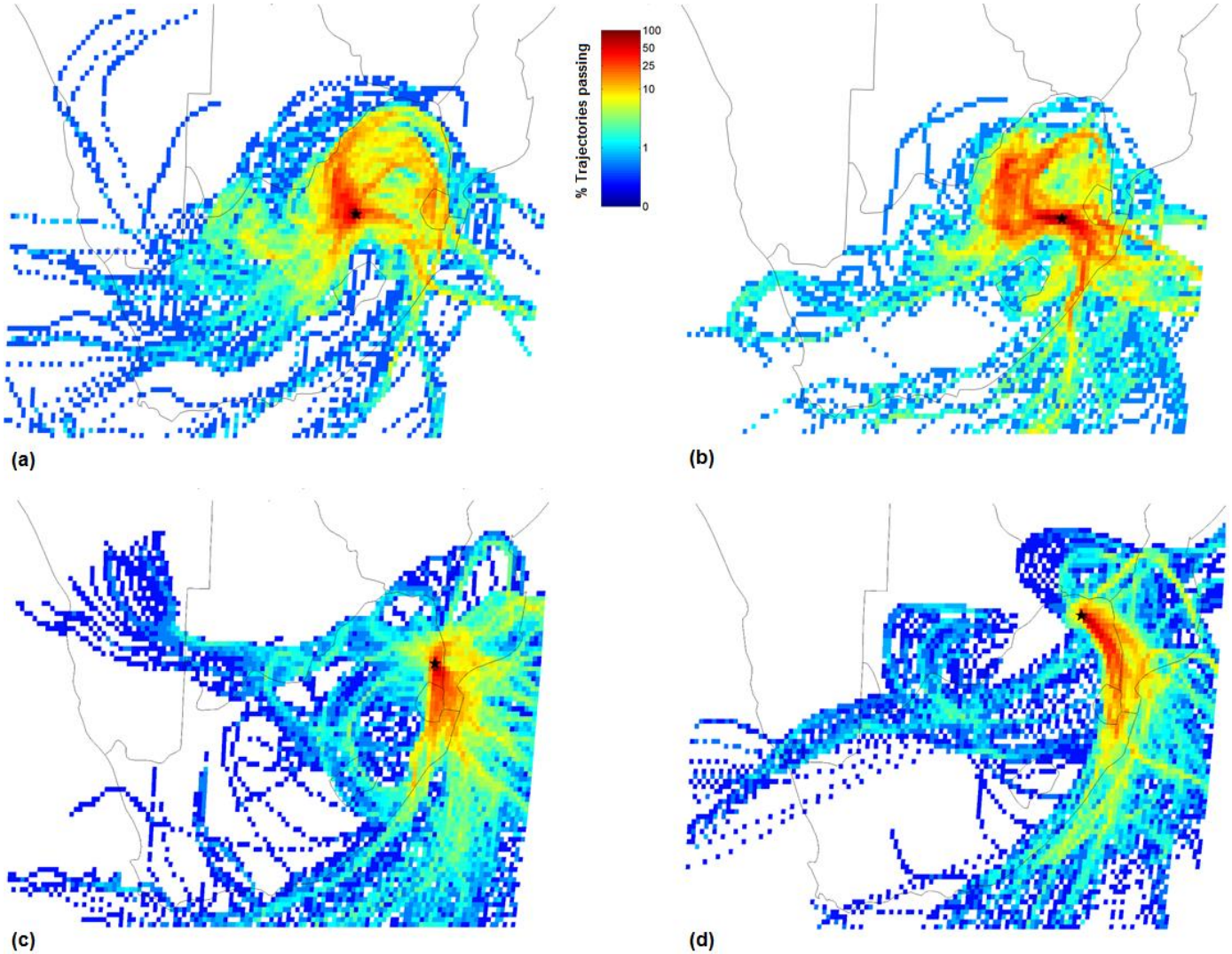

Figure 2-9: Overlay back trajectory maps (calculated as indicated in section 2.2.4) for VT (a), AF (b), SK (c) and LT (d) for all sampling days during the entire monitoring period (i.e. March 2009 to December 2015)

Considering the overlay back trajectory map (Figure 2-9a) for VT, it is evident that air masses had likely transported open biomass burning fire emissions (Figure 2-7) to the site. However, as was indicated by the seasonal patterns (Figure 2-5), this is not the dominant OC and EC source. The OC/EC ratio for this site clearly indicated that sources in relatively close proximity are dominant (Figure 2-3), while the seasonal patterns (Figure 2-5) indicated that this source is likely to be household combustion for space heating, especially during the cold winter months. Additionally, the overlay trajectory map (Figure 2-9a) and the population density map (Figure 2-8*)* clearly show that air masses, which had passed over the Johannesburg-Pretoria (Jhb-Pta) megacity, will influence VT. The Jhb-Pta megacity has more than 10 million inhabitants, with large semi- and informal settlements (Lourens et al., 2012; Lourens et al., 2016).

Considering the OC and EC seasonal patterns (Figure 2-5), elevated levels at LT were identified as being mostly due to open biomass burning (Figure 2-5 and associated text). However, it was also the site with the least number of fires occurring within 100 and 250 km radii, which seemed contradictory. However, it is evident from the overlay back trajectory map (Figure 2-9d) that the main fetch region (region with highest frequency of back trajectory overpass) for LT is over the Kruger National Park and the South African-Mozambique border, which is an area that has a high incidence of open biomass burning (Figure 2-7).

OC and EC seasonal patterns indicated that both household combustion for space heating and open biomass burning resulted in elevated levels (Figure 2-5) at AF and SK. The open biomass burning contribution at both these sites is obvious from Figure 2-6, Figure 2-7 and Figure 2-9. For AF, the household combustion influence is likely to be associated with small semi- and informal settlements from the town of Amersfoort (not the measurement site, but the town close to it), as well as air masses that had passed over the Jhb-Pta megacity (Figure 2-8 and Figure 2-9b). Although SK is situated in the Kruger National Park, which is a relatively pristine environment, in reality, relatively large and densely populated semi- and informal settlements occur less than 20 km north-west from the SK site (see zoomed-in area in Figure 2-8), which explains the observed household combustion for space heating influence in winter.

Recently, Chiloane et al. (2017) showed the influence of household combustion for space heating on eBC (measured online) at Elandsfontein (as indicated earlier, approximately 100km west north-west from AF), by indicating a correspondence between eBC and ambient temperature. Since the elevated OC and EC levels at VT during winter were mainly attributed to household combustion for space heating, the OC and EC concentrations measured at VT were plotted against the average ambient temperature during every 24-hour sample period, using a bivariate technique that considers uncertainty margins (Thirumalai et al., 2011) as indicated in Figure 2-10a and Figure 2-10b. In order to evaluate the correlation, guidelines similar to

Sheskin (2003) and Kleynhans et al. (2017) were employed, i.e. *"(i) if |r| ≥ 0.7 a correlation is considered to be strong/significant; (ii) if |0.3| ≥ |r| < 0.7 a correlation is considered to be moderate and (iii) if |r| < 0.3 a correlation is considered to be weak/insignificant"*. Considering these guidelines, OC correlated moderately (r = 0.48) to average temperature, while EC correlated to the high end of moderate, almost being significant (r = 0.62). However, it must be taken into consideration that household combustion for space heating in South African semi- and informal settlements usually only occurs in the evening to early morning during a typical winter day (Venter et al., 2012), since ambient temperature can vary from below 0°C in the early to morning to well above 25°C in the afternoon. Therefore, these correlations, which were based on average temperatures over the entire 24-hour sampling periods, are likely to be significantly improved if sampling times corresponded more with household combustion for space heating periods. The afore-mentioned correlations therefore support the notion that household combustion for space heating is the dominant source at VT, resulting in elevated OC and EC levels, especially during winter. In contrast, for LT, was insignificantly impacted by household combustion for space heating, the correlations (Figure 2-10c and Figure 2-10d) were completely insignificant (r = 0.12 for both OC and EC correlations with temperature).

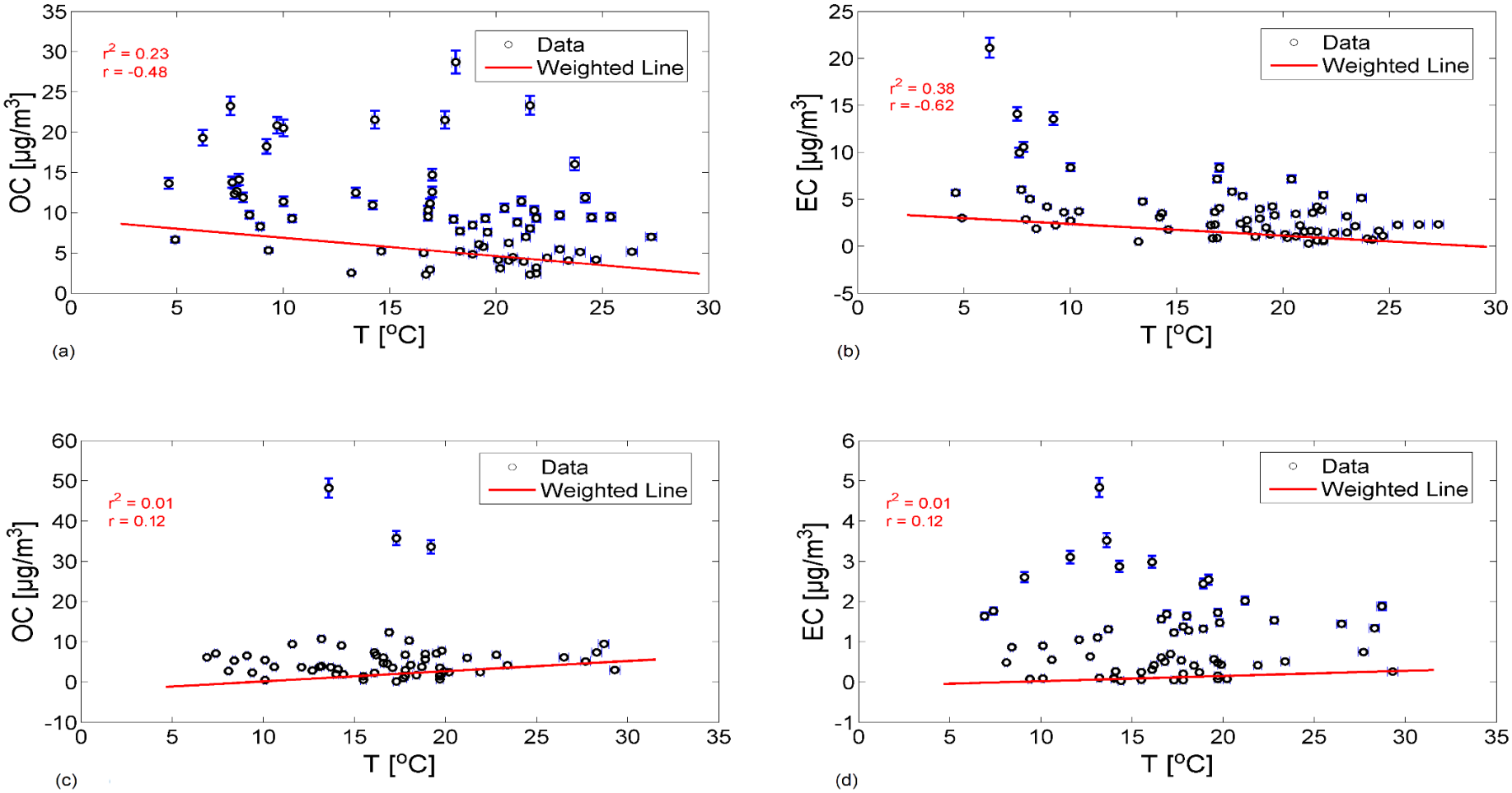

Figure 2-10: Bivariate correlation (Thirumalai et al., 2011) of $PM_{2.5}$ OC and EC concentrations against average ambient temperature during 24-hour sampling periods for VT (a and b) and LT (c and d)

2.4 Summary and conclusions

Maritz et al. (2015) did publish the results of the first two years (i.e. March 2009 till April 2011) of data included in this chapter. This chapter presents the first long-term (several years) OC and EC dataset for South Africa that covers multiple measurement sites, i.e. two regional background sites (SK and LT), an industrially influenced site (AF), and an urban/industrial site (VT). OC and EC mass fractions for all sites were lower than what is typical for the developed world. This was not due to lower OC and EC levels, but rather due to larger fractional contributions from other species, with specifically SO_4^{2-} making a significant contribution to aerosol chemical composition in South Africa.

OC and EC levels were significantly higher at VT than at the other sites. OC/EC ratios indicated that sources in close proximity to VT were likely the main contributors, while more distant sources possibly impacted AF, SK and LT. Seasonal OC and EC patterns indicated that household combustion for space heating in semi- and informal settlements was likely to be the most dominant source at VT, which was substantiated by correlating OC and EC concentrations to ambient temperature. Overlay back trajectory maps compiled for the sampling periods indicated that air mass that had passed over the Johannesburg-Pretoria (Jhb-Pta) megacity, where many semi- and informal settlements occur, also makes a contribution to OC and EC levels at VT. In addition, open biomass burning made a contribution, therefore the seasonal pattern observed for VT was as a result of both these sources, i.e. household combustion for space heating and biomass burning.

Seasonal OC and EC patterns indicated that elevated levels of OC and EC at LT were likely to be due to regional open biomass burning, which was confirmed by overlay back trajectory analysis within the context of open biomass burning fire locations. Both open biomass burning and household combustion resulted in elevated levels of OC and EC in the seasonal patterns of SK and AF, which were confirmed with back trajectory analysis, population densities and open biomass burning fire locations.

Overall, the results indicated that open biomass burning contributed to OC and EC levels on a regional scale, irrespective of site location in the South African interior. However, household combustion for space heating in semi- and informal settlements makes a significant local (e.g. at VT) and discernible regional (e.g. at AF and SK) OC and EC contribution, which has not previously been indicated, although Chiloane et al. (2017) did show that eBC from household combustion made a regional contribution to eBC. Industrial and vehicle emissions are likely to contribute to the baseline OC and EC levels measured throughout the year, while oxidation of VOCs during the rainy season will also contribute to OC levels during this period.

CHAPTER 3

PARTICULATE MATTER WATER-SOLUBLE INORGANIC IONS AND ORGANIC ACIDS ASSESSMENT

In this chapter… *Literature relevant to water-soluble inorganic ions and organic acids is presented in section 3.1. In section 3.2, experimental aspects, including sampling site description, filter preparation and sampling methods (section 3.2.1), analyses (section 3.2.2), ancillary data and data processing (section 3.2.3), as well as empirical calculations and statistical analysis (section 3.2.4) are discussed. Results and discussions are presented in section 3.3, which includes contextualisation of concentrations (section 3.3.1), spatial distribution (section 3.3.2), temporal assessment of the most important ions (section 3.3.3), acidity and neutralisation (section 3.3.4) and statistical evaluations along with source contributions (section 3.3.5). Section 3.4 summarises the conclusions drawn from this chapter. This chapter is linked to Objective 2, as stated in section 1.3.*

3.1 Literature survey

3.1.1 Introduction

Typical chemical species present in atmospheric aerosols include alumina-silicates (e.g. from wind-blown dust), black carbon (BC) or elemental carbon (EC) (definitions according to Petzold et al., 2013, depending on the analytical technique applied), organic carbon (OC), trace metal species, water-soluble inorganic ions (e.g. nitrate (NO_3^-), chloride (Cl^-), sulphate (SO_4^{2-}), fluoride (F^-), sodium (Na^+), ammonium (NH_4^+), potassium (K^+), magnesium (Mg^{2+}), calcium (Ca^{2+})) and organic acids (OA) (e.g. oxalic- ($(COOH)_2$), acetic- (CH_3COOH), formic- (CHOOH) and propionic- (C_2H_5COOH) acid). In this chapter, only the afore-mentioned water-soluble inorganic ions and organic acids are considered.

3.1.2 Impacts

Atmospheric aerosols can affect the environment negatively (Lin et al., 2014; Zhang et al., 2018) and can have adverse human health affects (Seaton et al., 1995; Lazaridis et al., 2002; Gauderman et al., 2004; Karthikeyan and Balasubramanian, 2006; Schlesinger et al., 2006). These effects depend on the aerosol concentration, as well as physical (e.g. size, mass, structure, and optical density) and chemical properties (e.g. chemical composition and solubility) (Seinfeld and Pandis, 2016). In subsequent paragraphs, these possible negative impacts are briefly considered.

3.1.2.1. Health impacts

Particulate matter (PM) smaller than 10 µm (PM_{10}) has been linked to causing asthma, respiratory diseases and even cancer (Callén et al., 2012), while crustal- and road dust in this size range were specifically associated with increased cardiovascular diseases (US EPA, 2009). Smaller aerosols, e.g. smaller than 2.5 µm ($PM_{2.5}$), have been identified as one of the main causes for cardiopulmonary morbidity and mortality (Zhou et al., 2015; Hsu et al., 2017). The finer particulate fractions in wood and biomass fuel burning smoke have been associated with increased respiratory illness of the upper respiratory tract, tuberculosis and lung cancer, while such particulate matter from traffic emissions has been linked with cardiovascular diseases (Bruce et al., 2000; US EPA, 2009). The US EPA (2009) stated that secondary sulphates from long-range transport, which are typically very fine (e.g. <100 nm), (Vakkari et al., 2015), were associated with higher mortality rates. All the afore-mentioned clearly indicates that aerosol size is very important within a human health perspective, since finer particles typically penetrate deeply into the respiratory system.

Many studies have shown that various health effects were specifically associated with water-soluble ions. SO_4^{2-} and NO_3^- are typically the most common inorganic components of PM sampled in the South African interior (Tiitta et al., 2014; Aurela et al., 2016). Aerosol SO_4^{2-} and NO_3^- are formed through the oxidation of sulphur dioxide (SO_2) and nitrogen oxides (NO_x), respectively. Since SO_4^{2-} occurs mainly in the $PM_{2.5}$ size fraction (Pandey et al., 2006; Reiss et al., 2007), it is likely to be transported and penetrate deeper into the lungs than species associated with larger particles (Pandey et al., 2006). Zhang et al. (2000) suggested that areas with high SO_4^{2-} concentrations had higher mortality rates. Chen et al. (2016) found that exposure to SO_4^{2-} was linked to elevated blood pressure and heart rate, as well as increased respiratory and cardiovascular problems. Secondary SO_4^{2-} species, e.g. $(NH_4)_2SO_4$, can also cause malignant growths of lung cancer, although the mechanisms by which SO_4^{2-} aerosols are responsible for these growths is still unknown (Yun et al., 2017). In contrast to SO_4^{2-}, very few epidemiological studies have positively identified health effects associated with NO_3^-. Lipfert et al. (2006) and Ostro et al. (2006) reported NO_3^- to be associated with mortality rates in California. Furthermore, a clinical study by Utell et al. (1980) reported other health effects associated with NO_3^-, such as reduced airway conductance in humans with influenza (Schlesinger, 2007).

Atmospheric NH_4^+ is formed from ammonia (NH_3) emissions. After N_2 and N_2O, NH_3 is the most abundant compound in the atmosphere that contains nitrogen (Seinfeld and Pandis, 2016). NH_4^+ can neutralise acid forming species present in the aerosol phase to produce ammonium salts (e.g. ammonium sulphate (NH_4HSO_4) and -bisulphate ($(NH_4)_2SO_4$), and/or ammonium nitrate (NH_4NO_3)) (Young et al., 2016). Identified health effects associated with NH_4^+ in the $PM_{2.5}$ size fraction, along with OC and EC, are increased cardiovascular- and respiratory

mortality (Atkinson et al., 2015; Hsu et al., 2017). Wang et al. (2015c) indicated that SO_4^{2-}, K^+ and NH_4^+ had high correspondence (in terms of occurrence) with water-soluble metals and therefore might contribute to more harmful effects in humans. Jones et al. (2015) found that SO_4^{2-}, NH_4^+ and NO_3^- were strongly associated with respiratory problems.

Chlorine-releasing agents (e.g. sodium hypochlorite (NaClO), calcium hypochlorite ($CaCl_2O_2$) and trichloro-S-triazinetrione ($C_3Cl_3N_3O_3$)) contribute to effects such as mucosal irritation, as well as bronchial hyper-reactivity, which can lead to more severe pulmonary diseases (Babu et al., 2008; Cao et al., 2017). In contrast, when chloride is emitted from marine sources (e.g. NaCl), it can have a therapeutic effect on people with airway infections and breathing disorders, viz. hoarseness, bronchitis and asthma (Cătălina et al., 2012).

F^- is emitted by some industries, specifically in countries with historically less stringent air quality legislations, e.g. China and India. Many employees of such industries have been diagnosed with fluorosis (i.e. excessive exposure to fluoride), which is indicated through the measurement of haemoglobin (Zhiliang et al., 1987; Joshi and Dudani, 2008; Susheela et al., 2013). Currently, F^- emissions do not seem to be a general problem in South Africa. Some everyday products contain F^- (Barbier et al., 2010). For instance, sodium fluoride (NaF) is used in water fluoridation and toothpaste (Dutta et al., 2017).

According to Seinfeld and Pandis (2016), CHOOH and CH_3COOH are the most commonly occurring carboxylic organic acids in the atmosphere, even though Graedel et al. (1986) and Niu et al. (2018) reported many aliphatic, olefinic and aromatic acids being present in the atmosphere. Particulate matter organic acids could contribute to pulmonary inflammation (Pöschl, 2005).

Mg^{2+} and Ca^{2+} occur commonly in both crustal sources and in fly ash emitted by industrial activities (Mahlaba et al., 2011). Fly ash poses increasing health risks for humans when ingested or inhaled, since it also contains heavy metals, which could be carcinogenic (Zhou et al., 2015).

3.1.2.2. Environmental impacts

The deposition of inorganic compounds can be either beneficial (e.g. nutrients) or detrimental (e.g. eutrophication) to the environment. Because nitrogen is a structural element of chlorophyll and amino acids (building blocks of protein molecules), the occurrence of nitrogen-containing species in the environment within certain limits is beneficial (Connell, 2005; Elminir, 2007), more so than for S-containing species. However, these beneficial levels are often exceeded. In general, the negative environmental effects of SO_4^{2-} and NO_3^- are reduction in vegetative photosynthesis, visibility impairment, temperature fluctuations, haze formation (Meng et al., 2016 and references therein) and its effects on the radiative balance through their optical and hygroscopic properties (Young et al., 2016). Xu et al. (2015) reported that the SO_2 and NO_x

measured during a haze period in Southeast Asia were oxidised and formed optically active secondary inorganic aerosols (i.e. NH_4NO_3 and $(NH_4)_2SO_4$ or NH_4HSO_4) that reduced visibility between 2.0 and 90.0%. Furthermore, Gao et al. (2015) also reported a lack of visibility caused by organic matter (OM), $(NH_4)_2SO_4$ and EC. The haze events mentioned in Xu et al. (2015) had decreasing effects on vegetative photosynthesis, which consequently led to fewer crops and increased atmospheric temperature (due to the lower uptake of CO_2 by crops). If this secondary effect (i.e. temperature increase) was dramatic, it could have led to more natural biomass burning. In South Africa it is however unlikely that this effect will be substantial (Kulmala et al., 2014; Keppel-Aleks and Washenfelder, 2016). In general, the direct radiative effect of both NO_3^- and SO_4^{2-} is cooling (i.e. negative aerosol forcing) (Charlson et al., 1992; IPCC, 2013; Wan et al., 2016). According to Jacobson (2001b), Cl^- also enhances cooling of the atmosphere. Environmental concerns with organic acids are acidification of rain water, which Keene and Galloway (1986a) indicated from precipitation samples collected in New York, USA. Detrimental environmental effects on terrestrial and aquatic ecosystems can be caused by disposed fly ash (may contain Mg^{2+} and Ca^{2+}), because heavy metals are leached from the ash that adversely affects water quality and plant growth (Wong and Wong, 1990; Babu and Reddy, 2011). Excessive NH_4^+ deposition can lead to eutrophication (i.e. excessive richness of nutrients) of ecosystems (i.e. terrestrial and water) (Bouwman et al., 1997; Asman et al., 1998).

3.1.3 Sources

Sources of the previously mentioned water-soluble ions and organic acids are explored in this section. SO_2 and NO_x (as the most important precursors of SO_4^{2-} and NO_3^-) are often co-emitted by coal-fired power plants (Collett et al., 2010; Amster et al., 2014; Pretorius et al., 2015) and household combustion for space heating and cooking (Lourens et al., 2011; Venter et al., 2012). SO_2 is mainly emitted from fossil fuel combustion activities (Graedel and Crutzen, 1995; Van Loon and Duffy, 2005; Engelbrecht, 2009; Lourens et al., 2011; Conradie et al., 2016), sulphide ore smelters (Jacobs, 2006) and volcanoes (Connell, 2005). Petrochemical operations are also known to emit either H_2S or SO_2, or a combination of both (Nunes et al., 2005; Lourens et al., 2011; Malakan et al., 2018). The atmospheric lifetime of H_2S is longer than SO_2 (Seinfeld and Pandis, 2016), but it can ultimately also result in SO_4^{2-} formation, via oxidation of SO_2. Seinfeld and Pandis (2016) reported global SO_2 and SO_4^{2-} emission estimates to be 56.3 and 2.2 Tg(S)/yr from fossil fuel combustion and industry, 1.3 and 0.1 Tg(S)/yr from biomass burning, and 6.6 and 2-4 Tg(S)/yr from volcanoes, while only the SO_4^{2-} emissions were estimated to be between 40 and 320 Tg(S)/yr from oceans and 2-4 Tg(S)/yr from plants and soils.

NO_x can be emitted from natural or anthropogenic sources. Natural sources include biogenic emissions and open biomass burning (if not anthropogenic), while the anthropogenic sources include biomass burning (both household combustion and anthropogenic open biomass

burning), fossil fuel combustion (e.g. coal-fired power stations, traffic emissions) (Niu et al., 2016; Lv et al., 2018; Sun et al., 2018) and vehicle emissions (Lourens et al., 2012; Lourens et al., 2016).

In general, the emissions of S- and N-containing species are relatively high in South Africa, since most of the local industries do de-SO_x or de-NO_x their process off-gas, as is common in first-world countries (Beukes et al., 2013a). The South African platinum industry is the exception, since it has implemented de-SO_x technology (Jacobs, 2006). Since a significant fraction of both SO_4^{2-} and NO_3^- is secondarily formed, long-range transport can also be a significant source at regional background sites (Vakkari et al., 2013; Liu et al., 2017).

As mentioned in the previous section, NH_4^+ is formed from NH_3 emissions. The main sources of NH_3 include industrial production of fertiliser (Brasseur et al., 1999; Van Loon and Duffy, 2005; Seinfeld and Pandis, 2016), petrochemical plants, ammonification of humus (i.e. decomposition of leaves and plant material by microorganisms) (Seinfeld and Pandis, 2016), agricultural activities, bacterial decomposition in nitrogen-based fertiliser mixed with soils (Schlesinger and Hartley, 1992; Kumar et al., 2018), wild fires and wood use for household combustion (Delmas et al., 1995; Brocard et al., 1996).

The marine environment is the main source for chloride (Cl^-) and sodium (Na^+) and also a significant source of Mg^{2+} (Li et al., 2014a; Conradie et al., 2016; Szép et al., 2018). In addition to the marine origin, Cl^- and Na^+ can also originate from other sources. Wan et al. (2016) found that these ions at Lhasa (China) in winter originated mainly from biomass burning. The results from Kumar et al. (2018) indicated Cl^- levels in New Delhi were from open biomass burning and burning of plastic waste as fuel in industrial and domestic activities. According to Liu et al. (2017), higher concentrations of Cl^- and Na^+ were measured during winter at an urban Beijing site and possible sources were identified as coal combustion and biomass burning, while Zhao and Gao (2008) indicated Cl^- (fine fraction) to be primarily from coal combustion in winter. Li et al. (2010) and Liu et al. (2017) indicated that potassium (K^+) concentrations decreased in winter along with the higher concentrations of Cl^- and Na^+, and therefore coal combustion was named the primary source of Cl^- and Na^+ emissions in these two studies.

Andreae et al. (1998), Wan et al. (2016), Liu et al. (2017) and Kumar et al. (2018) reported that K^+ in the fine fraction was emitted from biomass burning. In contrast, Wan et al. (2016) and Kumar et al. (2018) proposed that K^+ in the coarse fraction originated from crustal sources, while Shen et al. (2009) and Liu et al. (2017) both found it to be emitted from marine sources, in addition to the crustal origin. More recently, Aurela et al. (2016) found that K^+ in fresh biomass burning plumes formed KCl (Gao et al., 2003; Li et al., 2003). The concentrations of the total dissociated organic acids, together with K^+ and Cl^- were also used as an indicator for biomass

burning contribution in Conradie et al. (2016). Within Indian and Asian contexts, high particulate SO_4^{2-} and K^+ are often indicative of firework emissions (Cao et al., 2017).

According to Zhiliang et al. (1987), F^- is emitted in China by the metallurgical industry (e.g. aluminium and iron smelters), while in India it is emitted from industries producing aluminium from alumina by using cryolite (tri-sodium hexafluoro-aluminate, Na_3AlF_6) as a flux (Susheela et al., 2013). Kumar et al. (2018) stated that, in New Delhi, F^- is mainly emitted by the brick kiln industry, with a smaller contribution from coal combustion.

Mg^{2+} and Ca^{2+} could be from marine sources, terrigenous contribution, or elements in fly ash (Liu et al., 2017) emitted by pyro-metallurgical smelters (Mahlaba et al., 2011). The terrigenous contribution to the aerosol loading in South Africa is significant, since it is a semi-arid country. Kumar et al. (2018) reported Mg^{2+} and Ca^{2+} to be from heavy dust storms, while Wan et al. (2016) and Liu et al. (2017) stated that Ca^{2+} was primarily from dust sources (i.e. crustal materials such as calcite and dolomite, $CaCO_3$ and $CaMg(CO_3)_2$, respectively). Zhou et al. (2018) stated that a mixture of Ca^{2+} and Na^+ was primarily from crustal species and construction materials in Baotou, China.

Niu et al. (2018) indicated primary and/or secondary sources to be the origin of organic acids. Primary sources consist of direct vehicle emissions, marine and vegetation (Kawamura et al., 1985; Graedel and Eisner, 1988), while secondary sources consist of photochemical formation of organic acids (Bothe and Donahue, 2010; Gu et al., 2014; Niu et al., 2018). Niu et al. (2018) stated that CHOOH, CH_3COOH and $(COOH)_2$ combined accounted for more than 90.0% of the total atmospheric organic acid load, while Kawamura et al. (1985) indicated CH_3COOH as the main organic acid in the atmosphere, followed by CHOOH and C_2H_5COOH. The primary source of CHOOH and CH_3COOH, indicated by Kawamura et al. (1985), was used engine oil. Niu et al. (2018) and Keene and Galloway (1986a) found CHOOH and CH_3COOH to originate from primary biogenic sources. Lazaridis et al. (2008) and Gonçalves et al. (2017) indicated primary sources of organic acids (i.e. malonic- and succinic acids, $CH_2(COOH)_2$ and $(CH_2)_2(CO_2H)_2$, respectively) to be vehicular emissions, biomass burning and biogenic emissions. The study of Mochizuki et al. (2017) presented a more detailed description of the secondary formation of different organic acids, but also stated that CHOOH and CH_3COOH were formed in the atmosphere by photo-oxidation of biogenic volatile organic compounds (BVOCs), while $(COOH)_2$ was attained from biogenic, as well as anthropogenic VOCs.

3.1.4 Water-soluble inorganic ions and organic acids in southern and South Africa

As stated in section 2.1.5, South Africa is an important source region of atmospheric pollutant species. South Africa is the economic and industrial hub of southern Africa, which includes several large anthropogenic point sources (section 2.1.5) such as large coal-fired power stations (Mphepya et al., 2004; Collett et al., 2010; Lourens et al., 2011; Beukes et al., 2013a;

Pretorius et al., 2015; Chiloane et al., 2017; Venter et al., 2017), petrochemical operations (Lourens et al., 2011; Chiloane et al., 2017) and pyro-metallurgical smelters (Barcza, 1995; Roos, 2011; Kleynhans et al., 2016). Not many of these large point sources de-SO_x and de-NO_x their process off-gas, which leads to elevated atmospheric SO_4^{2-} and NO_3^- levels (Dhammapala, 1996; Engelbrecht, 2009; Conradie et al., 2016). In addition, contributing sources include household combustion of coal and wood for space heating and cooking by a large part of the population living in semi- and informal settlements in South Africa (Venter et al., 2012; Van Zyl et al., 2014; Hersey et al., 2015; Giannakaki et al., 2016; Nkosi et al., 2018). Emissions from vehicle transport in South Africa will contribute to the elevated levels of certain ions in the atmosphere (Kawamura et al., 1985; Conradie et al., 2016; Niu et al., 2018), especially since the South African vehicular fleet is relatively old (with a significant fraction of older technology) and not as well maintained as is common in first-world countries (Lourens et al., 2012; Lourens et al., 2016). Biomass burning also contributes significantly to elevated levels of atmospheric aerosols (Formenti et al., 2003; Mafusire et al., 2016; Vakkari et al., 2018), with specifically the organic (Tiitta et al., 2014) and K^+ (associated with Cl^-) aerosol contents increasing as a result thereof (Aurela et al., 2016). NH_4^+ from agricultural activities is important (Conradie et al., 2016; Sun et al., 2017; Nanus et al., 2018) and PM_1 chemical analysis by Tiitta et al. (2014) also indicated that industrial processes (e.g. petrochemical and chemical industries) are also likely to be a significant source for this species. Conradie et al. (2016) studied precipitation samples at the same sampling sites that were considered in this study and indicated that terrigenous and marine sources contributed significantly to the ionic species found in South African rainwater. Therefore, these sources will also be investigated in this study as possible sources.

According to reports on air quality in South Africa, exceedances of $PM_{2.5}$ and PM_{10} associated standard limits are frequent in many regions in South Africa (SAAQIS, 2018). South Africa is also the country with the highest frequency of new secondary aerosol formation and the highest growth rate of these newly formed aerosols (Nieminen et al., 2018). As was indicated in the preceding paragraphs, many possible sources could contribute to these observations. Notwithstanding the afore-mentioned, there are only a few published studies on aerosol composition for South Africa. Tiitta et al. (2014) used an Aerosol Chemical Speciation Monitor (ACSM) to measure and report the chemical composition of PM_1 aerosols at Welgegund, which included NO_3^-, Cl^-, SO_4^{2-}, organic aerosols and NH_4^+. Aurela et al. (2016) presented very limited data of inorganic water-soluble ions, OC and EC, as well as monosaccharide anhydrides, which was derived from samples collected over 14 days during 2007 and 2008 at a regional background site (i.e. Botsalano). This study (Aurela et al., 2016) also presented the composition of two samples (one measured for 44 and the other for 124 minutes) collected in fresh biomass burning plumes. In addition, water-soluble inorganic ionic aerosol species (i.e. SO_4^{2-}, NO_3^-, NH_4^+, Na^+, K^+, Cl^-, Ca^{2+}, Mg^{2+}, F^-) were reported for a one-year sampling campaign at Welgegund in the PM_1, $PM_{1\text{-}2.5}$ and $PM_{2.5\text{-}10}$ size fractions and for one year at Marikana (except

F^-) in the $PM_{2.5}$ and $PM_{2.5-10}$ size fractions (Venter et al., 2018a). Other studies such as Mphepya et al. (2004 and 2006) and Conradie et al. (2016) focused only on water-soluble species in precipitation samples. In addition to the South African work, some results have been published from studies conducted in southern Africa. Formenti et al. (2003) reported on a limited number of filter measurements collected during SAFARI 2000 on board an aircraft in a smoke haze layer over the Atlantic Ocean (offshore from Namibia and Angola) for which water-soluble inorganic ions (except F^- and organic acids) were reported. Limited aerosol composition measurements (two-week sampling period during the wet season and 12 days during the dry season) were also presented for Morogoro, Tanzania (Mkoma et al., 2013), which indicated the concentrations of water-soluble inorganic ions (except F^-). All the afore-mentioned studies related to South and southern Africa (Formenti et al., 2003; Mkoma et al., 2013; Tiitta et al., 2014; Aurela et al., 2016) will be discussed in greater detail within the context of results presented later in this chapter.

3.1.5 Literature conclusions

Considering the paucity of published literature related to aerosol chemistry in South Africa and more specifically on water-soluble inorganic ions and organic acids, it is evident that more such research is needed. Therefore, if the goals set out in Objective 2 (section 1.2) are achieved, this study will make a significant contribution to very relevant science. In order to accomplish this, samples collected during a long-term sampling campaign at four sites in the South African interior were analysed for water-soluble inorganic ions and organic acids. These results were explored in terms of spatial and temporal patterns, acidity and neutralisation, statistical evaluation, as well as possible source contributions.

3.2 Experimental

3.2.1 Sampling sites, filter preparation and sampling

Aerosol samples were collected at four different sampling sites in the northern interior of South Africa, operated within the Deposition of Biogeochemical Important Trace Species (DEBITS), International Network to study Deposition and Atmospheric chemistry in Africa (INDAAF) project (Galy-Lacaux et al., 2003; Martins et al., 2007), which is endorsed by the International Global Atmospheric Chemistry (IGAC) programme and the World Meteorological Organisation (WMO). A detailed description of the sampling sites (i.e. Vaal Triangle (VT), Amersfoort (AF), Skukuza (SK) and Louis Trichardt (LT)) was presented in section 2.2.1, therefore it is not repeated here again.

24-hour $PM_{2.5}$ and PM_{10} aerosol samples were collected on Teflon filters (with a deposit area of 12.56 cm^2). It was collected once a month from March 2009 to December 2015 at each of the

four sites for both size fractions. A total of 656 samples were collected for both $PM_{2.5}$ and PM_{10}, i.e. 164 samples per site.

Before sampling, the Teflon filters were inspected for any flaws, while wearing surgical gloves and using tweezers. After this, the filters were weighed with a Mettler Toledo scale (XS1005 DualRange) that was calibrated and accredited by SANAS. Afterwards the filter were placed into airtight Petri dishes and stored in a conventional refrigerator until sampling.

The Teflon filters were placed in a MiniVol sampler for sampling. These samplers were developed by the United States Environmental Protection Agency (US-EPA) and the Lane Regional Air Pollution Authority (Baldauf et al., 2001). The samplers were equipped with a pump, which was controlled by a programmable timer. This allows samples to be collected at a constant flow rate over a pre-determined time period. All samples in this study were collected at a flow rate of 5 L/min, which were verified by a handheld flow meter that was supplied with the MiniVol samplers.

After sampling, the Teflon filters were placed back into the same Petri dishes in which they were stored before. These holders were then sealed off, bagged and stored in a portable refrigerator for transport to the laboratory. At the laboratory, the sealed filters were stored in a conventional refrigerator until analysis.

Before analysis, all the filters were weighed again with the Mettler Toledo scale. The water-soluble ions were extracted by placing each filter into a pre-marked and clean Teflon cup with 10 ml deionised water (resistivity 18.2 MΩ/cm). The cups were sealed with lid and placed into a sonic bath for 30 minutes. After this, the water in each cup was poured into a pre-marked vile and analysed with an ion chromatograph (IC).

3.2.2 Ion Chromatograph (IC) analysis

A Dionex ICS-3000 IC system with two flow lines was utilised. The one flow line was used for the detection of anions and the other for cations. Water-soluble anions quantified were acetic- (CH_3COO^-), formic- (COO^-), propionic- ($C_2H_5COO^-$) and oxalic acid ($C_2O_4^{2-}$), as well as fluoride (F^-), chloride (Cl^-), sulphate (SO_4^{2-}) and nitrate (NO_3^-). The anion flow line was equipped with a 4 mm AS 15 analytical column, 4 mm AG 15 guard columns, a 4 mm CRD 200 carbonate removal device and an AERS (Anion Electrolytically Regenerated Suppressor) 500 4 mm suppressor. A multiple-step eluent program was employed and potassium hydroxide (KOH) was used as an eluent. Firstly, the eluent concentration was kept constant at 5 mM for 14 minutes, after which it was raised to 35 mM during a two-minute period. The eluent concentration was then kept constant at 35 mM for 18.5 minutes, after which it was reduced to 5 mM during a two-minute period and kept constant for 2.5 minutes. This eluent concentration profile ensured minimum analysis time, while enabling proper species peak separation. Throughout the 39-

minute program, the suppressor current was kept constant at 104 mA. A five-point calibration was performed with 0.1, 0.5, 1.0, 2.5 and 5.0 ppm standard solutions prepared from 1 000 ppm certified stock solutions obtained from Industrial Analytical. Analysis of the samples commenced only after the relative standard deviation of the calibration curve was below 5.0%. Detection limits (DLs) at a confidence level of 98.3% were determined according to the method presented by Skoog e5t al. (2014) for the various anionic species, as indicated in Table 3-1.

Water-soluble cations quantified were sodium (Na^+), ammonium (NH_4^+), potassium (K^+), magnesium (Mg^{2+}) and calcium (Ca^{2+}). The cation flow line was equipped with a CERS (Cation Electrolytically Regenerated Suppressor) 500 4 mm suppressor. A set of 3 mm CS-16 analytical column and 3 mm CG-16 guard column was fitted, and a constant methanesulphonic acid (MSA) eluent concentration of 25 mM was employed at a constant flow rate of 0.400 mL/min, while a suppressor current of 30 mA was applied. The program was set to run for 39 minutes per sample. A five-point calibration was also performed with 0.1, 0.5, 1.0, 2.5 and 5 ppm standard solutions prepared from 1 000 ppm certified stock solutions obtained from Industrial Analytical. The samples were only analysed after the relative standard deviation of the calibration curve was below 5.0%. Detection limits (DLs) at a confidence level of 98.3% were determined according to the method presented by Skoog et al. (2014) for the various cationic species, as indicated in Table 3-1.

Table 3-1: Detection limits (DLs) at a confidence level of 98.3% in ppb (i.e. µg/L) and µg/m^3 for the water-soluble ion species analysed with the IC

Inorganic ions	DLs (ppb)	DLs (µg/m^3)
NO_3^-	52.6	52600
Cl^-	17.5	17500
SO_4^{2-}	5.7	5700
F^-	10.7	10700
Na^+	33.6	33600
NH_4^+	20.1	20100
K^+	27.2	27200
Mg^{2+}	21.0	21000
Ca^{2+}	18.7	18700
Organic acids (OA):		
Acetic acid (CH_3COO^-)	28.1	28100
Formic acid (COO^-)	18.2	18200
Propionic acid ($C_2H_5COO^-$)	15.7	15700
Oxalic acid ($C_2O_4^{2-}$)	17.2	17200

3.2.3 Ancillary data and data processing

As indicated in section 2.2.4, 96-hour backward trajectories were calculated for each sampling hour, and overlay back trajectory figures were generated with Matlab.

3.2.4 Empirical calculations and statistical evaluations

The anionic and cationic species quantified with the IC in parts per billion (ppb) ($\frac{(\mu g)}{L}$) and were converted to mass concentration in microgram per cubic meter $\left(\frac{\mu g}{m^3}\right)$, as well as micro-equivalents per litre $(\mu Eq/L)$ by using Table 3-2, as well as Equations 3-1 to 3-3.

Table 3-2 shows the molar mass (M) (g/mol) and the equivalent weight of the different ionic species ($Eq.wt$) (g/mol).

Table 3-2: The molar mass (M) (g/mol) and equivalent weight (Eq.wt.) for all the ionic species

Ionic species	Molar Mass (M) (g/mol)	Equivalent weight (Eq.wt.) (g/mol)
Na^+	22.99	22.99
NH_4^+	18.05	18.05
K^+	39.10	39.10
Mg^{2+}	24.31	12.16
Ca^{2+}	40.08	20.04
NO_3^-	62.00	62.00
Cl^-	35.45	35.45
SO_4^{2-}	96.06	48.03
$COOH^-$	45.02	45.02
CH_3COO^-	59.04	59.04
$C_2H_5COO^-$	73.07	73.07
$C_2O_4^{2-}$	88.02	44.01

In Equation 3-1 the mass concentration is $(\mu g/m^3)$, the parts per billion (ppb) ($\frac{\mu g}{L}$) and the volume air is m^3. The value $0.01L$ is the amount of deionised water the sample was sonicated in for 10 minutes. Equation 3-2, the $Eq.wt$ is the equivalent weight (g/mol) (Table 3-2), M is the molar mass (g/mol) (Table 3-2) and n is the ionic charge. In Equation 3-3, c is the ion concentration (µg/L that is also ppb).

$$\frac{(\mu g)}{m^3} = \frac{\frac{(\mu g)}{L} x\ 0.01L}{Volume\ air(m^3)} \qquad (3-1)$$

$$Eq.wt. = M/|\pm n| \qquad (3-2)$$

$$\frac{(\mu Eq)}{L} = \frac{c}{Eq.wt} \qquad (3-3)$$

In order to determine the ionic balance of samples extracted from the filters, the anionic contributions (AE) in µEq/L (Equation 3-4), along with the cationic contribution (CE) in µEq/L (Equation 3-5) were required. The AE and CE were used to calculate the $total\ ionic\ load$ of each sample in µEq/L (Equation 3-6). After this, the ion difference percentage ($ID\%$) (Equation 3-7) was calculated. The AE included nitrate (NO_3^-), chloride (Cl^-), sulphate (SO_4^{2-}), fluoride (F^-), as well as dissociated oxalic- ($C_2O_4^{2-}$), acetic- (CH_3COO^-), formic- ($CHOO^-$) and propionic- ($C_2H_5COO^-$) acid. The CE included sodium (Na^+), ammonium (NH_4^+), potassium (K^+), magnesium (Mg^{2+}) and calcium (Ca^{2+}).

$$AE = \sum Anion\ concentrations \qquad (3-4)$$

$$CE = \sum Cation\ concentrations \qquad (3-5)$$

$$Total\ ionic\ load = AE + CE \qquad (3-6)$$

$$ID\% = \left|\left(\frac{(CE - AE)}{(CE + AE)}\right) \times 100\right| \qquad (3-7)$$

The neutralisation factor (NF) was calculated with Equation 3-8 to evaluate the neutralisation ability of the base cations (X) (i.e. Mg^{2+}, Ca^{2+} and NH_4^+) on the main inorganic acidic species (considered to be SO_4^{2-} and NO_3^-) in the aerosol sample (Laouali et al., 2012), while Equation 3-9 was used to evaluate the neutralisation ability of the afore-mentioned base cations on the main inorganic acidic species and dissociated OA (SO_4^{2-}, NO_3^- and dissociated OA).

$$(NF)_X = {}^{X}/_{(NO_3^- + SO_4^{2-})} \quad (3-8)$$

$$(NF)_X = {}^{X}/_{(NO_3^- + SO_4^{2-} + OA)} \quad (3-9)$$

The contributions of the sea-salt fractions (SSF) and non-sea-salt fractions (nSSF) were calculated for different ions (X) separately with Equations 3-10 (for SSF_X) and 3-11 (for $nSSF_X$). All Na^+ were assumed to be from sea salt, even though it was mentioned in section 3.1.3 that other sources could emit Na^+ and Cl^-. Southern Africa is surrounded by the Atlantic and Indian Oceans and oceans are therefore considered as the main sources of Na^+ and Cl^-. The SSF_X is the sea-salt fraction of element X (e.g. Cl^-, SO_4^{2-}, Mg^{2+}, Ca^{2+} and K^+), $nSSF_X$ is the non-sea-salt fraction of element X, $[Na^+]_{aerosol}$ is the sodium concentration in the aerosol sample (µEq/L), $[X/Na^+]_{seawater}$ is the ratio of element X concentration (µEq/L) to Na^+ concentration (µEq/L) in seawater (Keene et al., 1986b) (Table 3-6, section 3.3.5), and $[X]_{aerosol}$ is the concentration of element X in the aerosol sample (µEq/L).

$$SSF_X = [Na^+]_{aerosol} \times \left[{}^{X}/_{Na^+}\right]_{seawater} \quad (3-10)$$

$$nSSF_X = [X]_{aerosol} - \left([Na^+]_{aerosol} \times \left[{}^{X}/_{Na^+}\right]_{seawater}\right) = [X]_{aerosol} - SSF_X \quad (3-11)$$

Similar to Conradie et al. (2016) the SSFs values were used to indicate the marine contributions and since agricultural and biomass burning are large source contributions in southern Africa, NH_4^+ was used to suggest possible NH_4^+-associated contributions, which are not all from agricultural contributions, while OA for possible other sources (section3.1.3) that includes biomass burning contributions. SO_4^{2-} was also used as a reference ion for the anthropogenic activities in South Africa. To estimate the anthropogenic contributions, the $SSF_{(SO42-)}$ was subtracted from the determined SO_4^{2-} concentration values (µEq/L). The remaining SO_4^{2-} (i.e. $nSSF_{(SO42-)}$) is either from anthropogenic or terrigenous sources. Assuming that anthropogenic

SO_4^{2-} is in excess of that supplied by sea salt (i.e. $SSF_{(SO42-)}$) as mentioned and from terrigenous supplied by gypsum (i.e. the Ca^{2+} concentration), according to Delmas (1981), it was used as a reference element for continental crust, since Ca^{2+} is a common lithospheric component (Ding et al., 2013) and therefore subtracted from $nSSF_{(SO42-)}$ to indicate the anthropogenic part of SO_4^{2-} contributions ($[SO_4^{2-}]_{anthropogenic}$) (Equation 3-12) (as was also used by Conradie et al., 2016 and Mphepya et al., 2006). The terrigenous part of the SO_4^{2-} contribution ($[SO_4^{2-}]_{terrigenous}$) was calculated by counting $nSSF_{(Mg2+)}$, $nSSF_{(Ca2+)}$, $nSSF_{(K+)}$, $[Ca^{2+}]_{Continental\ crust}$ together (Equation 3-13) (used also by Mphepya et al., 2006). $[SO_4^{2-}]_{nSSF}$ is the non-sea-salt fraction of the SO_4^{2-} concentration (µEq/L), $[Ca^{2+}]_{nSSF}$ is the non-sea-salt fraction of the Ca^{2+} concentration (µEq/L), $[Mg^{2+}]_{nSSF}$ is the non-sea-salt fraction of the Mg^{2+} concentration (µEq/L), and $[K^+]_{nSSF}$ is the non-sea-salt fraction of the K^+ concentration (µEq/L).

$$[SO_4^{2-}]_{anthropogenic} = [SO_4^{2-}]_{nSSF} - 0.47\,[Ca^{2+}]_{nSSF} = [SO_4^{2-}]_{nSSF} - [Ca^{2+}]_{Continental\ crust} \quad (3-12)$$

$$[SO_4^{2-}]_{terrigenous} = [Mg^{2+}]_{nSSF} + [Ca^{2+}]_{nSSF} + [K^+]_{nSSF} + \left([SO_4^{2-}]_{nSSF} - [SO_4^{2-}]_{anthropogenic}\right) = [Mg^{2+}]_{nSSF} + [Ca^{2+}]_{nSSF} + [K^+]_{nSSF} + [Ca^{2+}]_{Continental\ crust} \quad (3-13)$$

The fossil fuel use contribution was calculated with Equation 3-14. $[NO_3^-]_{nSSF}$ is the non-sea-salt fraction of the NO_3^- concentration (µEq/L).

$$Fossil\ fuel\ use\ contribution = [NO_3^-]_{nSSF} + [SO_4^{2-}]_{anthropogenic} \quad (3-14)$$

Principal component analysis (PCA) is often used to indicate the possible sources of different ions (e.g. Conradie et al., 2016; Kumar et al., 2018; and Zhang et al., 2018). The dataset, of all

the ions in both size fractions and all the sites, was submitted to a Box-Cox transformation. Although there is no limit to the amount of factors that may be used and kept, it is recommended that only factors that are meaningful or with significant eigenvalues should be considered (Hosiokangas et al., 1999; Conradie et al., 2016). Only principal components that had eigenvalues higher than 1 were inspected, after which Varimax rotation followed. Three principal components were considered for all the sites in both size fractions, except for the $PM_{2.5}$ size fraction at LT that had two meaningful principal components. Some of the components identified represented more than one source type, while others only indicated a single source type.

3.3 Results and discussion

3.3.1 Contextualisation of concentrations

Considering that PM_{10} includes the $PM_{2.5}$ size fraction, $PM_{2.5}$ mass concentrations were subtracted from PM_{10} to determine the $PM_{2.5-10}$ size fraction concentrations. Table 3-3 presents the average mass concentrations of water-soluble ions in the $PM_{2.5}$ and $PM_{2.5-10}$ size fractions for the entire sampling period for all the measurement sites, as well as concentrations obtained at African and other international sites.

Table 3-3: $PM_{2.5}$ mean mass concentrations (µg/m^3) of particulate matter samples collected at the four South African INDAAF sites (i.e. VT, AF, SK, LT), compared to published $PM_{2.5}$ mean/median mass concentrations (µg/m^3) of particulate matter samples collected at various international locations

Source	Date	Place	Site	Mean/Median (µg/m^3)	NO_3^-	Cl^-	SO_4^{2-}	F^-	OA	Na^+	NH_4^+	K^+	Mg^{2+}	Ca^{2+}
This study	03/2009 -12/2015	Vaal Triangle	Grassland biome, Industrialised, Traffic, Household combustion	Mean $PM_{2.5}$	0.88	0.54	3.80	0.39	2.12	0.37	1.68	0.53	0.47	0.52
				Mean $PM_{2.5-10}$	0.67	0.22	0.89	0.07	0.94	0.26	0.31	0.09	0.18	0.31
		Amersfoort	Grassland biome in NO_2 hotspot	Mean $PM_{2.5}$	0.35	0.46	2.88	0.41	2.03	0.74	1.00	0.59	0.47	1.09
				Mean $PM_{2.5-10}$	0.35	0.28	0.75	0.08	0.63	0.25	0.23	0.10	0.22	0.23
		Skukuza	Savannah biome, background site	Mean $PM_{2.5}$	0.875	1.83	2.25	0.39	1.54	0.63	0.80	0.45	0.59	0.71
				Mean $PM_{2.5-10}$	0.42	0.64	0.61	0.06	0.35	0.59	0.15	0.18	0.18	0.28
		Louis Trichardt	Savannah biome, agricultural, background site	Mean $PM_{2.5}$	0.38	0.45	2.10	0.31	1.57	0.35	0.69	0.42	0.42	0.54
				Mean $PM_{2.5-10}$	0.49	0.47	1.28	0.08	0.65	0.51	0.41	0.13	0.31	0.99
Africa														
Aurela et al. (2016)	9-15/10/2007 and 01-02/2008	Botsalano, South Africa	Background dry savannah	Mean PM_1	0.03	-	3.92	-	-	0.05	1.02	0.18	-	-
Tiitta et al. (2014)	09/2010-08/2011	Welgegund, South Africa	Grassland savannah, grazed by cattle and sheep	Mean PM_1	0.5	0.03	2.4	-	-	-	0.9	-	-	-
Venter et al. (2018a)	24/11/2010-28/12/2011	Welgegund, South Africa	Grassland savannah, grazed by cattle and sheep	Median PM_1	0.02	0.005	1.35	0.015		0.16	0.44	0.032	0.003	0.019
	11/2008-10/2009	Marikana, South Africa	Small residential area	Median $PM_{2.5}$	0.27	0.07	1.83			0.09	0.55	0.09	0.02	0.08
Formenti et al. (2003)	6-16/09/2000	Atlantic Ocean offshore Namibia/Angola	Aged smoke	Mean PM_1	1.02	0.03	1.98	-	-	0.19	0.91	0.61	0.013	0.051
				Mean $PM_{>1}$	1.181	0.045	1.155	-	-	0.149	0.51	0.313	0.051	0.152
			Fresh smoke	Mean PM_1	1.415	0.272	1.935	-	-		1.591	4.46	-	0.104
				Mean $PM_{>1}$	4.193	0.261	1.343	-	-	0.659	1.141	1.36	0.642	2.192
Mkoma et al. (2013)	05-06/2011 and 07-08/2011	Morogoro, Tanzania	Agricultural, livestock, domestic and forest fires	Mean $PM_{2.5}$ WS	0.06	0.06	0.21	-	-	0.32	0.21	0.39	0.09	0.06
				Mean $PM_{2.5}$ DS	0.18	0.08	0.26	-	-	0.62	0.93	1.54	0.079	0.297
Other international locations														
Shao et al. (2018)	12/2016 -01/2017	Beijing, China	Urban, industrial, traffic, heavy haze	Mean $PM_{2.5}$	29.09	4.07	20.93	-	-	0.58	15.44	1.40	0.23	0.69
Qiu et al. (2016)	03/2012-03/2013	Xi'an High, Tech Zone, China	Urban, residential	Mean $PM_{2.5}$	17.10	3.80	22.20	0.30	-	1.70	9.60	1.30	0.30	2.50
		Xi'an Jiaotong University, China	Residential, traffic	Mean $PM_{2.5}$	17.20	3.90	22.80	0.30	-	1.60	9.10	1.50	0.30	2.50
		Xi'an North Third Ring, China	Suburban, traffic	Mean $PM_{2.5}$	17.80	4.50	23.70	0.20	-	1.10	9.20	1.60	0.40	2.80
		Weinan, China	Urban, fertilizer factory, power plants	Mean $PM_{2.5}$	18.00	3.00	24.70	0.10	-	1.30	10.00	1.30	0.20	1.60
		Baoji, China	Traffic	Mean $PM_{2.5}$	14.80	2.30	19.80	0.10	-	1.20	7.50	0.90	0.20	1.30
		Qinling Mountains, China	Background site, affected by Xi'an emissions	Mean $PM_{2.5}$	14.80	1.70	19.30	0.20	-	1.50	7.20	1.00	0.20	1.10
Shakya et al. (2017)	02-04/2014 and 07-08/2014	Kathmandu Valley, Nepal	Urban basin, mountains and hills	Mean $PM_{2.5}$	0.49	0.58	6.38	0.07	-	0.23	3.30	0.91	0.14	3.65
Kumar and Raman (2016)	01/2012-12/2013	VVNP Bhopal, Central India	Lake and hill	Mean $PM_{2.5}$	3.02	1.46	3.35	0.35	-	0.96	2.07	0.98	0.18	0.77
Chuang et al. (2016a)	09/2014-01/2015	Taoyuan, Taiwan	Open area, close to airport, highways and industries	Mean $PM_{2.5}$	8.90	1.00	9.60	-	-	0.20	5.00	0.30	0.20	0.40
Jusino-Atresino et al. (2016)	08/2006-09/2006	Cape San Juan, Puerto Rico	Clean environment, close to Atlantic Ocean	Mean $PM_{2.5}$	0.06	0.58	0.50	0.01	-	0.63	0.16	0.03	0.09	0.10
Szigeti et al. (2015)	06/2010-05/2013	Széna Square, Budapest, Hungary	Urban, traffic	Mean $PM_{2.5}$	2.14	0.11	2.84	-	-	0.22	1.33	0.18	0.05	0.16
Gawhane et al. (2017)	04/2015-04/2016	Pune, India	Urban, industrial, traffic	Mean $PM_{2.5}$	0.98	3.42	4.80	-	-	1.98	0.51	0.47	0.28	0.51
Bressi et al. (2013)	09/2009-09/2010	Paris, France	Suburban	Mean $PM_{2.5}$	2.90	0.18	2.10	-	-	0.16	1.50	0.13	0.03	0.08
			Urban	Mean $PM_{2.5}$	2.90	0.19	2.00	-	-	0.18	1.40	0.12	0.03	0.12
			North East Rural	Mean $PM_{2.5}$	2.20	0.16	1.90	-	-	0.14	1.20	0.12	0.02	0.05
			North West Rural	Mean $PM_{2.5}$	2.60	0.18	1.90	-	-	0.16	1.30	0.11	0.03	0.06
			South Rural	Mean $PM_{2.5}$	2.20	0.14	1.80	-	-	0.13	1.20	0.10	0.02	0.04
Castro et al. (2018)	03/2006-03/2006	Tecámac University, Mexico	Suburban	Mean $PM_{3.2}$	1.81	0.73	3.42	-	-	-	1.09	0.97	0.23	1.08

By considering the combined $PM_{2.5}$ and $PM_{2.5-10}$ results from this study in isolation, it is evident from Table 3-3 that SO_4^{2-} concentrations were the highest of all the water-soluble species, at all four sites. Differences between the four measurement sites considered in this thesis are not discussed further here, since spatial distribution is considered in detail later (section 3.3.2).

As previously indicated (section 3.1.4), very few aerosol chemical analyses have been published for southern- and South Africa. By considering Table 3-3, it is evident that all the South African sites considered in this study had significantly higher $PM_{2.5}$ mean ionic concentrations than reported for Morogoro (Tanzania), which was mostly influenced by agriculture and livestock, as well as domestic and open biomass burning emissions (Mkoma et al., 2013). Although $PM_{2.5}$ cannot be directly compared to PM_1, Formenti et al. (2003) reported similar or even higher mean concentrations of most of the ionic species in open biomass burning plumes measured offshore from Namibia and Angola, than the $PM_{2.5}$ mean concentrations reported for VT, AF, SK and LT. This indicates the significant regional influence of large-scale open biomass burning in southern Africa, which is endemic in this region (Swap et al., 2003). Aurela et al. (2016) reported higher mean SO_4^{2-} in PM_1 aerosols measured at Botsolano, than what was found in $PM_{2.5}$ at the relatively polluted VT and AF. This is understandable, considering that Botsalano is frequently impacted by air masses that had passed over the western Bushveld Complex. Here, numerous platinum group metal (PGM) smelters occur that emit high concentrations of SO_2 (Jacobs, 2006), due to sulphide-rich ore being smelted (Xiao and Laplante, 2004b). The PM_1 mean SO_4^{2-} and NO_3^- reported by Tiitta et al. (2014) for Welgegund, a regional background site in South Africa, were in the same range as $PM_{2.5}$ concentrations found at all four the sites considered in this study. The total PM_1 organic aerosol content (which also included non-water-soluble species) at Welgegund (3.6 µg/m^3) was significantly higher than the $PM_{2.5}$ OA (i.e. organic acid) levels found at VT, AF, SK and LT (1.54–2.12 µg/m^3), but this can at least partially be explained since only the water-soluble organic acids (OA) were quantified in the current study. The median PM_1 at Welgegund reported by Venter et al. (2018a) for NO_3^-, Cl^-, SO_4^{2-} and NH_4^+, was much lower when compared to the same ions in the PM_1 mean (Tiitta et al., 2014) and in the $PM_{2.5}$ at all four sites of the current study. In contrast, the $PM_{2.5}$ median of NO_3^- for Marikana (Venter et al., 2018a) compared well with the $PM_{2.5}$ mean concentrations at AF and LT, while the $PM_{2.5}$ median for NH_4^+ (Venter et al., 2018a) was in the same range as for SK and LT.

The average $PM_{2.5}$ ionic concentrations of the background sites SK and LT were substantially higher than reported for a true international background site, i.e. Cape San Juan (Puerto Rico) (Table 3-3) (Jusino-Atresino et al., 2016), which indicates the regional impact of anthropogenic pollution and open biomass burning in the South African interior. Furthermore, although the NO_3^- (0.88 and 0.35 µg/m^3), SO_4^{2-} (3.80 and 2.88 µg/m^3) and NH_4^+ (1.68 and 1.00 µg/m^3) $PM_{2.5}$ concentrations at VT and AF were relatively high within an African context, these levels were

substantially lower than NO_3^- (14.80-29.09 µg/m^3), SO_4^{2-} (19.3-24.70 µg/m^3) and NH_4^+ (7.20-15.44 µg/m^3) $PM_{2.5}$ concentrations reported for severely polluted areas in China (Table 3-3 and references therein). SO_4^{2-} $PM_{2.5}$ concentrations at the regional background sites SK and LT (2.25 and 2.10 µg/m^3) were in the same range as reported for Paris (1.80 and 2.10 µg/m^3) (Table 3-3 and references therein), which again indicates the regional impact of anthropogenic pollution in South Africa. NH_4^+ $PM_{2.5}$ concentrations at VT and AF (1.68 and 1.00 µg/m^3) were similar to levels reported in Paris (1.20 and 1.50 µg/m^3) (Table 3-3 and references therein). However, the NO_3^- levels in Paris (2.20 and 2.90 µg/m^3) were higher than found for VT, AF, SK and LT (0.35-0.88 µg/m^3) (Table 3-3 and references therein), mostly likely due to the high traffic volumes in this large city.

Currently, there is no South African air quality standard limit for total and/or water-soluble ionic content of PM. However, the WHO (2014) does propose annual guideline limits for $PM_{2.5}$ and PM_{10} as 10 and 20µg/m^3, respectively. The total $PM_{2.5}$ water-soluble ionic concentrations, as presented in Table A-1 (Appendix A), exceed the afore-mentioned guidelines at VT (11.31 µg/m^3), AF (10.02 µg/m^3) and SK (10.06 µg/m^3), which indicates that the ionic content of $PM_{2.5}$ in South Africa requires attention in terms of possible air quality impacts.

3.3.2 Spatial distribution

Presented in Figure 3-1 and Figure 3-2 are box and whisker plots (indicating median, mean, 25th and 75th percentiles and ±2.7 x standard deviation) of the water-soluble ion and OA mass concentrations (µg/m^3) of $PM_{2.5}$ and $PM_{2.5-10}$, respectively, for all the sites considered in this study. Each of these figures is divided into two, i.e. the top graph (a) indicates the actual mass concentrations, while in the bottom graph (b) some of the species concentrations were multiplied with constants (indicated next to the species name on the x-axis) to make the concentration values more legible on the y-axis. Consistent multiplying constants were applied in both Figure 3-1 and Figure 3-2.

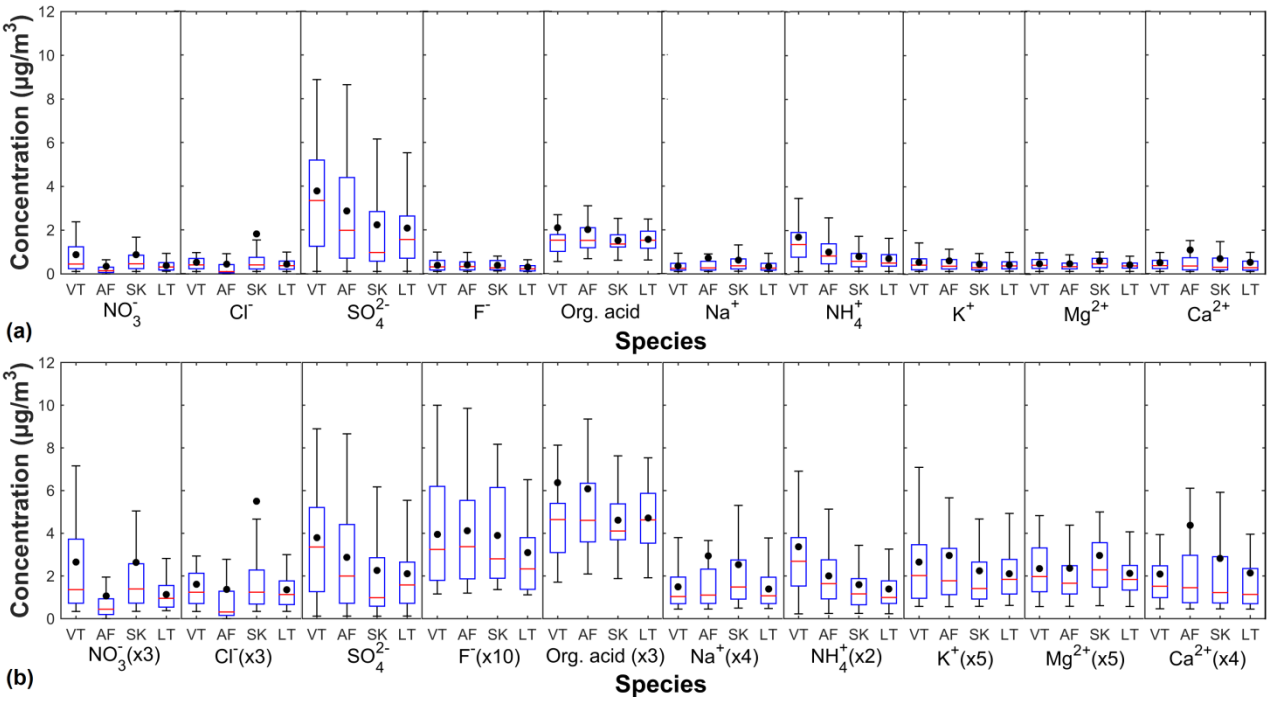

Figure 3-1: $PM_{2.5}$ mass concentrations (µg/m^3) of the water-soluble ions and OA for each of the INDAAF sites. The red line indicates the median, the black dot the mean, the top and bottom edges of the box the 25th and 75th percentiles and the whiskers the ±2.7 σ (99.3% coverage if the data have a normal distribution). Top graph (a) indicates the actual mass concentrations of the species, while the bottom graph (b) indicates the mass concentrations that were multiplied with constants (indicated next to the species name on the x-axis)

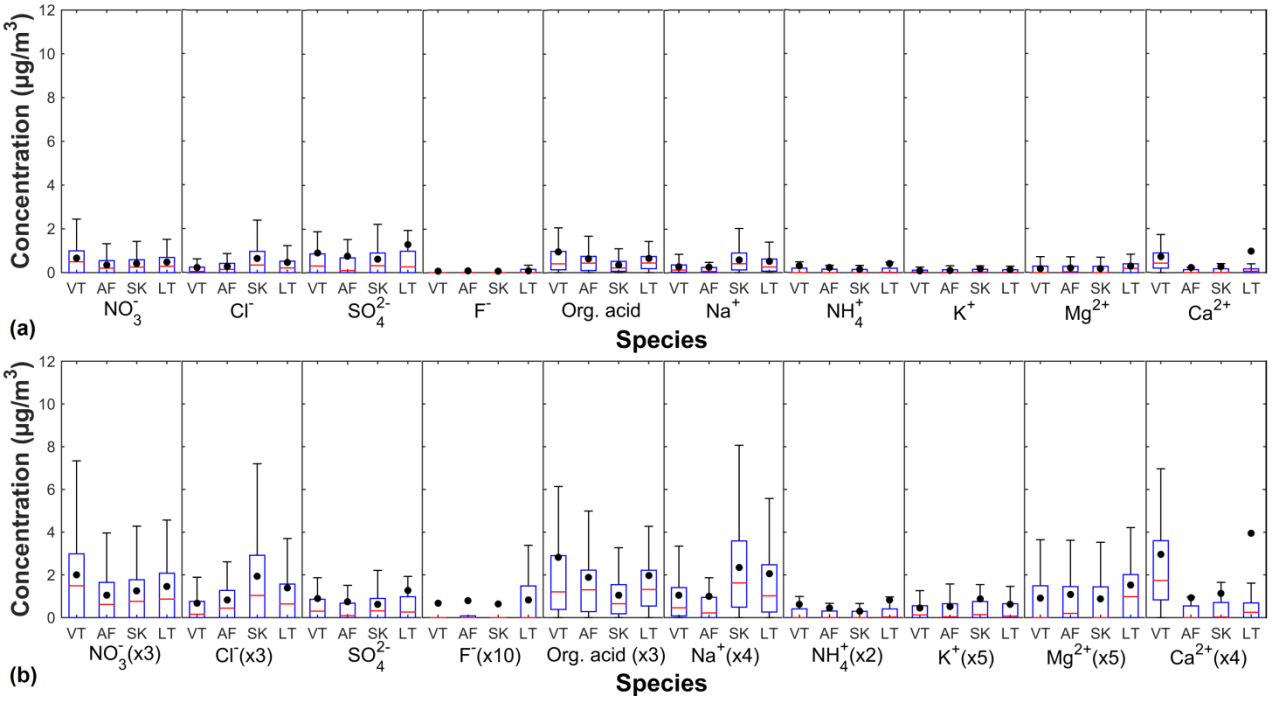

Figure 3-2: $PM_{2.5-10}$ mass concentrations (µg/m^3) of the water-soluble ions and OA for each of the INDAAF sites. The red line indicates the median, the black dot the mean, the top and bottom edges of the box the 25th and 75th percentiles and the whiskers the ±2.7 σ (99.3% coverage if the data have a normal distribution). Top graph (a) indicates the actual mass concentrations of the species, while the bottom graph (b) indicates the mass concentrations that were multiplied with constants (indicated next to the species name on the x-axis)

By comparing Figure 3-1a and Figure 3-2a, it is evident that a higher concentration of water-soluble ions occurred in the $PM_{2.5}$ than in the $PM_{2.5-10}$ size fraction. Moreover, in the $PM_{2.5}$ size fraction, SO_4^{2-} was the species with the highest concentration at all sites, while the organic acid

(OA) mass concentrations were 2nd highest. However, if total nitrogen (N) (determined from NO_3^- and NH_4^+) and total sulphur (S) (determined from SO_4^{2-}) are calculated (Table A-1, Appendix A), very similar N and S concentrations are found at each site. By considering the total water-soluble ionic concentration of both the size fractions (Table A-1, Appendix A), it is clear that aerosols at VT (15.25 µg/m^3) had the highest water-soluble ionic content, with AF (13.13 µg/m^3) and SK (13.52 µg/m^3) each with very similar levels, while LT (12.54 µg/m^3) had the lowest water-soluble ionic content. However, the relative contributions of the different species and size fractions varied at the different sites, as will subsequently be discussed.

Several studies indicate that SO_4^{2-} (as oxidation product of SO_2, and to a lesser degree from H_2S) and NO_3^- (as oxidation product of NO_x) in the South African interior mainly originate from industrial fossil fuel use (e.g. coal-fired power stations and petrochemical operations) and household combustion for space heating and cooking (Collett et al., 2010; Lourens et al., 2011; Venter et al., 2012; Pretorius et al., 2015). As previously stated, almost none of the industries in South Africa de-SO_x or de-NO_x their process off-gas (Beukes et al., 2013a) as is common in first-world countries, and therefore it is possible that these industrial sources are responsible for a significant fraction of the SO_4^{2-} and NO_3^- emissions. Open biomass burning (especially from August to middle October), biogenic emissions and traffic can also contribute significantly to NO_3^- levels (Lourens et al., 2012; Beukes et al., 2013a). Considering the variety of possible sources, SO_4^{2-} and NO_3^- levels are not always associated with one another. By comparing the average and/or median SO_4^{2-} concentrations at the different sites, it is evident that the VT had the highest concentrations, followed by AF, SK and LT. Aerosols at VT also had the highest average and/or median NO_3^- concentrations, notwithstanding that AF is situated in the well-known NO_2 hotspot identified with satellite measurements, while VT is situated on the edge of the afore-mentioned hotspot (Lourens et al., 2012). This indicates that emission heights of NO_3^- precursor species, which can be assumed to be mostly NO_x within the South African context, differ significantly between AF and VT. Most of the NO_x emissions in the Mpumalanga Highveld will be from industrial high-stack emissions (e.g. coal-fired power stations) (Pretorius et al., 2015), whereas, fractionally, a much greater proportion of NO_x emission will take place at ground level near VT, due to the larger population density there. Likely sources of such lower level emissions are traffic (Lourens et al., 2012), small industries and household combustion in semi- and informal settlements (Venter et al., 2012; Hersey et al., 2015; Nkosi et al., 2018). The comparison of the average and/or median NO_3^- concentrations at the different sites indicated that SK had the 2nd highest concentration, followed by AF and LT. Various reasons could contribute to lower NO_3^- levels at AF than SK, one of which are the high-stack emissions in the vicinity of AF, although the SO_4^{2-} is higher at AF than at SK. However, the atmospheric lifetime of SO_2 is generally shorter than NO_2 (Seinfeld and Pandis, 2016). Therefore, NO_3^- formation will take place over a wide area if compared to SO_4^{2-} formation.

By comparing the average and/or median NH_4^+ concentrations from Figure 3-1 and 3-2, it is evident that these levels are highest at VT, followed by AF, SK and LT. Fertilisers (an important possible source of NH_3) (Schlesinger and Hartley, 1992; Lian et al., 2018) are produced close to VT on a large scale and this site is also surrounded by more chemical-related industrial activities (Conradie et al., 2016) than AF and the other two sites, which explains the higher NH_4^+ levels. SK and LT are in the same concentration range and it can be expected that agricultural activities will make a contribution to NH_4^+ levels (Satsangi et al., 2013) at these sites, as well as open biomass burning (Paulot et al., 2017) and animal excrement (Schlesinger and Hartley, 1992).

According to Aurela et al. (2016), Cl^- and K^+ levels can be used as indicators of biomass burning influence, in addition to OA as indicated by Conradie et al. (2016). The OA correlation with acidity was used as indicative for biomass burning in Conradie et al. (2016) even though no seasonal cycle of OA was observed by the afore-mentioned authors. By comparing the average and/or median of Cl^-, K^+ and OA, in Figure 3-1, it is evident that the levels of the individual species were in the same range, except the Cl^- at AF that was a bit lower. It is therefore likely that open biomass burning is a possible source at all the sites.

Cl^- associated with Na^+ usually indicates a marine contribution (Conradie et al., 2016; Jusino-Atresino et al., 2016). In both size fractions (Figures 3-1 and 3-2), the Cl^- and Na^+ concentrations were the highest at SK, which is situated closest to the coast of the four sites considered, and therefore supports the notion that SK has a higher marine influence, if compared to the other three sites.

By comparing the average and/or median Mg^{2+} and Ca^{2+} concentrations, they seem to be in the same range at all the sites. Therefore, the results do not indicate whether fly ash (Mahlaba et al., 2011; Conradie et al., 2016), marine and/or terrigenous (Van Zyl et al., 2014; Conradie et al., 2016) sources dominate at the different sites.

In order to augment the concentration-based results presented in Figures 3-1 and 3-2, the mass fraction percentages (%) of the individual water-soluble ions and total organic acids determined for all four sites in the two size fractions, i.e. $PM_{2.5}$ and $PM_{2.5-10}$, are presented in Figures 3-3 and 3-4, respectively. Again, each of these figures indicates the actual mass fraction percentage (%) (graph a), as well as the results with some of the mass fraction percentages multiplied with constants (indicated next to the species name on the x-axis) to make the values more legible on the y-axis.

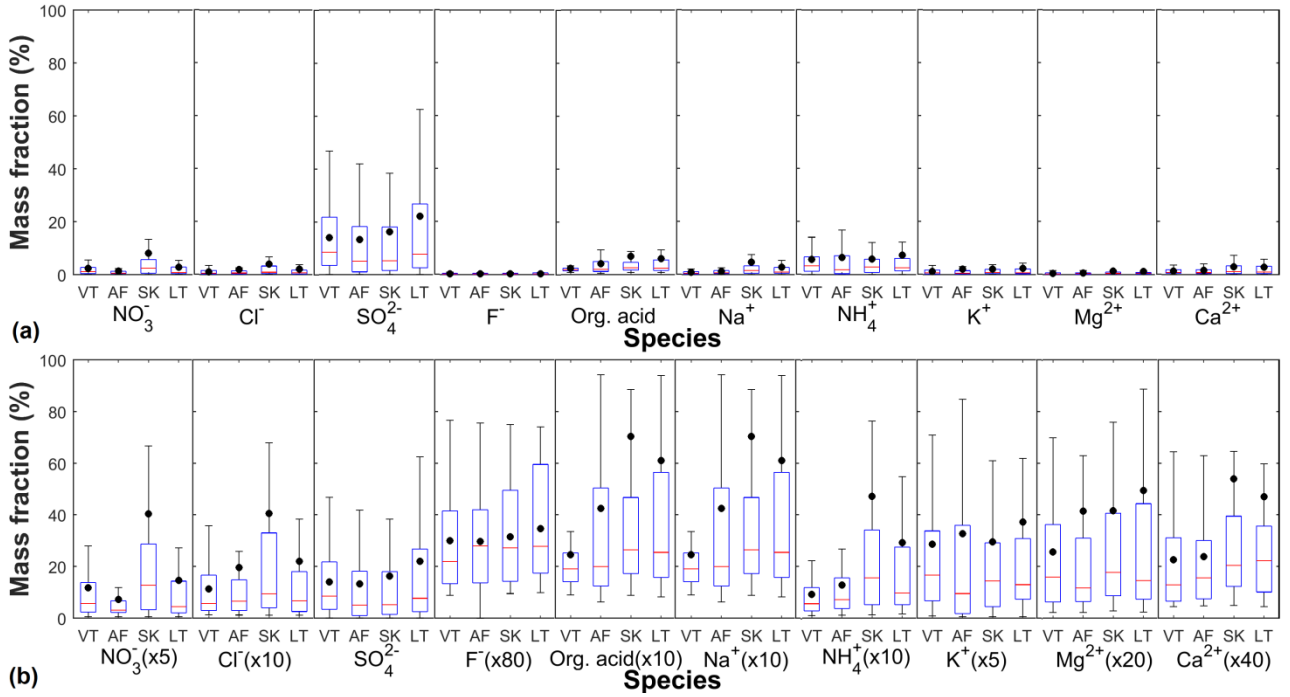

Figure 3-3: $PM_{2.5}$ mass fraction percentages (%) of the water-soluble ions and OA for each of the INDAAF sites. The red line indicates the median, the black dot the mean, the top and bottom edges of the box indicates the 25th and 75th percentiles and the whiskers the ±2.7 σ (99.3% coverage if the data have a normal distribution). Top graph (a) indicates the actual mass fraction percentages of the species, while the bottom graph (b) indicates the mass fraction percentages that were multiplied with constants (indicated next to the species name on the x-axis)

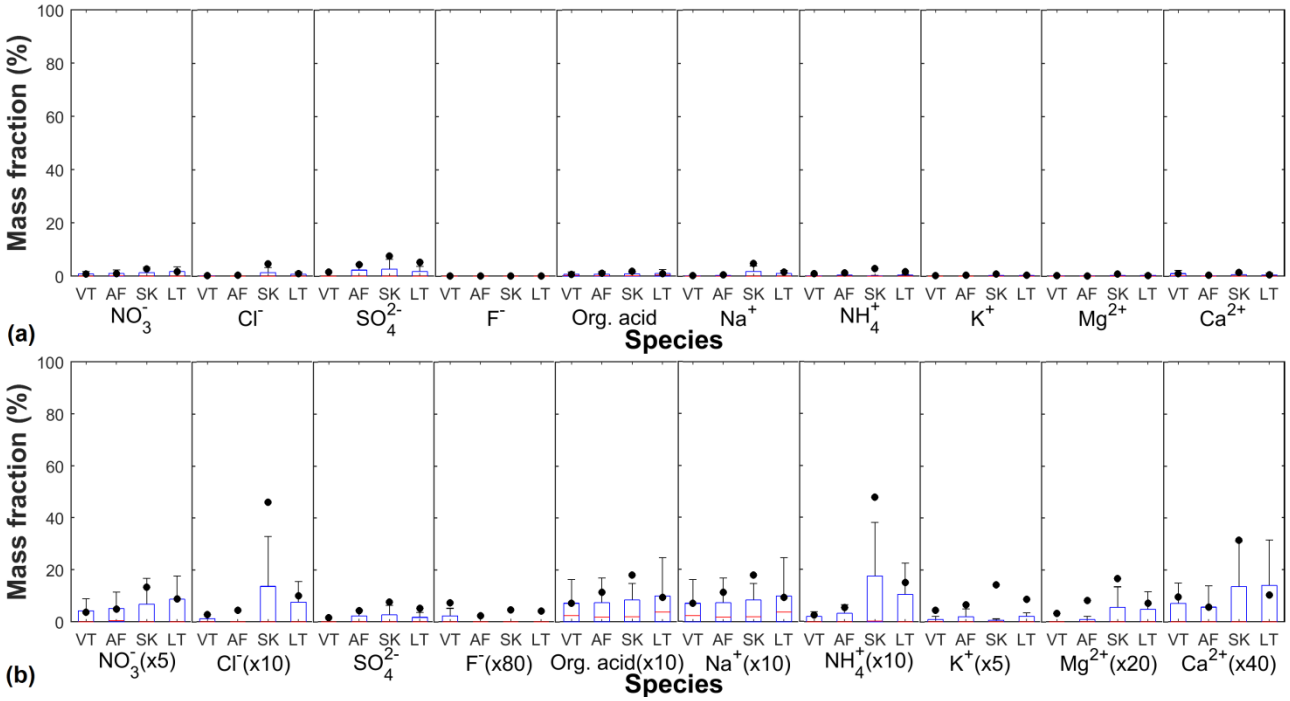

Figure 3-4: $PM_{2.5-10}$ mass fraction percentages (%) of the water-soluble ions and OA for each of the INDAAF sites. The red line indicates the median, the black dot the mean, the top and bottom edges of the box indicates the 25th and 75th percentiles and the whiskers the ±2.7 σ (99.3% coverage if the data have a normal distribution). Top graph (a) indicates the actual mass fraction percentages of the species, while the bottom graph (b) indicates the mass fraction percentages that were multiplied with constants (indicated next to the species name on the x-axis)

From Figures 3-3 and 3-4, it is obvious that SO_4^{2-} is the species with the highest fractional contribution of all the ionic species at all four sites considered. The mean mass fraction percentage

contribution of SO_4^{2-} for the four sites varied between 13.3 and 22.1%, while its median mass fraction percentage contribution varied between 5.2 and 8.6%. The mean ranges of $PM_{2.5}$ mass fraction for the other ions at all four sites were as follows: NO_3^- (1.4 and 8.1%), Cl^- (1.1 and 4.1%), F^- (approx. 0.4% for all sites), OA (2.5 and 7.0%), Na^+ (2.5 and 7.0%), NH_4^+ (0.9 and 4.7%), K^+ (5.7 and 7.4%), Mg^{2+} (1.3 and 2.1%) and Ca^{2+} (0.6 and 1.3%).

The significant mass fraction contribution of SO_4^{2-}, even at the background sites, again indicated the regional influence of anthropogenic emissions. As previously mentioned in Chapter 2, Conradie et al. (2016) also found that SO_4^{2-} was the dominant ion in rain water at the same sites (i.e. VT, AF, SK and LT) during the sampling period from 2009 to 2014. $SO_4^{2-}$was reported to be the dominant ionic species at Botsalano (Aurela et al., 2016) and Welgegund (Tiitta et al., 2014; Venter et al., 2018a), respectively. Aurela et al. (2016) and Tiitta et al. (2014) stated that the mean mass contributions of SO_4^{2-} were 44.0% at Botsalano and 33.0% of non-refractive PM_1 at Welgegund (27.0% if eBC is included in calculation). SK had the highest mean mass fractions for Cl^-, Na^+ and OA, with 4.1, 7.0 and 7.0%, respectively. This indicates the significant influences from marine and possible biomass burning sources at this site.

To contextualise the above-mentioned mass fraction percentages, some international references are considered. Shao et al. (2018) reported mass fractions of NO_3^- (i.e. 38.3%), SO_4^{2-} (i.e. 27.4%) and NH_4^+ (i.e. 21.7%) in the $PM_{2.5}$ fraction in Beijing. Kumar and Raman (2016) stated that the sum of SO_4^{2-}, NO_3^- and NH_4^+ contributed 61.0% to the total $PM_{2.5}$ ionic species in Bhopal (India), while Gawhane et al. (2017) reported that SO_4^{2-} (i.e. 13.0%) made the highest contribution in $PM_{2.5}$ in Pune (India). In Budapest, the ion with the highest mass fraction in summer was SO_4^{2-} with 21.5% (14.4% in the fall and 15.5% in spring), while NO_3^- was the ion with the highest mass percentage in winter, i.e. 13.0% (Szigeti et al., 2015). At five sites in Paris, the mass fraction percentages were between 17.0 and 22.0% for NO_3^-, 13.0 and 16.0% for nssSO_4^{2-}, 10.0 and 12.0% for NH_4^+, 2.0 and 5.0% for mineral dust and 3.0 and 4.0% for sea salt (Bressi et al., 2013), respectively. The dominance of NO_3^- over SO_4^{2-} percentages in a number of the afore-mentioned studies (Bressi et al., 2013; Szigeti et al., 2015; Gawhane et al., 2017) was attributed to traffic being the most significant source of precursors (NO_x), which is clearly not the case for the South African sites considered in this study. Parworth et al. (2015) reported 21.0% for NO_3^-, 12.0% for SO_4^{2-}, 9.4% for NH_4^+, 0.24% for Cl^-, 57.0% for organics at a background location in north-central Oklahoma, while Bressi et al. (2016) reported 58.0% of organics, 21.0% for NO_3^-, 12.0% for SO_4^{2-} and 8.0% of NH_4^+ at northwest of the Po Valley (i.e. background site) for the total non-refractive PM_1. Both these studies were measured with an ACSM instrument. For Cape San Juan, a true marine background site, Na^+ and Cl^- contributed 58.0% to the mean mass, which clearly indicates marine as the main source of ionic species (Jusino-Atresino et al., 2016). Therefore, although SK (and LT to a less degree) is significantly impacted by marine air masses, the fractional contribution thereof is not comparable to true marine background sites.

By considering Figures 3-1 and 3-2, as well as Figures 3-3 and 3-4, some deduction can already be made with regard to the distribution of the water-soluble ions and OA between the two different size fractions, i.e. $PM_{2.5}$ and $PM_{2.5-10}$. However, to enable proper assessment of this, Figure 3-5 presents the size distribution percentages (%) for each ion and OA, over the two size fractions for all the sites.

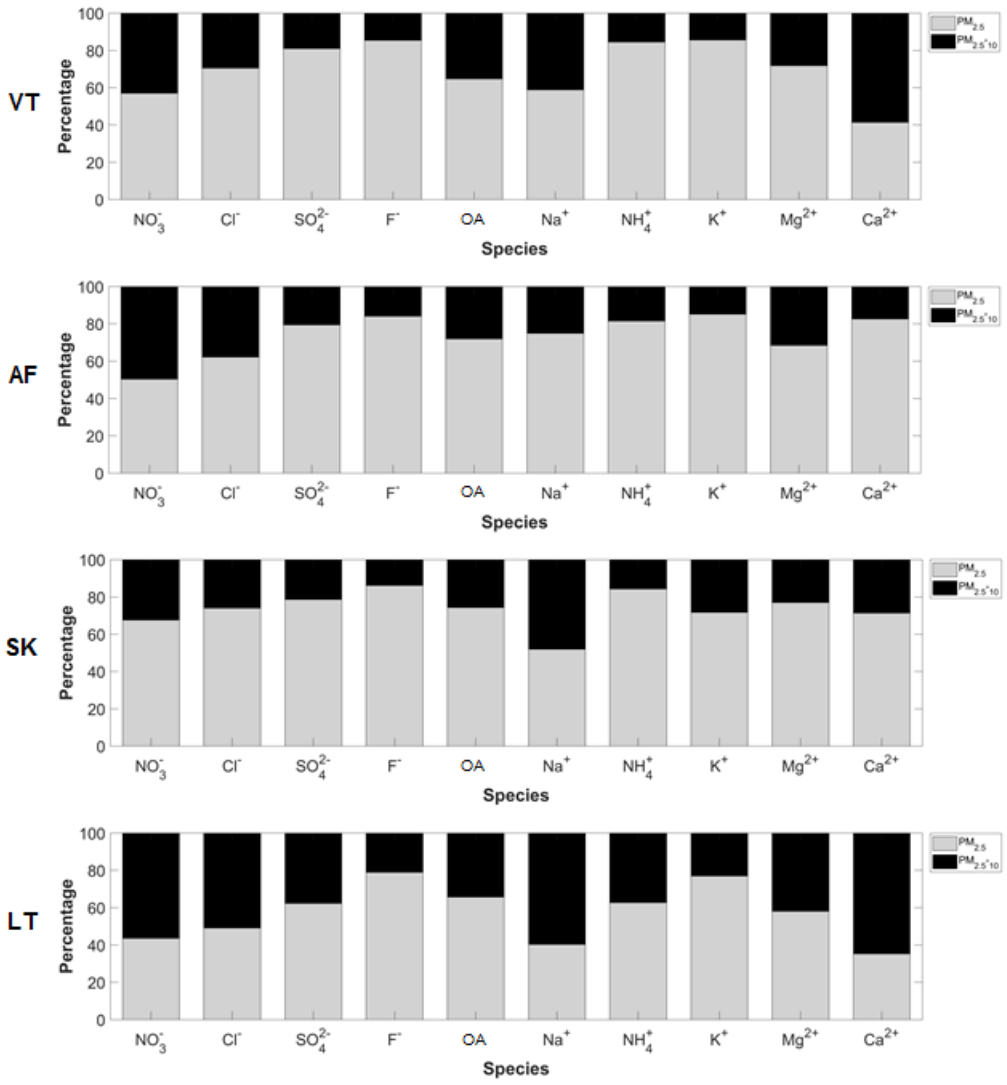

Figure 3-5: Size distribution of the water-soluble ionic species and OA for all four INDAAF sites

From Figure 3-5, it can be seen that most of the ions occur in the $PM_{2.5}$ size fraction at all sites. Seinfeld and Pandis (2006) defined two general size fractions to explain aerosol composition, i.e. PM_2 and $>PM_2$. PM_2 particles typically originate from primary emissions; condensation of secondary SO_4^{2-}, nitrate and organics from the gas phase; and coagulation of smaller particles. As is evident from Figure 3-5, SO_4^{2-} mainly occurred in $PM_{2.5}$ at all the sites, as expected (Seinfeld and Pandis, 2006). This is also in agreement with Venter et al. (2018a), who recently mentioned that SO_4^{2-} mainly occurred in the PM_1 size fraction at a regional background site in South Africa, i.e. Welgegund. However, a significant fraction of NO_3^- occurred in $PM_{2.5-10}$ (43.0%, 49.7%, 32.4% and 56.5%) for VT, AF, SK and LT, respectively, which indicates that the high SO_4^{2-} levels in the $PM_{2.5}$ size fraction result in substitution of NO_3^- in NH_4NO_3 to form

ammonium sulphate ($(NH_4)_2SO_4$). In addition, the higher NO_3^- in $PM_{2.5-10}$ suggests the influence of aged marine air masses, wherein NHO_3 reacts with some NaCl to form $NaNO_3$ and HCl (Turner and Colbeck, 2008). It is also obvious that SK and LT are influenced more by fresher marine air masses than the other sites, since Na^+ at these sites was significantly higher in the $PM_{2.5-10}$ size fraction. This was confirmed by overlay back trajectory figures (Figures 3-6a to d) that were compiled from back trajectories with arrival times coinciding with sampling times during the entire sampling period (March 2009 to December 2015). These figures clearly showed SK and LT being influenced more by marine air masses than VT and AF. In contrast, VT is influenced most by air masses that had passed over the surrounding industrial/developed/populated areas (including the Mpumalanga Highveld), as well as the Johannesburg-Pretoria megacity that is also significantly polluted (Lourens et al., 2012 and 2016). AF is mostly influenced by air masses that had passed over the surrounding Mpumalanga Highveld and the Vaal Triangle (where VT was situated). Detailed site descriptions, which include references to large point sources and the declaration of priority areas wherein VT and AF are located, were presented in section 2.2.1.

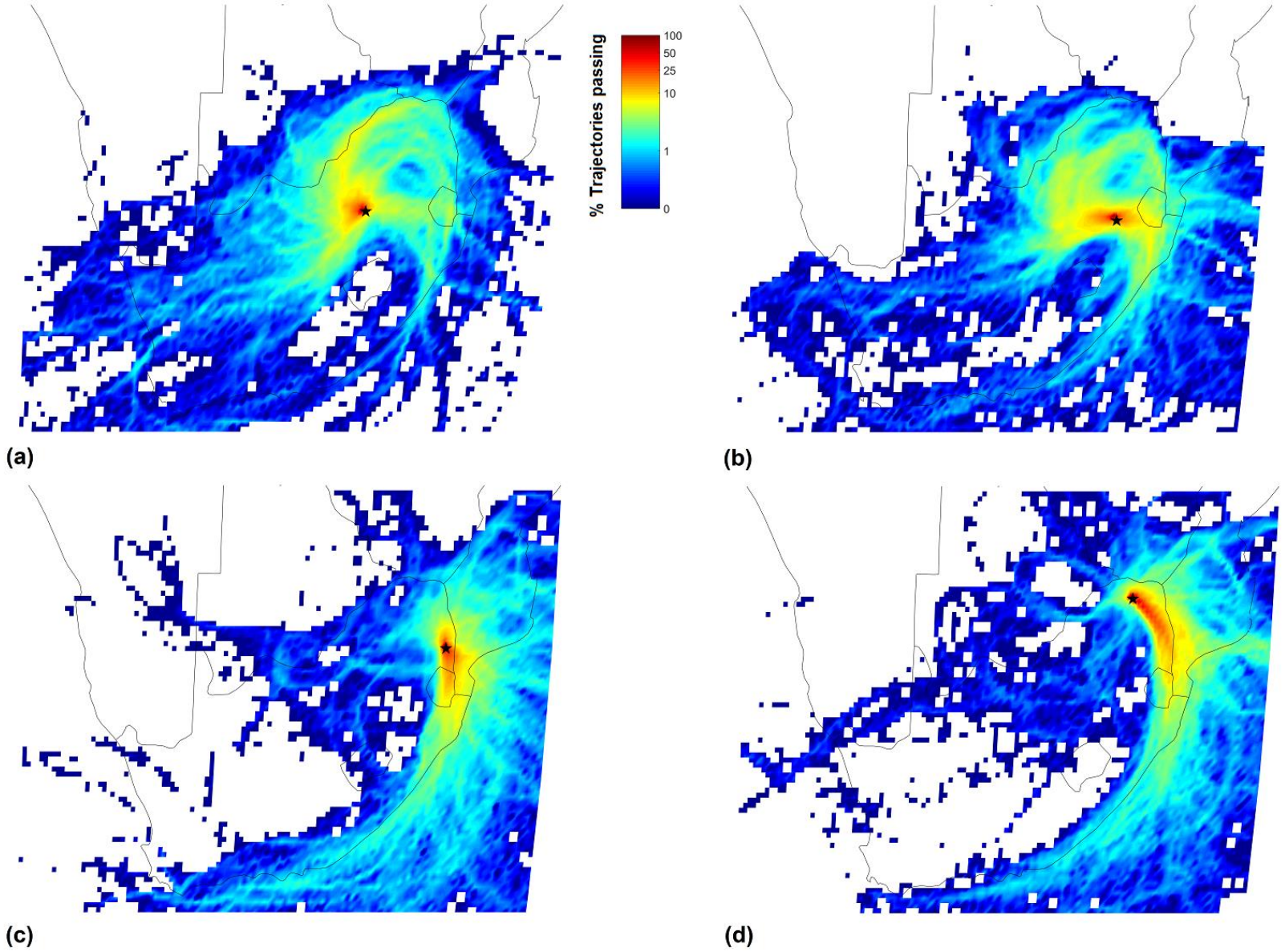

Figure 3-6: Overlay back trajectory figures of individual trajectories calculated during sampling times at VT (a), AF (b), SK (c) and LT (d) over the entire sampling period (i.e. March 2009 to December 2015). Similar figures were presented in section 2.3.1

3.3.3 Temporal assessment of the most important ions

According to results presented thus far in this chapter (i.e. Figures 3-1 to 3-4), SO_4^{2-}, NO_3^-, OA and NH_4^+ were the ions with the highest concentrations. This is in agreement with results from Venter et al. (2018a), who presented results for a regional background site (Welgegund) and an industrial/household combustion impacted site (Marikana). Therefore, only the temporal variations for these species, i.e. SO_4^{2-}, NO_3^-, OA and NH_4^+, are considered. The monthly median concentrations for both size fractions and each sampling site are presented in Figure 3-7, while the corresponding monthly average concentrations are presented in Figure 3-8.

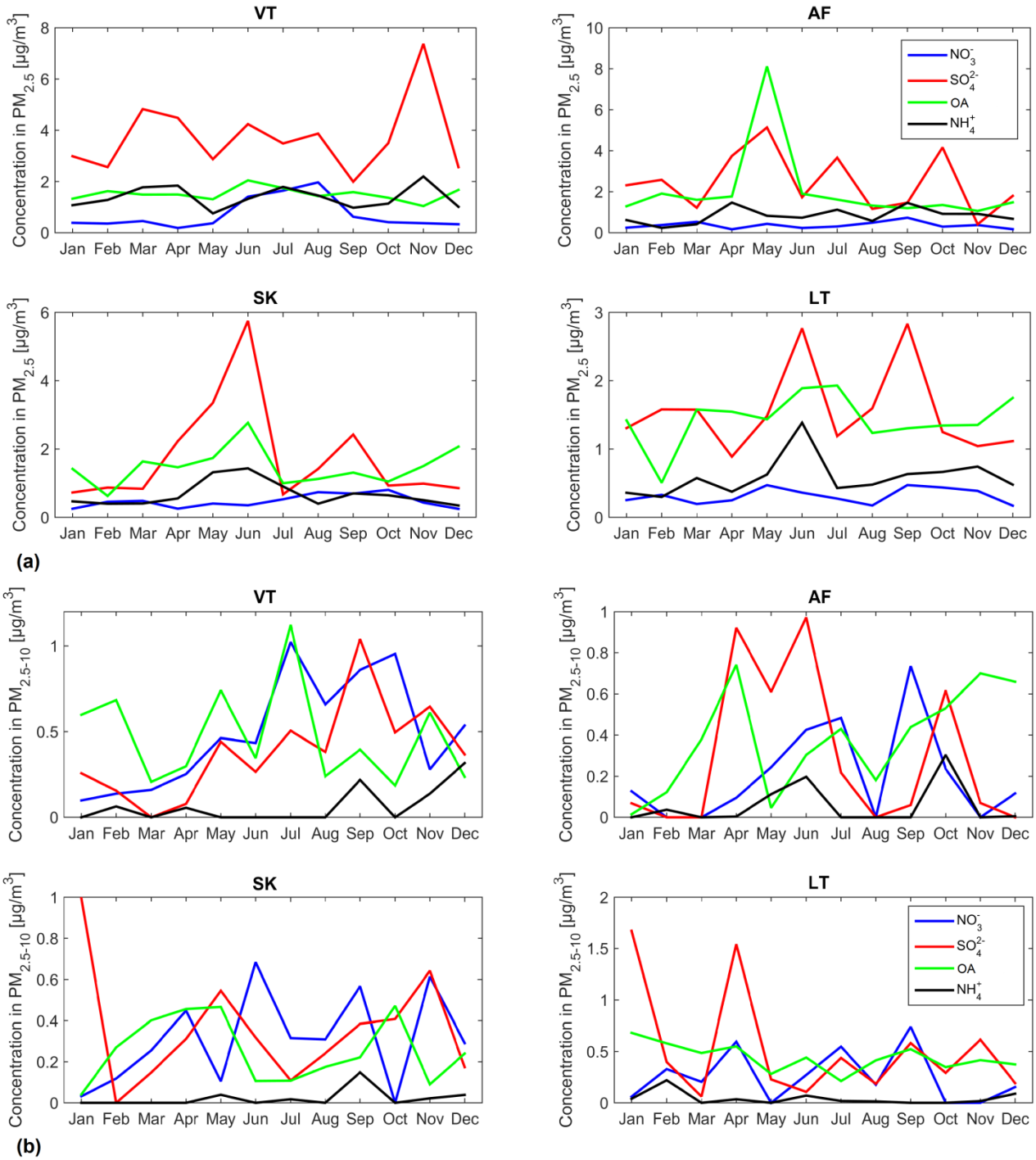

Figure 3-7: The monthly median concentrations of NO_3^- (blue line), SO_4^{2-} (red line), OA (green line) and NH_4^+ (black line) in the $PM_{2.5}$ (a) and $PM_{2.5-10}$ (b) size fraction, over the entire sampling period for all four INDAAF sites

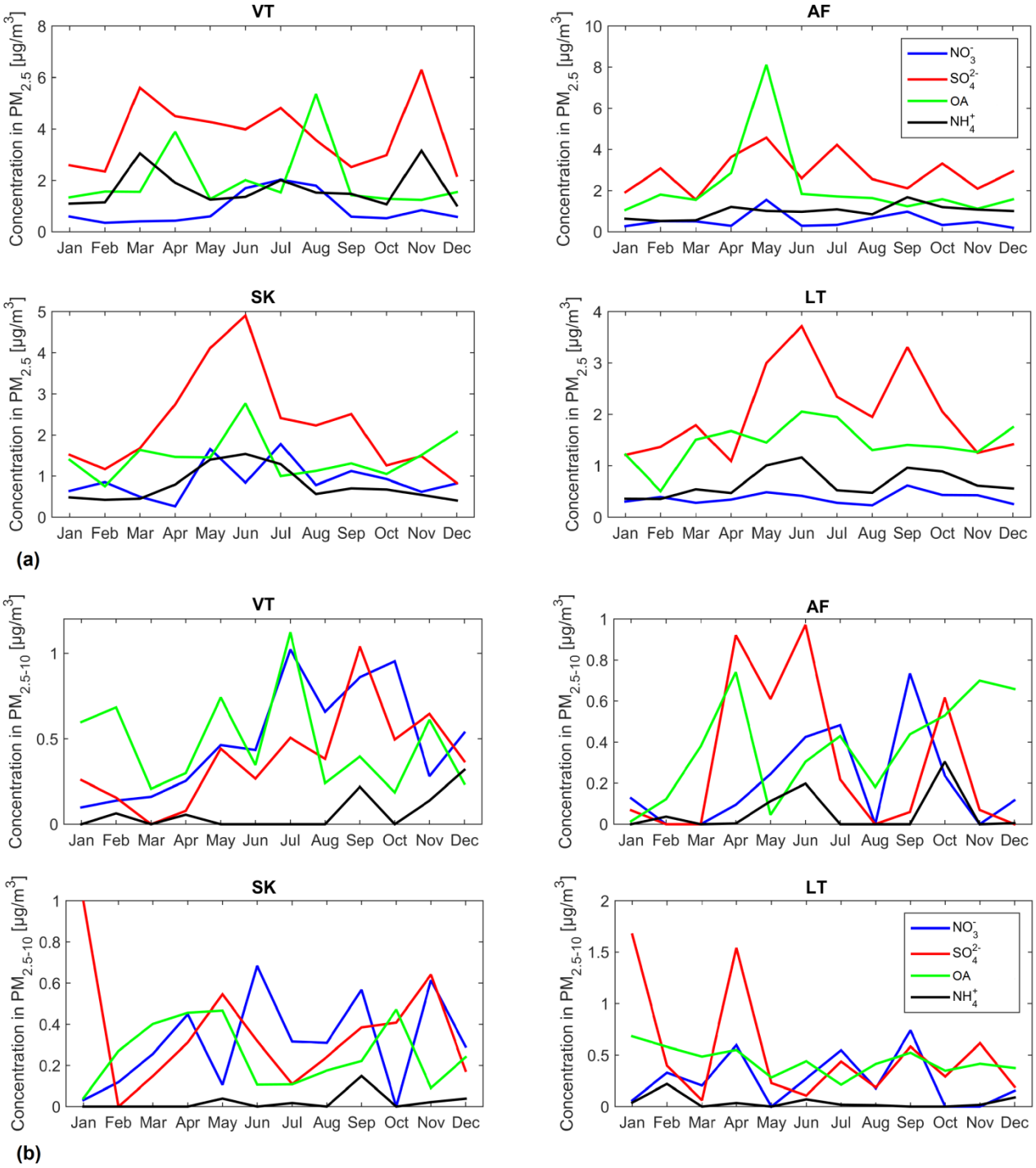

Figure 3-8: The monthly average concentrations of NO_3^- (blue line), SO_4^{2-} (red line), OA (green line) and NH_4^+ (black line) in the $PM_{2.5}$ (a) and $PM_{2.5-10}$ (b) size fraction, over the entire sampling period for all four INDAAF sites

Considering the results presented in Figures 3-7 and 3-8, it is difficult to state with a high level of confidence that clear seasonal patterns exist for any of the ions considered. One of the reasons why seasonal patterns are not obvious might be due to the sampling procedure applied, i.e. a monthly 24-hour sample at each site might not represent the monthly average/median concentrations, even over the ~6.5 year period considered here. A single 24-hour sample with an abnormally high or low concentration will significantly influence the

results, which would have been less likely if monthly composite samples were obtained. However, even Tiitta et al. (2014), who conducted high temporally resolved PM_1 ACSM measurements at Welgegund, could not identify clear seasonal patterns, except for organic aerosols that were higher in the open biomass burning season. In the current study, only OA was determined and not total organic aerosol content, and therefore it is difficult to compare to the results of Tiitta et al. (2014). Tiitta et al. (2014) also made some deductions regarding the seasonality of NO_3^-, but these authors only considered PM_1 that contains only a small fraction of NO_3- (as was also reported by Aurela et al., 2016, and Venter et al., 2018a).

The seasonality of the ionic content of PM in the South African interior will depend on many factors. For instance, the effect on warm and wetter summers, vs cold and dry winters (Laakso et al., 2012); seasonality of open biomass burning during the dry season as a source of PM (Mafusire et al., 2016, section 2.3.3); seasonal differences in wet deposition as a removal mechanism for PM (Conradie et al., 2016); influence of seasonal relative humidity on SO_2 oxidation to SO_4^{2-} (Connell, 2005); seasonal differences in circulation patterns over southern Africa (Garstang et al., 1996); seasonal differences in the formation of inversion layers in the South African interior (Garstang et al., 1996; Korhonen et al., 2014; Gierens et al., 2018); and obviously the sources that impact a specific site. However, all authors who have previously considered the seasonality of PM ionic content in the South African interior (Tiitta et al., 2014; Aurela et al., 2016; Venter et al., 2018a) have found that air mass history (i.e. over what source areas an air mass has passed) is very important in understanding the chemical composition.

In order to explore the effect of air mass history on ionic content, the chemical composition of individual samples was plotted in stacked bar plots over the entire sampling period for the VT site. This site was chosen as an example site, since it is influenced by a complex mixture of sources. Additionally, more consideration was given to the $PM_{2.5}$ size fraction, since it contained the majority of the mass concentrations of most of the ions, with much less mass occurring in the $PM_{2.5-10}$ size fraction (Figure 3-5). Considering the afore-mentioned, Figure 3-9 presents the $PM_{2.5}$ composition stacked bar plot of the 82 individual samples collected at VT. Samples 2, 5, 9 and 18 were carefully selected as case studies (indicated by the * in Figure 3-9). The back trajectories associated with sampling times of these selected case studies are presented in Figure 3-10. Figure 3-9 indicates organic matter (OM) and not OC, due to OC concentrations that were converted to OM concentrations by multiplying it with a factor of 1.71 (Hegg et al., 1997; Turpin and Lim, 2001). This was required, since the analytical technique that was applied (section 2.2.3) only quantified the carbon content of organic compounds (from there the term OC), while the actual weight of organic compounds is co-determined by the oxygen (O), hydrogen (H), nitrogen (N), sulphur (S), phosphor (P)

and other trace elements present in the molecular structures. Additionally, the OA mass fractions were not indicated separately, since OA forms part of the OM fraction. By converting measured OC to OM through this calculation, furthermore adds uncertainty to the new calculated OM that is <5.0% (Turpin et al., 2001). The uncertainty of the calculated OM values is also controlled by our limited knowledge about OM components.

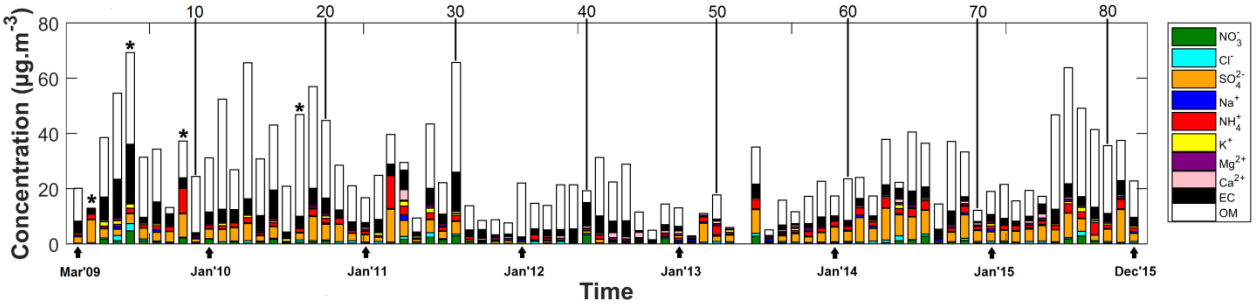

Figure 3-9: $PM_{2.5}$ stacked bar plot of the ion concentrations (µg/m^3) (including elemental carbon (EC) as presented in Chapter 2 and organic matter (OM)) of individual samples collected over the entire sampling period at VT. The samples are numbered at the top and the samples that were carefully selected as case studies are indicated by *

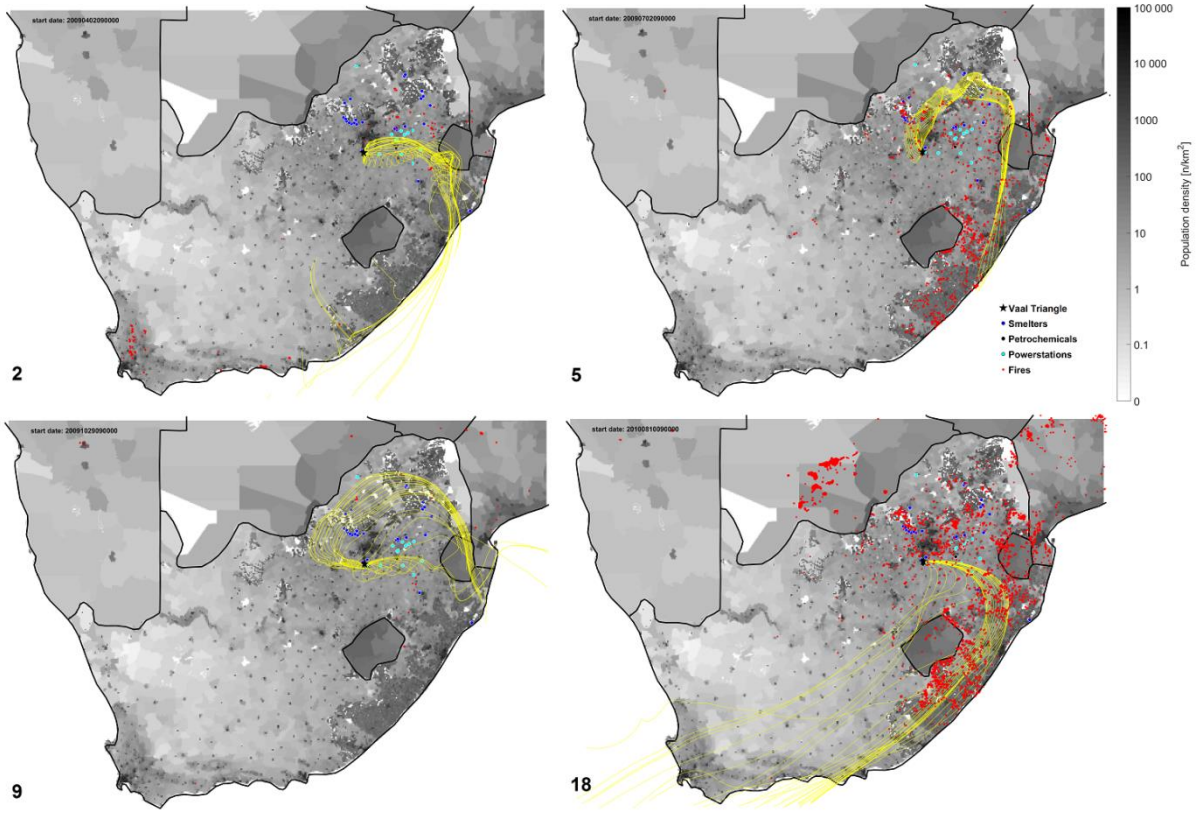

Figure 3-10: Back trajectories associated with $PM_{2.5}$ case studies (i.e. samples 2, 5, 9, 18) for the VT

As is evident in Figure 3-9, samples 31 to 52 (September 2011 to June 2013) had much lower ionic concentrations than the samples measured before and after this time period. This was due to the ionic concentration of some of the species being non-retrievable (thus therefore not quantified) from the analytical instrument. Therefore, case studies from this

period was not considered. The impact of these data limitations was limited during all calculations, since the missing data points that were treated as non-available data in Matlab calculations (i.e. not a number, NaN).

Case study and back trajectories associated with sample number 2 of VT

The chemical composition of this case study sample indicated elevated concentrations of SO_4^{2-}, and lower but notable NH_4^+ and EC concentrations (Figure 3-9). The back trajectories passed over the Mpumalanga Highveld with its array of coal-fired power stations (Figure 3-10, number 2) that are well known for high SO_2 and NO_x emissions. As explained earlier, SO_2 has a shorter atmospheric lifetime than NO_x (Seinfeld and Pandis, 2006), and therefore the higher SO_4^{2-} reported here makes sense. Additionally, substantial NO_3^- will only occur in the particle phase if there is enough NH_4^+ to fully neutralize SO_4^{2-}, and even then its occurrence is strongly dependant on temperature (Seinfeld and Pandis, 2006).

Case study and back trajectories associated with sample number 5 of VT

This case study sample exhibited elevated organic matter (OM) and EC, as well as K^+, NO_3^- and Cl^- concentrations. The associated back trajectories passed over many open biomass burning events that are common during the dry season (this specific sample was taken in July 2009). Such fires release the N (as NO_x) that was part of the biomass and it is also known that KCl is emitted (Aurela et al., 2016). The SO_4^{2-} concentration of this sample was also not negligible, since the air masses had passed over numerous pyro-metallurgical smelters in the western Bushveld Complex (near Rustenburg and Brits) that are known to emit relatively high concentrations of SO_2. However, the emitted flue gas concentrations do not matter, but total emitted SO_2 matters on a regional scale.

Case study and back trajectory associated with sample number 9 of VT

This case study sample had elevated concentrations of OM, NH_4^+ and SO_4^{2-}, with lower NO_3^- and EC concentrations. The back trajectories associated with it passed over a couple of pyro-metallurgical smelters and coal-fired power stations, which explains the elevated SO_4^{2-}. The NH_3 emissions from the production of fertiliser in the area and other chemical operation near VT explain the elevated NH_4^+ - such nearby sources are not easily explained by air mass back trajectory analysis, but at least the sources are known and can make a contribution. In contrast with the previously considered case study, almost no open biomass burning events occurred, which explains the low EC concentration. However, the elevated OM concentration can be explained by elevated biogenic VOC (BVOC) concentrations during the early part of the wet season (sample was taken in November 2009) that can be oxidised to form OM (Jaars et al., 2016).

Case study and back trajectories associated with sample number 18 of VT

The composition of the case study sample indicated the presence of a number of species that have already been considered in the previous case studies, e.g. NH_4^+, SO_4^{2-}, NO_3^- and Cl^-. However, what makes this case study particularly interesting is the elevated OM, but lower EC concentrations (Figure 3-9). The back trajectory associated with this sample passed over many open biomass burning events (Figure 3-10, number 18). However, the majority of these events were quite far from the site (mostly in KwaZulu-Natal and the Eastern Cape). It was indicated in Chapter 2 (section 2.3.1) that the OC/EC ratio indicates the freshness of a plume, since secondary OC concentration is enhanced during aging from biomass burning or biogenic VOC precursors, while EC concentration is reduced, due to wet and dry deposition. According to Vakkari et al. (2014) combustion phases also affect the ratio of BC to organic aerosol, resulting in higher OC/EC ratios for smouldering combustion. Therefore, the elevated OM and lower EC observed for this case study are not surprising.

As was previously stated, more consideration was given to the $PM_{2.5}$ than to the $PM_{2.5-10}$ size fraction during the discussion of case studies (Figures 3-9 and 3-10), since the former size fraction contained the majority of the mass concentration of most of the ions (Figure 3-5). However, a single $PM_{2.5-10}$ size fraction case study is also considered for the VT, i.e. sample 24 that was collected in February 2011, since it illustrated one particular source better than the previously discussed $PM_{2.5}$ case studies. Figure 3-11 presents the stacked bar plot of the $PM_{2.5-10}$ size fraction of VT, wherein it is evident that sample 24 contained a very significant amount of Na^+, Ca^{2+} and Mg^{2+} if compared to the other samples. This is indicative of marine aerosol, since Na^+, Mg^{2+} and Ca^{2+} are the most prevalent mineral ions in seawater (https://web.stanford.edu/group/Urchin/mineral.html). The marine origin is also confirmed by the back trajectory that is associated with this sample (Figure 3-12).

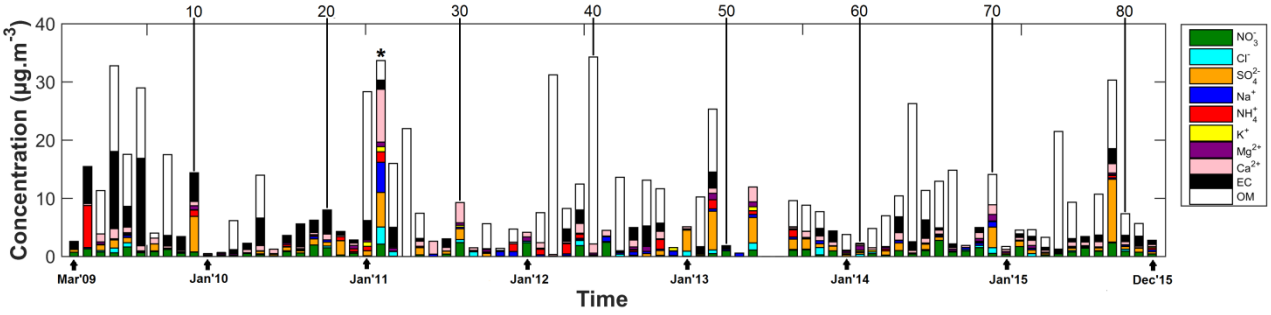

Figure 3-11: $PM_{2.5-10}$ stacked bar plot of the ion concentrations (µg/m^3) (including elemental carbon (EC) as presented in Chapter 2 and organic matter (OM)) of individual samples collected over the entire sampling period for VT. The samples are numbered at the top and the samples that were carefully selected as case studies are indicated by *

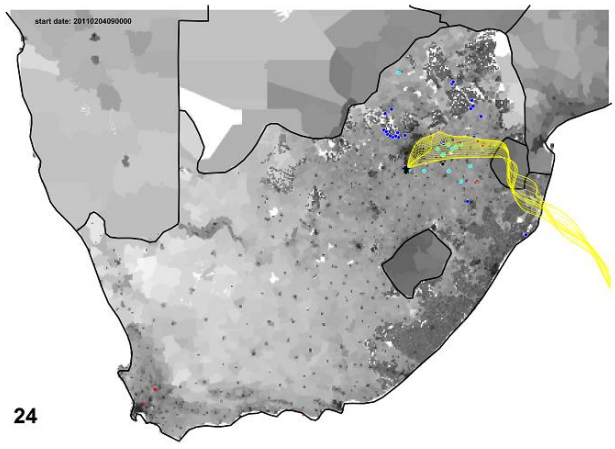

Figure 3-12: Back trajectory associated with $PM_{2.5-10}$ case study 24 for the VT

From all the case studies associated with VT, which was considered as an example site, it was evident that the lack of observed seasonal patterns in the ionic concentrations (Figures 3-7 and 3-8) is due to air mass history being the dominant determining factor for the ionic chemical composition, in addition to the seasonal occurrence of open biomass burning.

3.3.4 Acidity and neutralisation

In this section, the empirical calculations and statistical evaluations described in section 3.2.4 are applied. In contrast to guidelines for the ionic balance of wet precipitation samples prescribed by the World Meteorological Organization (WMO/GAW, 2004), no guideline(s) for aerosol water-soluble ionic species balance could be found by the candidate. Therefore, all the results obtained over the entire sampling period at all four sites were included in the data analyses. The average ion difference percentages (calculated with Equation 3-7) for the $PM_{2.5}$ size fractions were 17.9, 19.2, 22.2 and 18.1 %, while the ion difference percentages for the $PM_{2.5-10}$ size fractions were 29.4, 18.0, 21.6 and 22.0 %, for VT, AF, SK and LT, respectively. According to the principle of electro-neutrality, the aqueous aerosol extractions prepared in this study (section 3.2.1) should have no ion difference. However, all ionic species were not quantified, e.g. carbonate (CO_3^{2-}) and bicarbonate (HCO_3^-). In addition, H^+ occurring in acid condensate in aerosols (e.g. H_2SO_4) cannot conventionally be quantified. Also, Hennigan et al. (2015) found that the aerosol H^+ loading did not necessarily corresponded well with declining pH, therefore it was suggested that the ion balance may not be a very good indicator of aerosol acidity. Kerminen et al. (2001) observed that the ion balance depends on particle size, thereby suggesting that the smaller particles are more acidic when compared to super-micrometre particles. Therefore, the afore-mentioned ion difference percentages were expected and they are in the same range as reported for similar studies elsewhere (Satsangi et al., 2013; Wan et al., 2016).

In addition to the direct importance of aerosol acidity (e.g. the effect of acidity on deposited surface), has an influence on hygroscopicity of the aerosol, as well as the ability to produce heterogeneous sulphate and secondary organic aerosols (Jang et al., 2002; Pathak et al., 2011). According to Table 3-3, SO_4^{2-}, NO_3^- and dissociated OA are the anions that had the highest concentrations in samples at the sites considered. Cl^- was not considered here, due to its common association with Na^+ as a marine aerosol. Therefore, these ions (SO_4^{2-}, NO_3^- and dissociated OA) will contribute most to aerosol acidity. This is similar to previous findings related to aerosol acidity in the South African interior (Tiitta et al., 2014; Venter et al., 2018a), although none of these authors quantified OA. Similar to Satsangi et al. (2013), the three cations NH_4^+, Mg^{2+} and Ca^{2+} were considered as the most common neutralising species in aerosols for the afore-mentioned acid-forming species. Again, this is comparable to neutralisation calculations previously reported for aerosols sampled in South Africa (Tiitta et al., 2014; Venter et al., 2018a), with some differences. For instance, Tiitta et al. (2014) did not quantify Mg^{2+} and Ca^{2+}, while Venter et al. (2018a) did not consider the neutralisation effect of Mg^{2+} and Ca^{2+} although these species were quantified. Similar assumptions to that applied here (i.e. SO_4^{2-}, NO_3^- and dissociated OA as the main acid forming species, and

NH_4^+, Mg^{2+} and Ca^{2+} as the main neutralising species) have also been applied in wet deposition acidy calculations (Mphepya et al., 2004; Laouali et al., 2012). Figure 3-13 presents graphs of the $PM_{2.5}$ (a) and $PM_{2.5-10}$ (b) cation- (CE) (µEq/L) versus the anion (AE) (µEq/L) equivalent contributions (calculated with Equations 3-4 and 3-5) for each site, with CE representing the total NH_4^+, Mg^{2+} and Ca^{2+} equivalent concentrations and AE the total NO_3^-, SO_4^{2-} and OA equivalent concentrations.

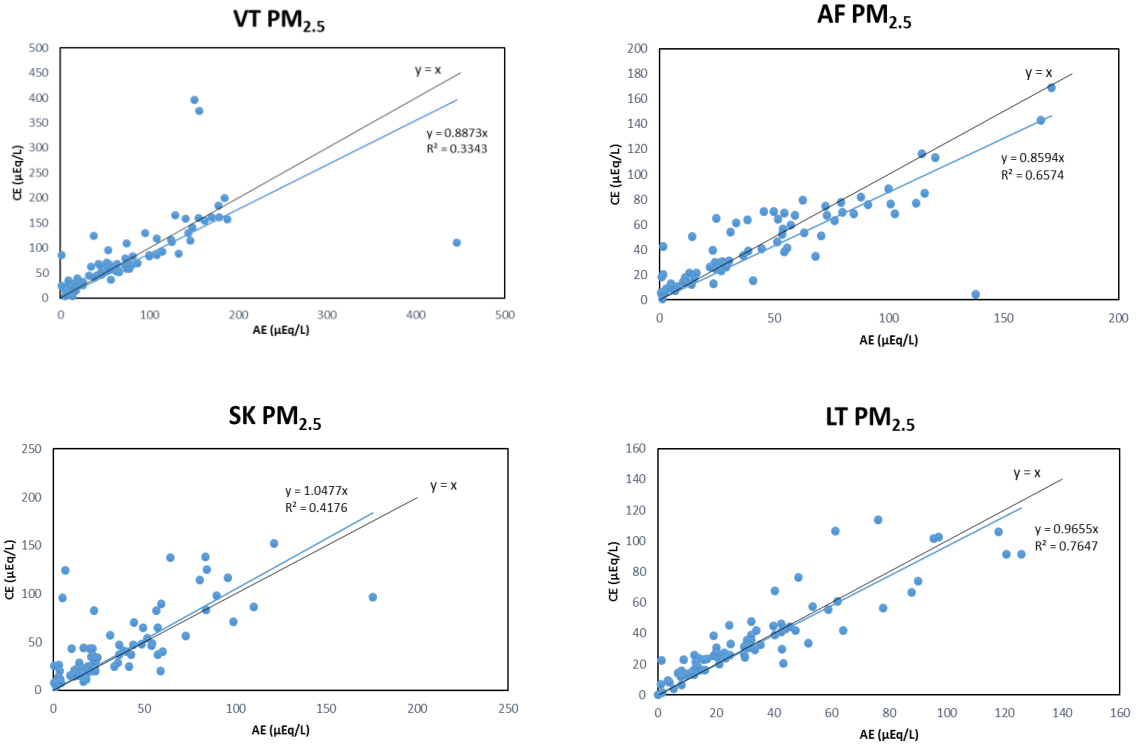

(a)

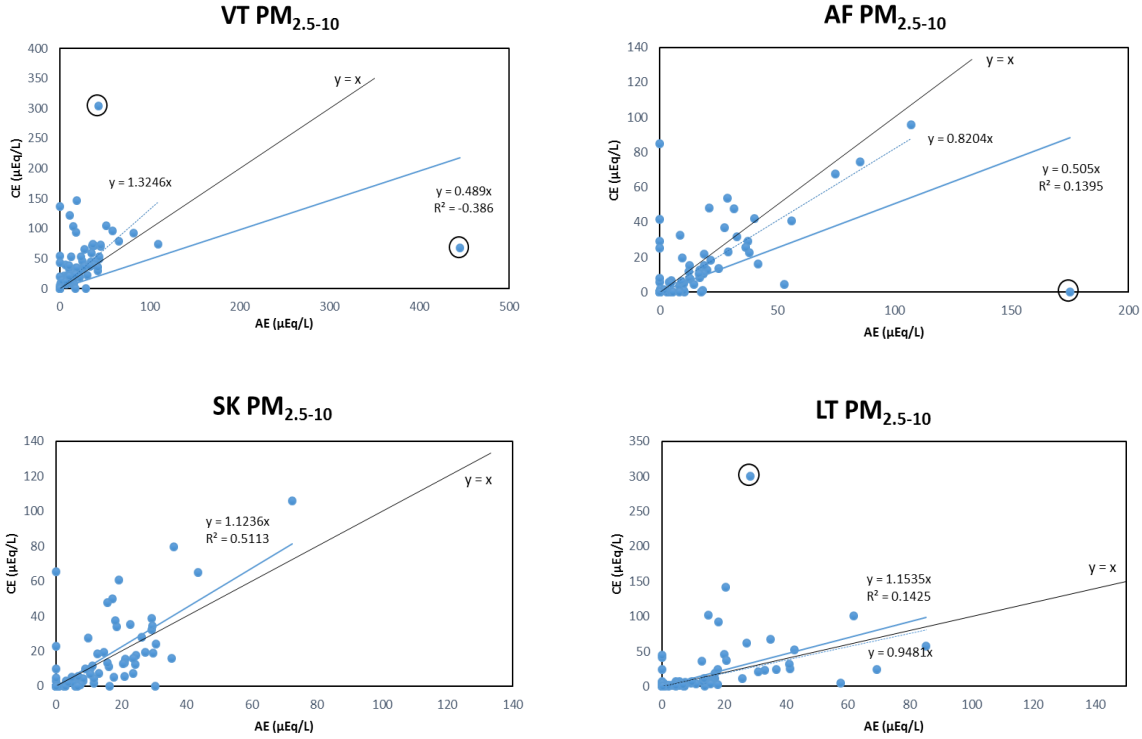

(b)

Figure 3-13: $PM_{2.5}$ (a) and $PM_{2.5-10}$ (b) cation (i.e. sum of NH_4^+, Mg^{2+}, Ca^{2+}) versus anion (i.e. sum of NO_3^-, SO_4^{2-}, OA) equivalent concentrations for each site. The solid black line is a 1:1 line; the solid blue line a linear fit of all data and the dotted blue line in some graphs indicate an alternative linear fit if one or more outliers (identified with black circle) were omitted

From Figure 3-13a, it is evident that the $PM_{2.5}$ size fractions at VT and AF are slightly acidic, with the calculated CE not fully accounting for calculated AE neutralisation. This is understandable, since $PM_{2.5}$ SO_4^{2-} concentrations (that are likely to be the dominant acid forming species in aerosols in the South African interior) at these two sites are significantly higher than at the other two sites (Figure 3-1). However, at SK and LT, it seems as if the $PM_{2.5}$ size fractions are fully neutralised. For the $PM_{2.5-10}$ size fraction (Figure 3-13b), it seems as if the particulate matter is fully neutralised, if a very limited number of outliers are ignored. The afore-mentioned results, i.e. that the $PM_{2.5}$ and $PM_{2.5-10}$ seem fully or almost fully neutralised differ from deductions made by Tiitta et al. (2014) and Venter et al. (2018a), who indicated that PM_1 is not fully neutralised. However, as previously mentioned, these authors did not account for the neutralising effect of Mg^{2+} and Ca^{2+}. When Ca^{2+} and Mg^{2+} were removed from these graphs (Figure 3-13), similar slopes as reported by Tiitta et al. (2014) and Venter et al. (2018a) were found. It is also interesting to note that Conradie et al. (2016) reported very acidic wet deposition (pH 4.32 to 4.89 volume weighted means) at the same measurement sites considered in the current study. Therefore, it is good (a positive result) to know that $PM_{2.5}$ and $PM_{2.5-10}$ compositions do not seem to further exacerbate the regional acid deposition problem over the South African interior.

To explore possible seasonal variations in aerosol acidity, Figure 3-14 illustrates $PM_{2.5}$ (a) and $PM_{2.5-10}$ (b) CE (µEq/L) versus AE (µEq/L) for the summer (i.e. January, February and December) and winter (i.e. June, July and August) months separately, for each site. As is evident from these results, there does not seem to be any significant seasonality with both size fractions being neutralised in both seasons at all sites, after a very limited number of outliers were omitted.

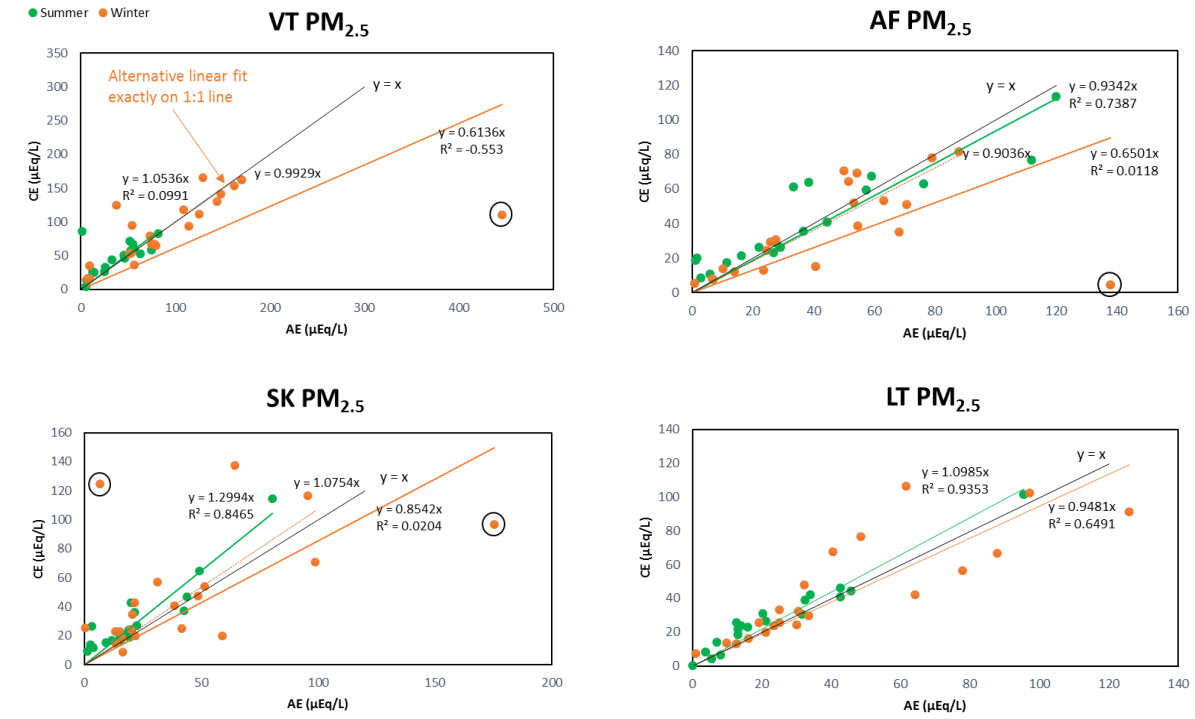

(a)

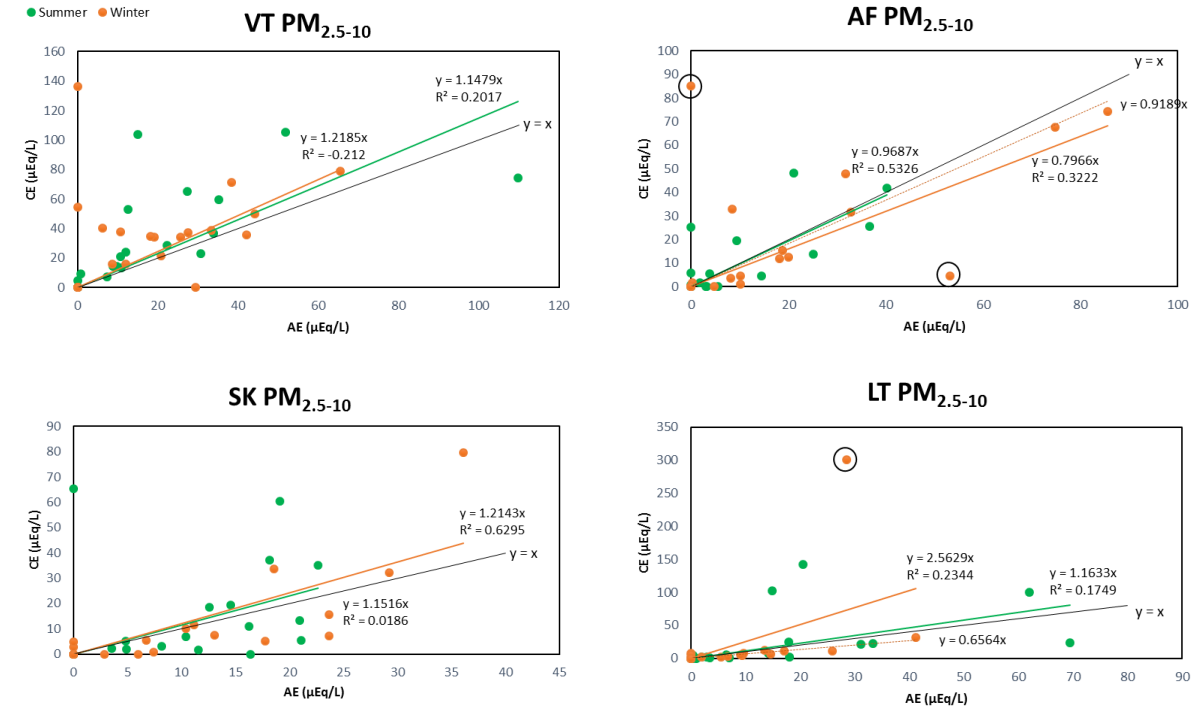

(b)

Figure 3-14: $PM_{2.5}$ (a) and $PM_{2.5-10}$ (b) cation (i.e. sum of NH_4^+, Mg^{2+}, Ca^{2+}) versus anion (i.e. sum of NO_3^-, SO_4^{2-}, OA) equivalent concentrations separately for summer (Dec, Jan and Feb) and winter (Jun, Jul and Aug) months for each site. The green dots and trend lines indicate summer months, while the orange dots and trend lines indicate winter months. The solid black line is a 1:1 line. The dotted linear lines in some graphs indicate an alternative linear fit if one or more outliers (identified with black circle) were omitted

The ability of cation species to neutralise anion species can be evaluated by calculating NF factors. The higher the NF factor, the more the specific cation species are able to neutralise strong acidic species. Average NF for NH_4^+, Mg^{2+} and Ca^{2+} was calculated with Equation 3-8 (if only SO_4^{2-} and NO_3^- are considered as acidic species) and Equation 3-9 (if SO_4^{2-}, NO_3^- and OA are considered as acidic species) for both size fractions and all the sites. These calculated average NF values are summarised in Table 3-4 (for acidic species SO_4^{2-} and NO_3^-) and Table 3-5 (for acidic species SO_4^{2-}, NO_3^- and OA) for $PM_{2.5}$ (a) and $PM_{2.5-10}$ (b).

Table 3-4: Average neutralisation factors (NF) of NH_4^+, Mg^{2+} and Ca^{2+} to neutralise SO_4^{2-} and NO_3^- in the $PM_{2.5}$ (a) and $PM_{2.5-10}$ (b) size fractions at all sites

(a)

Site	NF_{NH4+}	NF_{Mg2+}	NF_{Ca2+}
VT	0.91	0.12	0.23
AF	0.77	0.13	0.20
SK	0.72	0.34	0.42
LT	0.78	0.17	0.28

(b)

Site	NF_{NH4+}	NF_{Mg2+}	NF_{Ca2+}
VT	0.70	0.49	1.21
AF	0.63	0.22	0.24
SK	0.31	0.58	0.44
LT	0.83	0.45	0.48

Table 3-5: Average neutralisation factors (NF) of NH_4^+, Mg^{2+} and Ca^{2+} to neutralise SO_4^{2-}, NO_3^- and OA in the $PM_{2.5}$ (a) and $PM_{2.5-10}$ (b) size fractions at all sites

(a)

Site	NF_{NH4+}	NF_{Mg2+}	NF_{Ca2+}
VT	0.78	0.10	0.20
AF	0.69	0.12	0.18
SK	0.62	0.29	0.36
LT	0.68	0.15	0.25

(b)

Site	NF_{NH4+}	NF_{Mg2+}	NF_{Ca2+}
VT	0.45	0.31	0.77
AF	0.54	0.18	0.21
SK	0.27	0.51	0.38
LT	0.67	0.36	0.39

By considering Tables 3-4a and 3-5a, it is evident that NH_4^+ is likely the most important cation to neutralise the acidic ions in the $PM_{2.5}$ size fraction at all the sites, while Ca^{2+} is likely to be the second most important neutralising cation. This is similar to Conradie et al. (2016) who also found NH_4^+ and Ca^{2+} to be the most important and second most important cations to neutralise acidic species occurring in wet precipitation samples collected at the same sites considered in this study. However, if Tables 3-4b and 3-5b are considered, it is obvious that the likely neutralisation contribution of Mg^{2+} and Ca^{2+}, relative to NH_4^+, increases in the $PM_{2.5-10}$ size fraction. This is not unexpected, since higher Mg^{2+} and Ca^{2+} concentrations in the coarse fraction are likely due to wind-blown dust and marine aerosol (https://web.stanford.edu/group/Urchin/mineral.html) contributions. All sites considered in this study will be impacted by wind-blown dust, since South Africa is a semi-arid country. Additionally, fly ash from combustion sources (both industrial and household) is likely to make a significant contribution at VT. Due to the proximity of SK and LT to the Indian Ocean, and the air mass histories associated with these sites (Figure 3-6), marine aerosols will impact these sites significantly. VT and AF will also be impacted by marine aerosols, as was illustrated in the case study considered in Figure 3-13 and in previous work (Conradie et al., 2016; Venter et al., 2018a), though such influences will be less than at SK and LT. Internationally, it is also not always the case that NH_4^+ is the dominant neutralising species. For instance, in Agra (India), Ca^{2+} was the most important neutralising species, followed by Mg^{2+} and NH_4^+ (Satsangi et al., 2013).

3.3.5 Statistical evaluation and source contributions

Various methods can be used to assess the possible contribution of sources to the measured ambient aerosol concentrations. One of the simplest methods is to draw correlation graphs between different species to find possible linkages. However, it is unrealistic to draw and consider hundreds of these graphs. Therefore, many authors have compiled diagonal correlation graphs, which indicate the correlation coefficient(s) of species to one another, for various applications (Satsangi et al., 2013; Jaars et al., 2014; Conradie et al., 2016; Kleynhans et al., 2017; Liu et al., 2017; Mishra and Kulshrestha, 2017; Shakya et al., 2017). Such diagonal correlation graphs are presented in the left pane of Figures 3-15a to 3-15d and Figures 3-16a to 3-16d, for the $PM_{2.5}$ and $PM_{2.5-10}$ size fractions, respectively, for each site. Such diagonal correlation graphs do not inform the reader of possible auto-correlations and other data pitfalls; therefore, more advanced statistical processing is advised. In the current study, explorative principal component analysis (PCA) was conducted to identify possible factors associated with a source(s), similar to Conradie et al. (2016), Kumar et al. (2018) and Zhang et al. (2018). The term ‘explorative’ is specifically used within this context due to the relatively small dataset considered in this study (small in terms of

statistical evaluation), which implies that the PCA results cannot be considered as conclusive, but rather as indicative. The obtained meaningful PCA factors (with eigenvalues higher than 1, for each site in both size fractions) are presented in the right pane of Figures 3-15a to 3-15d and Figures 3-16a to 3-16d. These factors identified single or multiple source types.

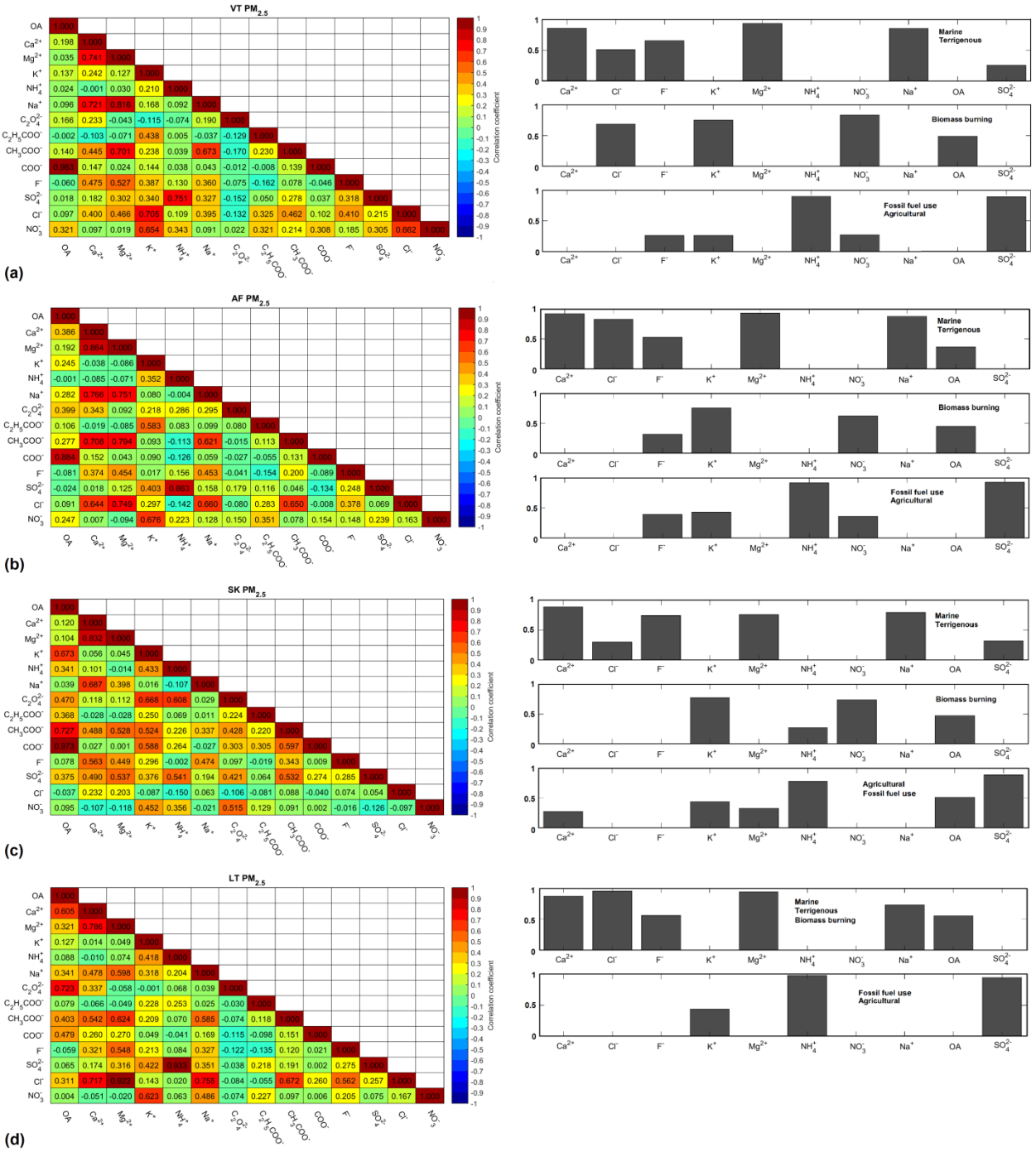

Figure 3-15: Diagonal correlation graphs indicating Pearson correlations (r) (left panes) and meaningful PCA factors (right pane) for each site in the $PM_{2.5}$ size fraction

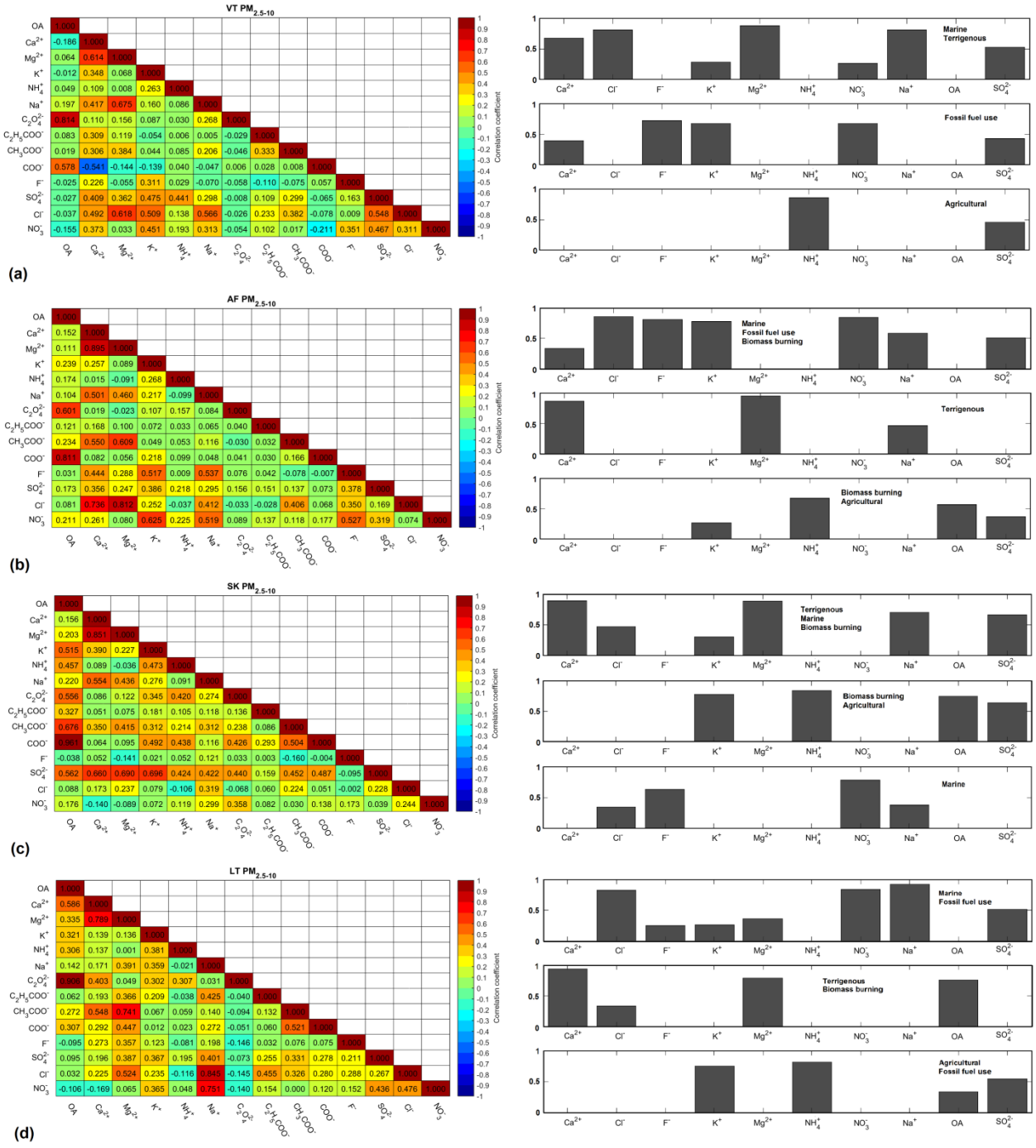

Figure 3-16: Diagonal correlation graphs indicating Pearson correlations (r) (left pane) and meaningful PCA factors (right pane) for each site in the $PM_{2.5-10}$ size fraction

Firstly, correlations between species in the $PM_{2.5}$ size fraction (Figure 3-15) are considered. However, the interpretation of correlations values is sometimes subjective. Therefore, the definitions suggested by Sheskin (2003) are employed to quantify the significance of a correlation coefficient, i.e., *"(i) if |r| ≥ 0.7 a correlation is considered to be strong/significant; (ii) if |0.3| ≥ |r| < 0.7 a correlation is considered to be moderate and (iii) if |r| < 0.3 a correlation is considered to be weak/insignificant",* which was also used by Kleynhans et al.

(2017). Strong positive correlations between SO_4^{2-} and NH_4^+ at VT (r = 0.751), AF (r = 0.863) and LT (r = 0.933), and moderate correlation at SK (r = 0.541), indicate the importance of neutralisation between these two species to form NH_4HSO_4 and/or $(NH_4)_2SO_4$. Weaker correlations (|r| = 0.063 to 0.356) were found between NH_4^+ and NO_3^-, which indicates that NH_4NO_3 formation is less significant in the fine fraction. Interestingly, dissociated acetic acid (CH_3COO^-) correlated moderately strong with Ca^{2+} and Mg^{2+} at all the sites (r = 0.445 to 0.794), which could indicate that this organic acid is mostly neutralised by the afore-mentioned cations, rather than NH_4^+. A strong correlation (r = 0.705) between K^+ with Cl^- was found at VT, but these species had weak correlations at the other sites (|r| = 0.087 to 0.297). This could indicate the impact of fresh biomass burning at VT, possibly from household combustion (e.g. wood burning), since Aurela et al. (2016) revealed the significant presence of KCl in fresh biomass burning plumes. Ca^{2+} and Mg^{2+} were strongly correlated (r = 0.741 to 0.864) at all sites, which could indicate terrigenous sources (Huang et al., 2008; Satsangi et al., 2013; Mishra and Kulshrestha, 2017), fly ash (Mahlaba et al., 2011) and/or marine aerosols (https://web.stanford.edu/group/Urchin/mineral.html) are meaningful sources. Na^+ was also moderate to strongly correlated (r = 0.398 to 0.766) to Ca^{2+} and Mg^{2+}, possibly also indicating the afore-mentioned sources. Obviously, it can be expected that fly ash at VT, from industrial sources and/or household combustion, and fly ash from industrial sources near AF will contribute to the observed Mg^{2+} and Ca^{2+} levels. Marine aerosols will have a fractionally more significant impact on SK and LT, than at VT and AF, as indicated by the air mass histories (Figure 3-6). Cl^- was strongly correlated to Ca^{2+} and Mg^{2+} (r = 0.717 and 0.922) and to Na^+ (0.755) at LT, which supports the notion of marine aerosol influence, but none of the afore-mentioned three species correlate significantly with Na^+ for SK. K^+ and NO_3^- correlated moderately (r = 0.452 to 0.676) at all sites, which could indicate the use of fertiliser across the region, wherein KNO_3 is often used as a source of soluble NO_3^- and K^+ that is free of Cl^- (https://www.cropnutrition.com/potassium-nitrate). K^+ and SO_4^{2-} correlated moderately (r = 0.340 to 0.422) at all sites, which along with the moderate K^+ and NO_3^- correlation could indicate ageing of biomass burning plumes (Li et al., 2003).

In general, strong correlations between species in the $PM_{2.5-10}$ size fraction were not as common as in the $PM_{2.5}$ size fraction. This was expected, since the majority of the water-soluble inorganic ions and OA occurred in fine fraction (Figure 3-5). Therefore, it might be presumptuous to make a significant deduction based on correlations for species in the $PM_{2.5-10}$ size fraction. However, fractionally, the NO_3^-, Na^+ and Ca^{2+} contributions were more substantial than for the other species in the coarse fraction (Figure 3-5). Therefore, these species are briefly considered. For LT, where NO_3^- occurred mostly in the coarse fraction (Figure 3-5), Na^+ correlated strongly (r = 0.751) to NO_3^-. However, the meaning thereof is not

clear at present. Ca^{2+} and Mg^{2+} correlated moderately to strong (r = 0.614 to 0.895) for all sites; possibly indicating similar sources, i.e. marine aerosols, fly ash and/or crustal emissions (dust).

For the VT, PCA yielded three meaningful $PM_{2.5}$ factors (Figure 3-15 right panes). The first $PM_{2.5}$ factor was associated with marine (due to high Na^+ and Cl^-, as well as Ca^{2+} and Mg^{2+} loading) and/or terrigenous (due to high Ca^{2+} and Mg^{2+} loading) sources. The second $PM_{2.5}$ factor was associated with biomass burning (due to high K^+, Cl^-, OA and NO_3^- loading), while the third factor was associated with fossil fuel use (due high SO_4^{2-} and NO_3^- loading) and agricultural activities (due to high K^+, NO_3^- and NH_4^+ loading). As indicated in section 3.1.3 other sources could also be responsible for OA emissions, not just biomass burning. Reference is made here to specifically 'fossil fuel use' for factors with high SO_4^{2-} loading, instead of 'fossil fuel combustion', since some sources emit H_2S that is the reduced form of gaseous sulphur. However, H_2S can also be oxidised to SO_2 and ultimately SO_4^{2-}. PCA also yielded three meaningful factors for the $PM_{2.5-10}$ size fraction at VT. The first was marine (due to high Na^+ and Cl^-, as well as Ca^{2+} and Mg^{2+} loading) and/or terrigenous (due to high Ca^{2+} and Mg^{2+} loading). Fossil fuel use was indicated as a possible source by the second factor (due to high SO_4^{2-} and NO_3^- loading), while agricultural (due to NH_4^+ loading) was implicated by the third factor. These factors explained 68.0 and 57.2% of the total variances for VT, in the $PM_{2.5}$ and $PM_{2.5-10}$ size fractions, respectively.

For AF, PCA yielded three meaningful $PM_{2.5}$ factors, which indicated similar species loading and sources to the three $PM_{2.5}$ factors of VT, and therefore these are not repeated. Three meaningful $PM_{2.5-10}$ factors were also identified, but their loadings indicated grouping of different source types if compared to the VT coarse fraction. The first AF $PM_{2.5-10}$ factor indicated marine (due to high Na^+ and Cl^- loading), fossil fuel use (due to high SO_4^{2-} and NO_3^- loading) and biomass burning (due to high K^+, Cl^- and NO_3^- loading) as possible sources. The second factor implied terrigenous sources (due to high Ca^{2+} and Mg^{2+} loading, while Na^+ and/or Cl^- was absent). Possible biomass burning (due to high OA and K^+ loading) and agricultural (due to NH_4^+ loading) were indicated by the third factor. These factors explained 70.2 and 59.0% of the total variances for AF in the $PM_{2.5}$ and $PM_{2.5-10}$ size fractions, respectively.

PCA again yielded three meaningful $PM_{2.5}$ factors for SK, which indicated similar species loading and sources to the three $PM_{2.5}$ factors identified for VT and AF, i.e. i) marine and terrigenous; ii) biomass burning; and iii) agriculture and fossil fuel use. Three meaningful $PM_{2.5-10}$ factors, with slightly different source combinations than those obtained for the $PM_{2.5-10}$ size fractions of VT and AF, were obtained. The first factor was associated with

terrigenous (due to high Ca^{2+} and Mg^{2+} loading), marine (due to high Na^{+} and Cl^{-} loading) and biomass burning (due to high K^{+} and Cl^{-} loading) sources. The second factor again implied possible biomass burning influence (due to high K^{+} and OA loading), in addition to agricultural emissions (due to NH_4^{+} loading), while the third factor again indicated the influence of marine aerosols (due to high Na^{+} and Cl^{-} loading). These factors explained 61.0 and 65.5% of the total variances in the $PM_{2.5}$ and $PM_{2.5-10}$ size fractions for SK, respectively.

For LT, PCA of the $PM_{2.5}$ size fraction only yielded two meaningful factors. The first indicated possible sources as marine (due to high Na^{+} and Cl^{-}, as well as Ca^{2+} and Mg^{2+} loading), terrigenous (due to high Ca^{2+} and Mg^{2+} loading) and possible biomass burning (due to high Cl^{-} and OA loading), while fossil fuel use (due to high SO_4^{2-} loading) and agriculture (due to high NH_4^{+} loading) were implied by the second factor. Analysis of the $PM_{2.5-10}$ size fraction for LT indicated three meaningful factors. The first was associated with marine (due to high Na^{+} and Cl^{-} loading) and fossil fuel use (due to high SO_4^{2-} loading). The second factor implied terrigenous (due to high Ca^{2+} and Mg^{2+} loading) and possible biomass burning (due to high Cl^{-} and OA loading) contributions. The last factor was related to agricultural emissions (due to high NH_4^{+} loading) and again fossil fuel (due to high SO_4^{2-} loading). These factors explained 64.9 and 68.8% of the total variances for the $PM_{2.5}$ and $PM_{2.5-10}$ size fractions for LT, respectively.

From literature, and from the results presented thus far in section 3.3.5, it is obvious that some species might originate from multiple possible sources. For instance, Ca^{2+} and Mg^{2+} might be from terrigenous (Satsangi et al., 2013; Mishra and Kulshrestha, 2017), fly ash (Mahlaba et al., 2011) or marine (https://web.stanford.edu/group/Urchin/mineral.html) sources. Therefore, to gain further insight into the origin of species, the sea-salt fractions (SSF) and non-sea-salt fractions (nSSF) were calculated according Equations 3-10 and 3-11, respectively. Table 3-6 indicates the ratios of different elements (i.e. Cl^{-}, SO_4^{2-}, Mg^{2+}, Ca^{2+} and K^{+}) in relation to Na^{+} in seawater (Keene et al., 1986b), which were used in these calculations. In addition, it was assumed that Na^{+} was completely of marine origin. Similar SSF and nSSF calculations have been performed by many previous authors (Sigha-Nkamdjou et al., 2003; Mphepya et al., 2004; Mphepya et al., 2006; Galy-Lacaux et al., 2009; Vet et al., 2014; Conradie et al., 2016).

Table 3-6: Seawater concentrations ratios of element X (µEq/L) to Na^+ (µEq/L) (Keene et al., 1986b)

X	$[X/Na^+]_{seawater}$
Cl^-	1.1600
SO_4^{2-}	0.1210
Mg^{2+}	0.2270
Ca^{2+}	0.0439
K^+	0.0218

Figures 3-17, 3-18, 3-19 and 3-20 present graphs for the nSSF against the SSF contributions calculated for Cl^-, SO_4^{2-}, Mg^{2+}, Ca^{2+} and K^+ in both size fractions for VT, AF, SK and LT, respectively. In these figures, a 1:1 line (in red) is also indicated. If the data were predominantly below this line, the SSF contribution dominated that implied marine origin, while the opposite is true if the data were mainly above the 1:1 line, i.e. non-marine origin.

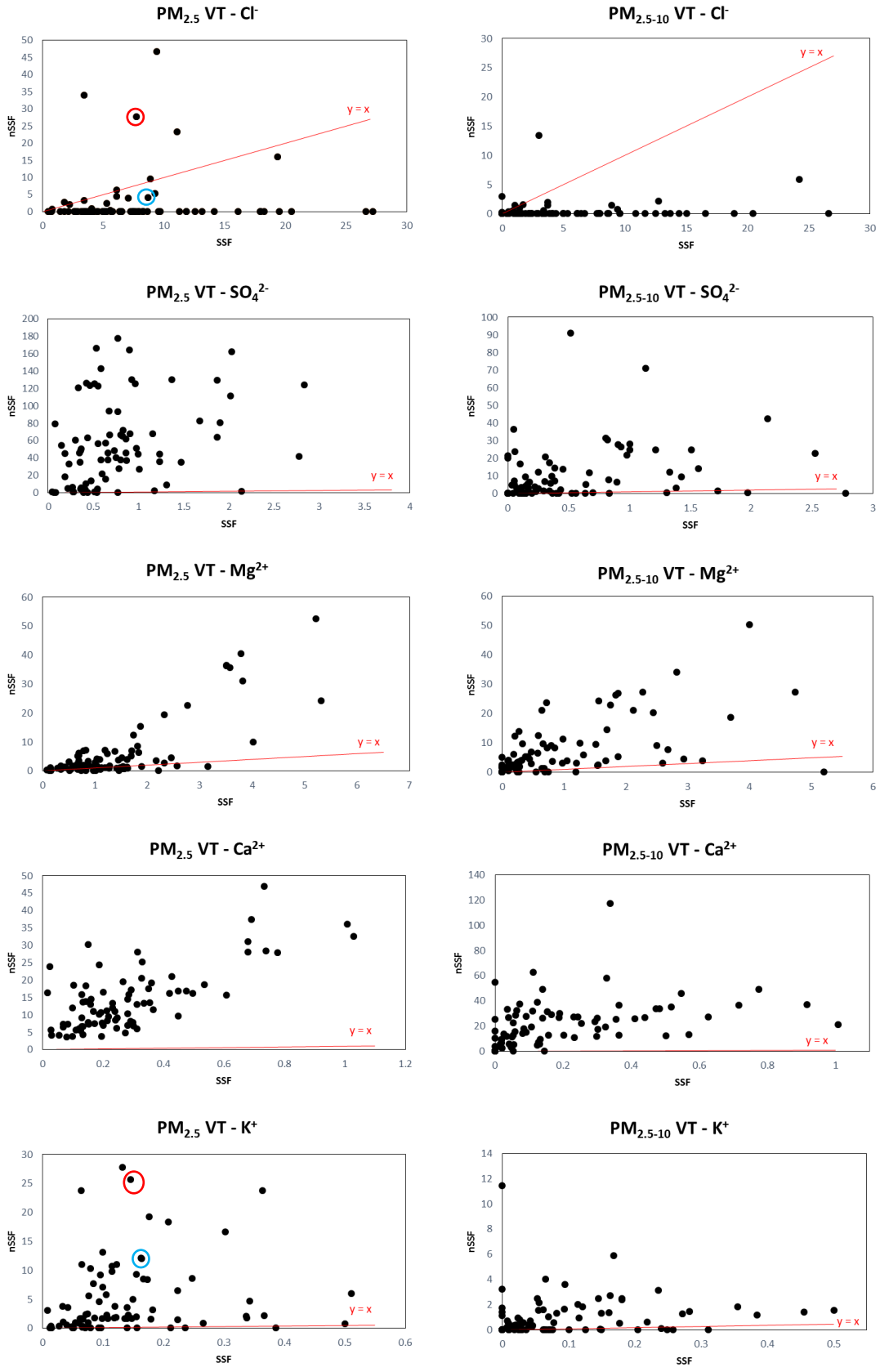

Figure 3-17: Graphs illustrating the nSSF versus the SSF for VT in the $PM_{2.5}$ (a) and $PM_{2.5-10}$ (b) size fractions. Red and blue circles show examples of fresh and aged biomass burning plumes, respectively

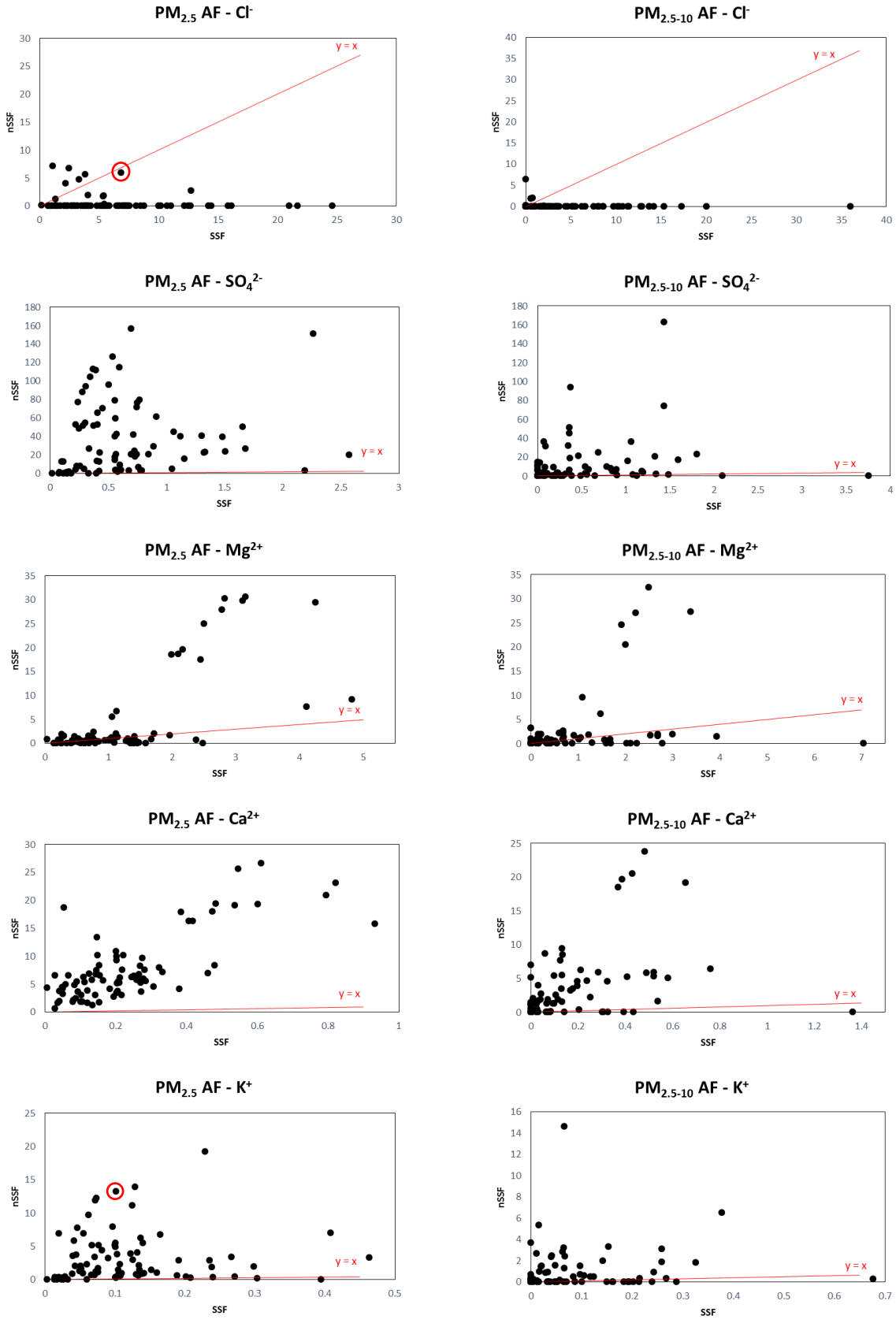

(a) **(b)**

Figure 3-18: Graphs illustrating the nSSF versus the SSF for AF in the $PM_{2.5}$ (a) and $PM_{2.5-10}$ (b) size fractions. Red circles show examples of fresh biomass burning plumes

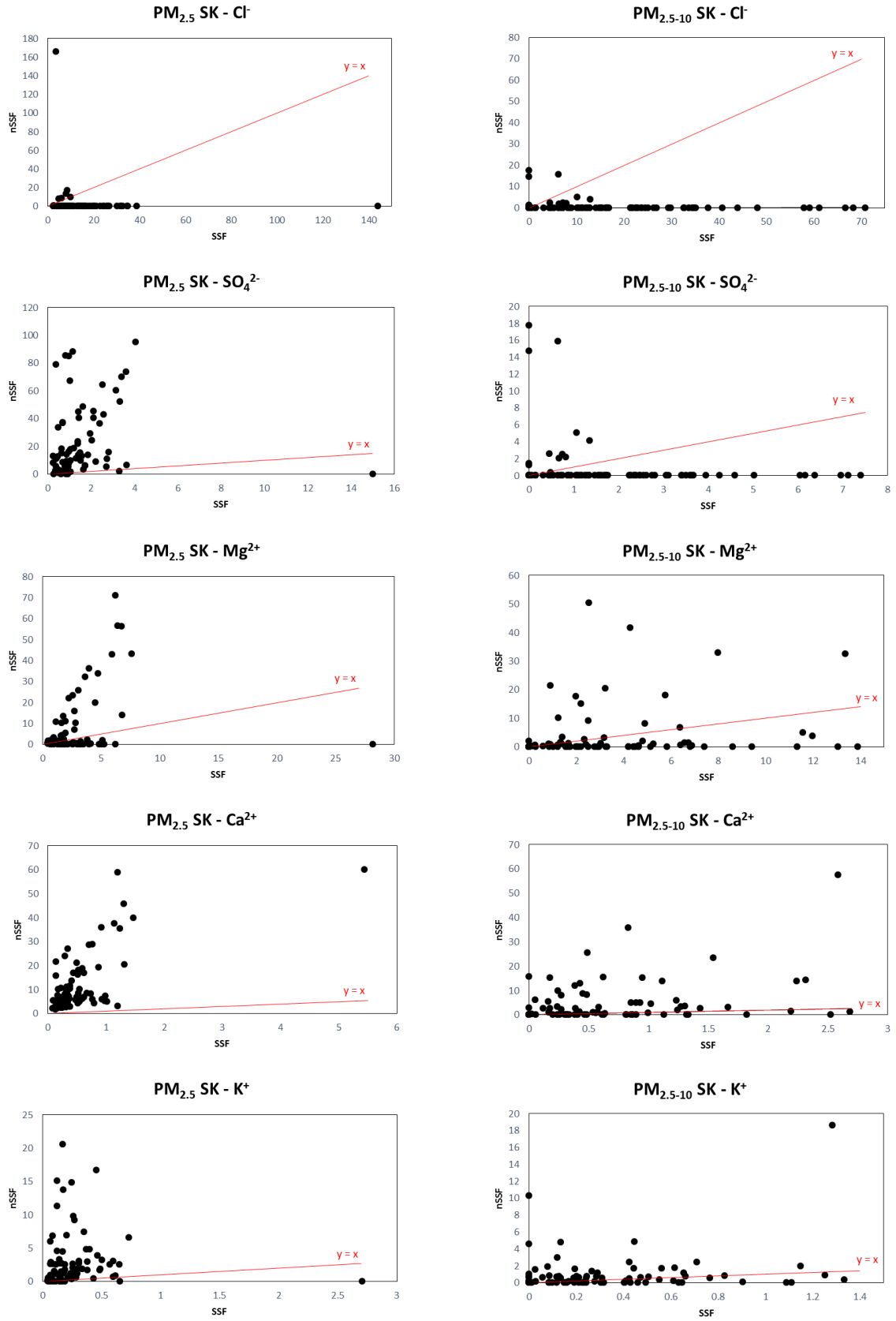

Figure 3-19: Graphs illustrating the nSSF versus the SSF for SK in the $PM_{2.5}$ (a) and $PM_{2.5-10}$ (b) size fractions

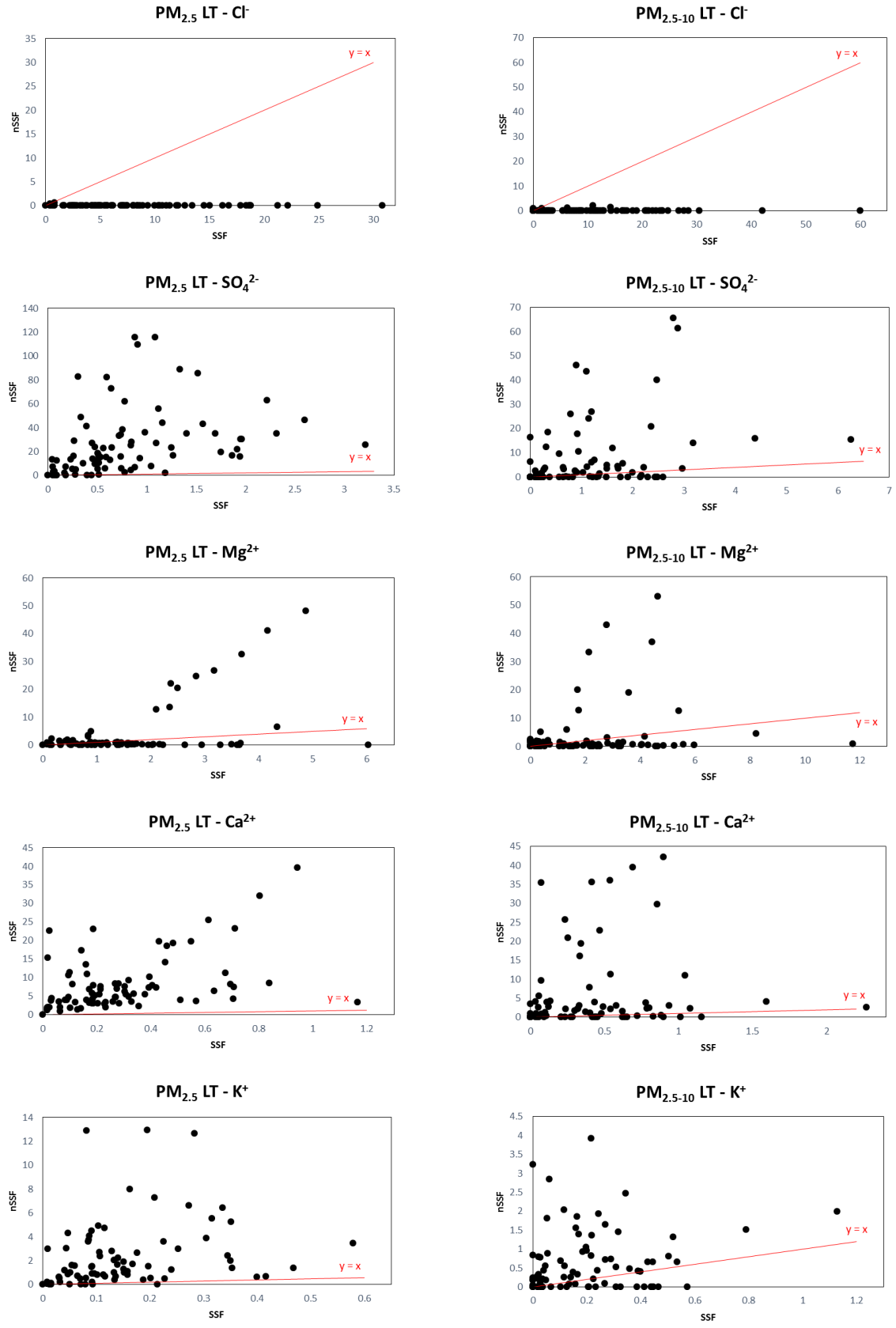

Figure 3-20: Graphs illustrating the nSSF versus the SSF for LT in the $PM_{2.5}$ (a) and $PM_{2.5-10}$ (b) size fractions

Considering Figures 3-17 to 3-20, it is evident for both size fractions that Cl^- was predominantly from marine origin at VT, AF and SK, while it was exclusively from marine origin at LT. SO_4^{2-} in the $PM_{2.5}$ size fraction was predominantly from non-marine origin at all sites. In the $PM_{2.5-10}$ size fraction, non-marine SO_4^{2-} also dominated at all sites, although fractionally more samples were associated with marine origin, if compared to the $PM_{2.5}$ size fraction. This was particularly true for SK and LT (Figures 3-19 and 3-20), since these two sites are influenced more than the other sites by air masses that have passed over the Indian Ocean (Figure 3-6). For Mg^{2+} at the VT (Figure 3-17), it is apparent that it is mostly from non-marine origin in both size fractions. However, at the other sites (AF, SK and LT, Figures 3-18 to 3-20), it seems that there are significant fractions of Mg^{2+} associated with both marine and non-marine origins in both size fractions. Ca^{2+} in both size fractions at all sites (Figures 3-17 to 3-20) was predominantly from non-marine origin, although a limited number of samples in the $PM_{2.5-10}$ size fraction at AF, SK and LT (Figures 3-18 to 3-20) reflected marine origin. K^+ in the $PM_{2.5}$ size fraction (Figures 3-17 to 3-20) was predominantly from non-marine origin at all sites, as well as in the $PM_{2.5-10}$ size fraction at VT and AF. Although this was also true for SK and LT in the $PM_{2.5-10}$ size fraction, it was obvious that the marine influence increased in this size fraction at these two sites.

Examples of High nSSF Cl^- and K^+ values, which might suggest fresh biomass burning plumes as a possible source are indicate with red circles in Figure 3-17 (during August 2015) and Figure 3-18 (during August 2009) in the $PM_{2.5}$ size fraction. Examples of low nSSF Cl^- and high nSSF K^+, which could possibly indicate an aged biomass plume as the source, are indicated with blue circles in Figure 3-17 (during August 2011) in the $PM_{2.5}$ size fraction. Such examples could be further explored in subsequent studies.

In addition to the above-mentioned SSFs and nSSFs, calculated according Equations 3-10 and 3-11, respectively, additional source deductions were made by applying Equations 3-12, 3-13 and 3-14 described in section 3.2.4. Thereby the SSF was considered to be entirely from marine origin. The nSSF for Cl^-, Mg^{2+}, Ca^{2+} and K^+ were assumed to be from terrigenous (crustal) sources, while the nSSF of SO_4^{2-} was divided between terrigenous and anthropogenic source contributions. To estimate the anthropogenic contributions of SO_4^{2-}, the $SSF_{(SO42-)}$ was subtracted from the determined SO_4^{2-} values (µEq/L). The remaining SO_4^{2-} (i.e. $nSSF_{(SO42-)}$) was then assumed to be either from anthropogenic or terrigenous sources. Assuming that anthropogenic SO_4^{2-} is in excess of that supplied by gypsum ($CaSO_4 \cdot 2H_2O$) (Delmas, 1981), Ca^{2+} was used as a reference element for continental crustal emissions (Ding et al., 2013), and therefore anthropogenic SO_4^{2-} contributions were calculated with Equation 3-12, while the terrigenous SO_4^{2-} contributions were calculated with

Equation 3-13. The fossil fuel use source contribution was then calculated with Equation 3-14, which totalled the anthropogenic SO_4^{2-} and NO_3^- nSSF. With the empirical source contribution calculations applied, it was impossible to differentiate between NH_4^+ contributions from bacterial decomposition of urea in animal excreta and from natural/fertilised soils (Schlesinger and Hartley, 1992), open biomass burning fires and household combustion of wood (Delmas et al., 1995; Brocard et al., 1996), fertiliser production (Brasseur et al., 1999; Van Loon and Duffy, 2005; Seinfeld and Pandis, 2016) and petrochemical plant emissions (Mirbagheri et al., 2010; Khan et al., 2016). Therefore, this source group was merely indicated as 'NH_4^+-associated' contributions. Conradie et al. (2016) attributed OA only to biomass burning. However, other sources could also make a contribution to this species. Therefore, "OA-associated" was indicated as a separate contribution, which is likely to be mainly of biomass burning origin, although other sources could also contribute. Considering all the afore-mentioned, Figure 3-21 presents pie graphs of the estimated source contributions to the determined chemical content of the analysed ions of $PM_{2.5}$ (a) and $PM_{2.5-10}$ (b) size fractions for all sites. Each of these source contributions is subsequently discussed separately.

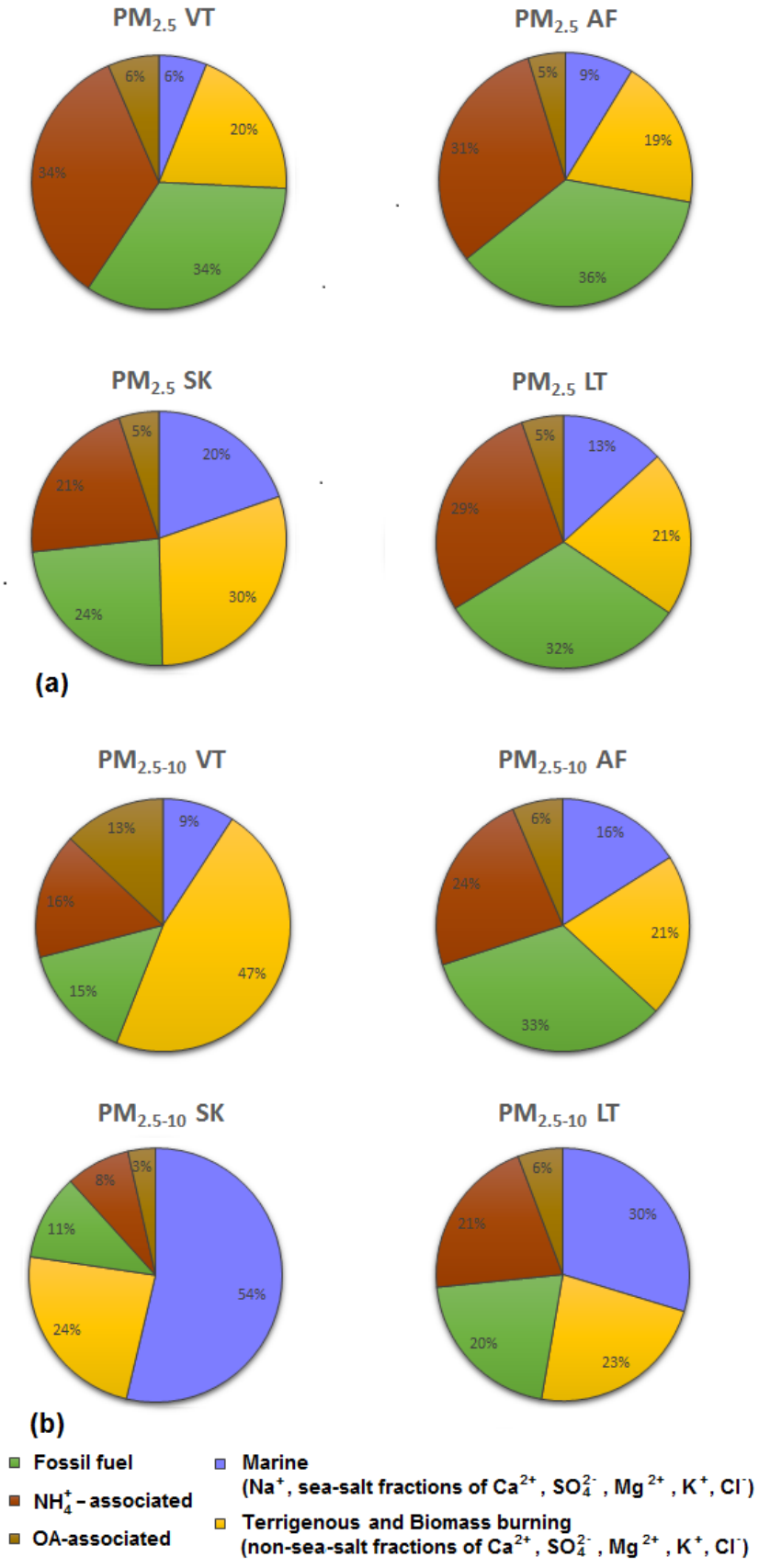

Figure 3-21: Estimations of source contributions to the chemical content of dry aerosol loading at each site for analysed ions in $PM_{2.5}$ (a) and $PM_{2.5-10}$ (b) size fractions

Marine contributions: The marine contributions on the water-soluble aerosol contents were calculated to be 6.0, 9.0, 20.0 and 13.0% in the $PM_{2.5}$ size fraction, while in the $PM_{2.5-10}$ size fraction they were 9.0, 16.0, 54.0 and 30.0% for VT, AF, SK and LT, respectively (Figure 3-21). By comparing all these values, it is evident that the marine influences at SK, followed by LT, were most significant. This was expected, since SK and LT are situated closest to the coast of the four sites considered (Figure 2-1), and the air mass histories of these two sites suggested significant marine influences (Figure 3-6). Conradie et al. (2016), who investigated wet deposition (rain) chemistry at the same sites considered in this study, also reported the marine influences to be most significant at SK and LT. By comparing the $PM_{2.5}$ (Figure 3-21a) and $PM_{2.5-10}$ size fractions (Figure 3-21b), it is apparent that the marine influence is much more significant in the coarse fraction than the fine fraction at all sites.

Terrigenous (crustal) and Biomass burning contributions: These two contributions were presented together, since the $nSSF_{(K+)}$ are part of terrigenous contributions, but together with $nSSF_{(Cl-)}$ it is part of biomass burning contributions. As indicated by Figure 3-21, the terrigenous and biomass burning contributions to the water-soluble aerosol contents at all sites were in similar ranges, i.e. between 19.0 and 30.0% in the $PM_{2.5}$ and between 21.0 and 24.0% in the $PM_{2.5-10}$ size fraction. The exception to this was VT in the $PM_{2.5-10}$ size fraction, for which the contribution was 47.0%. The terrigenous contribution is associated with wind-blown dust species and is considered an important contributor to the aerosol load in South Africa (Van Zyl et al., 2014), since it is a semi-arid country. Therefore, the meaningful terrigenous contributions at all sites make sense. The extremely high terrigenous contribution in the coarse fraction at VT could be due to two possible reasons. Firstly, the assumption applied that the nSSFs of Mg^{2+}, Ca^{2+} and K^+ were from terrigenous (crustal) sources, could inflate the contribution at VT. Here, industrial fly ash and fly ash from household combustion from semi- and informal settlements are likely to contribute to the main terrigenous associated species. However, industries use bag filter and/or electrostatic precipitator technologies to limit fly ash emissions (Pretorius et al., 2015). Therefore, ambient fly ash from this source type is expected to be fine (i.e. passing through bag filters and/or electrostatic precipitators) and reports mostly to the $PM_{2.5}$ size fraction. In contrast, household combustion emissions are unfiltered and will contribute to elevated $PM_{2.5-10}$ levels. This deduction is supported by the earlier observation (Figure 3-15 left pane) that a strong correlation between K^+ and Cl^- was only observed for VT. Fresh biomass burning, such as household combustion of wood, is characterised by KCl emissions (Aurela et al., 2016). Secondly, Venter et al. (2018b) reported that the eastern Free State, which is by volume the largest maize (staple food in South Africa) producing region in South Africa, is one of the most significant wind-blown dust source regions. Typically, cultivated land is ploughed just

before the first rains, which results in high amounts of dust being liberated by wind erosion from the unprotected soil. Since the VT site is situated on the north-western border of the eastern Free State, this site is likely to be significantly impacted by wind-blown dust, which was associated with terrigenous sources in this study. The terrigenous contribution reported here was in the same range or higher than that reported by Conradie et al. (2016) (14.0 to 24.0%) in wet deposition (rain) at the same sites considered in this study. As previously stated, open biomass burning is endemic to southern Africa (Swap et al., 2003), and will make a contribution at all the sites considered. The higher biomass burning contribution in the $PM_{2.5}$ size fraction for VT can possibly be explained by household combustion of biomass (wood) that will be a more important source at this site, than at any of the other sites. Conradie et al. (2016) reported the biomass burning contributions in wet deposition (rain) to be in the 6.0 to 15.0% range, which is similar to the aerosol contributions reported here for both size fractions at all sites. Even though OA is not included for this contribution it is also likely to be from biomass burning, while other sources could also contribute to OA emissions as mentioned in section 2.1.3. Therefore, OA-associated sources was indicated as a separate contribution.

Fossil fuel use contributions: The fossil fuel contributions to the water-soluble aerosol contents were 34.0, 36.0, 24.0 and 32.0% in the $PM_{2.5}$ and 15.0, 33.0, 11.0 and 20.0% in the $PM_{2.5-10}$ size fraction at VT, AF, SK and LT, respectively (Figure 3-21). These results indicate the very significant regional influence of fossil fuel use in South Africa, since even the remote background sites such as SK and LT are significantly impacted. This regional impact is mainly due to most industries in South Africa not yet applying de-SO_x and de-NO_x technologies. Conradie et al. (2016) also reported fossil fuel contributions in wet deposition (rain) at all the sites considered in this study to be between 18.0 and 47.0%, which is in the same range and even higher than calculated aerosol contributions. The same authors found SO_4^{2-} to be the species with the highest volume weighted mean concentrations at all the sites, with NO_3^- also having relatively high concentrations.

NH_4^+-associated contributions: Figure 3-21 indicates that the NH_4^+-associated contributions for analysed ions were 34.0, 31.0, 21.0 and 29.0% in the $PM_{2.5}$, and 16.0, 24.0, 8.0 and 21.0% in the $PM_{2.5-10}$ size fraction at VT, AF, SK and LT, respectively. Most of the NH_4^+ reported to $PM_{2.5}$ (Figure 3-5), therefore this size fraction is of particular interest. As previously stated, various sources of NH_3 that results in NH_4^+ formation are known. Some of these sources are expected to make a contribution at all sites, e.g. bacterial decomposition of urea in animal excreta and from natural/fertilised soils (Schlesinger and Hartley, 1992) and open biomass burning (Delmas et al., 1995; Brocard et al., 1996; Swap et al., 2003).

Furthermore, it was indicated earlier that K^+ and NO_3^- correlated moderately at all sites in the $PM_{2.5}$ size fraction (Figure 3-15 left pane), which suggested fertiliser use emissions across the region, since KNO_3 is often used as a source of soluble NO_3^- and K^+ that are free of Cl^- (https://www.cropnutrition.com/potassium-nitrate). K^+ and SO_4^{2-} also correlated moderately at all sites, which along with the moderate K^+ and NO_3^- correlation could indicate ageing of biomass burning plumes (Li et al., 2003). However, VT and AF are located in the biomes where food associated crop cultivation in South Africa mainly occurs (Mucina and Rutherford, 2006; Jaars et al., 2016), which will result in more significant fertiliser application levels and associated higher NH_3 atmospheric emissions. Therefore, the higher NH_4^+-associated contributions in the $PM_{2.5}$ size fractions at the afore-mentioned two sites are understandable. Additionally, emissions of fertiliser production and the chemical industries near VT could contribute to it being the site with the higher NH_4^+-associated contribution in the $PM_{2.5}$ size fractions. As a comparison to the aerosol results presented here, Conradie et al. (2016) reported NH_4^+-associated contributions (indicated as agriculture contributions by these authors) in wet deposition (rain) at all the sites considered in this study to be between 14.0 and 20.0%. This is in the same range as reported here, except for the afore-mentioned higher contribution at VT in the $PM_{2.5}$ size fractions. Lastly, it is important to remember that NH_4^+ are usually associated with SO_4^{2-} and/or NO_3^-, therefore this source contribution also partially reflect the occurrence of the latter two species.

OA-associated contributions: The contributions of this fraction of the analysed ions illustrated by Figure 3-21 were 6.0, 5.0, 5.0 and 5.0% in the $PM_{2.5}$, and 13.0, 6.0, 3.0 and 6.0% in the $PM_{2.5-10}$ size fraction at VT, AF, SK and LT, respectively. Biomass burning will make a significant contribution to this fraction (Conradie et al., 2016), however, other sources will also contribute to OA.

3.4 Summary and conclusions

The literature survey indicated that few similar studies, i.e. to quantify aerosol water-soluble contents, have been conducted for southern and South Africa, and indeed Africa in general (section 3.1.4). The total $PM_{2.5}$ water-soluble ionic concentrations at VT, AF and SK (Table A-1, Appendix A) exceeded the guideline set by the WHO (2014), which indicates that the ionic content of $PM_{2.5}$ in South Africa requires attention in terms of possible air quality impacts.

The results suggested that the highest concentration of water-soluble ions occurred in the $PM_{2.5}$ size fraction (Figures 3-1, 3-2 and 3-5), and in this size fraction, SO_4^{2-} had the highest concentrations, followed by OA. The high fractional contribution of SO_4^{2-} at all four sites considered (Figures 3-3 and 3-4) indicated the regional influence of anthropogenic

emissions. SO_4^{2-} that mainly occurred in $PM_{2.5}$ size fraction indicated substitution of NO_3^- in NH_4NO_3 to form ammonium sulphate ($(NH_4)_2SO_4$), but ($(NH_4)_2SO_4$) will also form without NO_3^- if there is SO_4^{2-} present in the particle phase (Seinfeld and Pandis, 2006). The significant fraction of NO_3^- that occurred in the $PM_{2.5-10}$ size fraction suggested the influence of aged marine air masses wherein HNO_3 reacts with some NaCl to form $NaNO_3$ and HCl (Turner and Colbeck, 2008). Spatial assessment (Figures 3-1 and 3-2) revealed that the VT had the highest SO_4^{2-} and NH_4^+ concentrations, followed by AF, SK and LT, while the NO_3^- concentrations were the highest at VT, followed by SK, AF and LT. The higher NO_3^- levels at SK instead of AF (as expected) were explained by the high-stack emissions in the vicinity of AF and the atmospheric lifetime of NO_2 that is generally longer than that of SO_2 (Seinfeld and Pandis, 2016). However, NO_3^- concentrations depends on various factors other than only NO_2 concentrations, therefore it is possible that other sources could be responsible for the differences between the sites, since the air mass histories of the sites differ significantly.

Temporal variations for the most prominent species, i.e. SO_4^{2-}, NO_3^-, OA and NH_4^+, were considered. However, no clear seasonal patterns could be identified (Figures 3-7 and 3-8). The sampling procedure applied, i.e. taking one 24hr sample per site per month, could have attributed to this observation, since a specific 24hr sample will not represent an entire month. However, previous authors who have conducted highly temporarily resolved aerosol chemical measurements also could not identify clear seasonal patterns (Tiitta et al., 2014). Regardless of sampling limitations, it was found that air mass histories (Figures 3-6, 3-9 to 3-12) are very important in understanding the chemical compositions at regionally representative sites, as considered in this study.

The acidity and neutralisation calculations suggested that the main acid forming species (i.e. SO_4^{2-}, NO_3^- and OA) both in the $PM_{2.5}$ and the $PM_{2.5-10}$ size fractions were in essence nearly fully neutralised (by NH_4^+, Mg^{2+} and Ca^{2+}) over the entire sampling period (Figure 3-13) as well as during summer and winter (Figure 3-14). These results indicate that $PM_{2.5}$ and $PM_{2.5-10}$ compositions do not seem to further exacerbate the regional acid deposition problem over the South African interior (Conradie et al., 2016). Calculated neutralisation factors (Tables 3-4a and 3-5a) indicated that NH_4^+ is probably the most important cation to neutralise the acidic ions in the $PM_{2.5}$ size fraction at all the sites, while Ca^{2+} is likely to be the second most important neutralising cation. These results also proposed the likely neutralisation contribution of Mg^{2+} and Ca^{2+}, relative to NH_4^+ increases in the $PM_{2.5-10}$ size fraction, which are likely due to wind-blown dust and marine aerosol (https://web.stanford.edu/group/Urchin/mineral.html) contributions.

The diagonal correlations graph analysis (Figure 3-15 left pane) indicated strong positive correlations between SO_4^{2-} and NH_4^+ in the $PM_{2.5}$ size fraction at VT, AF and LT, and moderate correlation at SK, which stipulates the importance of neutralisation between these two species to form NH_4HSO_4 and/or $(NH_4)_2SO_4$. Much weaker correlations were found between NH_4^+ and NO_3^-, which indicates that NH_4NO_3 formation is less significant in the fine fraction. Strong correlations between K^+ with Cl^- at VT only indicated the likely impact of fresh biomass (as suggested by Aurela et al., 2016) from household combustion (e.g. wood burning) and possible contributions from open biomass burning. Ca^{2+} and Mg^{2+} were strongly correlated at all sites, which could indicate terrigenous sources (Huang et al., 2008; Satsangi et al., 2013; Mishra and Kulshrestha, 2017), fly ash (Mahlaba et al., 2011) and/or marine aerosols (https://web.stanford.edu/group/Urchin/mineral.html) are meaningful sources. K^+ and NO_3^- correlated moderately at all sites, which could indicate the use of fertiliser across the region, wherein KNO_3 is often used as a source of soluble NO_3^- and K^+ that is free of Cl^- (https://www.cropnutrition.com/potassium-nitrate). K^+ and SO_4^{2-} also correlated moderately at all sites, which along with the moderate K^+ and NO_3^- correlation could indicate the contribution from aged biomass burning plumes (Li et al., 2003). In general, strong correlations between species in the $PM_{2.5-10}$ size fraction (Figure 3-15 left pane) were not as common as in the $PM_{2.5}$ size fraction.

PCA yielded three meaningful $PM_{2.5}$ (Figure 3-15 right pane) and three meaningful $PM_{2.5-10}$ (Figure 3-16 right pane) factors for all sites, except for LT, for which only two meaningful factors were obtained in the $PM_{2.5}$ size fraction. All factors represented single or multiple combinations of emissions associated with marine, terrigenous, biomass burning, fossil fuel use and agricultural emissions. These factors explained 61.0 to 70.2% and 57.2 to 68.8% of the total variances for the analysed ions in the $PM_{2.5}$ and $PM_{2.5-10}$ size fractions, respectively.

By plotting SSF vs. nSSF (Figures 3-17 to 3-20), it was evident for both size fractions that Cl^- was predominantly from marine origin. SO_4^{2-} in both size fractions was predominantly from non-marine origin at all sites, although fractionally more samples were associated with marine origin in the $PM_{2.5-10}$ size fraction, if compared to the $PM_{2.5}$ size fraction. For Mg^{2+} at the VT (Figure 3-17), it is apparent that it is mostly from non-marine origin in both size fractions, which could indicate the influence of fly ash (industry and/or household combustion origin). Ca^{2+} in both size fractions at all sites (Figures 3-17 to 3-20) was predominantly from non-marine origin, which is likely due to wind-blown dust.

Additional processing of the SSF and nSSF data led to the deduction of estimated source contributions to the determined chemical analysed ion content of the $PM_{2.5}$ (Figure 3-21a) and $PM_{2.5-10}$ (Figure 3-21b) size fractions for all sites. Marine, terrigenous together with

biomass burning, fossil fuel use, NH_4^+-associated and OA-associated contributions were quantified. Fossil fuel use, NH_4^+-associated, terrigenous and biomass burning source contributions were most significant at all sites in the $PM_{2.5}$ size fraction (Figure 3-21a). However, the marine contribution was comparatively stronger at SK and LT, than at the other sites, which made sense considering the air mass histories (Figure 3-6). As expected, the contributions associated with marine, terrigenous and biomass burning sources increased in the $PM_{2.5-10}$ size faction (Figure 3-21b), if compared to the $PM_{2.5}$ size faction (Figure 3-21a). OA-associated sources made consistent contributions in both size fractions, ranging from 3.0 to 13.0%.

CHAPTER 4

MASS CLOSURE ASSESSMENT

In this chapter… *A brief introduction is presented (section 4.1), before the results and discussions relating to mass closure of all the species studied in Chapters 2 and 3 are presented (section 4.2). Thereafter, section 4.3 presents the conclusions. This chapter is linked to Objective 1 and 2, as stated in section 1.3.*

4.1 Introduction

Particulate matter is studied because of its possible environmental and human health impacts (section 3.1.2). As indicated in the previous chapter, various deductions can be made from the chemical compositions of aerosols and numerous methods can be applied to identify possible sources and/or source contributions. However, aerosol composition also needs to be considered within the context of mass closure, in order to understand the contribution of individual species to the overall aerosol mass concentration (Sillanpää et al., 2006; Yang et al., 2011; Gu et al., 2014). Without this understanding, specific sources cannot be targeted to reduce the overall aerosol mass, which is particularly problematic within the context of the South African interior (SAAQIS, 2018). As was previously indicated (section 3.1.4) very limited aerosol chemical composition data have been reported for South Africa (Tiitta et al., 2014; Maritz et al., 2015; Aurela et al., 2016; Venter et al., 2018a). Of these, even fewer considered mass closure.

Tiitta et al. (2014) correlated the total non-refractive PM_1 chemical composition (NR-PM_1) measured with an Aerosol Chemical Speciation Monitor (ASCM) and PM_1 black carbon (BC), with aerosol mass calculated from differential mobility particle sizer (DMPS) measurements to attempt mass closure. Although the correlation coefficient (r) between the afore-mentioned species was 0.94, the slope of the linear line was 0.84, which indicated that a significant fraction of aerosol mass was not accounted for. Maritz et al. (2015) published limited mass fractions for OC and EC, but did not consider any other species. Similar to Tiitta et al. (2014), Aurela et al. (2016) used PM_1 aerosol mass calculated from DMPS measurements to indicate that water-soluble ions, organic matter (OM) and EC comprised most of the PM_1 mass, but could not make further mass closure deductions based on the very small dataset considered. Although these authors (Aurela et al., 2016) also measured $PM_{1\text{-}2.5}$ and $PM_{2.5\text{-}10}$, no mass closure results relating to these size fractions were presented.

In addition to these limited literature results, OC and EC mass fractions (section 2.3.1), as well as inorganic water-soluble ion and organic acid (OA) mass fractions (section 3.3.2) were presented in this study. In the current chapter, the afore-mentioned organic mass (i.e. OM, calculated from OC) and EC mass fractions, as well as the inorganic water-soluble mass fractions are presented within the context of the overall aerosol mass.

4.2 Results and discussion

Figures 4-1 and 4-2 present the mass fraction percentages of all the species considered in Chapters 2 (i.e. OC and EC) and 3 (i.e. SO_4^{2-}, NO_3^-, Cl^-, F^-, Na^+, NH_4^+, K^+, Mg^{2+} and Ca^{2+}), as well as the mass fraction that could not be attributed to any of these species, in both size fractions at all the INDAAF sites. Some ions contributed very little to the mass fractions that were grouped together, as indicated by the legend in each figure. As mentioned in Chapter 3, the OC concentrations were converted to OM concentrations by multiplying it with a factor of 1.71 (Hegg et al., 1997; Turpin and Lim, 2001).

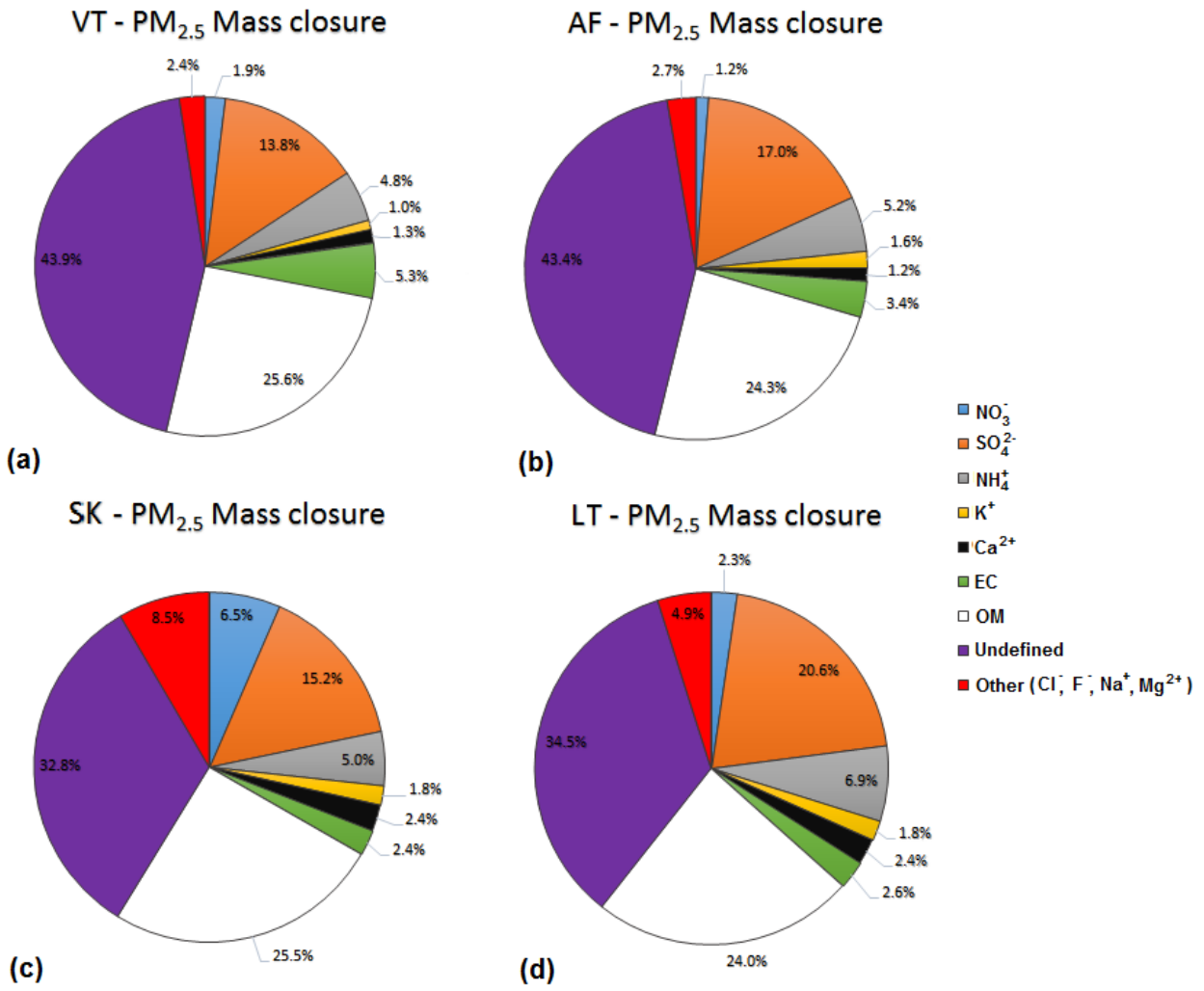

Figure 4-1: Average $PM_{2.5}$ mass fraction contribution percentages (%) of the aerosol species present in the total aerosol load at the INDAAF sites, i.e. VT (a), AF (b), SK (c) and LT (d), respectively

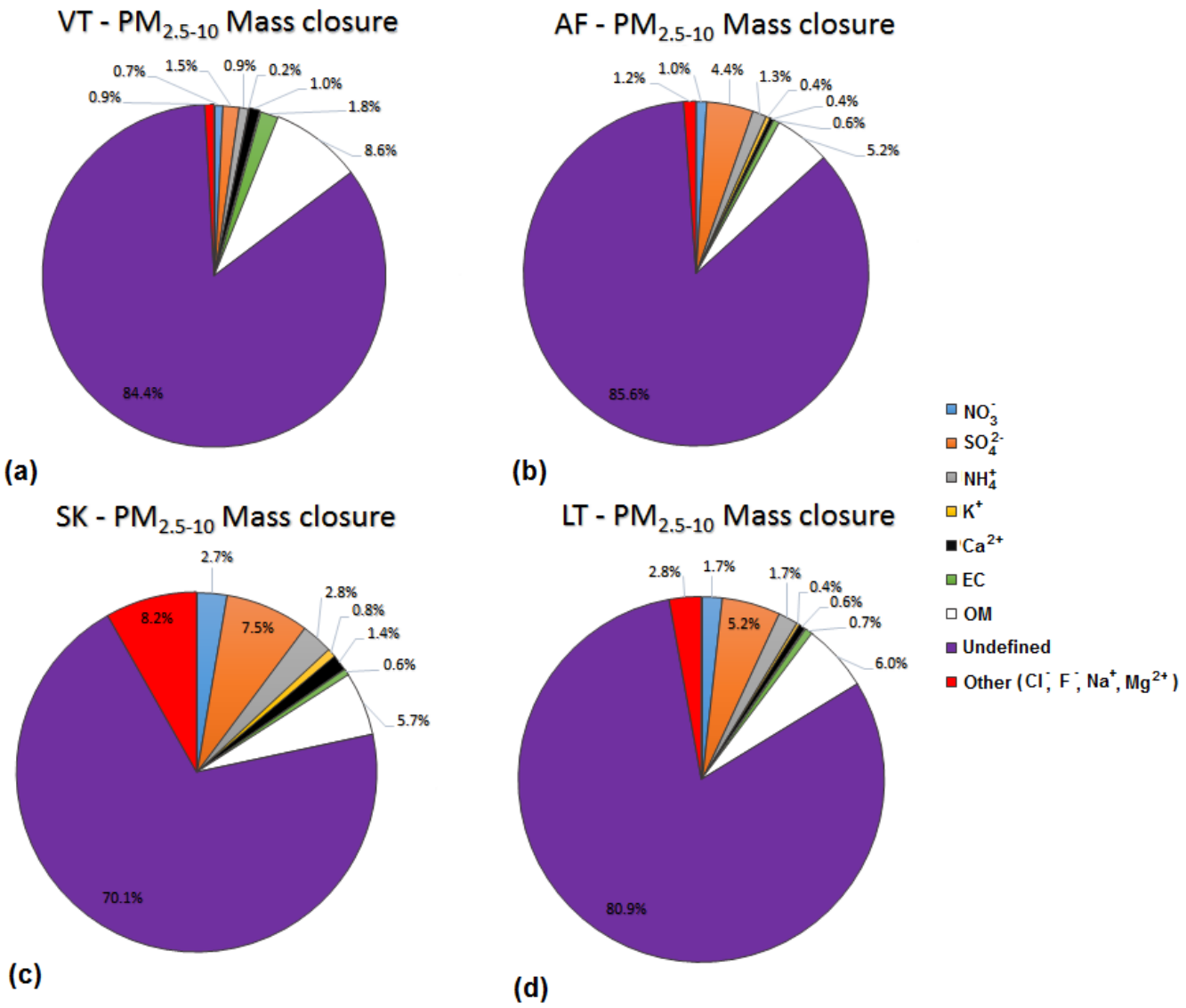

Figure 4-2: Average $PM_{2.5-10}$ mass fraction contribution percentages (%) of the aerosol species present in the total aerosol load of the INDAAF sites, i.e. VT (a), AF (b), SK (c) and LT (d), respectively

It is evident from the results that the quantified chemical mass contributions accounted for more than half (56.1 to 67.2%) of the $PM_{2.5}$ size fraction for all the sites, while the undefined fraction (i.e. that was not quantified chemically) accounted for the majority (70.1 to 85.6%) of the mass in the $PM_{2.5-10}$ size fraction. The undefined fractions in both size fractions at all sites are likely to primarily comprise of wind-blown dust (i.e. mineral dust) from crustal sources (Piketh et al., 1999; Van Zyl et al., 2014), since South Africa is a semi-arid country (Mphepya et al., 2004; Maritz et al., 2015). Receptor modelling results, based on measurements conducted at several regional background sites in South Africa, indicated that wind-blown dust contributed between 29.0 and 69.0% to the total inorganic aerosol PM_{10} load, depending on location and season (Piketh et al., 1999). Mineral dust contains various phases that are insoluble, such as alumina silicates. Fly ash from large point sources (Mahlaba et al., 2011) could also contribute to the insoluble mineral matter reporting to the undefined mass in the $PM_{2.5}$ size fraction. Since South African industries employ bag filter and/or electrostatic precipitator technologies to limit fly ash emissions (Pretorius et al., 2015), ambient fly ash from such sources is expected to be fine (i.e. passing through bag filters and/or electrostatic precipitators). However, insoluble mineral matter present in household combustion emissions are unfiltered and could contribute to the undefined mass in both the $PM_{2.5}$ and $PM_{2.5-10}$ size fractions, especially at VT where various large semi- and informal settlements are nearby.

Considering the significance of the quantified chemical mass contributions in the $PM_{2.5}$ size fraction at all the sites (accounting for 56.1 to 67.2% of total aerosol mass), this size fraction (Figure 4.1) is considered further. From Figure 4-1, it is evident that OM, SO_4^{2-}, NH_4^+ and EC combined accounted for the majority of the chemically quantified $PM_{2.5}$ aerosol mass. The total aerosol mass percentage contributions of these four species were 49.5, 49.9, 48.1 and 54.1%, at VT, AF, SK and LT, respectively. Of these four species, OM made the largest overall $PM_{2.5}$ aerosol mass percentage contributions at all sites (24.0 to 25.6%), with SO_4^{2-} making the second largest contribution at all sites (13.8 to 20.6%). The overall $PM_{2.5}$ aerosol mass percentage contributions of NH_4^+ (4.8 to 6.9%) and EC (2.4 to 5.3%) were substantially less than that of OM and SO_4^{2-}, but significantly higher than other quantified species.

In Chapter 3 (section 3.3.3), it was stated that no obvious seasonal patterns were observed for the water-soluble ionic species concentrations, due to air mass histories being such a dominant determining factor. To explore possible seasonal variations in the aerosols mass contributions, Figure 4-3 ($PM_{2.5}$) and Figure 4-4 ($PM_{2.5-10}$) present the mass fraction percentages for the individual seasons at every site and in both size fractions. The months

for each season included September till November for spring, December till February for summer, March till May for autumn and June till August for winter.

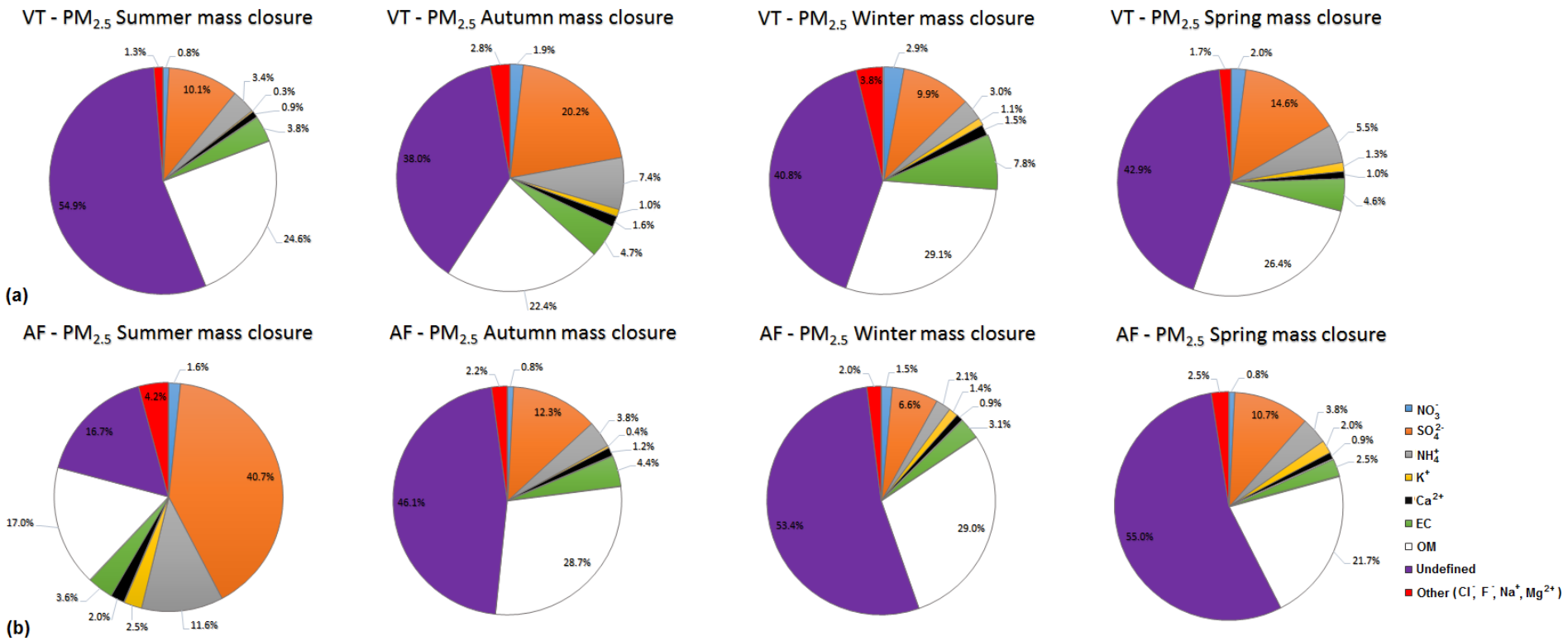

Figure 4-3: Average $PM_{2.5}$ size fraction contribution percentages (%) of the aerosol species present in each season of the INDAAF sites, i.e. VT (a), AF (b), SK (c) and LT (d), respectively

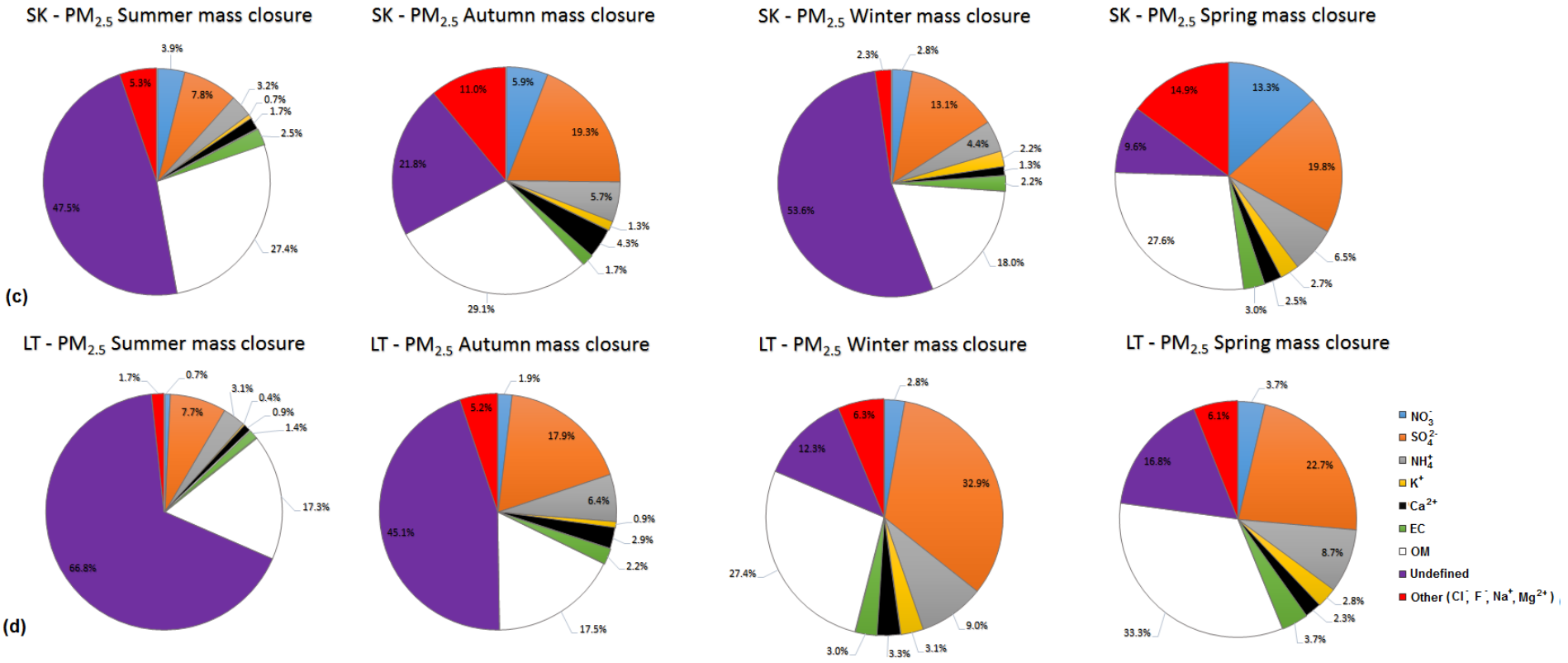

Figure 4-3 (continued): Average $PM_{2.5}$ size fraction contribution percentages (%) of the aerosol species present in each season of the INDAAF sites, i.e. VT (a), AF (b), SK (c) and LT (d), respectively

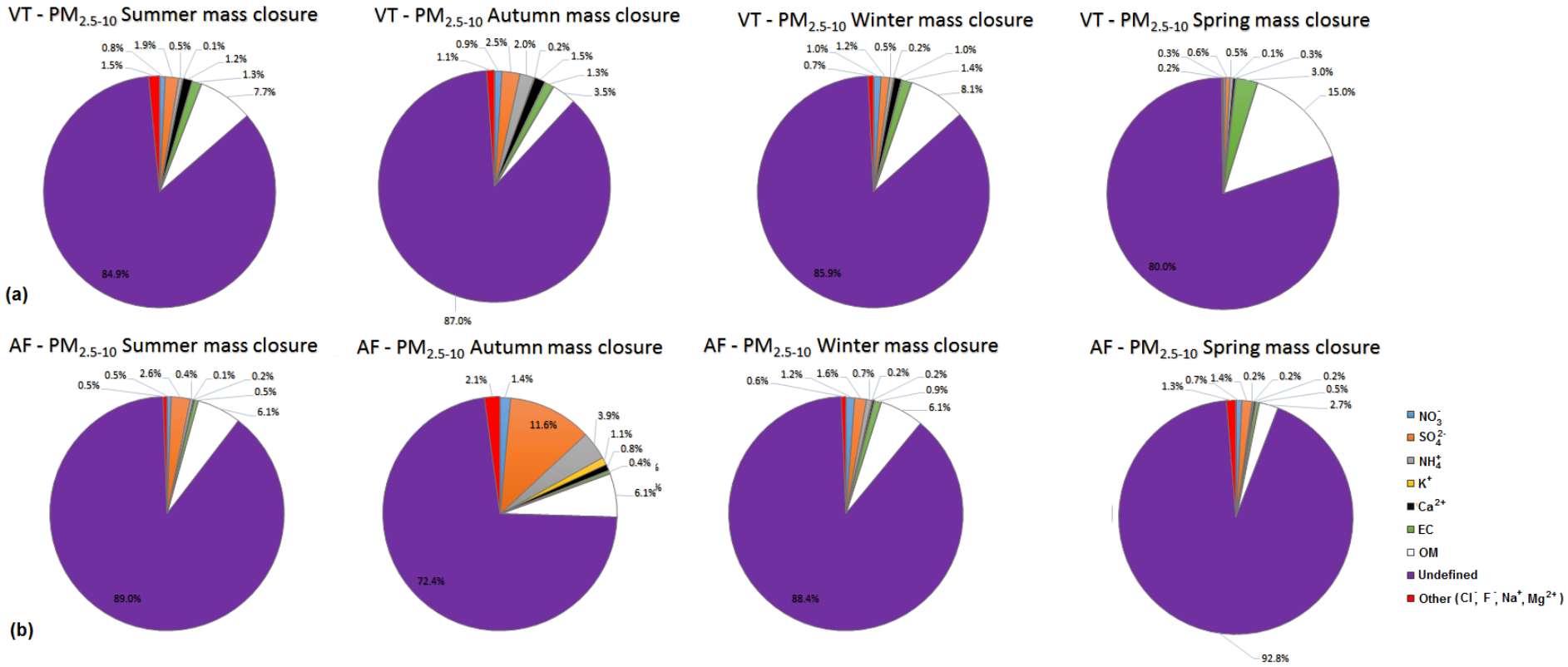

Figure 4-4: Average $PM_{2.5-10}$ size fraction contribution percentages (%) of the aerosol species present in each season of the INDAAF sites, i.e. VT (a), AF (b), SK (c) and LT (d), respectively

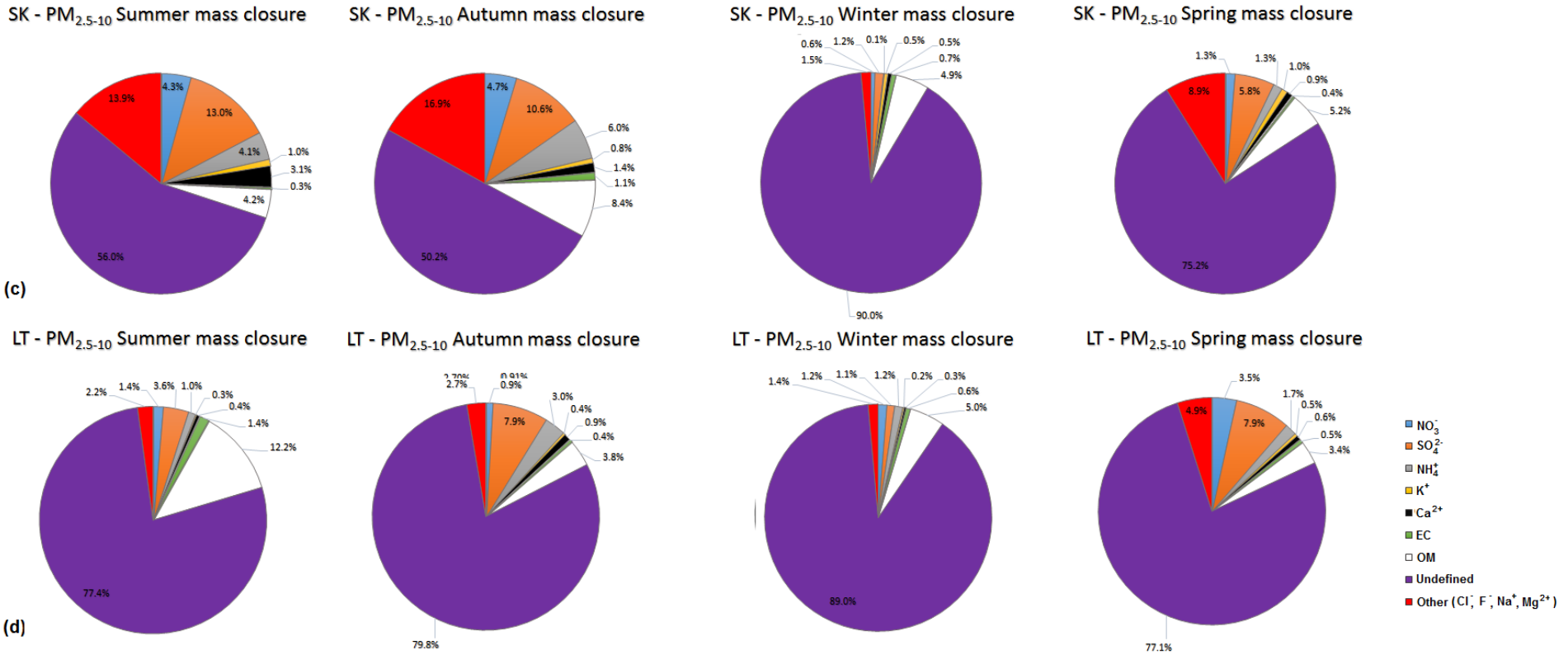

Figure 4-4 (continued): Average $PM_{2.5-10}$ size fraction contribution percentages (%) of the aerosol species present in each season of the INDAAF sites, i.e. VT (a), AF (b), SK (c) and LT (d), respectively

It was earlier hypothesised that most of the mass in the undefined fractions in both size fractions, at all sites, is likely to primarily comprise of wind-blown dust and fly ash. If wind-blown dust was the main source, one would intuitively have expected the undefined mass fraction to be lower in summer (due to lower dust generation of wetter surfaces and wet scavenging of aerosols) than in winter (due to dryer surfaces and almost no wet scavenging). However, this was not consistently the case at all sites, in both size fractions. In the $PM_{2.5}$ size fraction only at AF in summer there was a significantly lower undefined mass fraction observed than in winter, while this was only observed at SK in the $PM_{2.5-10}$ size fraction.

In addition to the temporal mass closure aspects considered in Figures 4.3 and 4.4, stacked bar plots of the $PM_{2.5}$ and $PM_{2.5-10}$ mass fractions (%) at all the sites, i.e. VT (a), AF (b), SK (c) and LT (d), for individual samples collected over the entire sampling period are presented in shown in Figures A-2 and A-3 (Appendix A).

4.3 Summary and conclusions

The quantified chemical mass contributions accounted for more than half of the $PM_{2.5}$ size fraction for all the sites, while the undefined fraction (i.e. that was not quantified chemically) accounted for the majority of the mass in the $PM_{2.5-10}$ size fraction. The undefined fractions in both size fractions at all sites are likely to primarily comprise of wind-blown dust, as well as fly ash from large point sources and household combustion. As was indicated in section 2.3.2, even SK that is considered as a regional background site, is likely to be impacted by household combustion. OM, SO_4^{2-}, NH_4^+ and EC combined accounted for the majority of the chemically quantified $PM_{2.5}$ aerosol mass. OM made the largest overall $PM_{2.5}$ aerosol mass percentage contributions at all sites, with SO_4^{2-} making the second largest contribution at all sites.

As was the case with water-soluble ionic species seasonal patterns (section 3.3.3), no obvious seasonal pattern could be identified for the aerosol mass contributions in both size ranges. This uncertainty in explaining the results and the large contribution of the undefined fraction clearly indicates that chemical/mineralogical identification and quantification of the species in this fraction need to receive more research attention in future.

CHAPTER 5

FINAL CONCLUSIONS, PROJECT EVALUATION AND FUTURE PERSPECTIVES

In this chapter… *Section 5.1 presents the final conclusions, while section 5.2 considers the project evaluation within the context of the objectives set in section 1.2. Section 5.3 provides future perspectives and recommendations.*

5.1 Final conclusions

This thesis (specifically Chapter 2) presented the first long-term (several years) OC and EC dataset for the South African interior that covers multiple measurement sites, i.e. two regional background sites (SK and LT), an industrially influenced site (AF) and an urban/industrial site (VT). OC and EC mass fractions at all the sites were lower than what is typical within a developed world context. This was not due to lower OC and EC levels at the South African sites, but rather due to larger fractional contributions from other species, with specifically SO_4^{2-} making a significant contribution (as mentioned in Chapters 3 and 4). OC and EC levels were significantly higher at VT than at the other sites. OC/EC ratios implied that sources in close proximately to this site (VT) were likely the main contributors, while more distant sources impacted AF, SK and LT more substantially. Seasonal assessment indicated that household combustion for space heating in semi- and informal settlements was likely to be the most dominant OC and EC source at VT. This was substantiated by correlating OC and EC concentrations to ambient temperature. Additionally, overlay back trajectory maps compiled for the sampling periods indicated that air masses that had passed over the Johannesburg-Pretoria (Jhb-Pta) megacity, which is also a relatively polluted area, made a contribution to OC and EC levels measured at VT. Open biomass burning made a contribution at all sites, but its impact at VT was obscured by the influence of household combustion for space heating.

Seasonal OC and EC patterns also indicated that elevated levels of OC and EC at LT were likely to be due to regional open biomass burning. This was confirmed by overlay back trajectory analysis, within the context of open biomass burning fire locations. Open biomass burning and household combustion both contributed to elevated levels of OC and EC in the seasonal patterns of SK and AF, which were confirmed with considering back trajectory analysis, population densities and open biomass burning fire locations.

Overall, the OC- and EC-related results (Chapter 2) indicated that open biomass burning contributed to elevated OC and EC levels on a regional scale in the South African interior. Household combustion for space heating in semi- and informal settlements makes a substantial local (e.g. at VT) and noticeable regional (e.g. at AF and SK) OC and EC contribution, which has not previously been indicated. Additionally, industrial and/or vehicle emissions contributed to the baseline OC and EC levels year-round, while oxidation of VOCs during the wet season will also contribute to OC levels. The low OC/EC levels at VT supports the notion of emitting sources being close to this measurement site, while the higher OC/EC ratios at the other sites indicates emitting sources to be further away from the measurement site.

Chapter 3 presented the first long-term (several years) $PM_{2.5}$ and $PM_{2.5-10}$ inorganic water-soluble and organic acid (OA) dataset for the South African interior, again for the same measurement sites introduced in Chapter 2. The highest concentration of water-soluble ions occurred in the $PM_{2.5}$ size fraction, wherein SO_4^{2-} had the highest concentrations, followed by OA. VT had the highest SO_4^{2-} and NH_4^+ concentrations, followed by AF, SK and LT, while NO_3^- concentrations were the highest at VT, followed by SK, AF and LT. Higher NO_3^- levels at SK, instead of at AF (as expected), were explained by the high-stack emissions at AF and the atmospheric lifetime of NO_2 that is normally longer than that of SO_2. However, NO_3^- concentrations depends on various factors other than only NO_2 concentrations, therefore it is possible that other sources could be responsible for the differences between the sites, since the air mass histories differ significantly.

No clear seasonal patterns could be identified for the most prominent species, i.e. SO_4^{2-}, NO_3^-, OA and NH_4^+. Instead, it was found that air mass histories have a significant impact on the chemical compositions.

Acidity and neutralisation calculations demonstrated that the main acid forming species (i.e., SO_4^{2-}, NO_3^- and OA) in both size fractions were, in principle, completely neutralised by NH_4^+, Mg^{2+} and Ca^{2+}. This is a very important result, since it indicates that aerosol composition does not further aggravate the regional acid deposition problem over the South African interior (Conradie et al., 2016). Calculated neutralisation factors indicated that NH_4^+ is probably the most important cation to neutralise the acidic ions in the $PM_{2.5}$ size fraction, while Ca^{2+} is likely to be the second most important. The results further suggested that the likely neutralisation contribution of Mg^{2+} and Ca^{2+}, relative to NH_4^+, increased in the $PM_{2.5-10}$ size fraction.

Diagonal correlation graph analysis indicated strong positive correlations between SO_4^{2-} and NH_4^+ in the $PM_{2.5}$ size fraction at VT, AF and LT, and a moderate correlation at SK, which demonstrated the significance of neutralisation between these two species to form NH_4HSO_4 and/or $(NH_4)_2SO_4$. Much weaker correlations were found between NH_4^+ and NO_3^- in the fine

fraction, indicating that NH_4NO_3 formation is less significant. Strong correlation between K^+ and Cl^- only at VT demonstrated the probable impact of fresh biomass from household combustion (e.g. wood burning) at this site. Ca^{2+} and Mg^{2+} were strongly correlated at all sites, which indicated that terrigenous sources, fly ash and/or marine aerosols could make meaningful contributions. K^+ and NO_3^- correlated moderately at all sites, indicating the use of fertiliser across the region, wherein Cl^--free KNO_3 is often used as a source of soluble NO_3^- and K^+. K^+ and SO_4^{2-} also correlated moderately at all sites, which along with the moderate K^+ and NO_3^- correlation could indicate the contribution of aged biomass burning plumes (Li et al., 2003). Overall, strong correlations between species in the $PM_{2.5-10}$ size fraction were not common.

Meaningful factors obtained from principal component analysis (PCA) indicated that marine, terrigenous, biomass burning, fossil fuel use and agricultural emissions make contributions at all sites. By plotting sea-salt fractions (SSFs) vs. non-sea-salt fractions (nSSFs), it was obvious that Cl^- was predominantly from marine origin in both size fractions. At all sites, SO_4^{2-} in both size fractions was predominantly from non-marine origin. Mg^{2+} and Ca^{2+} in both size fractions, at all sites, were strongly correlated, which indicate similar source(s).

Estimated source contributions for marine, terrigenous together with biomass burning, fossil fuel use, NH_4^+-associated and OA-associated sources were calculated. Fossil fuel use, terrigenous, biomass burning and NH_4^+-associated sources made the most significant contributions to analysed ions at all sites in the $PM_{2.5}$ size faction. However, marine contributions were comparatively stronger at SK and LT, than at the other sites. The contributions associated with marine, terrigenous and biomass burning sources also increased in the $PM_{2.5-10}$ size faction, if compared to the fine fraction. The OA-associated sources made relatively small, but consistent contributions in both size fractions at all sites. OA is likely to be from biomass burning (Conradie et al., 2016), however, other sources could also contribute to OA.

In Chapter 4, the overall mass balances for both size fractions at all sites were presented. The quantified chemical mass contributions, i.e. organic mass (OM, calculated from OC), EC and water-soluble ions, accounted for more than half of the $PM_{2.5}$ size fraction for all the sites, while the undefined fraction accounted for the majority of the coarse fraction. The undefined portions in both size fractions are likely to comprise primarily wind-blown dust, as well as industrial fly ash and household combustion fly ash. Combined, OM, SO_4^{2-}, NH_4^+ and EC accounted for the majority of the chemically quantified $PM_{2.5}$ aerosol mass. OM made the largest overall $PM_{2.5}$ aerosol mass percentage contributions at all sites, with SO_4^{2-} making the second largest contribution.

5.2 Project evaluation

In order to evaluate the project, the outcomes were compared with the objectives set in Chapter 1, section 1.2. Therefore, each objective is again repeated here, followed by a short discussion on how this objective was achieved.

Objective 1:

"Perform long-term assessment of OC and EC aerosol concentrations in the South African interior. This assessment should include evaluating spatial and temporal patterns, mass fractions of the total aerosol mass and possible source contributions."

Long-term measurements of OC and EC aerosol concentrations were conducted at two regional background sites (i.e. SK and LT), as well as two sites that are more directly impacted by nearby emissions (i.e. VT and AF). Specifically, it was decided to collect filter samples, which were analysed off-line to yield OC and EC contents, since continuous online measurements at the relatively remote regional background sites were not possible. Samples were collected for a period of 6.5 years. From this dataset, spatial and temporal patterns, mass fraction contributions, and possible source contributions were deduced. A summary of the main findings was presented in section 5.1. These findings included several important deductions, which significantly improved the level of scientific understanding of OC and EC in the South African interior.

Objective 2:

"Conduct similar (to Objective 1) assessment of aerosol water-soluble inorganic ions and organic acids at the same sampling sites."

Concurrently to the OC and EC sample collection (associated with Objective 1), samples were collected over 6.5 years at the same sites (i.e. VT, AF, SK and LT) that were used to quantify aerosol water-soluble inorganic ions and organic acids concentrations. These samples were also analysed off-line, since online analyses of all the species at all the sites were not feasible. Spatial and temporal patterns, mass fraction contributions, and possible source contributions were derived from this dataset. A summary of the main findings related to the water-soluble ions and OA was presented in section 5.1. These findings included several important deductions, which significantly improved the current level of scientific understanding of these species in the South African interior. One drawback of the sampling methodology employed was identified during data analysis, i.e. a 24-hour sample per month does not necessarily represent the average monthly concentrations, which possibly contributed no clear seasonal patterns being observed for the main ions. However, from a previous study at a regional South African background site, during which highly temporally resolved measurements of ionic species were conducted (Tiitta et al., 2014), only vague seasonal patterns could be deduced.

5.3 Future perspectives

If highly temporally resolved measurements are not possible, a recommendation would be to collect composite monthly samples rather than a single 24-hour sample per month, as in this study. Such composite monthly samples might be better suited to assess seasonal cycles. However, it will be more complicated to assess the air mass histories of monthly composite samples, than 24-hour samples.

The total $PM_{2.5}$ water-soluble ionic concentrations at VT, AF and SK (Table A-1, Appendix A) exceeded the guideline set by the WHO (2014), which indicated that the ionic content of $PM_{2.5}$ in South Africa requires attention in terms of possible air quality impacts. This should be brought to the attention of the Department of Environmental Affairs (DEA) and similar studies at more sites should be encouraged to verify the extent of the problem.

The uncertainty related to the chemical/mineralogical composition of the very significant undefined mass fractions should be addressed in future studies. Furthermore, if possible, differentiation should be made between wind-blown dust, industrial fly ash and household combustion fly ash source contributions. No published works were found by the candidate to aid in measurements that might distinguishing between these source contributions and currently no known experimental studies are on-going to differentiate between the above mentioned contributions.

As far as the candidate could assess, aerosol dry deposition, based on actual measurements, has not yet been presented for South Africa. If deposition velocities for the two size fractions considered can be calculated or modelled, the concentration-based results presented in this study could be used to calculate such deposition. Experimental studies are planned to start soon on the assessment of aerosol dry deposition.

BIBLIOGRAPHY

AMSTER, E. D., HAIM, M., DUBNOV, J. & BRODAY, D. M. 2014. Contribution of nitrogen oxide and sulfur dioxide exposure from power plant emissions on respiratory symptom and disease prevalence. *Environmental Pollution,* 186**,** 20-28. http://dx.doi.org/10.1016/j.envpol.2013.10.032

ANDREAE, M., ANDREAE, T., ANNEGARN, H., BEER, J., CACHIER, H., LE CANUT, P., ELBERT, W., MAENHAUT, W., SALMA, I. & WIENHOLD, F. 1998. Airborne studies of aerosol emissions from savanna fires in southern Africa: 2. Aerosol chemical composition. *Journal of Geophysical Research: Atmospheres,* 103**,** 32119-32128.

ARL. 2014. *Air Resources Laboratory: Gridded Meteorological Data Archives* [Online]. Available: http://www.ready.noaa.gov/archives.php [Accessed 24 February 2014].

ASMAN, W. A., SUTTON, M. A. & SCHJØRRING, J. K. 1998. Ammonia: emission, atmospheric transport and deposition. *The New Phytologist,* 139**,** 27-48.

ATKINSON, R. W., MILLS, I. C., WALTON, H. A. & ANDERSON, H. R. 2015. Fine particle components and health—a systematic review and meta-analysis of epidemiological time series studies of daily mortality and hospital admissions. *Journal of Exposure Science and Environmental Epidemiology,* 25**,** 208. DOI: 10.1038/jes.2014.63

AURELA, M., BEUKES, J. P., VAN ZYL, P., VAKKARI, V., TEINILÄ, K., SAARIKOSKI, S. & LAAKSO, L. 2016. The composition of ambient and fresh biomass burning aerosols at a savannah site, South Africa. *South African Journal of Science,* 112**,** 1-8. DOI: 10.17159/sajs.2016/20150223

BABU, A. G. & REDDY, M. S. 2011. Dual inoculation of arbuscular mycorrhizal and phosphate solubilizing fungi contributes in sustainable maintenance of plant health in fly ash ponds. *Water, Air and Soil Pollution,* 219**,** 3-10. DOI: 10.1007/s11270-010-0679-3

BABU, R. V., CARDENAS JR, V. & SHARMA, G. 2008. Acute respiratory distress syndrome from chlorine inhalation during a swimming pool accident: a case report and review of the literature. *Journal of Intensive Care Medicine,* 23**,** 275-280. DOI: 10.1177/0885066608318471

BAE, M.-S. & PARK, S.-S. 2013. Thermal distribution of size-resolved carbonaceous aerosols and water soluble organic carbon in emissions from biomass burning. *Asian Journal of Atmospheric Environment,* 7**,** 95-104. http://dx.doi.org/10.5572/ajae.2013.7.2.095

BALDAUF, R. W., LANE, D. D., MAROTZ, G. A. & WIENER, R. W. 2001. Performance evaluation of the portable MiniVOL particulate matter sampler. *Atmospheric Environment,* 35**,** 6087-6091. DOI: 10.1016/S1352-2310(01)00403-4

BARBIER, O., ARREOLA-MENDOZA, L. & DEL RAZO, L. M. 2010. Molecular mechanisms of fluoride toxicity. *Chemico-Biological Interactions,* 188**,** 319-333. DOI: 10.1016/j.cbi.2010.07.011

BARCZA, N. 1995. Presidential Address: The role of pyrometallurgy in the development of South Africa. *Journal of the Southern African Institute of Mining and Metallurgy,* 96**,** 229-239. http://hdl.handle.net/10520/AJA0038223X_2396

BEUKES, J. P., VAN ZYL, P. G., VENTER, A. D., JOSIPOVIC, M., JAARS, K., TIITTA, P., PIENAAR, J. J., LAAKSO, L., VAKKARI, V. & KULMALA, M. 2013a. Source region plume characterisation of the interior of South Africa as observed at Welgegund. *Clean Air Journal/Tydskrif vir Skoon Lug,* 23**,** 7-10. http://hdl.handle.net/10520/EJC148129

BIRCH, M. 1998. Analysis of carbonaceous aerosols: interlaboratory comparison. *Analyst,* 123**,** 851-857. DOI: 10.1039/A800028J

BIRCH, M. & CARY, R. 1996. Elemental Carbon-Based Method for Monitoring Occupational Exposures to Particulate Diesel Exhaust. *Aerosol Science and Technology,* 25**,** 221-241. DOI: 10.1080/02786829608965393

BODHAINE, B. A. 1995. Aerosol absorption measurements at Barrow, Mauna Loa and the south pole. *Journal of Geophysical Research: Atmospheres,* 100**,** 8967-8975. DOI: 10.1029/95JD00513

BOND, T. C., DOHERTY, S. J., FAHEY, D. W., FORSTER, P. M., BERNTSEN, T., DEANGELO, B. J., FLANNER, M. G., GHAN, S., KÄRCHER, B., KOCH, D., KINNE, S.,

KONDO, Y., QUINN, P. K., SAROFIM, M. C., SCHULTZ, M. G., SCHULZ, M., VENKATARAMAN, C., ZHANG, H., ZHANG, S., BELLOUIN, N., GUTTIKUNDA, S. K., HOPKE, P. K., JACOBSON, M. Z., KAISER, J. W., KLIMONT, Z., LOHMANN, U., SCHWARZ, J. P., SHINDELL, D., STORELVMO, T., WARREN, S. G. & ZENDER, C. S. 2013. Bounding the role of black carbon in the climate system: A scientific assessment. *Journal of Geophysical Research: Atmospheres,* 118**,** 5380-5552. DOI: 10.1002/jgrd.50171

BOND, T. C. & SUN, H. 2005. Can reducing black carbon emissions counteract global warming? *Environmental Science and Technology,* 39(11)**,** 5921-5926. DOI: 10.1021/es0480421

BOOYENS, W., VAN ZYL, P. G., BEUKES, J. P., RUIZ-JIMENEZ, J., KOPPERI, M., RIEKKOLA, M.-L., JOSIPOVIC, M., VENTER, A. D., JAARS, K., LAAKSO, L., VAKKARI, V., KULMALA, M. & PIENAAR, J. J. 2015. Size-resolved characterisation of organic compounds in atmospheric aerosols collected at Welgegund, South Africa. *Journal of Atmospheric Chemistry,* 72**,** 43-64. DOI: 10.1007/s10874-015-9304-6

BOTHE, M. & DONAHUE, N. M. 2010. Organic aerosol formation in citronella candle plumes. *Air Quality, Atmosphere and Health,* 3**,** 131-137. DOI: 10.1007/s11869-009-0061-z

BOUWMAN, A., LEE, D., ASMAN, W., DENTENER, F., VAN DER HOEK, K. & OLIVIER, J. 1997. A global high-resolution emission inventory for ammonia. *Global Biogeochemical Cycles,* 11**,** 561-587.

BRASSEUR, G., ORLANDO, J. J. & TYNDALL, G. S. 1999. *Atmospheric chemistry and global change*, Oxford University Press.

BRESSI, M., SCIARE, J., GHERSI, V., BONNAIRE, N., NICOLAS, J., PETIT, J.-E., MOUKHTAR, S., ROSSO, A., MIHALOPOULOS, N. & FÉRON, A. 2013. A one-year comprehensive chemical characterisation of fine aerosol ($PM_{2.5}$) at urban, suburban and rural background sites in the region of Paris (France). *Atmospheric Chemistry and Physics,* 13**,** 7825-7844. DOI: 10.5194/acp-13-7825-2013

BRESSI, M., CAVALLI, F., BELIS, C. A., PUTAUD, J.-P., FRÖHLICH, R., MARTINS DOS SANTOS, S., PETRALIA, E., PRÉVÔT, A. S. H., BERICO, M., MALAGUTI, A. AND CANONACO, F. 2016. Variations in the chemical composition of the submicron aerosol and in the sources of the organic fraction at a regional background site of the Po Valley (Italy). Atmospheric Chemistry and Physics, 16(20), 12875–12896. DOI:10.5194/acp-16-12875-2016

BROCARD, D., LACAUX, C., LACAUX, J.-P., KOUADIO, G. & YOBOUE, V. 1996. Emissions from the combustion of biofuels in western Africa. *Biomass Burning and Global Change,* 1**,** 350-360.

BRUCE, N., PEREZ-PADILLA, R. & ALBALAK, R. 2000. Indoor air pollution in developing countries: a major environmental and public health challenge. *Bulletin of the World Health Organization,* 78**,** 1078-1092.

BUTT, E. W., RAP, A., SCHMIDT, A., SCOTT, C. E., PRINGLE, K. J., REDDINGTON, C. L., RICHARDS, N. A. D., WOODHOUSE, M. T., RAMIREZ-VILLEGAS, J., YANG, H., VAKKARI, V., STONE, E. A., RUPAKHETI, M., PRAVEEN, P. S., VAN ZYL, P. G., BEUKES, J. P., JOSIPOVIC, M., MITCHELL, E. J. S., SALLU, S. M., FORSTER, P. M. & SPRACKLEN, D. V. 2015. The impact of residential combustion emissions on atmospheric aerosol, human health and climate. *Atmospheric Chemistry and Physics Discussions,* 15**,** 20449-20520. DOI: 10.5194/acpd-15-20449-2015

CALLÉN, M., LÓPEZ, J. & MASTRAL, A. 2012. Apportionment of the airborne PM_{10} in Spain. Episodes of potential negative impact for human health. *Journal of Environmental Monitoring,* 14**,** 1210-1219.

CAO, J., LEE, S., HO, K., ZOU, S., FUNG, K., LI, Y., WATSON, J. G. & CHOW, J. C. 2004. Spatial and seasonal variations of atmospheric organic carbon and elemental carbon in Pearl River Delta Region, China. *Atmospheric Environment,* 38**,** 4447-4456. DOI: 10.1016/j.atmosenv.2004.05.016

CAO, X., ZHANG, X., TONG, D. Q., CHEN, W., ZHANG, S., ZHAO, H. & XIU, A. 2017. Review on physicochemical properties of pollutants released from fireworks: environmental and health effects and prevention. *Environmental Reviews,* 26**,** 133-155. DOI: 10.1016/j.atmosenv.2004.05.016

CASERINI, S., GALANTE, S., OZGEN, S., CUCCO, S., DE GREGORIO, K. & MORETTI, M. 2013. A methodology for elemental and organic carbon emission inventory and results for Lombardy region, Italy. *Science of the Total Environment,* 450**,** 22-30. DOI: 10.1016/j.scitotenv.2013.01.073

CASTRO, T., PERALTA, O., SALCEDO, D., SANTOS, J., SAAVEDRA, M. I., ESPINOZA, M. L., SALCIDO, A., CELADA-MURILLO, A.-T., CARREÓN-SIERRA, S. & ÁLVAREZ-OSPINA, H. 2018. Water-soluble inorganic ions of size-differentiated atmospheric particles from a suburban site of Mexico City. *Journal of Atmospheric Chemistry,* 75**,** 155-169. DOI: 10.1007/s10874-017-9369-5

CĂTĂLINA, S., CĂTĂLIN, S. & ION, S. 2012. Impact assessment of saline aerosols on exercise capacity of athletes. *Procedia-Social and Behavioral Sciences,* 46**,** 4141-4145.

CAVALLI, F., ALASTUEY, A., ARESKOUG, H., CEBURNIS, D., ČECH, J., GENBERG, J., HARRISON, R. M., JAFFREZO, J. L., KISS, G., LAJ, P., MIHALOPOULOS, N., PEREZ, N., QUINCEY, P., SCHWARZ, J., SELLEGRI, K., SPINDLER, G., SWIETLICKI, E., THEODOSI, C., YTTRI, K. E., AAS, W. and PUTAUD, J. P. 2016. A European aerosol phenomenology -4: Harmonized concentrations of carbonaceous aerosol at 10 regional background sites across Europe. Atmospheric Environment, 144, 133–145, DOI:https://doi.org/10.1016/j.atmosenv.2016.07.050

CHARLSON, R. T., SCHWARZ, S. J., HALES, J. M., CESS, R. D., COAKLEY, J. A., HANSEN JR., J. E. & HOFMANN, D. J. 1992. Climate Forcing by Anthropogenic Aerosols. *American Association for the Advancement of Science,* 255**,** 423-430. http://www.jstor.org/stable/2876009

CHEN, X., SUN, Y., ZHAO, Q., SONG, X., HUANG, W., HAN, Y., SHANG, J., ZHU, T., WU, A. & LUAN, S. 2016. Design and characterization of human exposure to generated sulfate and soot particles in a pilot chamber study. *Journal of the Air and Waste Management Association,* 66**,** 366-376. DOI: 10.1080/10962247.2015.1136712

CHILOANE, K. E., BEUKES, J. P., VAN ZYL, P. G., MARITZ, P., VAKKARI, V., JOSIPOVIC, M., VENTER, A. D., JAARS, K., TIITTA, P., KULMALA, M., WIEDENSOHLER, A., LIOUSSE, C., MKHATSHWA, G. V., RAMANDH, A. & LAAKSO, L. 2017. Spatial, temporal and source contribution assessments of black carbon over the northern interior of South Africa. *Atmospheric Chemistry and Physics,* 17**,** 6177-6196. DOI: 10.5194/acp-17-6177-2017

CHOW, J., WATSON, J. G., CROW, D., LOWENTHAL, D. H. & MERRIFIELD, T. 2001. Comparison of IMPROVE and NIOSH carbon measurements. *Aerosol Science and Technology,* 34**,** 23-34. DOI: 10.1080/02786820119073

CHOW, J., WATSON, J. G., KUHNS, H., ETYEMEZIAN, V., LOWENTHAL, D. H., CROW, D., KOHL, S. D., ENGELBRECHT, J. P. & GREEN, M. C. 2004. Source profiles for industrial, mobile, and area sources in the Big Bend Regional Aerosol Visibility and Observational study. *Chemosphere,* 54**,** 185-208. DOI: 10.1016/j.chemosphere.2003.07.004

CHOW, J., WATSON, J. G., PRITCHETT, L. C., PIERSON, W. R., FRAZIER, C. A. & PURCELL, R. G. 1993. The DRI thermal/optical reflectance carbon analysis system: description, evaluation and applications in US air quality studies. *Atmospheric Environment. Part A. General Topics,* 27**,** 1185-1201. DOI: 10.1016/0960-1686(93)90245-T

CHUANG, M.-T., CHEN, Y.-C., LEE, C.-T., CHENG, C.-H., TSAI, Y.-J., CHANG, S.-Y. & SU, Z.-S. 2016a. Apportionment of the sources of high fine particulate matter concentration events in a developing aerotropolis in Taoyuan, Taiwan. *Environmental Pollution,* 214**,** 273-281.

CIESIN. 2010. *Center for international Earth Science Information Network (CIESIN)* [Online]. Socioeconomic Data and Applications Center (SEDAC), Palisades, Colombia University, New York: United Nations Food and Agricultural Programme (FOA) and Centro Internacional de Agriculture Tropical (CIAT,) 2005. Available: http://sedac.ciesin.columbia.edu/gpw [Accessed 01 August 2010].

COLLETT, K. S., PIKETH, S. J. & ROSS, K. E. 2010. An assessment of the atmospheric nitrogen budget on the South African Highveld. *South African Journal of Science,* 106.

CONNELL, D. W. 2005. *Basic concepts of environmental chemistry*, CRC Press.

CONRADIE, E. H., VAN ZYL, P. G., PIENAAR, J. J., BEUKES, J. P., GALY-LACAUX, C., VENTER, A. D. & MKHATSHWA, G. V. 2016. The chemical composition and fluxes of

atmospheric wet deposition at four sites in South Africa. *Atmospheric Environment,* 146**,** 113-131. DOI: 10.1016/j.atmosenv.2016.07.033

DAFF 2016. Abstract of agricultural activities 2016. *In:* DEPARTMENT OF AGRICULTURE, F. A. F.-R. O. S. A. (ed.). Pretoria: Department of Agriculture, Forestry and Fisheries.

DECESARI, S., FACCHINI, M. C., FUZZI, S. & TAGLIAVINI, E. 2000. Characterization of water-soluble organic compounds in atmospheric aerosol: A new approach. *Journal of Geophysical Research: Atmospheres,* 105**,** 1481-1489.

DELMAS, R. 1981. *Contribution à l'étude des forêts équatoriales commesources naturelles de dérivés soufrés atmosphériques.* PhD Thesis, Université Paul Sabatier de Toulouse.

DELMAS, R., LACAUX, J. P., MENAUT, J. C., ABBADIE, L., LE ROUX, X., HELAS, G. & LOBERT, J. 1995. Nitrogen compound emission from biomass burning in tropical African savanna FOS/DECAFE 1991 experiment (Lamto, Ivory Coast). *Journal of Atmospheric Chemistry,* 22**,** 175-193.

DHAMMAPALA, R. S. 1996. Use of diffusive samplers for the sampling of atmospheric pollutants.

DING, X., HU, Y., ZHANG, H., LI, C., LING, M. & SUN, W. 2013. Major Nb/Ta fractionation recorded in garnet amphibolite facies metagabbro. *The Journal of Geology,* 121**,** 255-274. DOI: 10.1086/669978

DRAXLER, R. R. & HESS, G. 1997. Description of the HYSPLIT4 modeling system. *NOAA Technical Memorandum ERL ARL-224***,** 1-27.

DUTTA, M., RAJAK, P., KHATUN, S. & ROY, S. 2017. Toxicity assessment of sodium fluoride in Drosophila melanogaster after chronic sub-lethal exposure. *Chemosphere,* 166**,** 255-266. http://dx.doi.org/10.1016/j.chemosphere.2016.09.112

EHN, M., THORNTON, J. A., KLEIST, E., SIPILA, M., JUNNINEN, H., PULLINEN, I., SPRINGER, M., RUBACH, F., TILLMANN, R., LEE, B., LOPEZ-HILFIKER, F., ANDRES, S., ACIR, I.-H., RISSANEN, M., JOKINEN, T., SCHOBESBERGER, S., KANGASLUOMA, J., KONTKANEN, J., NIEMINEN, T., KURTEN, T., NIELSEN, L. B., JORGENSEN, S., KJAERGAARD, H. G., CANAGARATNA, M., MASO, M. D., BERNDT, T., PETAJA, T., WAHNER, A., KERMINEN, V.-M., KULMALA, M., WORSNOP, D. R., WILDT, J. and MENTEL, T. F. 2014. A large source of low volatility secondary organic aerosol. Nature, 506(7489), 476–479.

ELMINIR, H. K. 2007. Relative influence of air pollutants and weather conditions on solar radiation–Part 1: Relationship of air pollutants with weather conditions. *Meteorology and Atmospheric Physics,* 96**,** 245-256. DOI: 10.1007/s00703-006-0209-4

ENGELBRECHT, W. 2009. *Characterisation of organic compounds in atmospheric aerosols utilising 2D gas chromatography and mass spectrometry. MSc Dissertation, North-West University*.

ENVIRONMENTAL. 2008. *Environmental analysis facility - Standard operating procedure* [Online]. Available: Laboratoired'Aérologie, UMR 5560. http://www.aero.obs-mip.fr/spip.php?article489 [Accessed 18 July 2011].

FACCHINI, M. C., FUZZI, S., ZAPPOLI, S., ANDRACCHIO, A., GELENCSÉR, A., KISS, G., KRIVÁCSY, Z., MÉSZÁROS, E., HANSSON, H. C. & ALSBERG, T. 1999. Partitioning of the organic aerosol component between fog droplets and interstitial air. *Journal of Geophysical Research: Atmospheres,* 104**,** 26821-26832.

FEIG, G. T., VERTUE, B., NAIDOO, S., NCGUKANA, N. & MABASO, D. 2015. Measurement of atmospheric black carbon in the Vaal Triangle and Highveld Priority Areas. *Clean Air Journal/Tydskrif vir Skoon Lug,* 25**,** 46-50. http://dx.doi.org/10.17159/2410-972X/2015/v25n1a4

FORMENTI, P., ELBERT, W., MAENHAUT, W., HAYWOOD, J., OSBORNE, S. & ANDREAE, M. 2003. Inorganic and carbonaceous aerosols during the Southern African Regional Science Initiative (SAFARI 2000) experiment: Chemical characteristics, physical properties, and emission data for smoke from African biomass burning. *Journal of Geophysical Research: Atmospheres,* 108. DOI: 10.1029/2002JD002408

FOURIE, G. D. 2006. *Modelling the long-range transport and transformation of air pollutants over the Southern African region, PhD Thesis, North-West University.*

GALY-LACAUX, C., AL OURABI, H., LACAUX, J., GARDRAT, E., MPHEPYA, J. & PIENAAR, K. Dry and wet atmospheric nitrogen deposition in Africa. EGS-AGU-EUG Joint Assembly, 2003. 9644.

GALY-LACAUX, C., LAOUALI, D., DESCROIX, L., GOBRON, N. & LIOUSSE, C. 2009. Long term precipitation chemistry and wet deposition in a remote dry savanna site in Africa (Niger). *Atmospheric Chemistry and Physics,* 9**,** 1579-1595. www.atmos-chem-phys.net/9/1579/2009/

GAO, S., HEGG, D.A., HOBBS, P.V., KIRCHSTETTER, T.W., MAGI, B.I., SADILEK, M. 2003. Water-soluble organic components in aerosols associated with savanna fires in southern Africa: Identification, evolution, and distribution. Journal of Geophysical Research, 108(D13): 8491. http://dx.doi.org/10.1029/2002JD002324

GAO, Y., LAI, S., LEE, S.-C., YAU, P. S., HUANG, Y., CHENG, Y., WANG, T., XU, Z., YUAN, C. & ZHANG, Y. 2015. Optical properties of size-resolved particles at a Hong Kong urban site during winter. *Atmospheric Research,* 155**,** 1-12. http://dx.doi.org/10.1016/j.atmosres.2014.10.020

GARSTANG, M., TYSON, P., SWAP, R., EDWARDS, M., KÅLLBERG, P. & LINDESAY, J. 1996. Horizontal and vertical transport of air over southern Africa. *Journal of Geophysical Research: Atmospheres,* 101**,** 23721-23736. https://doi.org/10.1029/95JD00844

GAUDERMAN, W. J., AVOL, E., GILLILAND, F., VORA, H., THOMAS, D., BERHANE, K., MCCONNELL, R., KUENZLI, N., LURMANN, F. & RAPPAPORT, E. 2004. The effect of air pollution on lung development from 10 to 18 years of age. *New England Journal of Medicine,* 351**,** 1057-1067. DOI: 10.1056/NEJMoa040610

GAWHANE, R. D., RAO, P. S. P., BUDHAVANT, K. B., WAGHMARE, V., MESHRAM, D. C. & SAFAI, P. D. 2017. Seasonal variation of chemical composition and source apportionment of $PM_{2.5}$ in Pune, India. *Environmental Science and Pollution Research,* 24**,** 21065-21072. DOI: 10.1007/s11356-017-9761-3

GAZETTE, G. 2005. Government Gazette - Republic of South Africa.

GIANNAKAKI, E., PFÜLLER, A., KORHONEN, K., MIELONEN, T., LAAKSO, L., VAKKARI, V., BAARS, H., ENGELMANN, R., BEUKES, J. P. & VAN ZYL, P. G. Free tropospheric aerosols over South Africa. EPJ Web of Conferences [Conference], 2016. EDP Sciences, 23015. DOI: 10.1051/epjconf/201611923015

GIERENS, R. T., HENRIKSSON, S., JOSIPOVIC, M., VAKKARI, V., VAN ZYL, P. G., BEUKES, J. P., WOOD, C. R. & O'CONNOR, E. J. 2018. Observing continental boundary-layer structure and evolution over the South African savannah using a ceilometer. *Theoretical and Applied Climatology***,** 1-14. https://doi.org/10.1007/s00704-018-2484-7

GOLDBERG, E. D. 1985. Black carbon in the environment: properties and distribution.

GONÇALVES, C., FIGUEIREDO, B. R., ALVES, C. A., CARDOSO, A. A. & VICENTE, A. M. 2017. Size-segregated aerosol chemical composition from an agro-industrial region of São Paulo state, Brazil. *Air Quality, Atmosphere and Health,* 10**,** 483-496. DOI: 10.1007/s11869-016-0441-0

GRAEDEL, T. & EISNER, T. 1988. Atmospheric formic acid from formicine ants: a preliminary assessment. *Tellus B,* 40**,** 335-339.

GRAEDEL, T., HAWKINS, D. & CLAXTON, L. 1986. *Atmospheric chemical compounds. Sources, occurrence and bioassay*.

GRAEDEL, T. E. & CRUTZEN, P. J. 1995. *Atmosphere, climate and change*, Scientific American Library.

GU, J., DU, S., HAN, D., HOU, L., YI, J., XU, J., LIU, G., HAN, B., YANG, G. & BAI, Z.-P. 2014. Major chemical compositions, possible sources, and mass closure analysis of $PM_{2.5}$ in Jinan, China. *Air Quality, Atmosphere and Health,* 7**,** 251-262. DOI: 10.1007/s11869-013-0232-9

GUILLAUME, B., LIOUSSE, C., GALY-LACAUX, C., ROSSET, R., GARDRAT, E., CACHIER, H., BESSAGNET, B. & POISSON, N. 2008. Modeling exceptional high concentrations of carbonaceous aerosols observed at Pic du Midi in spring–summer 2003: Comparison with Sonnblick and Puy de Dôme. *Atmospheric Environment,* 42**,** 5140-5149. DOI: 10.1016/j.atmosenv.2008.02.024

GUNSCH, M. J., MAY, N. W., WEN, M., BOTTENUS, C. L., GARDNER, D. J., VANREKEN, T. M., BERTMAN, S. B., HOPKE, P. K., AULT, A. P. & PRATT, K. A. 2018. Ubiquitous

influence of wildfire emissions and secondary organic aerosol on summertime atmospheric aerosol in the forested Great Lakes region. *Atmospheric Chemistry and Physics,* 18**,** 3701-3715. https://doi.org/10.5194/acp-18-3701-2018

HEGG, D. A., LIVINGSTON, J., HOBBS, P. V., NOVAKOV, T. & RUSSELL, P. 1997. Chemical apportionment of aerosol column optical depth off the mid-Atlantic coast of the United States. *Journal of Geophysical Research: Atmospheres,* 102**,** 25293-25303.

HENNIGAN, C. J., IZUMI, J., SULLIVAN, A. P., WEBER, R. J. AND NENES, A. 2015. A critical evaluation of proxy methods used to estimate the acidity of atmospheric particles. Atmospheric Chemistry And Physics, 15(5), 2775–2790, DOI:10.5194/acp-15-2775-2015

HERLEKAR, M., JOSEPH, A. E., KUMAR, R. & GUPTA, I. 2012. Chemical speciation and source assignment of particulate (PM_{10}) phase molecular markers in Mumbai. *Aerosol and Air Quality Research,* 12**,** 1247-1260. DOI: 10.4209/aaqr.2011.07.0091

HERSEY, S., GARLAND, R. M., CROSBIE, E., SHINGLER, T., SOROOSHIAN, A., PIKETH, S. & BURGER, R. 2015. An overview of regional and local characteristics of aerosols in South Africa using satellite, ground, and modeling data. *Atmospheric Chemistry and Physics,* 15**,** 4259. DOI: 10.5194/acp-15-4259-2015

HIRSIKKO, A., TIITTA, P., BEUKES, J., LAAKSO, L. & VAKKARI, V. 2012. Characterisation of sub-micron particle number concentrations and formation events in the western Bushveld Igneous Complex, South Africa. *Atmospheric Chemistry & Physics,* DOI: 10.5194/acp-12-3951-2012

HOSIOKANGAS, J., RUUSKANEN, J. & PEKKANEN, J. 1999. Effects of soil dust episodes and mixed fuel sources on source apportionment of PM_{10} particles in Kuopio, Finland. *Atmospheric Environment,* 33**,** 3821-3829.

HSU, C. Y., CHIANG, H. C., CHEN, M. J., CHUANG, C. Y., TSEN, C. M., FANG, G. C., TSAI, Y. I., CHEN, N. T., LIN, T. Y., LIN, S. L. & CHEN, Y. C. 2017. Ambient $PM_{2.5}$ in the residential area near industrial complexes: Spatiotemporal variation, source apportionment, and health impact. *Science of the Total Environment,* 590-591**,** 204-214. DOI: 10.1016/j.scitotenv.2017.02.212

HTTPS://WEB.STANFORD.EDU/GROUP/URCHIN/MINERAL.HTML. *Mineral makeup of seawater* [Online]. Available: https://web.stanford.edu/group/Urchin/mineral.html [Accessed 2018/11/08].

HTTPS://WWW.CROPNUTRITION.COM/POTASSIUM-NITRATE. *Mosaic Crop Nutrition - Potassium Nitrate* [Online]. [Accessed 2018/11/12].

HUANG, K., ZHUANG, G., XU, C., WANG, Y. & TANG, A. 2008. The chemistry of the severe acidic precipitation in Shanghai, China. *Atmospheric Research,* 89**,** 149-160. DOI: 10.1016/j.atmosres.2008.01.006

HUFFMAN, J., DOCHERTY, K., AIKEN, A., CUBISON, M., ULBRICH, I., DECARLO, P., SUEPER, D., JAYNE, J., WORSNOP, D. & ZIEMANN, P. 2009. Chemically-resolved aerosol volatility measurements from two megacity field studies. *Atmospheric Chemistry and Physics,* 9**,** 7161-7182. www.atmos-chem-phys.net/9/7161/2009/

HUTTUNEN, K., SIPONEN, T., SALONEN, I., YLI-TUOMI, T., AURELA, M., DUFVA, H., HILLAMO, R., LINKOLA, E., PEKKANEN, J. & PENNANEN, A. 2012. Low-level exposure to ambient particulate matter is associated with systemic inflammation in ischemic heart disease patients. *Environmental Research,* 116**,** 44-51. DOI: 10.1016/j.envres.2012.04.004

HYVÄRINEN, A.-P., VAKKARI, V., LAAKSO, L., HOODA, R., SHARMA, V., PANWAR, T., BEUKES, J., VAN ZYL, P., JOSIPOVIC, M. & GARLAND, R. 2013. Correction for a measurement artifact of the Multi-Angle Absorption Photometer (MAAP) at high black carbon mass concentration levels. *Atmospheric Measurement Techniques,* 6**,** 81. DOI: 10.5194/amt-6-81-2013

IPCC 2013. *STOCKER, T. Climate change 2013: the physical science basis: Working Group I contribution to the Fifth assessment report of the Intergovernmental Panel on Climate Change*, Cambridge University Press.

JAARS, K., BEUKES, J. P., VAN ZYL, P. G., VENTER, A. D., JOSIPOVIC, M., PIENAAR, J. J., VAKKARI, V., AALTONEN, H., LAAKSO, H., KULMALA, M., TIITTA, P., GUENTHER, A., HELLÉN, H., LAAKSO, L. & HAKOLA, H. 2014. Ambient aromatic hydrocarbon measurements at Welgegund, South Africa. *Atmospheric Chemistry and Physics Discussions,* 14**,** 4189-4227.

JAARS, K., VAN ZYL, P. G., BEUKES, J. P., HELLÉN, H., VAKKARI, V., JOSIPOVIC, M., VENTER, A. D., RÄSÄNEN, M., KNOETZE, L., CILLIERS, D. P., SIEBERT, S. J., KULMALA, M., RINNE, J., GUENTHER, A., LAAKSO, L. & HAKOLA, H. 2016. Measurements of biogenic volatile organic compounds at a grazed savannah grassland agricultural landscape in South Africa. *Atmospheric Chemistry and Physics,* 16**,** 15665-15688. DOI: 10.5194/acp-16-15665-2016

JACOBS, M. 2006. Process description and abbreviated history of Anglo Platinum's Waterval Smelter. *Southern African Pyrometallurgy***,** 17-23.

JACOBSON, M. Z. 2001b. Global direct radiative forcing due to multicomponent anthropogenic and natural aerosols. *Journal of Geophysical Research: Atmospheres,* 106**,** 1551-1568.

JANG, M., CZOSCHKE, N. M., LEE, S. & KAMENS, R. M. J. S. 2002. Heterogeneous atmospheric aerosol production by acid-catalyzed particle-phase reactions. 298**,** 814-817.

JEN, P. H. S. & WU, C. H. 2008. Echo duration selectivity of the bat varies with pulse-echo amplitude difference. *Neuroreport,* 19**,** 373-377. 10.1097/WNR.0b013e3282f52c61

JI, D., ZHANG, J., HE, J., WANG, X., PANG, B., LIU, Z., WANG, L. & WANG, Y. 2016. Characteristics of atmospheric organic and elemental carbon aerosols in urban Beijing, China. *Atmospheric Environment,* 125**,** 293-306. DOI: 10.1016/j.atmosenv.2015.11.020

JONES, R. R., HOGREFE, C., FITZGERALD, E. F., HWANG, S.-A., ÖZKAYNAK, H., GARCIA, V. C. & LIN, S. 2015. Respiratory hospitalizations in association with fine PM and its components in New York State. *Journal of the Air and Waste Management Association,* 65**,** 559-569. DOI: 10.1080/10962247.2014.1001500

JOSHI, S. & DUDANI, I. 2008. Environmental health effects of brick kilns in Kathmandu valley. *Kathmandu University Medical Journal (KUMJ),* 6**,** 3-11.

JOSIPOVIC, M., ANNEGARN, H. J., KNEEN, M. A., PIENAAR, J. J. & PIKETH, S. J. 2010. Concentrations, distributions and critical level exceedance assessment of SO_2, NO_2 and O_3 in South Africa. *Environmental Monitoring and Assessment,* 171**,** 181-196. DOI: 10.1007/s10661-009-1270-5

JUSINO-ATRESINO, R., ANDERSON, J. & GAO, Y. 2016. Ionic and elemental composition of $PM_{2.5}$ aerosols over the Caribbean Sea in the Tropical Atlantic. *Journal of Atmospheric Chemistry,* 73**,** 427-457. DOI: 10.1007/s10874-016-9337-5

KANAKIDOU, M., SEINFELD, J., PANDIS, S., BARNES, I., DENTENER, F., FACCHINI, M., DINGENEN, R. V., ERVENS, B., NENES, A. & NIELSEN, C. 2005. Organic aerosol and global climate modelling: a review. *Atmospheric Chemistry and Physics,* 5**,** 1053-1123. www.atmos-chem-phys.org/acp/5/1053/

KARTHIKEYAN, S. & BALASUBRAMANIAN, R. 2006. Determination of water-soluble inorganic and organic species in atmospheric fine particulate matter. *Microchemical Journal,* 82**,** 49-55. DOI: 10.1016/j.microc.2005.07.003

KAWAMURA, K., NG, L. L. & KAPLAN, I. R. 1985. Determination of organic acids (C_1-C_{10}) in the atmosphere, motor exhausts, and engine oils. *Environmental Science and Technology,* 19**,** 1082-1086.

KEENE, W. C. & GALLOWAY, J. N. 1986a. Considerations regarding sources for formic and acetic acids in the troposphere. *Journal of Geophysical Research: Atmospheres,* 91**,** 14466-14474. https://doi.org/10.1029/JD091iD13p14466

KEENE, W. C., PSZENNY, A. A., GALLOWAY, J. N. & HAWLEY, M. E. 1986b. Sea-salt corrections and interpretation of constituent ratios in marine precipitation. *Journal of Geophysical Research: Atmospheres,* 91**,** 6647-6658. https://doi.org/10.1029/JD091iD06p06647

KEPPEL-ALEKS, G. AND WASHENFELDER, R. A. 2016. The effect of atmospheric sulfate reductions on diffuse radiation and photosynthesis in the United States during 1995–2013. Geophysical Research Letters, 43(18), 9984–9993. DOI:10.1002/2016GL070052.

KERMINEN, V.-M., HILLAMO, R., TEINILÄ, K., PAKKANEN, T., ALLEGRINI, I. AND SPARAPANI, R. 2001. Ion balances of size-resolved tropospheric aerosol samples: implications for the acidity and atmospheric processing of aerosols. Atmospheric Environment, 35(31), 5255–5265. https://doi.org/10.1016/S1352-2310(01)00345-4

KHAN, A., AL-AWADI, L., AL-RASHIDI, M. J. J. O. T. A. & ASSOCIATION, W. M. 2016. Control of ammonia and urea emissions from urea manufacturing facilities of Petrochemical

Industries Company (PIC), Kuwait. *Journal of the Air and Waste Management Association,* 66**,** 609-618. DOI: 10.1080/10962247.2016.1145154

KISS, G., VARGA, B., GALAMBOS, I. & GANSZKY, I. 2002. Characterization of water-soluble organic matter isolated from atmospheric fine aerosol. *Journal of Geophysical Research: Atmospheres,* 107. DOI: 10.1029/2001JD000603

KLEYNHANS, E., BEUKES, J., VAN ZYL, P., BUNT, J., NKOSI, N. & VENTER, M. 2017. The effect of carbonaceous reductant selection on chromite pre-reduction. *Metallurgical and Materials Transactions B,* 48**,** 827-840. DOI: 10.1007/s11663-016-0878-4

KLEYNHANS, E. L. J., NEIZEL, B. W., BEUKES, J. P. & VAN ZYL, P. G. 2016. Utilisation of pre-oxidised ore in the pelletised chromite pre-reduction process. *Minerals Engineering,* 92**,** 114-124. DOI: 10.1016/j.mineng.2016.03.005

KORHONEN, K., GIANNAKAKI, E., MIELONEN, T., PFÜLLER, A., LAAKSO, L., VAKKARI, V., BAARS, H., ENGELMANN, R., BEUKES, J. & VAN ZYL, P. 2014. Atmospheric boundary layer top height in South Africa: measurements with lidar and radiosonde compared to three atmospheric models. *Atmospheric Chemistry and Physics,* 14**,** 4263-4278. DOI: 10.5194/acp-14-4263-2014

KUIK, F., LAUER, A., BEUKES, J., VAN ZYL, P., JOSIPOVIC, M., VAKKARI, V., LAAKSO, L. & FEIG, G. 2015. The anthropogenic contribution to atmospheric black carbon concentrations in southern Africa: a WRF-Chem modeling study. *Atmospheric Chemistry and Physics,* 15**,** 8809-8830. DOI: 10.5194/acp-15-8809-2015

KULMALA, M., NIEMINEN, T., NIKANDROVA, A., LEHTIPALO, K., MANNINEN, H. E., KAJOS, M. K., KOLARI, P., LAURI, A., PETÄJÄ, T., KREJCI, R., HANSSON, H.-C., SWIETLICKI, E., LINDROTH, A., CHRISTENSEN, T. R., ARNETH, A., HARI, P., BÄCK, J., VESALA, T. AND KERMINEN, V.-M. 2014. CO_2-induced terrestrial climate feedback mechanism: From carbon sink to aerosol source and back. Boreal Environment Research, 19, 122–131.

KUMAR, P., KUMAR, S. & YADAV, S. 2018. Seasonal variations in size distribution, water-soluble ions, and carbon content of size-segregated aerosols over New Delhi. *Environmental Science and Pollution Research,* 25**,** 6061-6078. https://doi.org/10.1007/s11356-017-0954-6

KUMAR, S. & RAMAN, R. S. 2016. Inorganic ions in ambient fine particles over a National Park in central India: Seasonality, dependencies between SO_4^{2-}, NO_3^-, and NH_4^+, and neutralization of aerosol acidity. *Atmospheric Environment,* 143**,** 152-163. http://dx.doi.org/10.1016/j.atmosenv.2016.08.037

LAAKSO, L., VAKKARI, V., LAAKSO, H., VIRKKULA, A., KULMALA, M., BEUKES, J., VAN ZYL, P., PIENAAR, J., CHILOANE, K. & GILARDONI, S. 2010. South African EUCAARI–measurements: a site with high atmospheric variability. *Atmospheric Chemistry and Physics Discussions,* 10**,** 30691-30729. DOI: 10.5194/acpd-10-30691-2010

LAAKSO, L., VAKKARI, V., VIRKKULA, A., LAAKSO, H., BACKMAN, J., KULMALA, M., BEUKES, J., VAN ZYL, P., TIITTA, P. & JOSIPOVIC, M. 2012. South African EUCAARI measurements: seasonal variation of trace gases and aerosol optical properties. *Atmospheric Chemistry and Physics,* 12**,** 1847-1864. DOI: 10.5194/acp-12-1847-2012

LAOUALI, D., GALY-LACAUX, C., DIOP, B., DELON, C., ORANGE, D., LACAUX, J. P., AKPO, A., LAVENU, F., GARDRAT, E. & CASTERA, P. 2012. Long term monitoring of the chemical composition of precipitation and wet deposition fluxes over three Sahelian savannas. *Atmospheric Environment,* 50**,** 314-327. DOI: 10.1016/j.atmosenv.2011.12.004

LASKIN, A., LASKIN, J. and NIZKORODOV, S. A. 2015. Chemistry of Atmospheric Brown Carbon, Chemical Reviews, 115(10), 4335–4382. DOI: 10.1021/cr5006167

LAZARIDIS, M., LATOS, M., ALEKSANDROPOULOU, V., HOV, Ø., PAPAYANNIS, A. & TØRSETH, K. 2008. Contribution of forest fire emissions to atmospheric pollution in Greece. *Air Quality, Atmosphere and Health,* 1**,** 143-158. DOI: 10.1007/s11869-008-0020-0

LAZARIDIS, M., SEMB, A., LARSSEN, S., HJELLBREKKE, A.-G., HOV, Ø., HANSSEN, J. E., SCHAUG, J. & TØRSETH, K. 2002. Measurements of particulate matter within the framework of the European Monitoring and Evaluation Programme (EMEP): I. First results. *Science of the Total Environment,* 285**,** 209-235. DOI: 10.1016/S0048-9697(01)00932-9

LI, C., QIN, X., DING, M., GUO, R., XIAO, C., HOU, S., BIAN, L., QIN, D. & REN, J. 2014a. Temporal variations in marine chemical concentrations in coastal areas of eastern

Antarctica and associated climatic causes. *Quaternary International,* 352**,** 16-25. http://dx.doi.org/10.1016/j.quaint.2014.03.016

LI J, PÓSFAI M, HOBBS P, BUSECK P. 2003. Individual aerosol particles from biomass burning in southern Africa: 2, Compositions and aging of inorganic particles. Journal of Geophysical Research, 108(D13):8484. http://dx.doi. org/10.1029/2002JD002310

LI, W., SHAO, L. & BUSECK, P. 2010. Haze types in Beijing and the influence of agricultural biomass burning. *Atmospheric Chemistry and Physics,* 10**,** 8119-8130. DOI: 10.5194/acp-10-8119-2010

LIAN, Z., OUYANG, W., HAO, F., LIU, H., HAO, Z., LIN, C. & HE, M. 2018. Changes in fertilizer categories significantly altered the estimates of ammonia volatilizations induced from increased synthetic fertilizer application to Chinese rice fields. *Agriculture, Ecosystems & Environment,* 265**,** 112-122. https://doi.org/10.1016/j.agee.2018.05.025

LIN, J., PAN, D., DAVIS, S. J., ZHANG, Q., HE, K., WANG, C., STREETS, D. G., WUEBBLES, D. J. & GUAN, D. 2014. China's international trade and air pollution in the United States. *Proceedings of the National Academy of Sciences,* 111**,** 1736-1741. www.pnas.org/lookup/suppl/doi:10.1073/pnas.1312860111/-/DCSupplemental

LIOUSSE, C., PENNER, J., CHUANG, C., WALTON, J., EDDLEMAN, H. & CACHIER, H. 1996. A global three-dimensional model study of carbonaceous aerosols. *Journal of Geophysical Research: Atmospheres,* 101**,** 19411-19432. DOI: 10.1029/95JD03426

LIPFERT, F., BATY, J., MILLER, J. & WYZGA, R. 2006. $PM_{2.5}$ constituents and related air quality variables as predictors of survival in a cohort of US military veterans. *Inhalation Toxicology,* 18**,** 645-657. DOI: 10.1080/08958370600742946

LIU, S., AHLM, L., DAY, D. A., RUSSELL, L. M., ZHAO, Y., GENTNER, D. R., WEBER, R. J., GOLDSTEIN, A. H., JAOUI, M. & OFFENBERG, J. H. 2012. Secondary organic aerosol formation from fossil fuel sources contribute majority of summertime organic mass at Bakersfield. *Journal of Geophysical Research: Atmospheres,* 117. DOI: 10.1029/2012JD018170, 2012

LIU, Z., XIE, Y., HU, B., WEN, T., XIN, J., LI, X. & WANG, Y. 2017. Size-resolved aerosol water-soluble ions during the summer and winter seasons in Beijing: Formation mechanisms of secondary inorganic aerosols. *Chemosphere,* 183**,** 119-131. http://dx.doi.org/10.1016/j.chemosphere.2017.05.095

LOURENS, A., BEUKES, J. P., VAN ZYL, P. G., FOURIE, G. D., BURGER, J. W., PIENAAR, J. J., READ, C. E. & JORDAAN, J. H. 2011. Spatial and temporal assessment of gaseous pollutants in the Highveld of South Africa. *South African Journal of Science,* 107**,** 1-8. DOI: 10.4102/sajs.v107i1/2.269

LOURENS, A., BUTLER, T. M., BEUKES, J. P., VAN ZYL, P. G., BEIRLE, S., WAGNER, T. K., HEUE, K.-P., PIENAAR, J. J., FOURIE, G. D. & LAWRENCE, M. G. 2012. Re-evaluating the NO_2 hotspot over the South African Highveld. *South African Journal of Science,* 108**,** 83-91. http://dx.doi.org/10.4102/sajs.v108i11/12.1146

LOURENS, A., BUTLER, T. M., BEUKES, J. P., VAN ZYL, P. G., FOURIE, G. D. & LAWRENCE, M. G. 2016. Investigating atmospheric photochemistry in the Johannesburg-Pretoria megacity using a box model. *South African Journal of Science,* 112**,** 01-11. DOI: 10.17159/sajs.2016/2015-0169

LV, W., HU, Y., LI, E., LIU, H., PAN, H., JI, S., HAYAT, T., ALSAEDI, A. & AHMAD, B. 2018. Evaluation of vehicle emission in Yunnan province from 2003 to 2015. *Journal of Cleaner Production,* 207**,** 814-825. https://doi.org/10.1016/j.jclepro.2018.09.227

MAFUSIRE, G., ANNEGARN, H. J., VAKKARI, V., BEUKES, J. P., JOSIPOVIC, M., ZYL, P. G. & LAAKSO, L. 2016. Submicrometer aerosols and excess CO as tracers for biomass burning air mass transport over southern Africa. *Journal of Geophysical Research: Atmospheres,* 121. DOI: 10.1002/2015JD023965

MAHLABA, J. S., KEARSLEY, E. P. & KRUGER, R. A. 2011. Physical, chemical and mineralogical characterisation of hydraulically disposed fine coal ash from SASOL Synfuels. *Fuel,* 90**,** 2491-2500. DOI: 10.1016/j.fuel.2011.03.022

MALAKAN, W., KEAWBOONCHU, J. & THEPANONDH, S. 2018. Comparison of AERMOD Performance using Observed and Prognostic Meteorological Data. *Environment Asia,* 11. DOI: 10.14456/ea.2018.21

MARITZ, P., BEUKES, J. P., VAN ZYL, P. G., CONRADIE, E. H., VENTER, A. D., PIENAAR, J. J., LIOUSSE, C., GALY-LACAUX, C., CASTERA, P. & RAMANDH, A. 2015. Spatial and temporal assessment of organic and black carbon at four sites in the interior of South Africa. *Clean Air Journal/Tydskrif vir Skoon Lug,* 25**,** 20-33. DOI: 10.17159/2410-972X/2015/v25n1a1

MARTINS, J., DHAMMAPALA, R., LACHMANN, G., GALY-LACAUX, C. & PIENAAR, J. 2007. Long-term measurements of sulphur dioxide, nitrogen dioxide, ammonia, nitric acid and ozone in southern Africa using passive samplers. *South African Journal of Science,* 103**,** 336-342.

MARTINS, J. J. 2009. *Concentrations and deposition of atmospheric species at regional sites in southern Africa, PhD Thesis, North-West University*.

MASSEY, D., KULSHRESTHA, A., MASIH, J. & TANEJA, A. 2012. Seasonal trends of PM_{10}, $PM_{5.0}$, $PM_{2.5}$ & $PM_{1.0}$ in indoor and outdoor environments of residential homes located in North-Central India. 47, 223-231. DOI: 10.1016/j.buildenv.2011.07.018

MATSUMOTO, K., ISHII, Y., KIM, S., KANEYASU, N. & KOBAYASHI, H. 2014. Volatility of water-soluble organic carbon in ambient aerosols. *Journal of Aerosol Science,* 67**,** 38-47. http://dx.doi.org/10.1016/j.jaerosci.2013.09.005

MAYOL-BRACERO, O., GUYON, P., GRAHAM, B., ROBERTS, G., ANDREAE, M., DECESARI, S., FACCHINI, M., FUZZI, S. & ARTAXO, P. 2002. Water-soluble organic compounds in biomass burning aerosols over amazonia 2. Apportionment of the chemical composition and importance of the polyacidic fraction. *Journal of Geophysical Research: Atmospheres,* 107. DOI: 10.1029/2001JD000522

MBENGUE, S., FUSEK, M., SCHWARZ, J., VODIČKA, P., ŠMEJKALOVÁ, A. H. and HOLOUBEK, I. 2018. Four years of highly time resolved measurements of elemental and organic carbon at a rural background site in Central Europe. Atmospheric Environment, 182, 335–346, https://doi.org/10.1016/j.atmosenv.2018.03.056

MENG, C. C., WANG, L. T., ZHANG, F. F., WEI, Z., MA, S. M., MA, X. & YANG, J. 2016. Characteristics of concentrations and water-soluble inorganic ions in $PM_{2.5}$ in Handan City, Hebei province, China. *Atmospheric Research,* 171**,** 133-146. DOI: 10.1016/j.atmosres.2015.12.013

MILLS, N. L., DONALDSON, K., HADOKE, P. W., BOON, N. A., MACNEE, W., CASSEE, F. R., SANDSTRÖM, T., BLOMBERG, A. & NEWBY, D. E. 2008a. Adverse cardiovascular effects of air pollution. *Nature Clinical Practice Cardiovascular Medicine,* 6**,** 36-44. DOI: 10.1038/ncpcardio1399

MIRBAGHERI, S. A., POSHTEGAL, M. K. & PARISAI, M. S. J. D. 2010. Removing of urea and ammonia from petrochemical industries with the objective of reuse, in a pilot scale: Surveying of the methods of waste water treatment. *Desalination,* 256**,** 70-76. DOI: 10.1016/j.desal.2010.02.011

MISHRA, M. & KULSHRESTHA, U. J. J. O. A. C. 2017. Chemical characteristics and deposition fluxes of dust-carbon mixed coarse aerosols at three sites of Delhi, NCR. *Journal of Atmospheric Chemistry,* 74**,** 399-421. DOI: 10.1007/s10874-016-9349-1

MIYAZAKI, Y., KONDO, Y., HAN, S., KOIKE, M., KODAMA, D., KOMAZAKI, Y., TANIMOTO, H. & MATSUEDA, H. 2007. Chemical characteristics of water-soluble organic carbon in the Asian outflow. *Journal of Geophysical Research: Atmospheres,* 112. DOI: 10.1029/2007JD009116

MKOMA, S., KAWAMURA, K. & FU, P. 2013. Contributions of biomass/biofuel burning to organic aerosols and particulate matter in Tanzania, East Africa, based on analyses of ionic species, organic and elemental carbon, levoglucosan and mannosan. *Atmospheric Chemistry and Physics,* 13**,** 10325-10338. DOI: 10.5194/acp-13-10325-2013

MOCHIZUKI, T., KAWAMURA, K., MIYAZAKI, Y., WADA, R., TAKAHASHI, Y., SAIGUSA, N. & TANI, A. 2017. Secondary formation of oxalic acid and related organic species from biogenic sources in a larch forest at the northern slope of Mt. Fuji. *Atmospheric Environment,* 166**,** 255-262. http://dx.doi.org/10.1016/j.atmosenv.2017.07.028

MODIS. 2014. *MODIS - Obtaining and processing MODIS data.* [Online]. Available: http://www.yale.edu/ceo/Documentation/MODIS_data.pdf [Accessed 14 February 2014].

MOFFET, R. C. & PRATHER, K. A. 2009. In-situ measurements of the mixing state and optical properties of soot with implications for radiative forcing estimates. *Proceedings of the*

National Academy of Sciences, 106**,** 11872-11877. www.pnas.org/cgi/doi/10.1073/pnas.0900040106

MPHEPYA, J., GALY-LACAUX, C., LACAUX, J., HELD, G. & PIENAAR, J. 2006. Precipitation chemistry and wet deposition in Kruger National Park, South Africa. *Journal of Atmospheric Chemistry,* 53**,** 169-183. DOI: 10.1007/s10874-005-9005-7

MPHEPYA, J., PIENAAR, J., GALY-LACAUX, C., HELD, G. & TURNER, C. 2004. Precipitation chemistry in semi-arid areas of Southern Africa: a case study of a rural and an industrial site. *Journal of Atmospheric Chemistry,* 47**,** 1-24.

MUCINA, L. & RUTHERFORD, M. 2006. The vegetation of South Africa, Lesotho and Swaziland. Strelitzia 19, South African National Biodiversity Institute, Pretoria. *Memoirs of the Botanical Survey of South Africa*.

MUKHERJEE, A. & AGRAWAL, M. 2017. World air particulate matter: sources, distribution and health effects. *Environmental Chemistry Letters,* 15**,** 283-309. DOI: 10.1007/s10311-017-0611-9

NANUS, L., CAMPBELL, D. H., LEHMANN, C. M. & MAST, M. A. 2018. Spatial and temporal variation in sources of atmospheric nitrogen deposition in the Rocky Mountains using nitrogen isotopes. *Atmospheric Environment,* 176**,** 110-119. https://doi.org/10.1016/j.atmosenv.2017.12.023

NIEMINEN, T., KERMINEN, V.-M., PETÄJÄ, T., AALTO, P. P., ARSHINOV, M., ASMI, E., BALTENSPERGER, U., BEDDOWS, D., BEUKES, J. P., COLLINS, D. J. A. C. & PHYSICS 2018. Global analysis of continental boundary layer new particle formation based on long-term measurements. *Atmospheric Chemistry & Physics,* 18**,** 14737-14756. https://doi.org/10.5194/acp-18-14737-2018

NIU, X., CAO, J., SHEN, Z., HO, S. S. H., TIE, X., ZHAO, S., XU, H., ZHANG, T. & HUANG, R. 2016. $PM_{2.5}$ from the Guanzhong Plain: Chemical composition and implications for emission reductions. *Atmospheric Environment,* 147**,** 458-469. http://dx.doi.org/10.1016/j.atmosenv.2016.10.029

NIU, Y., LI, X., PU, J. & HUANG, Z. 2018. Organic acids contribute to rainwater acidity at a rural site in eastern China. *Air Quality, Atmosphere and Health,* 11**,** 459-469. https://doi.org/10.1007/s11869-018-0553-9

NKOSI, N. C., PIKETH, S. J. & BURGER, R. P. 2018. Fine PM emission factors from residential burning of solid fuels using traditional cast-iron coal stoves. *Clean Air Journal/Tydskrif vir Skoon Lug,* 28**,** 35-41. http://dx.doi.org/10.17159/2410-972X/2018/v28n1a10

NUNES, L., TAVARES, T. M., DIPPEL, J. & JAESCHKE, W. 2005. Measurements of atmospheric concentrations of reduced sulphur compounds in the All Saints Bay area in Bahia, Brazil. *Journal of Atmospheric Chemistry,* 50**,** 79-100.

OBERDORSTER, G., SHARP, Z., ATUDOREI, V., ELDER, A., GELEIN, R., KREYLING, W. & COX, C. 2004. Translocation of inhaled ultrafine particles to the brain. *Inhalation Toxicology,* 16**,** 437-45. DOI: 10.1080/08958370490439597

OSTRO, B., FENG, W.-Y., BROADWIN, R., GREEN, S. & LIPSETT, M. 2006. The effects of components of fine particulate air pollution on mortality in California: results from CALFINE. *Environmental Health Perspectives,* 115**,** 13-19. DOI: 10.1289/ehp.9281

PANDEY, S. K., TRIPATHI, B., MISHRA, V. & PRAJAPATI, S. 2006. Size fractionated speciation of nitrate and sulfate aerosols in a sub-tropical industrial environment. *Chemosphere,* 63**,** 49-57. DOI: 10.1016/j.chemosphere.2005.07.035

PARWORTH, C., FAST, J., MEI, F., SHIPPERT, T., SIVARAMAN, C., TILP, A., WATSON, T. AND ZHANG, Q. 2015. Long-term measurements of submicrometer aerosol chemistry at the Southern Great Plains (SGP) using an Aerosol Chemical Speciation Monitor (ACSM). Atmospheric Environment, 106, 43–55. https://doi.org/10.1016/j.atmosenv.2015.01.060

PATHAK, R. K., WANG, T., HO, K. & LEE, S. J. A. E. 2011. Characteristics of summertime $PM_{2.5}$ organic and elemental carbon in four major Chinese cities: Implications of high acidity for water-soluble organic carbon (WSOC). *Atmospheric Environment,* 45**,** 318-325. DOI: 10.1016/j.atmosenv.2010.10.021

PAULOT, F., PAYNTER, D., GINOUX, P., NAIK, V., WHITBURN, S., VAN DAMME, M., CLARISSE, L., COHEUR, P. F. & HOROWITZ, L. 2017. Gas-aerosol partitioning of ammonia in biomass burning plumes: Implications for the interpretation of spaceborne

observations of ammonia and the radiative forcing of ammonium nitrate. *Geophysical Research Letters,* 44**,** 8084-8093. DOI: 10.1002/2017GL074215

PETZOLD, A., OGREN, J. A., FIEBIG, M., LAJ, P., LI, S.-M., BALTENSPERGER, U., HOLZER-POPP, T., KINNE, S., PAPPALARDO, G. & SUGIMOTO, N. 2013. Recommendations for reporting "black carbon" measurements. *Atmospheric Chemistry and Physics,* 13**,** 8365-8379. DOI: 10.5194/acp-13-8365-2013

PFEIFFER, R. 2005. Sampling for PM_{10} and $PM_{2.5}$ particulates. *Publications from USDA-ARS / UNL Faculty - Micrometeorology in Agricultural Systems,* 47**,** 227-245. http://digitalcommons.unl.edu/usdaarsfacpub/1393

PIKETH, S., ANNEGARN, H. & TYSON, P. J. J. O. G. R. A. 1999. Lower tropospheric aerosol loadings over South Africa: The relative contribution of aeolian dust, industrial emissions, and biomass burning. 104**,** 1597-1607.

PIO, C., CERQUEIRA, M., HARRISON, R. M., NUNES, T., MIRANTE, F., ALVES, C., OLIVEIRA, C., DE LA CAMPA, A. S., ARTÍÑANO, B. & MATOS, M. 2011. OC/EC ratio observations in Europe: Re-thinking the approach for apportionment between primary and secondary organic carbon. *Atmospheric Environment,* 45**,** 6121-6132. DOI: 10.1016/j.atmosenv.2011.08.045

POPE III, C. A. & DOCKERY, D. W. 2006. Health effects of fine particulate air pollution: lines that connect. *Journal of the Air and Waste Management Association,* 56**,** 709-742. DOI: 10.1080/10473289.2006.10464485

PÖSCHL, U. 2005. Atmospheric aerosols: composition, transformation, climate and health effects. *Angewandte Chemie International Edition,* 44**,** 7520-7540. DOI: 10.1002/anie.200501122

PRETORIUS, I., PIKETH, S., BURGER, R. & NEOMAGUS, H. 2015. A perspective on South African coal fired power station emissions. *Journal of Energy in Southern Africa,* 26**,** 27-40.

PUTAUD, J.-P., RAES, F., VAN DINGENEN, R., BRÜGGEMANN, E., FACCHINI, M.-C., DECESARI, S., FUZZI, S., GEHRIG, R., HÜGLIN, C. & LAJ, P. 2004. A European aerosol phenomenology—2: chemical characteristics of particulate matter at kerbside, urban, rural and background sites in Europe. *Atmospheric Environment,* 38**,** 2579-2595. DOI: 10.1016/j.atmosenv.2004.01.041

QIU, X., DUAN, L., GAO, J., WANG, S., CHAI, F., HU, J., ZHANG, J. & YUN, Y. 2016. Chemical composition and source apportionment of PM_{10} and $PM_{2.5}$ in different functional areas of Lanzhou, China. *Journal of Environmental Sciences,* 40**,** 75-83. https://doi.org/10.1016/j.jes.2015.10.021

RAMANATHAN, V. & FENG, Y. 2009. Air pollution, greenhouse gases and climate change: Global and regional perspectives. *Atmospheric Environment,* 43**,** 37-50. DOI: 10.1016/j.atmosenv.2008.09.063

REISS, R., ANDERSON, E. L., CROSS, C. E., HIDY, G., HOEL, D., MCCLELLAN, R. & MOOLGAVKAR, S. 2007. Evidence of health impacts of sulfate-and nitrate-containing particles in ambient air. *Inhalation Toxicology,* 19**,** 419-449. DOI: 10.1080/08958370601174941

RIDDLE, E. E., VOSS, P. B., STOHL, A., HOLCOMB, D., MACZKA, D., WASHBURN, K. & TALBOT, R. W. 2006. Trajectory model validation using newly developed altitude-controlled balloons during the International Consortium for Atmospheric Research on Transport and Transformations 2004 campaign. *Journal of Geophysical Research: Atmospheres,* 111. DOI: 10.1029/2006JD007456

RIEMER, N. & WEST, M. 2013. Quantifying aerosol mixing state with entropy and diversity measures. *Atmospheric Chemistry and Physics,* 13**,** 11423-11439. DOI: 10.5194/acp-13-11423-2013

ROOS, H. 2011. *Thermomechanical analysis of raw materials used in the production of Soderberg electrode paste, MSc Dissertation, North-West University.*

ROY, D. P., BOSCHETTI, L., JUSTICE, C. O. & JU, J. 2008. The collection 5 MODIS burned area product — Global evaluation by comparison with the MODIS active fire product. *Remote Sensing of Environment,* 112**,** 3690-3707. DOI: 10.1016/j.rse.2008.05.013

SAAQIS. 2018. *SAAQIS - South African air quality information system.* [Online]. Environmental affairs. Republic of South Africa. Available: http://www.saaqis.org.za/ [Accessed 25 October 2018 2018].

SATSANGI, A., PACHAURI, T., SINGLA, V., LAKHANI, A. & KUMARI, K. M. 2013. Water soluble ionic species in atmospheric aerosols: Concentrations and sources at Agra in the Indo-Gangetic Plain (IGP). *Aerosol and Air Quality Research,* 13**,** 1877-1889. DOI: 10.4209/aaqr.2012.08.0227

SCHLESINGER, R., KUNZLI, N., HIDY, G., GOTSCHI, T. & JERRETT, M. 2006. The health relevance of ambient particulate matter characteristics: coherence of toxicological and epidemiological inferences. *Inhalation Toxicology,* 18**,** 95-125. DOI: 10.1080/08958370500306016

SCHLESINGER, R. B. 2007. The health impact of common inorganic components of fine particulate matter ($PM_{2.5}$) in ambient air: a critical review. *Inhalation Toxicology,* 19**,** 811-832. DOI: 10.1080/08958370701402382

SCHLESINGER, W. H. & HARTLEY, A. E. 1992. A global budget for atmospheric NH_3. *Biogeochemistry,* 15**,** 191-211.

SEATON, A., GODDEN, D., MACNEE, W. & DONALDSON, K. 1995. Particulate air pollution and acute health effects. *The Lancet,* 345**,** 176-178.

SEHLOHO, T., BEUKES, J. P., MARITZ, P., VAN ZYL, P. G., JAARS, K., LIOUSSE, C., JOSIPOV, M., VENTER, A. D., VAKKARI, V., KULMALA, M. & LAAKSO, L. 2017. Levels, seasonal patterns and possible sources of organic and elemental carbon at a regional background site in South Africa. *In preparation for submission.***,** 34.

SEINFELD, J. & PANDIS, S. 2006. Atmospheric Chemistry and Physics, A Wiley-Inter Science Publication. John Wiley & Sons Inc, New York.

SEINFELD, J. H. & PANDIS, S. N. 2016. *Atmospheric chemistry and physics: from air pollution to climate change*, John Wiley & Sons. 1120.

SHAH, J. J. & RAU, J. A. 1990. *Carbonaceous species methods comparison study: Interlaboratory round robin interpretation of results*, Research Division, California Air Resources Board.

SHAKYA, K. M., RUPAKHETI, M., SHAHI, A., MASKEY, R., PRADHAN, B., PANDAY, A., PUPPALA, S. P., LAWRENCE, M. & PELTIER, R. E. 2017. Near-road sampling of $PM_{2.5}$, BC, and fine-particle chemical components in Kathmandu Valley, Nepal. *Atmospheric Chemistry and Physics,* 17**,** 6503-6516. https://doi.org/10.5194/acp-17-6503-2017

SHAO, P., TIAN, H., SUN, Y., LIU, H., WU, B., LIU, S., LIU, X., WU, Y., LIANG, W. & WANG, Y. 2018. Characterizing remarkable changes of severe haze events and chemical compositions in multi-size airborne particles (PM_1, $PM_{2.5}$ and PM_{10}) from January 2013 to 2016–2017 winter in Beijing, China. *Atmospheric Environment,* 189**,** 133-144. https://doi.org/10.1016/j.atmosenv.2018.06.038

SHARMA, S. K., SHARMA, A., SAXENA, M., CHOUDHARY, N., MASIWAL, R., MANDAL, T. K. & SHARMA, C. 2016. Chemical characterization and source apportionment of aerosol at an urban area of Central Delhi, India. *Atmospheric Pollution Research,* 7**,** 110-121. DOI: 10.1016/j.apr.2015.08.002

SHEN, Z., CAO, J., ARIMOTO, R., HAN, Z., ZHANG, R., HAN, Y., LIU, S., OKUDA, T., NAKAO, S. & TANAKA, S. 2009. Ionic composition of TSP and $PM_{2.5}$ during dust storms and air pollution episodes at Xi'an, China. *Atmospheric Environment,* 43**,** 2911-2918. DOI: 10.1016/j.atmosenv.2009.03.005

SHESKIN, D. J. 2003. *Handbook of Parametric and Nonparametric Statistical Procedures. 3rd Ed.,* Boca Raton, Chapman an Hall/CRC Press. 1193.

SIGHA-NKAMDJOU, L., GALY-LACAUX, C., PONT, V., RICHARD, S., SIGHOMNOU, D. & LACAUX, J. J. J. O. A. C. 2003. Rainwater chemistry and wet deposition over the equatorial forested ecosystem of Zoétélé (Cameroon). *Journal of Atmospheric Chemistry,* 46**,** 173-198.

SILLANPÄÄ, M., HILLAMO, R., SAARIKOSKI, S., FREY, A., PENNANEN, A., MAKKONEN, U., SPOLNIK, Z., VAN GRIEKEN, R., BRANIŠ, M. & BRUNEKREEF, B. J. A. E. 2006. Chemical composition and mass closure of particulate matter at six urban sites in Europe. *Atmospheric Environment,* 40**,** 212-223. DOI: 10.1016/j.atmosenv.2006.01.063

SIPONEN, T., YLI-TUOMI, T., AURELA, M., DUFVA, H., HILLAMO, R., HIRVONEN, M.-R., HUTTUNEN, K., PEKKANEN, J., PENNANEN, A. & SALONEN, I. 2015. Source-specific fine particulate air pollution and systemic inflammation in ischaemic heart disease patients.

Occupational and Environmental Medicine, 72**,** 277-283. DOI: 10.1136/oemed-2014-102240

SKOOG, D. A., WEST, D. M., HOLLER, F. J. & CROUCH, S. R. 2014. *Fundamentals of Analytical Chemistry.*, 9th Ed. (International Edition). Brooks/Cole,Cengage Learning: Belmont. 985pp. 985.

SLANINA, S. & ZHANG, Y. 2004. Aerosols: connection between regional climate change and air quality (Iupac Technical Report). *Pure and Applied Chemistry,* 76**,** 1241-1253. DOI: 10.1351/pac200476061241

STOHL, A. 1998. Computation, accuracy and applications of trajectories—a review and bibliography. *Atmospheric Environment,* 32**,** 947-966. DOI: 10.1016/S1352-2310(97)00457-3

SULLIVAN, A. P. & WEBER, R. J. 2006. Chemical characterization of the ambient organic aerosol soluble in water: 1. Isolation of hydrophobic and hydrophilic fractions with a XAD-8 resin. *Journal of Geophysical Research: Atmospheres,* 111. DOI: 10.1029/2005JD006485

SUN, L., DI, D., LI, G., KRONZUCKER, H. J. & SHI, W. 2017. Spatio-temporal dynamics in global rice gene expression (Oryza sativa L.) in response to high ammonium stress. *Journal of Plant Physiology,* 212**,** 94-104. http://dx.doi.org/10.1016/j.jplph.2017.02.006

SUN, W., SHAO, M., GRANIER, C., LIU, Y., YE, C. & ZHENG, J. 2018. Long-Term Trends of Anthropogenic SO_2, NO_x, CO, and NMVOCs Emissions in China. *Earth's Future,* 6**,** 1112-1133.

SUSHEELA, A., MONDAL, N. & SINGH, A. 2013. Exposure to fluoride in smelter workers in a primary aluminum industry in India. *The International Journal of Occupational and Environmental Medicine,* 4**,** 160-61-72.

SWANSON, K. J., MADDEN, M. C. & GHIO, A. J. 2007. Biodiesel exhaust: the need for health effects research. *Environmental Health Perspectives,* 115**,** 496. DOI: 10.1289/ehp.9631

SWAP, R., ARANIBAR, J., DOWTY, P., GILHOOLY, W. & MACKO, S. A. 2004. Natural abundance of ^{13}C and ^{15}N in C_3 and C_4 vegetation of southern Africa: patterns and implications. *Global Change Biology,* 10**,** 350-358. DOI: 10.1111/j.1365-2486.2003.00702.x

SWAP, R. J., SZUBA, T. A., GARSTANG, M., ANNEGARN, H. J., MARUFU, L. & PIKETH, S. J. 2003. Spatial and temporal assessment of sources contributing to the annual austral spring mid-tropospheric ozone maxima over the tropical South Atlantic. *Global Change Biology,* 9**,** 336-345.

SZÉP, R., MATEESCU, E., NIȚĂ, I.-A., BIRSAN, M.-V., BODOR, Z. & KERESZTESI, Á. 2018. Effects of the Eastern Carpathians on atmospheric circulations and precipitation chemistry from 2006 to 2016 at four monitoring stations (Eastern Carpathians, Romania). *Atmospheric Research,* 214**,** 311-328. https://doi.org/10.1016/j.atmosres.2018.08.009

SZIDAT, S., RUFF, M., PERRON, N., WACKER, L., SYNAL, H.-A., HALLQUIST, M., SHANNIGRAHI, A. S., YTTRI, K. E., DYE, C. & SIMPSON, D. 2009. Fossil and non-fossil sources of organic carbon (OC) and elemental carbon (EC) in Göteborg, Sweden. *Atmospheric Chemistry and Physics,* 9**,** 1521-1535. www.atmos-chem-phys.net/9/1521/2009/

SZIGETI, T., ÓVÁRI, M., DUNSTER, C., KELLY, F. J., LUCARELLI, F. & ZÁRAY, G. 2015. Changes in chemical composition and oxidative potential of urban $PM_{2.5}$ between 2010 and 2013 in Hungary. *Science of the Total Environment,* 518**,** 534-544. http://dx.doi.org/10.1016/j.scitotenv.2015.03.025

THATCHER, T. L. & LAYTON, D. W. J. A. E. 1995. Deposition, resuspension, and penetration of particles within a residence. 29, 1487-1497.

THIRUMALAI, K., SINGH, A. & RAMESH, R. 2011. A MATLAB™ code to perform weighted linear regression with (correlated or uncorrelated) errors in bivariate data. *Journal of the Geological Society of India,* 77**,** 377-380. DOI: 10.1007/s12594-011-0044-1

TIITTA, P., VAKKARI, V., CROTEAU, P., BEUKES, J., VAN ZYL, P., JOSIPOVIC, M., VENTER, A., JAARS, K., PIENAAR, J. & NG, N. 2014. Chemical composition, main sources and temporal variability of PM_1 aerosols in southern African grassland. *Atmospheric Chemistry and Physics,* 14**,** 1909-1927. DOI: 10.5194/acp-14-1909-2014

TUMMON, F., SOLMON, F., LIOUSSE, C. & TADROSS, M. 2010. Simulation of the direct and semidirect aerosol effects on the southern Africa regional climate during the biomass

burning season. *Journal of Geophysical Research: Atmospheres,* 115. DOI: 10.1029/2009JD013738

TURNER, J. & COLBECK, I. J. E. C. O. A. 2008. Physical and chemical properties of atmospheric aerosols. *Environmental Chemistry of Aerosols***,** 1-29.

TURPIN, B. J., CARY, R., HUNTZICKER, J. J. A. S. & TECHNOLOGY 1990. An in situ, time-resolved analyzer for aerosol organic and elemental carbon. 12, 161-171.

TURPIN, B. J. & LIM, H.-J. 2001. Species contributions to $PM_{2.5}$ mass concentrations: Revisiting common assumptions for estimating organic mass. *Aerosol Science and Technology,* 35**,** 602-610. https://doi.org/10.1080/02786820119445

TYSON, P. D. & PRESTON-WHYTE, R. A. 2000. *The weather and climate of southern Africa,* Cape Town, Oxford University Press.

US EPA 2009. Ross, Mary A. Integrated science assessment for particulate matter. *NCAR-RTP Division. Office of Research and Development, Research Triangle Park, NC, USA. EPA/600/R-08/139F. US Environmental Protection Agency: Washington DC, USA***,** 61-161.

UTELL, M. J., AQUILINA, A. T., HALL, W. J., SPEERS, D. M., DOUGLAS JR, R. G., GIBB, F. R., MORROW, P. E. & HYDE, R. W. 1980. Development of airway reactivity to nitrates in subjects with influenza. *American Review of Respiratory Disease,* 121**,** 233-241.

VAKKARI, V., BEUKES, J., LAAKSO, H., MABASO, D., PIENAAR, J., KULMALA, M. & LAAKSO, L. 2013. Long-term observations of aerosol size distributions in semi-clean and polluted savannah in South Africa. *Atmospheric Chemistry and Physics,* 13**,** 1751-1770. DOI: 10.5194/acp-13-1751-2013

VAKKARI, V., BEUKES, J. P., DAL MASO, M., AURELA, M., JOSIPOVIC, M. & VAN ZYL, P. G. 2018. Major secondary aerosol formation in southern African open biomass burning plumes. *Nature Geoscience***,** 1.

VAKKARI, V., KERMINEN, V. M., BEUKES, J. P., TIITTA, P., ZYL, P. G., JOSIPOVIC, M., VENTER, A. D., JAARS, K., WORSNOP, D. R. & KULMALA, M. 2014. Rapid changes in biomass burning aerosols by atmospheric oxidation. *Geophysical Research Letters,* 41**,** 2644-2651. DOI: 10.1002/2014GL059396

VAKKARI, V., LAAKSO, H., KULMALA, M., LAAKSONEN, A., MABASO, D., MOLEFE, M., KGABI, N. & LAAKSO, L. 2011. New particle formation events in semi-clean South African savannah. *Atmospheric Chemistry and Physics,* 11**,** 3333-3346. DOI: 10.5194/acp-11-3333-2011

VAKKARI, V., TIITTA, P., JAARS, K., CROTEAU, P., BEUKES, J. P., JOSIPOVIC, M., KERMINEN, V. M., KULMALA, M., VENTER, A. D. & ZYL, P. G. 2015. Reevaluating the contribution of sulfuric acid and the origin of organic compounds in atmospheric nanoparticle growth. *Geophysical Research Letters,* 42. DOI: 10.1002/2015GL066459

VAN LOON, G. & DUFFY, S. 2005. Organic matter in water. *Environmental Chemistry: A Global Perspective, 2nd Ed., Oxford University Press, New York*.

VAN ZYL, P. G., BEUKES, J. P., DU TOIT, G., MABASO, D., HENDRIKS, J., VAKKARI, V., TIITTA, P., PIENAAR, J. J., KULMALA, M. & LAAKSO, L. 2014. Assessment of atmospheric trace metals in the western Bushveld Igneous Complex, South Africa. *South African Journal of Science,* 110**,** 01-10. http://dx.doi.org/10.1590/sajs.2014/20130280

VENTER, A. D., VAKKARI, V., BEUKES, J. P., VAN ZYL, P. G., LAAKSO, H., MABASO, D., TIITTA, P., JOSIPOVIC, M., KULMALA, M. & PIENAAR, J. J. 2012. An air quality assessment in the industrialised western Bushveld Igneous Complex, South Africa. *South African Journal of Science,* 108**,** 1-10. http://dx.doi.org/10.4102/sajs.v108i9/10.1059

VENTER, A. D., VAN ZYL, P. G., BEUKES, J. P., JOSIPOVIC, M., HENDRIKS, J., VAKKARI, V. & LAAKSO, L. 2017. Atmospheric trace metals measured at a regional background site (Welgegund) in South Africa. *Atmospheric Chemistry and Physics,* 17**,** 4251-4263. DOI: 10.5194/acp-17-4251-2017

VENTER, A. D., VAN ZYL, P. G., BEUKES, J. P., SWARTZ, J.-S., JOSIPOVIC, M., VAKKARI, V., LAAKSO, L. & KULMALA, M. J. J. O. A. C. 2018a. Size-resolved characteristics of inorganic ionic species in atmospheric aerosols at a regional background site on the South African Highveld. *Journal of Atmospheric Chemistry***,** 1-20. https://doi.org/10.1007/s10874-018-9378-z

VENTER, M., BEUKES, J., VAN ZYL, P., VAKKARI, V., VIRKKULA, A., JOSIPOVIC, M., KULMALA, M. & LAAKSO, L. 2018b. Long-term observations of aerosol optical properties

at a southern African grassland savannah site. *In preparation for submission to Atmospheric Chemistry and Physics*.

VET, R., ARTZ, R. S., CAROU, S., SHAW, M., RO, C.-U., AAS, W., BAKER, A., BOWERSOX, V. C., DENTENER, F. & GALY-LACAUX, C. 2014. A global assessment of precipitation chemistry and deposition of sulfur, nitrogen, sea salt, base cations, organic acids, acidity and pH, and phosphorus. *Atmospheric Environment,* 93**,** 3-100. http://dx.doi.org/10.1016/j.atmosenv.2013.10.060

WAN, X., KANG, S., XIN, J., LIU, B., WEN, T., WANG, P., WANG, Y. & CONG, Z. 2016. Chemical composition of size-segregated aerosols in Lhasa city, Tibetan Plateau. *Atmospheric Research,* 174**,** 142-150. http://dx.doi.org/10.1016/j.atmosres.2016.02.005

WANG, Q., MA, Y., TAN, J., ZHENG, N., DUAN, J., SUN, Y., HE, K. & ZHANG, Y. 2015c. Characteristics of size-fractionated atmospheric metals and water-soluble metals in two typical episodes in Beijing. *Atmospheric Environment,* 119**,** 294-303. http://dx.doi.org/10.1016/j.atmosenv.2015.08.061

WATSON, J. G., CHOW, J. C. & CHEN, L.-W. A. 2005. Summary of Organic and Elemental Carbon/Black Carbon Analysis Methods and Intercomparisons. *Aerosol and Air Quality Research,* 5**,** 65-102.

WHO 2014. Ambient (outdoor) air quality and health. *Fact sheet N° 313*.

WMO/GAW 2004. Manual for the WMO/GAW precipitation chemistry programme. *WMO/GAW Report,* 160.

WONG, J. W. & WONG, M. 1990. Effects of fly ash on yields and elemental composition of two vegetables, Brassica parachinensis and B. chinensis. *Agriculture, Ecosystems and Environment,* 30**,** 251-264.

WOZNIAK, A. S., BAUER, J. E. & DICKHUT, R. M. 2012. Characteristics of water-soluble organic carbon associated with aerosol particles in the eastern United States. *Atmospheric Environment,* 46**,** 181-188. DOI: 10.1016/j.atmosenv.2011.10.001

XIAO, Z. & LAPLANTE, A. 2004b. Characterizing and recovering the platinum group minerals—a review. *Minerals Engineering,* 17**,** 961-979. DOI: 10.1016/j.mineng.2004.04.001

XU, J., TAI, X., BETHA, R., HE, J. & BALASUBRAMANIAN, R. 2015. Comparison of physical and chemical properties of ambient aerosols during the 2009 haze and non-haze periods in Southeast Asia. *Environmental Geochemistry and Health,* 37**,** 831-841. DOI: 10.1007/s10653-014-9667-7

YANG, F., TAN, J., ZHAO, Q., DU, Z., HE, K., MA, Y., DUAN, F., CHEN, G. J. A. C. & PHYSICS 2011. Characteristics of $PM_{2.5}$ speciation in representative megacities and across China. *Atmospheric Chemistry and Physics,* 11**,** 5207-5219. DOI: 10.5194/acp-11-5207-2011

YOUNG, L.-H., LI, C.-H., LIN, M.-Y., HWANG, B.-F., HSU, H.-T., CHEN, Y.-C., JUNG, C.-R., CHEN, K.-C., CHENG, D.-H., WANG, V.-S., CHIANG, H.-C. & TSAI, P.-J. 2016. Field performance of a semi-continuous monitor for ambient $PM_{2.5}$ water-soluble inorganic ions and gases at a suburban site. *Atmospheric Environment,* 144**,** 376-388. DOI: 10.1016/j.atmosenv.2016.08.062

YU, J. Z., TUNG, J. W. T., WU, A. W. M., LAU, A. K. H., LOUIE, P. K.-K. & FUNG, J. C. H. 2004a. Abundance and seasonal characteristics of elemental and organic carbon in Hong Kong PM_{10}. *Atmospheric Environment,* 38**,** 1511-1521. DOI: 10.1016/j.atmosenv.2003.11.035

YU, X., MA, J., AN, J., YUAN, L., ZHU, B., LIU, D., WANG, J., YANG, Y. & CUI, H. 2016. Impacts of meteorological condition and aerosol chemical compositions on visibility impairment in Nanjing, China. *Journal of Cleaner Production,* 131**,** 112-120. DOI: 10.1016/j.jclepro.2016.05.067

YUN, Y., GAO, R., YUE, H., GUO, L., LI, G. & SANG, N. 2017. Sulfate aerosols promote lung cancer metastasis by epigenetically regulating the epithelial-to-mesenchymal transition (EMT). *Environmental Science and Technology,* 51**,** 11401-11411. DOI: 10.1021/acs.est.7b02857

ZAPPOLI, S., ANDRACCHIO, A., FUZZI, S., FACCHINI, M., GELENCSER, A., KISS, G., KRIVACSY, Z., MOLNAR, A., MESZAROS, E. & HANSSON, H.-C. 1999. Inorganic, organic and macromolecular components of fine aerosol in different areas of Europe in relation to their water solubility. *Atmospheric Environment,* 33**,** 2733-2743.

ZHANG, J., SONG, H., TONG, S., LI, L., LIU, B. & WANG, L. 2000. Ambient sulfate concentration and chronic disease mortality in Beijing. *Science of the Total Environment,* 262**,** 63-71.

ZHANG, J., TONG, L., HUANG, Z., ZHANG, H., HE, M., DAI, X., ZHENG, J. & XIAO, H. 2018. Seasonal variation and size distributions of water-soluble inorganic ions and carbonaceous aerosols at a coastal site in Ningbo, China. *Science of the Total Environment,* 639**,** 793-803. https://doi.org/10.1016/j.scitotenv.2018.05.183

ZHANG, Q., JIMENEZ, J. L., CANAGARATNA, M. R., ALLAN, J. D., COE, H., ULBRICH, I., ALFARRA, M. R., TAKAMI, A., MIDDLEBROOK, A. M., SUN, Y. L., DZEPINA, K., DUNLEA, E., DOCHERTY, K., DECARLO, P. F., SALCEDO, D., ONASCH, T., JAYNE, J. T., MIYOSHI, T., SHIMONO, A., HATAKEYAMA, S., TAKEGAWA, N., KONDO, Y., SCHNEIDER, J., DREWNICK, F., BORRMANN, S., WEIMER, S., DEMERJIAN, K., WILLIAMS, P., BOWER, K., BAHREINI, R., COTTRELL, L., GRIFFIN, R. J., RAUTIAINEN, J., SUN, J. Y., ZHANG, Y. M. & WORSNOP, D. R. 2007b. Ubiquity and dominance of oxygenated species in organic aerosols in anthropogenically-influenced Northern Hemisphere midlatitudes. *Geophysical Research Letters,* 34**,** 6. DOI: 10.1029/2007gl029979

ZHAO, H., CHE, H., ZHANG, X., MA, Y., WANG, Y., WANG, H. & WANG, Y. 2013. Characteristics of visibility and particulate matter (PM) in an urban area of Northeast China. *Atmospheric Pollution Research,* 4**,** 427-434. DOI: 10.5094/APR.2013.049

ZHAO, Y. & GAO, Y. 2008. Mass size distributions of water-soluble inorganic and organic ions in size-segregated aerosols over metropolitan Newark in the US east coast. *Atmospheric Environment,* 42**,** 4063-4078. DOI: 10.1016/j.atmosenv.2008.01.032

ZHILIANG, Y., YIHUA, L., LIANSHENG, Z. & ZHENGPING, Z. 1987. Industrial fluoride pollution in the metallurgical industry in China. *Fluoride,* 20**,** 118-125.

ZHOU, H., LÜ, C., HE, J., GAO, M., ZHAO, B., REN, L., ZHANG, L., FAN, Q., LIU, T. & HE, Z. 2018. Stoichiometry of water-soluble ions in $PM_{2.5}$: Application in source apportionment for a typical industrial city in semi-arid region, Northwest China. *Atmospheric Research,* 204**,** 149-160. https://doi.org/10.1016/j.atmosres.2018.01.017

ZHOU, J., WU, S., PAN, Y., ZHANG, L., CAO, Z., ZHANG, X., YONEMOCHI, S., HOSONO, S., WANG, Y. & OH, K. 2015. Enrichment of heavy metals in fine particles of municipal solid waste incinerator (MSWI) fly ash and associated health risk. *Waste Management,* 43**,** 239-246. http://dx.doi.org/10.1016/j.wasman.2015.06.026

APPENDIX A

Table A-1: Average $PM_{2.5}$ and $PM_{2.5-10}$ water-soluble ion concentrations (µg/m^3), as well as the calculated total nitrogen (N) (determined from NO_3^- and NH_4^+) and total sulphur (S) (determined from SO_4^{2-}) concentrations (µg/m^3) for the four South African INDAAF sites, for the entire sampling period

	Average concentration (µg/m^3)							
Species	**Vaal Triangle (VT)**		**Amersfoort (AF)**		**Skukuza (SK)**		**Louis Trichardt (LT)**	
	$PM_{2.5}$	**$PM_{2.5-10}$**	**$PM_{2.5}$**	**$PM_{2.5-10}$**	**$PM_{2.5}$**	**$PM_{2.5-10}$**	**$PM_{2.5}$**	**$PM_{2.5-10}$**
Nitrate (NO_3^-)	0.884	0.667	0.353	0.348	0.875	0.419	0.375	0.486
Chloride (Cl^-)	0.537	0.225	0.455	0.278	1.833	0.644	0.449	0.465
Sulphate (SO_4^{2-})	3.795	0.892	2.878	0.746	2.250	0.612	2.101	1.277
Fluoride (F^-)	0.394	0.067	0.412	0.078	0.390	0.063	0.309	0.083
Organic acids (OA)	2.122	0.943	2.029	0.630	1.537	0.351	1.573	0.655
Sodium (Na^+)	0.373	0.260	0.737	0.248	0.634	0.586	0.346	0.515
Ammonium (NH_4^+)	1.684	0.310	1.001	0.228	0.798	0.149	0.692	0.413
Potassium (K^+)	0.531	0.090	0.592	0.103	0.447	0.177	0.419	0.126
Magnesium (Mg^{2+})	0.468	0.184	0.471	0.218	0.591	0.176	0.423	0.306
Calcium (Ca^{2+})	0.521	0.306	1.092	0.230	0.705	0.283	0.537	0.987
Total concentration	11.309	3.944	10.02	3.107	10.06	3.46	7.224	5.313
Total of $PM_{2.5}$ and $PM_{2.5-10}$	15.253		13.127		13.52		12.537	
Total Nitrogen (N)	1.507	0.391	0.857	0.255	0.817	0.211	0.622	0.430
Total Sulphur (S)	1.267	0.298	0.961	0.249	0.751	0.204	0.701	0.426

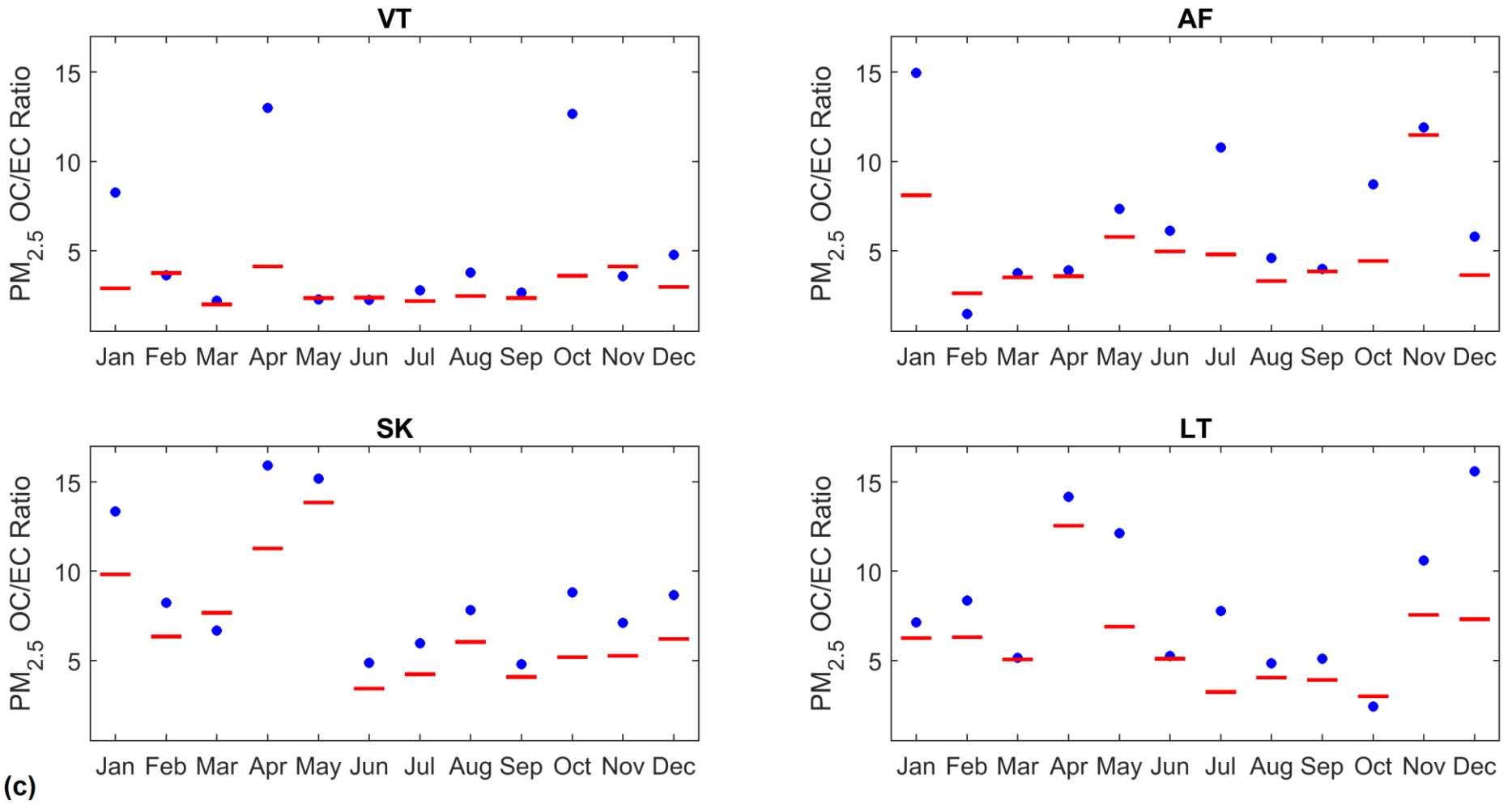

Figure A-1: **$PM_{2.5}$ monthly temporal distribution of OC (a) and EC (b) and OC/EC ratios (c) for each site over the entire monitoring period. Similar to Figure 2-3 and Figure 2-4, the blue dots indicate mean values and the red lines median values**

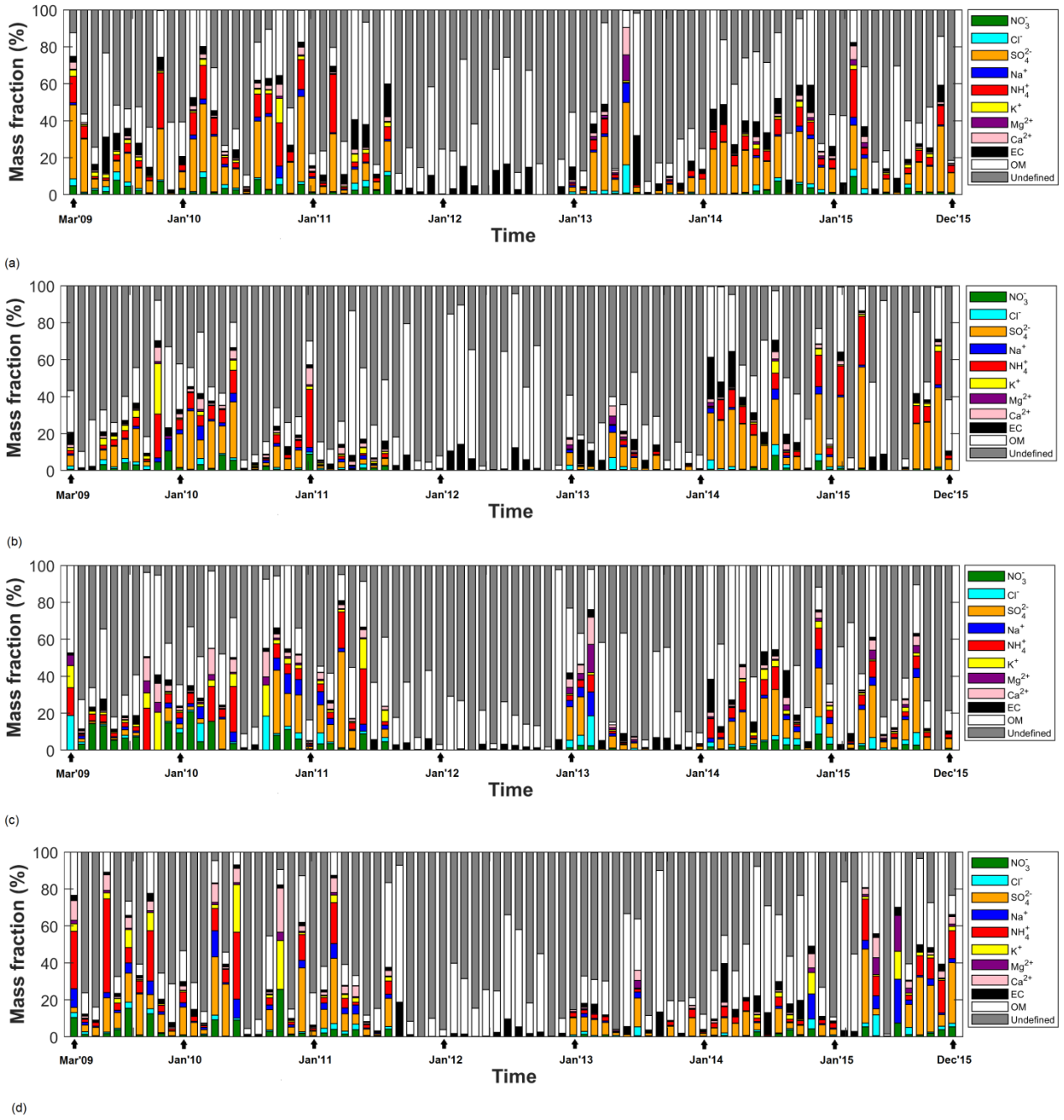

Figure A-2: Monthly stacked bar plots of the $PM_{2.5}$ mass fractions (%) at all the sites, i.e. VT (a), AF (b), SK (c) and LT (d), of individual samples collected over the entire sampling period. Note that concentrations of water-soluble ions were not available from September 2011 to December 2012

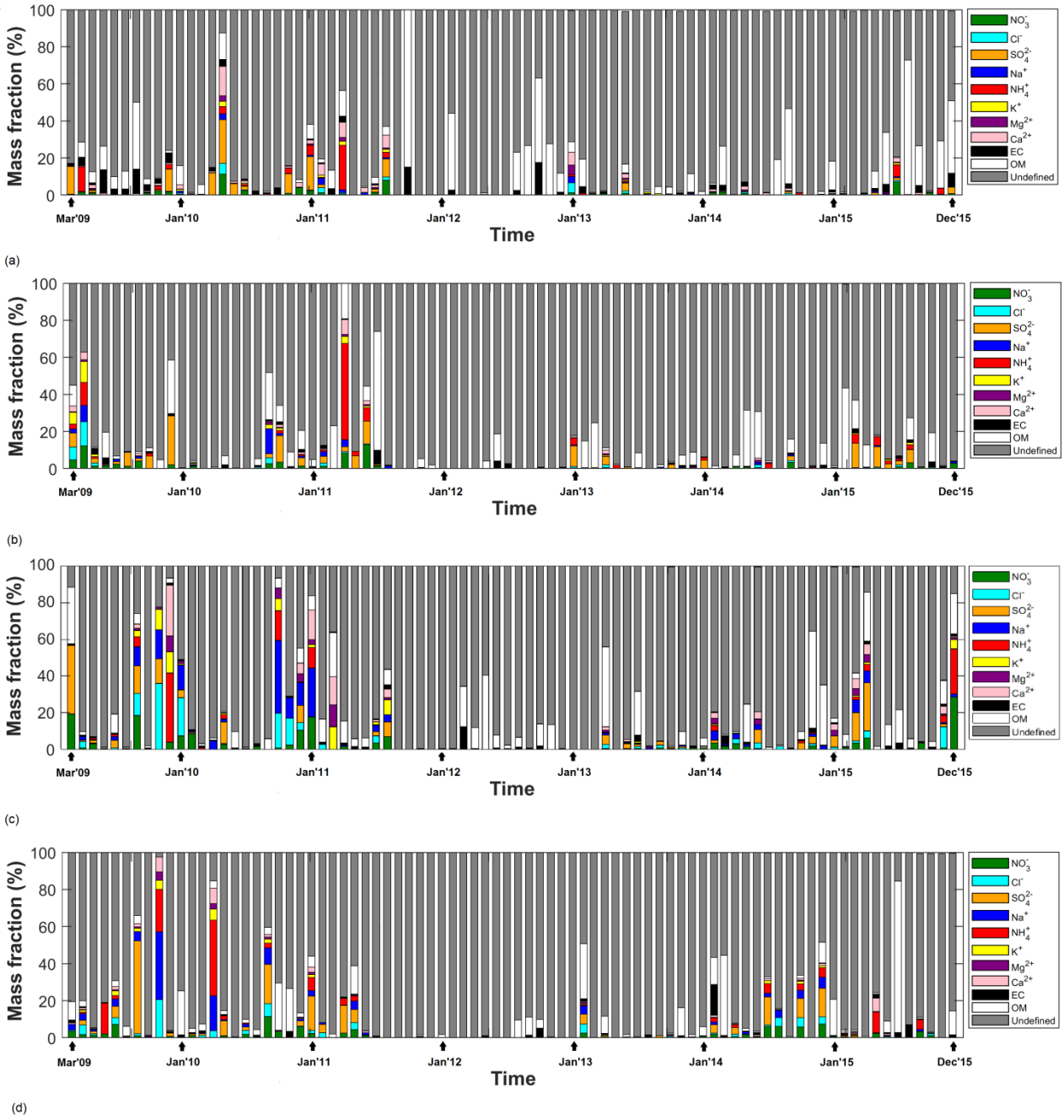

Figure A-3: Monthly stacked bar plots of the $PM_{2.5-10}$ mass fractions (%) at all the sites, i.e. VT (a), AF (b), SK (c) and LT (d), of individual samples collected over the entire sampling period. Note that concentrations of water-soluble ions were not available from September 2011 to December 2012